THE UNIVERSITY
of EDINBURGH

Development of Novel Molecular Tools for the Characterisation of Zebrafish Renin

Scott Hoffmann, BSc, MSc

A thesis submitted for the degree of
Doctor of Philosophy with Integrated Study

Optical Medical Imaging with Healthcare
Innovation & Entrepreneurship

2020

Acknowledgements

First and foremost I would like to thank my supervisors Professor John Mullins, Professor Mark Bradley and Dr Sebastien Rider for their support advice and help throughout this PhD. In particular I would like to thank Professor John Mullins for his time, for the meetings leading to interesting discussions, for the new ideas and for the continuous support for this project. I would also like to thank Dr Sebastien Rider for all the training and patience in teaching me all the techniques which have been performed throughout this thesis. I am grateful to Audrey Peter for tolerating and answering my never ending flow of questions and helping with so many experiments in the lab. Additionally, I would like to thank Dr Linda Mullins for her guidance and support throughout this project.

From the Bradley group I have to give particular thanks to Dr Jessica Clavadetscher who was able to teach a biologist how to do chemistry and successfully taught me how to synthesise FRET probes and peptides. Although I still look lost in a chemistry lab, I would have never managed to complete the chemistry related parts of this PhD without her help.

Many thanks to all the BVS staff for their incredible work, time and effort in helping with all the fish work in this project.

Anna, I would probably never have completed the writing of this thesis if it wasn't for your amazing work-ethic as well as the much needed breaks with many laughs. Thank you for being amazing and supporting me through this busy time!

Enormous thanks to Ruth and Christoph for the incredible support in getting this thesis finished and of course their Latex wizardry without which this would probably never have been printed correctly or looked anything like a book.

I would also like to thank all my friends who have made this PhD such an amazing experience.

Lastly, this thesis is dedicated to my parents, Christoph and Maria, who have shaped my entire life and are a big reason as to why I ended up here. I owe you enormous amounts for all the things you have done to ensure I got the best possible eduction. I hope you will enjoy having this book on your bedside table.

Abstract

The renin angiotensin system (RAS) is highly conserved across vertebrates. However, until recently it has not been extensively explored in zebrafish, an important model organism suitable for developmental studies, high-resolution *in vivo* imaging, and genetic and chemical screens. In common with mammals, the adult zebrafish kidney contains specialised renin-expressing mural cells that contain granules indicative of the processing and regulated secretion of active renin. Due to the translucent nature of zebrafish larvae, the functional pronephros is easily accessible for real-time imaging and *in vivo* studies of the RAS.

The primary aim of this project was to develop novel tools to help elucidate the function of renin and the role of the RAS in zebrafish. I designed a zebrafish renin-luciferase reporter transgene using a previously published promoter sequence to investigate the transcriptional regulation of renin in real-time. The expression vector was injected into fertilised WIK zebrafish eggs and successful integration of the plasmid into the zebrafish genome was demonstrated. An *in vivo* assay was designed to select for highest luciferase expressers, but bioluminescent imaging revealed that the high signal stemmed from the yolk sac of zebrafish. Yolk sac expression appeared to originate from episomal transcription of the injected plasmid and, in the F0 fish, masked potential bona fide expression from the renin-expressing cells of the pronephros. A new transgene was generated using two reporters, driven by the same promoter sequence and the two reporters were separated by a '2A' sequence which codes for a self-cleaving peptide. This zebrafish line was generated to permit selection of tg(*ren*:LUC-2A-mCherry) fish for the strongest mCherry signal originating from renin expressing cells. However, no expression was observed at the anterior mesenteric artery (AMA). Further investigation revealed that when generating novel transgenic zebrafish, the reporter proteins are transiently expressed in the yolk sac of F0 founder fish and the ectopic expression can influence studies relying on quantitative reporters.

Current studies largely rely on the transcriptional activity of RAS components and are restricted to timepoint-specific observations. The lack of antibodies prevents the measurement of RAS proteins in zebrafish. The amino acid sequence for zebrafish angiotensinogen is known and by comparison to mammalian sequences, I identified the amino acid sequences for angiotensin (Ang) I and II. The production of zebrafish Ang I and II peptides by solid phase peptide synthesis provided standards for the development of assays for zebrafish angiotensins. I used these

assays to demonstrate that Captopril, which in mammals prevents the conversion of Ang I to Ang II by inhibiting the Angiotensin Converting Enzyme (ACE), is active in zebrafish, and that its administration leads to a dramatic decrease in Ang II. In parallel I designed and synthesised a fluorescent resonant energy transfer (FRET) probe to enable zebrafish renin activity to be measured. Using various zebrafish models I was able to demonstrate dynamic changes in renin activity and measure these using the first renin zebrafish FRET probe.

I characterised a renin knockout zebrafish, generated by CrispRCas9 gene editing. Knockouts were identified by DNA sequencing which identified an 8bp deletion in exon 2 of the renin gene, causing a frameshift mutation and early termination of renin translation. Renin knockout fish proved to be viable and were screened for a phenotype using the high throughput automated screening system (VAST) which permits the precise imaging of a large number of live fish. Imaging revealed delayed development of the swim bladder and reduced fish length compared to age-matched controls. This was indicative of an overall developmental delay. The knockout fish were intercrossed with existing renal reporter lines to investigate phenotypes at a cellular level. *Ren*$^{-/-}$ tg(*wt1b*:EGFP) fish showed a delay in glomerular fusion of the pronephric kidney and a cross of the *ren*$^{-/-}$ with tg(*ren*:RFP-LifeAct) fish indicated a dramatic increase in renin-expressing cell along the renal mesonephric vasculature. Moreover, morphological examination revealed vacuolation of proximal tubules in the mesonephric kidney. The intercrossing of the *ren*$^{-/-}$ zebrafish to the tg(*ren*:RFP-LifeAct) and tg(*acta2*:EGFP) fluorescent reporters lead to the optimisation of a FAC sorting protocol and resulted in the first zebrafish *ren*- and *acta2*-expressing cells to be cultured and imaged using high-resolution microscopy imaging.

In summary, my work has led to the first successful measurement of zebrafish AngI and AngII in mesonephric zebrafish tissue to demonstrate the effectiveness of Captopril in zebrafish as well as the first development of a zebrafish renin FRET probe to allow the measurement and quantification of renin activity in zebrafish, enabling more accurate studies of the zebrafish RAS. Lastly, successful phenotypic characterisation of the *ren*$^{-/-}$ fish will further our understanding of the role of renin and the RAS in zebrafish.

Lay Abstract

The renin-angiotensin system (RAS) is a hormonal system responsible for blood pressure control and water regulation in the body. A vital component of that system is the enzyme renin, which is produced by specialised cells located in the kidney. Although various studies have investigated the function of renin, many questions remain regarding its role in cardiovascular diseases and kidney development. These studies have been performed predominantly in mammals, which have a very complex kidney. Recently, zebrafish have become a crucial model organism for studying the kidney. The main reasons are that during the early stages of zebrafish development, the zebrafish has a functional but simple kidney. Despite its simplicity, the types of cells that make up the zebrafish kidney are also present within the adult human kidney. Furthermore, the zebrafish is optically transparent during the early stages of development, allowing imaging of the kidney in living zebrafish. Recent studies have shown that the zebrafish possesses the crucial RAS enzyme renin, alongside other essential components. These studies have been able to show that the cells expressing renin have a similar structure to the renin cells found in the adult human kidney and respond to environmental stresses such as low salt concentrations in a comparable manner. Most of these studies have focused on the characterisation of these cells. However, there is a lack of tools to permit studying the active component renin in zebrafish.

During this project, I have generated a new transgenic zebrafish, which utilises bioluminescence instead of the commonly used fluorescence. Bioluminescence is based on the chemistry that allows fireflies to produce light. By placing regulatory elements required by renin in front of the gene coding for the bioluminescent protein and inserting it into the genome of zebrafish, it can be used as a surrogate marker for the renin gene. Due to the rapid bioluminescent reaction, the gene function can be assessed in living fish. I have used qualitative as well as quantitative data to asses whether bioluminescence can be used to measure renin activity in the larval zebrafish.

I was also able to identify and synthesise two components of the RAS in zebrafish. Using a blood pressure lowering drug I was able to evoke a dynamic change in the concentration of these components which were subsequently measured using a mass spectrometry assay provided by Attoquant Diagnostics. To investigate the function of the renin protein, I have developed chemical probes that can be injected or added to water to enter the fishes' blood supply. The probes

are designed by synthesising a sequence of amino acids which renin recognises and interacts with by breaking the amino acid chain. On either end of the chain, a fluorophore is attached. A fluorophore is a protein which fluoresces when it is excited by the correct wavelength of light. On the opposite end, a further molecule is attached which, when the amino acid chain is intact, inhibits the fluorescent protein from fluorescing. However, upon the interaction with renin, the probe is broken up, restoring the fluorescent property of the fluorophore. The fluorescence can be quantified and permits the investigation of renin activity. Similar probes have been designed for human and rat renin, however, this is the first probe of its kind for zebrafish renin. In this project, I describe the synthesis and also test the probe and how well it interacts with zebrafish renin.

Lastly, to understand the function of a gene within an organism, gene editing techniques are used to delete or disable a gene. The causes of the deletion can be investigated and give insight into the mechanisms for which the gene is required. I had the opportunity to characterise the first zebrafish with a mutation in the renin gene, causing a complete lack of renin. Using a high-throughput imaging system, I was able to determine that the growth of the zebrafish is delayed as well as severe differences in kidney structure in the adult zebrafish. Combination of the zebrafish line lacking renin with previous zebrafish lines used to characterise the renin expressing cells showed an increase in renin cells which is a response similar to that seen in mammals.

In this project, I was able to measure accurately the first dynamic change of RAS components and was able to synthesise these successfully. Furthermore, the first renin fluorescent probe was designed and tested and results have indicated that it is capable of recognising and reporting on zebrafish renin activity. Lastly, the characterisation of the first zebrafish lacking active renin by various imaging modalities has furthered the understanding of the function of renin in zebrafish. All of the designed tools in this project will permit to design more accurate and previously impossible experiments to further the understanding of the role of renin using the zebrafish as a model organism.

Contents

List of Figures

List of Tables

Glossary

ACE Angiotensin-converting enzyme

AMA Anterior mesenteric artery

AngII Angiotensin II

AngI Angiotensin I

Asn Asparagine

cAMP Cyclic adenosine monophosphate

CBP CREB-binding protein

CRISPR Clustered regularly interspaced short palindromic repeat

CW Conditioned water

DA Dorsal aorta

DIC N,N'-Diisopropylcarbodiimide

DMC Dimethyl carbonate

DMF Dimethylformamide

Dpf Days post fertilisation

EDTA Ethylenediaminetetraacetic acid

EGFP Enhanced green fluorescent protein

FACS Flow activated cell sorting

Glu Glutamic acid

His Histidine

Hpf Hours post fertilisation

JGA Juxtaglomerular apparatus

JG Juxtaglomerular

LUC Luciferase

Oxyma Ethyl cyanohydroxyiminoacetate

PBS Phosphate-buffered saline

PCR Polymerase chain reaction

PFA Paraformaldehyde

Phe Phenylalanine

PMA Proximal mesenteric artery

Pro Proline

QPCR Quantitative polymerase chain reaction

RAS Renin-angiotensin system

Ren Renin

RFP-LifeAct Red fluorescent protein

Ser Serine

TAE Tris-acetate-EDTA

TBST Trisaminomethane-buffered saline with Tween

TBS Trisaminomethane-buffered saline

Tris Trisaminomethane

VEGF Vascular endothelial growth factor

Chapter 1

Introduction

1.1 Overview

The renin-angiotensin system (RAS) is the primary hormonal system responsible for blood pressure and water regulation. The RAS rate-limiting enzyme, renin, is secreted and predominantly synthesised in specialised renal cells called the juxtaglomerular (JG) cells. Renin is secreted in response to reduced blood flow and low salt concentration and is required for the formation of angiotensin I (AngI) and ultimately angiotensin II (Ang II), the main effector of the canonical RAS. Many studies have elucidated the different roles of renin and the RAS in mammalian model systems. However, the role of renin and the RAS in the establishment of cardiovascular homeostasis and their involvement in cardiovascular and renal diseases remain unclear. Recent work using transgenic zebrafish has shown that zebrafish possess specialised renal mural cells expressing renin. Although there are many similarities of the zebrafish RAS to the mammalian RAS, the zebrafish model still lacks specific tools that allow investigation of the role of zebrafish renin. Developing tools such as new renin bioluminescent transgenic zebrafish lines, mutant RAS knockout animals and chemical probes for measuring RAS activity will further the zebrafish as a crucial model for kidney research.

1.2 Kidney Structure

The kidney is a highly complex multicellular organ. A nephron is the functional unit of the kidney and constitutes of a glomerulus, where blood is filtered through blood vessels and nutrients are reabsorbed in the tubule [1, 2]. Although the number of nephrons per kidney in humans varies strongly dependant on the size of the human, it is estimated that on average, an adult kidney consists of 1,000,000 nephrons [3]. Afferent arterioles provide blood in into the renal corpuscle where blood vessels form a knotted structure inside a capsule made up of epithelial cells. This blood-filtering structure is known as the glomerulus. The glomerulus is the main blood filtering structure, and the vessels inside the glomerular capsule are enveloped by specialised epithelial cells called podocytes. Podocytes project foot-like processes forming filtration slits which are bridged by the slit diaphragm. These slits enable the passing of molecules and proteins up to a specific size to pass through and into the urinary space of the tubule. The tubule is segmented by specialised cells with specific abilities to absorb and excrete different nutrients. The

convoluted tubule, posterior to the glomerulus and the first segment of the proximal tubule, specialises in the reabsorption of potassium, sodium and water, as well as certain amino acids. The loop of Henle followed by the convoluted proximal tubule predominantly reabsorbs water. The distal tubule, of which a small segment also contains the macula densa cells further absorbs sodium and hydrogen ions and senses the sodium concentration with the macula densa cells and is in contact with the JG-cells. The tubule connects into a collecting tubule which transports the remaining solutes into the bladder where they are excreted.

1.3 The Renin-Angiotensin System

The RAS is the primary regulator of blood pressure and fluid balance. Renin, the rate limiting enzyme of the RAS, is almost exclusively synthesised within specialised perivascular mural cells of the kidney called the JG cells. JG cells are located along the afferent arterioles, proximal to the glomerulus and comprise a crucial anatomical and functional feature of the juxtaglomerular apparatus (JGA) [4]. The main effector of the RAS is AngII, which is generated by sequential cleavage of peptides from the main substrate molecule angiotensinogen (Figure 1.1).

Angiotensinogen is freely secreted from the liver, and its C-terminus is cleaved by renin to generate the biologically inactive decapeptide AngI [5]. Subsequent cleavage of AngI by the angiotensin-converting enzyme (ACE) generates the biologically active octapeptide, AngII [6]. Binding of AngII to the AT_1 and AT_2 receptors triggers multiple systems affecting the heart, kidney, vasculature and the immune system [7]. The two receptors differ in spatial distribution, physiological function and signalling pathways. Most AngII effects occur via binding and activation of the AT_1 receptor which is highly present on vascular smooth muscle cells. Binding of AngII to the AT_1 receptor evokes an increase in intracellular calcium which induces the contraction of vascular smooth muscle cells and ultimately leads to an increase in blood pressure [8]. Furthermore, binding of AngII to the AT_1 receptor stimulates the production of aldosterone in the adrenal cortex, which acts on the principal cells of the kidney, leading to an increase in sodium reabsorption [9]. More recent studies have been investigating the function of the AT_2 receptor. The AT_2 receptor is highly expressed during early development; however, its expression is reduced postnatally in mammals [10]. Although the AT_1 receptor is dominant in adult organisms, an increase of AT_2 expression has been observed in response to vascular

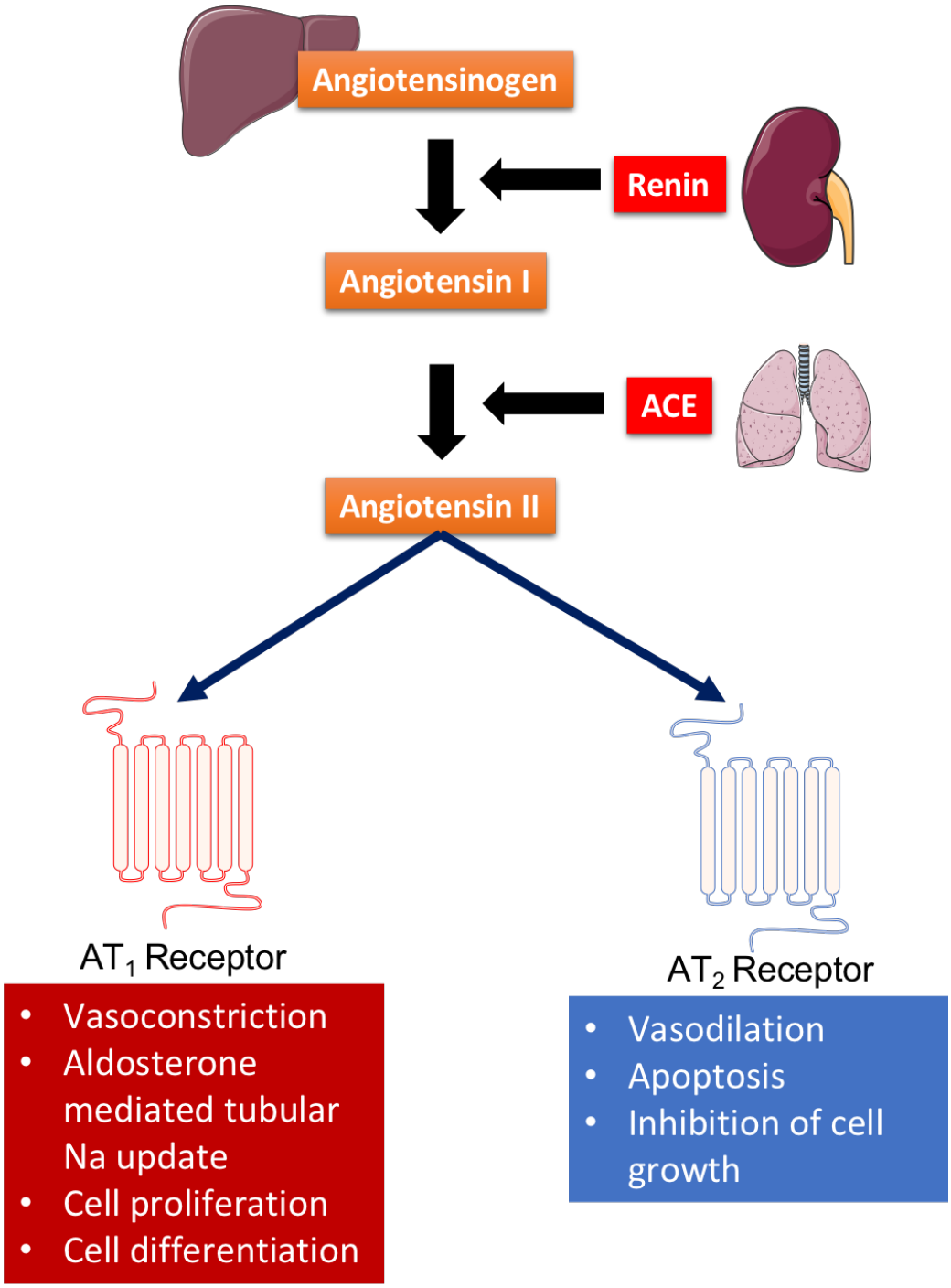

Figure 1.1 | **Schematic representation of the renin-angiotensin system** Angiotensinogen is freely secreted from the liver. Renin, secreted from specialised cells within the kidney, cleaves angiotensinogen and converts it to angiotensin I. Subsequent cleavage by ACE, released from the lung converts it to angiotensin II. Angiotensin II acts via the AT_1 and AT_2 receptors.

injury [11]. Mice lacking a gene coding for the AT_2 receptor have increased blood pressure, which was reversed using an AT_1 receptor antagonists [12]. Furthermore, studies have suggested that the observed increase in blood pressure using AT_2 antagonists suggests that the AT_2 might mediate vasodilatation [13, 14]. The opposing functions of the AT_2 receptor, to that of the AT_1 receptor implicates that the functions of the AT_2 receptor may have a protective effect against the overstimulation of the AT_1 receptor. In addition to the classical RAS, many additional smaller peptides have been described, which only recently gained pharmacological significance [15, 16, 17]. Besides the circulating RAS, several so-called 'local RAS' have been identified in different tissues such as the heart, brain and adrenal glands. These tissues can express all components of the RAS, although, the functionality of the RAS can differ to that of the circulating RAS [18].

1.4 Renin

Renin is the rate-limiting enzyme of the RAS, making it the central hormone for controlling blood pressure and water balance. However, renin is also involved in various other functions. Renin and the RAS were first discovered by Tigerstedt and Bergman, who observed an increase in blood pressure when injecting rabbit kidney extracts into rabbits [19]. The substance causing the raise in blood pressure was named renin after the renal substance it derived from. Renin is a protein-coding gene, which in humans encodes for 406 amino acids. Moreover, the enzyme renin belongs to the class of aspartyl proteases and has a high affinity to its substrate angiotensinogen and studies have demonstrated that in many cases renin is unable to cleave angiotensinogen from different species [20]. Synthesis of renin predominantly occurs in specialised JG cells in the kidney, which are located along the afferent arterioles, proximal to the glomerulus and comprise a crucial anatomical and functional feature of the JGA [4]. Renin expression and secretion is regulated by baroreceptors on JG cells sensing the perfusion in the afferent arteriole and via the macula densa cells, which sense sodium chloride concentration and signal to JG cells [21, 22, 23, 24]. Renin is synthesised in the JG cells as an inactive pre-pro-protein [25, 26]. The pre-segment acts as a signal peptide and removal of the pre-peptide from the N-terminus of renin produces the inactive form of renin, prorenin [26]. Prorenin is packed into vesicles, continuously in its inactive form as prorenin [27]. However, a small subset of prorenin is glycosylated in the Golgi Ap-

paratus and packaged into dense-core storage granules [28]. In those dense-core storage granules, a still unknown mechanism removes the pro-segment, activating it to renin, before being secreted via a regulated secretory pathway. It is still debated whether the precursor of renin, prorenin has a distinct physiological role. Circulating prorenin levels are reported to be 10-fold higher than concentrations of active renin [29, 30]. The recent identification of a prorenin receptor suggests that binding of prorenin to the receptor leads to conformational changes of prorenin, making it catalytically active, allowing it to produce AngII locally [31, 32, 33]. Moreover, there is evidence of prorenin uptake by cardiomyocytes, which subsequently can activate prorenin to renin [34].

Renin is highly selective for its substrate angiotensinogen and the specific amino acid sequence necessary for cleavage was first determined by isolation of a 14 amino acid sequence following trypsin digestion of horse plasma [35]. Although the tetradeca peptide amino acid sequence has demonstrated the best affinity as a substrate for renin, the shortest possible amino acid sequence, still cleaved by renin, is that of 10 amino acids [36]. A study has investigated the requirement of different amino acids in the decapeptide sequence using various alanine replacements. This study was able to demonstrate that the three amino acid sequence His^{6}-Pro^{7}-Phe^{8} is crucial for the cleavage of a substrate by renin [37]. Unsurprisingly, this sequence is conserved across all species that express renin and angiotensinogen [37]. The actual amino acids of the peptide bond cleaved by renin, however, vary dependant on species. In particular, the renin cleavage of human angiotensinogen occurs at the peptide bond of Leu^{10}-Leu^{11} whereas that of other mammalian species including rat, mouse, horse and sheep including other mammalian species is cleaved at Leu10-Val11 [38]. Zebrafish angiotensinogen also contains the His^{6}-Pro^{7}-Phe^{8} motif, which is essential for angiotensinogen cleavage by renin, however the peptide is cleaved between the Leu^{10}-Phe^{11} amino acids. These studies investigating the renin cleavage further suggest that the Leucine on the N-terminus of the renin cleaved amino acid is essential for the renin cleavage, whereas the C-terminal amino acid is variable [39].

1.5 Zebrafish Renin

Liang *et al.* first showed the presence of a renin gene in two non-mammalian species, the zebrafish, and the pufferfish [40]. Furthermore, Fournier *et al.* utilised

the published gene and protein sequence databases to investigate the evolution of the RAS [41]. During the analysis, Fournier identified multiple orthologous gene sequences of human RAS proteins. The zebrafish was shown to contain eight out of the nine sequences orthologous to the human genes: Ace1, Ace2, angiotensinogen, AT_1, AT_2, renin receptor, mineralocorticoid receptor, and renin. Zebrafish lack an orthologous gene sequence for the Mas receptor [41]. Although the function of the RAS in the zebrafish remains to be elucidated, the RAS in teleost has been linked to the ability to survive in water of fluctuating osmolarity [42]. In zebrafish, diluted salt water increases renin expression and circulating AngII levels in a comparable manner to the effect of low salt diets for mammals, suggesting an involvement of the RAS in salt handling [43,44,45]. AngII, the main effector of the system, acts via the AT_1 receptor. Tucker *et al.* demonstrated the presence of an AT_1 like receptor in zebrafish tissues involved in ion regulation [46]. Although it is suggested that the RAS is required for salt handling in zebrafish, the zebrafish has additional mechanisms that permit the maintenance of salt and water balance. In particular, the gills contain many specialised epithelial cells, ionicytes, which actively take up ions from the environment.

The identification of a zebrafish renin gene permitted the development of a novel transgenic fluorescent zebrafish reporter [47]. The fluorescent reporter plasmid to be injected into zebrafish to generate a transgenic line, utilised a 6.4kb segment of the zebrafish renin promoter, driving the fluorescent reporter protein RFP-LifeAct. The RFP-LifeAct fluorophore binds to intracellular actin, permitting visualisation of actin filaments [48]. The fluorescent zebrafish renin reporter enabled visualisation of renin cells as early as 48 hours post fertilisation (hpf) in the zebrafish pronephros. The cells first appear along the anterior mesenteric artery (AMA) in a post-glomerular position and expand along the dorsal aorta (DA) (Figure 1.2).

There are also renin-expressing cells present along the proximal mesenteric artery (PMA) that are not directly associated with the pronephric kidney [47]. The cellular location of renin-expressing cells in the mesonephric zebrafish kidney resembles that seen in the mammalian metanephros. Renin expressing cells are located proximal to the glomerulus along afferent arterioles [49]. Furthermore, the use of Lyostracker Green staining, which permits the intracellular labelling of acidic structures, suggested the presence of acidic granules in the renin-expressing cells [49]. Mammalian intrarenal renin cells contain a large number of acidic secretory granules that store and process prorenin into the active renin form [50]. The cross-

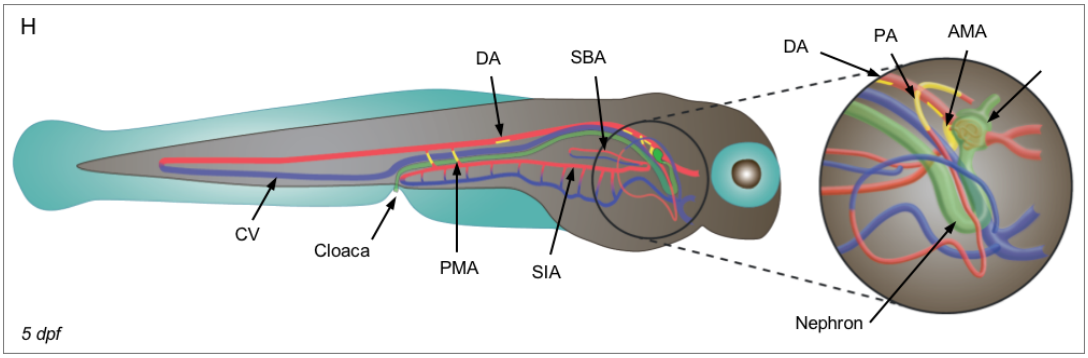

Figure 1.2 | **Renin cells in the zebrafish pronephros** Illustration of the larval zebrafish vasculature at 5 days post fertilisation (dpf). Renin-expressing cells are highlighted in yellow along the anterior mesenteric artery (AMA) and the dorsal aorta (DA) and the posterior mesenteric arteries (PMA). CV, caudal vein; PA, pectoral artery; SBA, swim bladder artery; SIA, Supraintestinal artery. Taken from Rider *et al.* [47].

ing of the tg(*ren*:RFP-LifeAct) zebrafish line to endothelial cell-deficient (cloche) and notch pathway impaired mib$^{ta52b-/-}$ mutants further demonstrated the requirement of a functional notch pathway and endothelium for the expression of renin [47].

1.6 Zebrafish Salt Handling

Zebrafish live in a hypotonic environment, making them hyperosmotic and hyperionic to their surroundings. Comparable with the mammalian kidney, the zebrafish kidney reabsorbs ions through active transcellular actions. Zebrafish possess specialised epithelial cells, termed ionocytes, which are predominantly located in the gills, that allow them to actively absorb electrolytes from the water. In addition to the ionocytes located on the gills, zebrafish are also capable of taking up electrolytes from food via epithelial cells located in the gut and subsequently through specialised cells within their kidneys [51, 52, 53]. During early development and prior proper establishment of the gills, zebrafish utilise ionocytes on their skin, allowing them for proper salt handling during larval stages [54]. Studies investigating the salt handling of freshwater fish have shown that zebrafish possess 4 different types of ionocytes, which are analogous to the transporting cells found in the different segments of the mammalian kidney tubules [55]. Namely, H^+- ATPase-rich(HR), Na^+-K^+- ATPase-rich(NaR), Na^+-Cl^-- element cotransporter-expressing

(NCC) and K^+-secreting cells are responsible for the sodium, calcium, and chloride uptake, respectively [56, 57]. A major difference between teleosts and mammals is that terrestrial mammals are required to actively take up water in order to prevent dehydration. However, teleosts live in an aquatic environment and constantly excrete huge amounts of highly diluted urine, in order to maintain their osmotic balance [58]. The main regulatory mechanisms, by which zebrafish maintain ion homeostasis, is via the endocrine system. The osmoregulation in vertebrates by the endocrine system has been widely studied, however only few studies have implicated several hormones that might be involved in osmoregulation in zebrafish [59]. These include the atrial natriuretic peptide (ANP), which is secreted in response to an increase in blood volume and promotes excretion of water and sodium, and the renin-angiotensin system, which is discussed in section 1.3 and 1.4. Lastly, prolactin the function of which includes promoting lactation in the mammary gland, has been implicated in the involvement for osmoregulation in fish. In particular in euryhaline fish, prolactin is required for the adaption to fresh water by promoting the uptake of ions [60]. Zebrafish are particularly interesting for the investigation of various endocrine responses as they are stenohaline, allowing them to adapt to freshwater salinity changes. Despite many similarities between zebrafish and mammals in endocrine responses to salinity changes, several differences exist due to the relationship of the control of blood volume and sodium concentration in the plasma. In terrestrial mammals, the blood volume control occurs in the same direction as the plasma sodium. However, in teleost the direction of blood volume control is opposite to that of the sodium plasma control. A great example of this is that in mammals ANP and renin have opposing effects. ANP promotes excretion of water and sodium, whereas renin promote reabsorption [61]. In zebrafish, ANP and renin have been suggested to be regulated in the same direction when exposed to low saltwater, suggesting that ANP may have a water excretion role in zebrafish whilst renin is implicated in sodium reabsorption [43].

1.7 Renin Knockout Models

To elucidate the function of renin, various studies in different mammals using knockout strategies have been performed [62, 63, 64]. Mice, depending on the strain, differ from other mammals and fish, as some strains have two renin genes, termed *Ren-1*^{d} and *Ren-2*, while other strains such as the C57BL/6 only have one renin

gene, *Ren-1^c*. The second renin gene is believed to have originated from a gene duplication on chromosome 1 [65]. The *Ren-2* gene sequence is highly homologous to *Ren-1^d*, with differences in the glycosylation sites required for post-translational modifications. Deletion of the *Ren-2* gene in mouse strains with two renin genes, leaving the *Ren-1^d* gene intact, does not result in any distinct phenotype [64]. *Ren-2* knockout mice are viable, do not display increased blood pressure, although an increase in active plasma renin can be measured. Knocking out the *Ren-1^d* gene in mice with two copies of the renin gene, leaving only the *Ren-2* as a functioning renin gene, resulted in hypotension in female mice but no change in blood pressure was observable in male mice [63]. Most interestingly, however, is the complete absence of secretory electron-dense granules in the JG cells [63]. A homozygous *Ren-1^c* knockout presents a very similar phenotype to a complete Agt knockout mouse [66]. Viability is significantly reduced, and daily saline injections are required to prevent death shortly after birth. The *Ren-1^c* knockout mice are polyureic, severely hypotensive and morphological changes to the kidneys include interstitial fibrosis, focal glomerulosclerosis and perivascular infiltration [62]. Prior to my thesis there has been no report describing the generation of a renin knockout zebrafish.

1.8 Renin Expressing Cells

Renin-expressing cells are specialised smooth muscle cells that are anatomically restricted to the JGA in the mammalian and metanephros and have also been characterised along the anterior mesenteric artery, dorsal aorta and the posterior mesenteric artery in the larval zebrafish pronephros, and along afferent arterioles in the zebrafish mesonephros [47, 67, 68]. Renin cells descend from Foxd1-expressing stromal cells [69]. The precursor cell to the Foxd1-expressing cells also gives rise to smooth muscle cells, mesangial cells, as well as interstitial pericytes. It has been suggested that renin precursor cells are crucial for the development of the kidney vasculature [70]. During kidney development in the mouse and rat, renin cells are located at kidney vessel sprouting points [71]. A similar observation has been made in the pronephric zebrafish kidney, where AMA angiogenesis was inhibited with the VGEF inhibitor axitinib. Renin-expressing cells were observed at the position of the expected initiation site of the AMA, suggesting a role in angiogenesis [47]. In rats and mice, the sprouting arteriolar vessels during kidney

development are enveloped by renin cells, and with the maturation of the vessels and the kidney, these cells lose their renin expressing identity and differentiate into smooth muscle cells [72]. Renin cells are then restricted to the juxtaglomerular position along the afferent arterioles in the metanephric mammalian kidney (Figure 1.3).

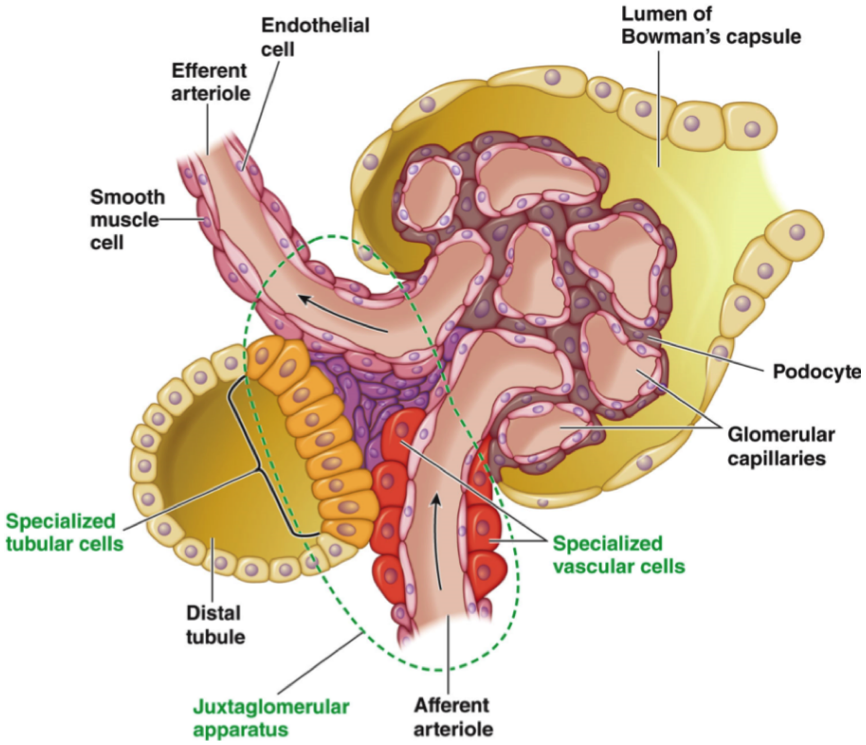

Figure 1.3 | **Mammalian glomerulus** Structure of the glomerulus. Afferent arterioles provide the glomerulus with blood and create a knot like structure. The juxtaglomerular apparatus constitutes of the granulated juxtaglomerular cells (specialised vascular cells in red) capable of renin expression and storage, extra glomerular mesangial cells (purple), and the macula densa cells (specialised tubular cells in yellow). The glomerular vasculature is lined by podocytes which filter small enough proteins into the lumen of the Bowman's capsule, attached to the tubule. Image from Lauralee Sherwood [73].

The smooth muscle cells along the afferent arterioles retain the ability to re-express renin in response to physiological stress [74]. Although renin cells express smooth muscle cell makers, as well as pericyte markers, the expression levels of these appear to be variable. Reports have shown that in comparison to smooth muscle cells along the afferent arterioles, which express high levels of α-smooth muscle actin, renin-expressing cells have low expression [75]. Although the exact mechanism for the transition of smooth muscle cells to renin cells in response

to physiological stress remains to be described, recent findings have suggested that the cAMP pathway involving CBP and p300 are essential for the induction of renin expression during development. Furthermore, as renin cells originate from a vascular progenitor cell, it remains to be elucidated whether renin-expressing cells are required for, and directly involved in the angiogenesis of the renal vasculature. RAS inhibition during kidney development or knockout of RAS genes results in renal vascular defects [76, 77, 78]. Renin-expressing cells release renin in response to various signals, which include the renal baroreceptors located on the JG cells, the macula densa mechanism, and via the β-adrenergic receptor mechanism. Renal baroreceptors sense the decrease in perfusion, which results in the release of renin. The cells of the macula densa sense the chloride concentration of the tubular fluid [79]. In response to high chloride concentrations macula densa cells release ATP, which induces vasoconstriction of the smooth muscle cells of the juxtaglomerular apparatus via purinergic receptors [80]. Reports have suggested that ATP may also be hydrolysed to adenosine before acting on the adenosine A1 receptors expressed on the smooth muscle cells [23]. A1 receptors induce a receptor-mediated inhibition of cAMP activity in renin cells, which is directly linked to regulation of renin gene expression via the CERB on the renin promoter region [81]. In response to low tubular chloride concentrations the macula densa cells have been shown to release prostaglandin E2 (PGE2) [82]. PGE acts via the PGE receptors and binding to the EP2 and EP4 receptors activates adenylyl cyclase which leads in an accumulation of intracellular cAMP, resulting in stimulating renin release [81]. Lastly, renin cells can also release renin in response to stimulation of their β2-receptors by cAMP [83]. Moreover, it has been shown that an increase in the concentration of circulating renin is predominantly due to an increase in renin-expressing cells rather than individual cells releasing more renin [84]. cAMP is a potent regulator of renin transcription, and renin release and the renin gene harbours a cAMP-responsive element which is required for renin expression [85]. Renin secretion is a tightly regulated and complex process. Activation of AT_1 receptors by AngII inhibits renin secretion and forms the AngII-mediated negative feedback loop of the RAS. The AngII inhibitory effect on renin secretion has been demonstrated by using various RAS targeting drugs that inhibit the formation of AngII. Application of these drugs as well as AT_1 receptor targeting drugs was shown to increase circulating renin, suggesting enhanced secretion of renin from JG cells [86].

1.9 The Zebrafish as a Model Organism

The zebrafish (*Danio Rerio*) is a bony (teleost) freshwater fish, native to South Asia. The zebrafish has become an important model for understanding numerous biological pathways and its applications extend well beyond developmental biology. The zebrafish was first established as a model species by George Streisinger [87], however research using the zebrafish for developmental and reproductive studies dates back to the 1930s, when its benefits over mammalian models were recognised [88]. Zebrafish are simpler to maintain and to manipulate compared to mice. Further advantages include that zebrafish pairings can generate many offspring (50-200 eggs) and many studies can be undertaken during the larval stage. The high number of offspring permits large phenotypic and drug screens using fish with the same genetic background. During early development, the zebrafish larvae are optically transparent, and the use of chemical compounds can delay the development of pigment at later stages. Zebrafish have high genetic similarity to humans and 70% of zebrafish genes have a human orthologous gene [89]. This genetic homology and the relative ease of using genetic editing techniques such as zinc finger nucleases, transcription activator-like effector nucleases (TALENs), and the 'clustered regularly interspaced short palindromic repeat' (CRISPR)-Cas9 system in zebrafish, permits the efficient use of this species for the study of gene function. Furthermore, the ability to easily generate transgenic zebrafish lines has permitted cell labelling and cell lineage tracing. Fluorescent zebrafish reporters have genetically incorporated fluorescent markers downstream of a promoter of a gene to be studied. The fluorescent reporter then allows visual tracking of the cells expressing the gene of interest.

Zebrafish transgenic lines are most commonly developed by using the tol2 transposon system. The tol2 transposon system utilises DNA transposons, which are present and make up significant parts of many genomes. Transposons identify, excise, and reinsert DNA that is tagged with inverted terminal repeats. The first active DNA transposon (tol2) was identified in Medaka fish and permitted the characterisation of its mRNA [90]. Its activity was further demonstrated by injecting a non-autonomous element alongside tol2 mRNA into zebrafish eggs, generating a germline transgenic zebrafish [90]. Generation of new transgenic lines still utilises the co-injection of tol2 mRNA alongside a plasmid carrying the desired expression cassette, placed between tol2 inverted terminal repeats [91]. The injection of tol2 mRNA ensures transient expression of the transposase due to mRNA degradation.

Since the discovery of the tol2 transposase, further transposases have been identified and used for the generation of transgenic zebrafish lines. However, the tol2 system remains the most successful tool for generating novel transgenic zebrafish lines. A crucial step for utilising the tol2 system is the cloning strategy used to place the expression cassette between the two inverted tol2 terminal repeats, recognised by the transposase.

Gateway Cloning multisite destination vectors are commercially available and already contain a reporter cassette [92]. The Gateway Cloning system permits DNA fragment transfer between different cloning vectors using a set of recombination sequences. DNA fragments initially are cloned between Gateway att sites to generate a 5'-entry, middle-entry and 3'-entry clone. Each plasmid contains specific recombination sites. The 5'-entry clone commonly carries the promoter region for the gene of interest, whereas the middle-entry clone contains the gene coding for the desired fluorescent reporter protein. Lastly, the 3'-entry clone contains the polyadenylation repeats. Specific enzyme mixes then allow recombination of the 3 plasmids into a destination vector while maintaining the reading frame. Although the gateway cloning method is more expensive than the more commonly used restriction enzyme and ligase-based cloning, it permits for faster and more efficient development of expression clones. Generation of transgenic zebrafish lines often utilises a dominant reporter cassette within the desired expression plasmid to aid in identifying successful transgenic animals visually and for subsequent genotyping. Commonly the reporter cassette constitutes a promoter such as a gamma-crystallin or the cardiac myosin light chain (*cmlc2*) promoter, driving the expression of a fluorescent protein. Both reporters are expressed very early during embryonic development, allowing for more accessible selection of transgenic carriers. Nowadays, the zebrafish is commonly employed for studying the nervous system due to the ability of the zebrafish to regenerate its nervous system. However, a considerable amount of work has been performed on zebrafish for renal studies. There are various advantages in using the species such as the simplicity of the pronephric embryonic kidney, the regenerative mesonephric zebrafish kidney, and the ability to generate fluorescent transgenic zebrafish lines and image the kidney function and cells of interest *in vivo*.

1.10 Transgenic Zebrafish for studying Zebrafish RAS

The ease of generating transgenic zebrafish has allowed the establishment of numerous tissue-specific transgenic zebrafish lines. These have helped our understanding of zebrafish kidney development. The most notable lines, some of which have been used as part of this project, are discussed below.

1.10.1 Tg(*ren*:RFP-LifeAct)

The *ren*:RFP-LifeAct was the first fluorescent transgenic zebrafish line that allowed high-resolution imaging of renin cells in the *in vivo* pronephric, as well as the *ex vivo* mesonephric zebrafish kidney. The transgenic zebrafish line was constructed by cloning a 6.4kb promoter region of the zebrafish renin promoter, containing essential cAMP and RBP-J binding sites [47]. The cloned renin promoter region drives the expression of the red fluorescent protein, RFP-LifeAct. This particular fluorophore binds to intracellular actin filaments, visualising the structure of the renin cells. Additionally, staining with dyes that bind to acidic compartments within cells, confirmed the presence of acidic granules within these cells [49]. The *ren*:RFP-LifeAct transgene also indicated the presence of renin cells at vascular sprouting tips, further suggesting the involvement of renin and renin cells in renal angiogenesis. Moreover, the generation of this transgenic line enabled intercrossing of the tg(*ren*:RFP-LifeAct) zebrafish to other existing lines such as the tg(*acta2*:EGFP) zebrafish to demonstrate the co-expression of the smooth muscle cell marker in zebrafish renin cells, as as reported in mammalian organisms. Lastly, the tg(*ren*:RFP-LifeAct) line visualised that the cells along the efferent arterioles, compared to the cells along the afferent arterioles, are flatter suggesting that, similarly to mammalian organisms the renin cells along the efferent arterioles in the zebrafish are not granulated [49, 93].

1.10.2 Tg(*wt1b*:EGFP)

The Wilms' tumor gene WT1 encodes a zinc finger transcription factor and is a major regulator of mesenchymal progenitors in various organs including the heart, kidney, spleen and gonads [94]. WT1b expression is required for proper kidney development and maintenance of the glomerulus [95]. Dysregulation of the *wt1b* gene is linked to abnormalities in the urogenital tract and a paediatric renal cancer

[96]. Zebrafish have two homologues of the WT1 gene termed *wt1a* and *wt1b* [97]. Despite high sequence homology, studies using morpholinos to knockdown either gene have suggested that the genes exert different roles. Knockdown of *wt1a* induces oedemas in larval zebrafish, whereas knockdown of *wt1b* results in subtle oedema and body curvature [98, 99]. A transgenic zebrafish line was generated using the promoter region for *wt1b* to drive the enhanced green fluorescent protein (EGFP) and studies showed that *wt1b* is strongly expressed during nephrogenesis [97, 99]. Furthermore dysregulation of zebrafish *wt1b* results in the formation of renal cysts which is similar to the wt1 deregulatory effects observed in humans [99]. The transgenic zebrafish recapitulates the expression of *wt1b* during kidney development and presents an powerful tool for studying kidney development and nephrogenesis *in vivo*.

1.10.3 Tg(*flk*:EGFP)

The promoter for the endothelial-specific gene flk-1 has been used to drive expression of fluorescent reporters to visualise endothelial cells in zebrafish. Flk-1 encodes for a protein tyrosine kinase and is first expressed in hemangioblasts, a precursor of endothelial cells, making Flk-1 one of the earliest markers of endothelial cells [100]. The most commonly used reporters are mCherry and EGFP and were chosen with consideration to the downstream application. Transgenic zebrafish expressing a fluorescent endothelial reporter have been used to study the vasculature of the zebrafish but have also been used to investigate the distinction between renin-expressing cells and the endothelium [49, 100].

1.11 Zebrafish Pronephros

The pronephros is the first kidney structure to form across all vertebrates [101]. The pro-nephros lacks blood filtering ability in higher vertebrates, however it is functional as a blood filtration organ in fish and amphibians [102, 103]. The use of fluorescent dextran of different molecular sizes demonstrated that blood filtering activity in the zebrafish pronephros commences from 3dpf and dextran smaller than 10kDa in size are filtered by the glomerulus [104, 105]. The pronephros is a simple structure consisting of two tubules fused at the glomerulus at the midline of the zebrafish (Figure 1.4) [106].

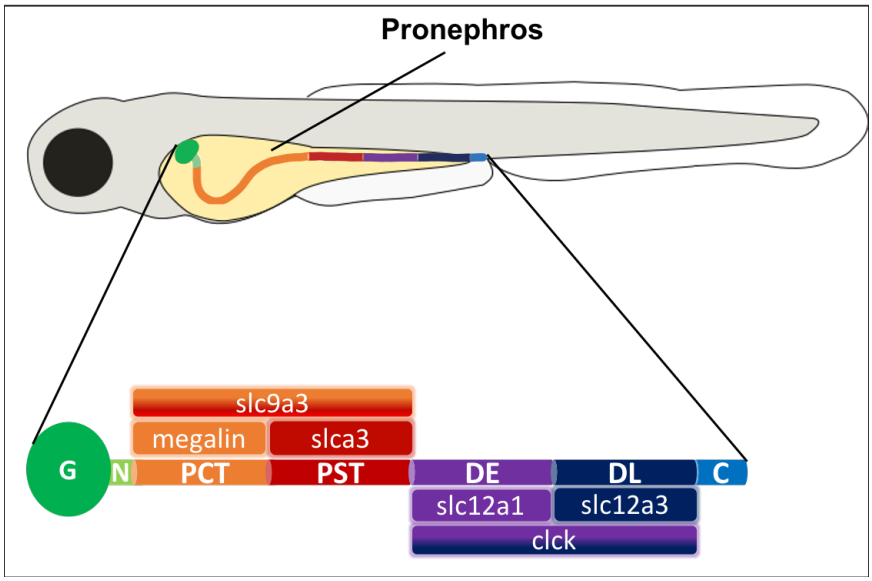

Figure 1.4 | **Zebrafish pronephros** Illustration of a 4dpf straightened zebrafish larvae with the pronephric structure. (G) Glomerulus, (N) Neck, (PCT) Proximal Convoluted Tubule, (PST) Proximal Straight Tubule, (DE) Distal Early, (DL) Distal Late, (C) Cloaca. Specific segments of the pronephric kidney show conservation of mammalian tubular kidney markers.

The zebrafish glomerular anatomy is comparable to that of the human glomerulus, although a significant difference between the mammalian and zebrafish urinary systems is the lack of a bladder in fish. The tubule segmentation is conserved with that of the more complex metanephric mammalian tubule and gene expression patterns within the segments are also conserved [107]. The zebrafish pronephros consists of eight distinct regions, defined by specialised cells destined for the reabsorption of nutrients [107, 108]. In comparison, the mammalian metanephric nephron contains nine distinct regions [109]. A significant difference in tubular segmentation between the mammalian and fish tubule is the lack of the loop of Henle in zebrafish, which in mammals functions predominantly for the reabsorption of water. The pronephric tubule contains a short neck segment expressing rfx2, a marker for ciliated cells [4]. The tubular epithelium of the pronephros is subdivided into two proximal and two distal segments. Similarly to mammals, the proximal segment is defined by the expression of the gene coding for the sodium hydrogen exchanger, slc9a3 [110, 111]. The proximal segment is further subdivided into a proximal convoluted tubule (PCT) and proximal straight tubule (PST), expressing megalin and slc13a3, respectively [108, 112]. In particular, the expression of slc13a3 further suggests the presence of ciliated cells in this part of the tubule [107]. Despite gene

conservation showing many similarities between the simple pronephric tubule and the mammalian metanephros, the latter has developed a highly complex collecting duct system into which the tubules drain. In the pronephros, the excretion system is simplified with the two tubules coming together at the pronephric duct and draining directly into the cloaca.

1.12 Zebrafish Mesonephros

Nephrogenesis proceeds through a series of phases marked by three different kidney structures, each more advanced than the previous. Nephrogenesis commences with the development of the pronephros, the most immature kidney structure, and progresses through a mesonephric structure to the metanephros, the most advanced kidney structure and the final kidney structure persisting as the definitive adult kidney in many vertebrates [113, 114]. The mesonephros in zebrafish develops at around 12dpf, following the thickening and convolution of the pronephric duct, by the formation of a new pair of glomeruli on either side of the pronephric duct [115] (Figure 1.5).

The nephrons fuse to the distal region of the existing pronephros [116]. The mesonephric kidney development was carefully investigated using the tg(*pod*:EGFP) and tg(*cadherin17*:EGFP) transgenic zebrafish [115]. In the trunk region of the zebrafish mesonephros, nephrons contain secondary branching tubules which are comparable to that seen in the metanephric mammalian kidney [71]. The mesonephros is a continually developing organ, maintaining the ability to form new nephrons, contrary to the mammalian metanephros which is a final structure. However, the zebrafish contains approximately 150 nephrons, depending on the size of the fish and new nephrons are formed to replenish damaged ones [115, 117]. The meso-nephros is capable of commencing regeneration within 48 hours following gentamicin-based kidney injury [115]. This fast response to renal damage makes the zebrafish mesonephros an incredibly useful model for studying kidney development and disease without the complexity of the mammalian metanephric kidney.

1.13 Circadian Rhythm of Blood Pressure

The circadian clock evolved for organisms to adapt to the 24 hours cycles of light and dark. The circadian rhythm has been identified to regulate physiological func-

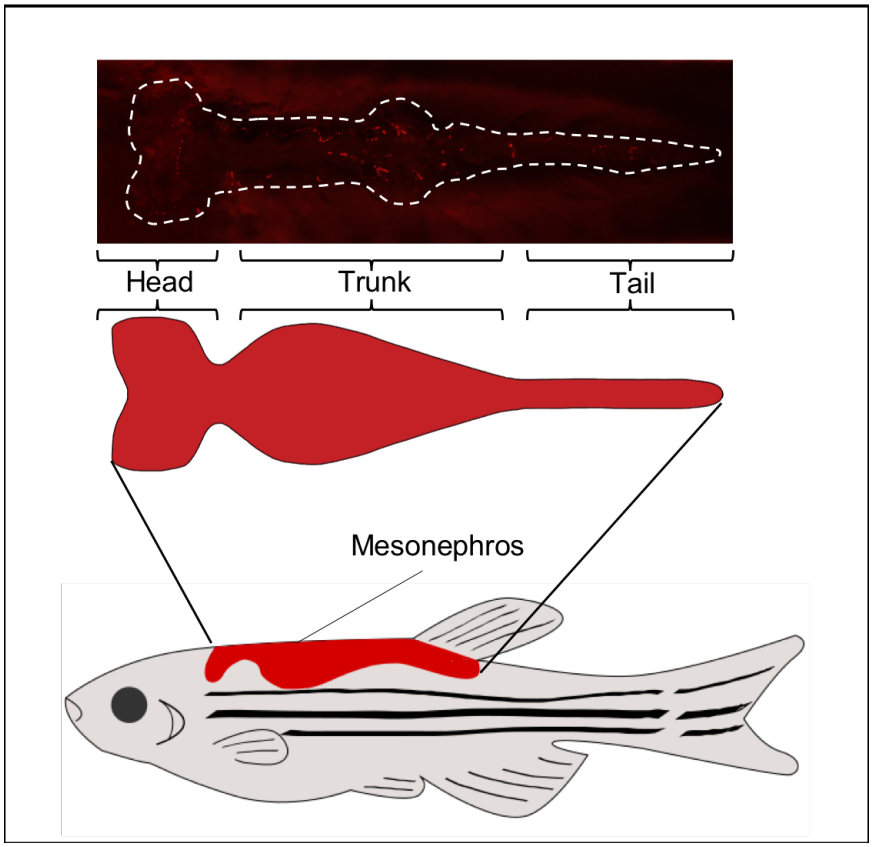

Figure 1.5 | **Zebrafish mesonephros** The mesonephros in the adult zebrafish is located on the distal side against the spine. The Mesonephros is divided into three anatomical different parts; head, trunk and tail. Top panel shows the mesonephros highlighted by dashed white lines of a tg(*ren*:RFP-LifeAct) transgenic zebrafish.

tion in organisms of various complexity, from bacteria to humans. In higher vertebrates, a master regulator is located within the suprachiasmatic nucleus of the brain and oscillates with an approximately 24 hour period even in the absence of external stimuli [118, 119]. However, peripheral circadian clocks are present in most tissues and cell types, regulating cell expression and are synchronised via hormonal and neuronal signals. The circadian clock mechanism is regulated by a series transcriptional, post-transcriptional and translatory feedback loops with a periodicity of approximately 24 hours [120, 121]. The circadian mechanism is governed by transcription factors, which function through a series of feedback loops, driving circadian gene expression of clock regulated genes. The transcription factors BMAL1 and CLOCK comprise the positive feedback loop of the circadian mechanism in mammals. BMAL1 and CLOCK drive the expression of two further transcription

factors, Period (Per) and Cryptochrome (Cry). Per and Cry form the negative feedback loop by antagonising the BMAL1/CLOCK transcriptional activity. This mechanism is predominantly synchronised to the light dark cycle and BMAL/CLOCK are highly expressed during the light cycle, whereas Per and Cry are high during the low light/dark period. The circadian rhythm is crucial for the maintenance of body function and homeostasis. Disruption of circadian rhythms is linked to various inflammatory diseases, cardiovascular diseases and cancer. It is well known that the renin-angiotensin system has a circadian rhythm, which was predominantly assessed by measuring the plasma renin activity at different time points [122, 123]. The study by Gordon et al. investigated patients that were placed on the same diet and identified that the plasma renin activity was higher in the morning than in the afternoon [123]. The study further revealed that the circadian rhythm of renin was unaffected by changes in diet or posture. The circadian rhythmicity of the RAS was further demonstrated by plasma concentration measurements of circulating AngII which revealed that AngII, the main effector of the RAS, exhibits diurnal variation with highest concentrations in the morning and lowest values in the evening [54]. Ultimately, the circadian rhythm of the RAS is linked with the blood pressure (BP) variation. In humans, blood pressure decreases at night, increases strongly in the morning and peaks in the late afternoon. In healthy individuals, BP drops by 10% - 20% at night [124]. However, so-called non-dippers do not experience a minimum decrease of 10% at night. This lack of blood pressure decrease is linked to the activation of the RAS, and ultimately, these individuals are at increased risk of chronic kidney disease [120,121]. Since, the circadian rhythm of the RAS has been identified in various different species, however, not in zebrafish. Homologous gene sequences to the mammalian clock genes have been identified in zebrafish [125]. Furthermore, the molecular mechanisms that govern the circadian rhythm are similar to that in the more extensively studied mammalian systems. Most of the zebrafish clock genes are rhythmically expressed, however, there is a lack studies investigating the circadian clock protein expression in zebrafish *in vivo* and their regulation of tissue specific genes.

1.14 Basic Principles of FRET

Fluorescence Resonance Energy Transfer (FRET) peptides are a novel and excellent tool for studying enzyme kinetics and for the investigation of enzyme kinetics *in vitro* and *in vivo*. FRET peptides are commonly designed to encompass two fluorophores that are separated by a peptide sequence which is recognised and cleaved by an enzyme of interest. Foster first described the resonance mechanism, and it occurs whenever the emission spectrum of the acceptor molecule overlaps with that of the emission molecule [126]. FRET is highly dependent on the distance of the two molecules and distances greater than 10nm are too far for FRET to occur [127]. For FRET probes, it is common to choose a fluorescent acceptor molecule that is quenched by a non-fluorescent emission molecule (Figure 1.6).

A peptide sequence separates the two molecules and, when intact, the probe exhibits internal fluorescent quenching. However, cleavage of the peptide sequence separates the two molecules and liberates the fluorescence property of the acceptor molecule, allowing quantitative and qualitative measurement and assessment of the enzyme activity. A significant advantage of FRET probes is that they have low toxicity [128]. Many peptides and fluorophores are not toxic and, due to the sensitivity of fluorophores, only low concentrations of the FRET probes are required for most applications.

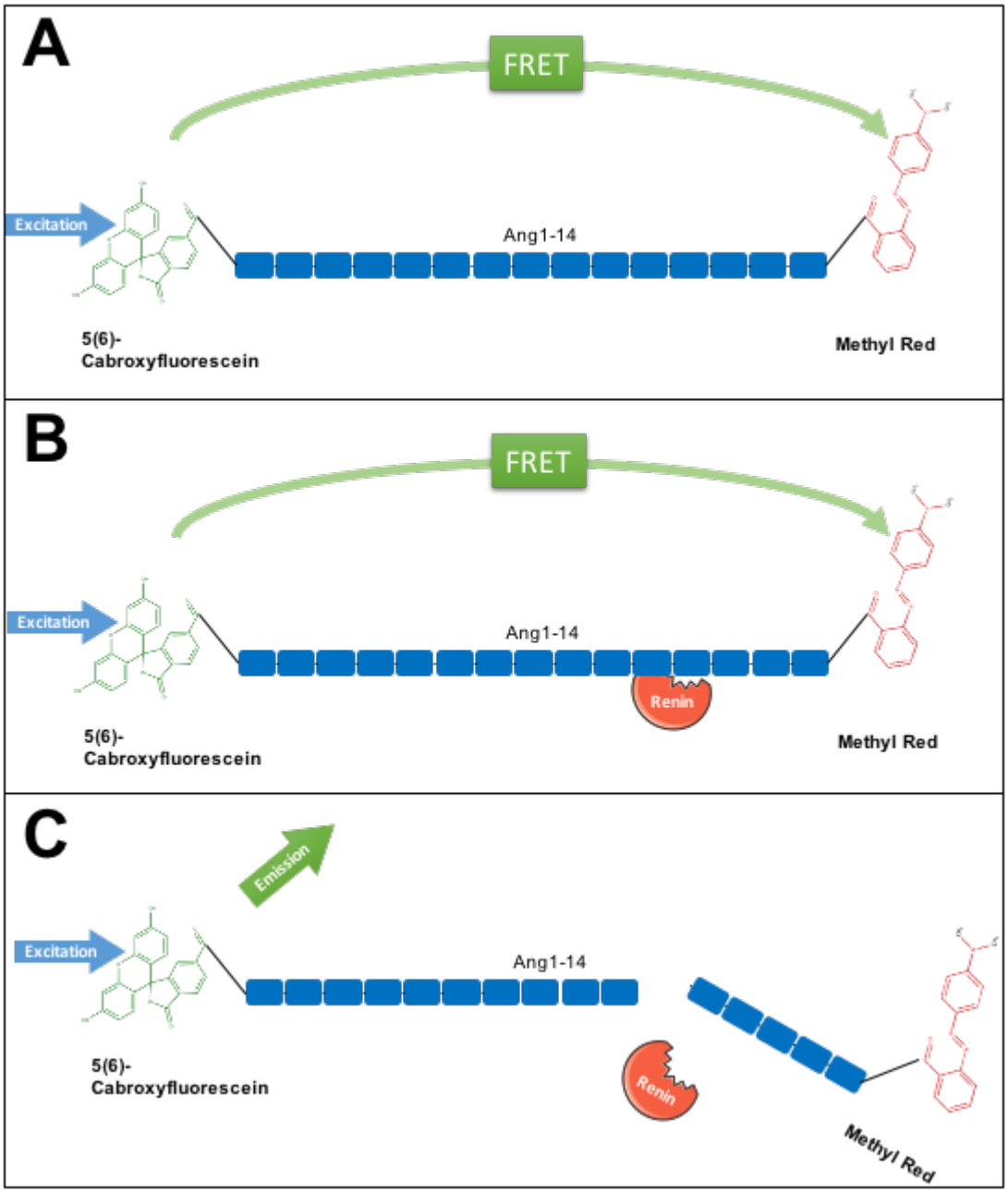

Figure 1.6 | **Schematic representation of the FRET peptide mechanism** A) Methyl red quenches the fluorescence of 5(6)-carboxyfluorescein when the peptide sequence is intact. B) Renin recognises and cleaves the Ang1-14 peptide sequence. C) Cleavage removes the N-terminus and C-terminus interrupting the FRET and restoring the fluorescent property of the 5(6)-carboxyfluorescein.

1.15 Renin FRET Probes

There is limited literature on the use of FRET probes to measure renin activity although FRET probes for mouse, rat and human renins are commercially available. Briefly, FRET probes consist of two fluorophores connected by a peptide sequence from angiotensinogen, which contains the renin cleavage site. In the absence of renin activity, the acceptor molecule on one end of the peptide sequence quenches the fluorophore activity of the fluorescent molecule on the opposing end of the peptide sequence, due to the fluorescent energy transfer between the two molecules. Cleavage by renin separates the two molecules and the inter-molecule distance becomes too great for FRET to occur and thus preventing quenching. This fluorescence-based technique is, in principle, an excellent alternative to the previously commonly-used radioimmuno method of assaying renin as it directly measures renin activity rather than measuring angiotensinogen conversion to AngI by renin. Noteworthy is the work conducted by Peter-Peterdi, which uses a commercially available FRET probe to measure and image renin release *in vitro* [129]. The FRET probe uses a 10 amino acid angiotensinogen sequence containing the renin cleavage site with the EDANS fluorophore, which is quenched by DABCYL when the peptide sequence is intact in the absence of renin. Renin release was stimulated by administration of isoproterenol, a β-adrenoreceptor stimulant, and an increase in EDANS fluorescence was observed. Other attempts to use the renin FRET probe have been for renin quantification in the plasma of rats and humans [130]. The problem with peptide based FRET probes is that the amino acid sequence is often recognised and cleaved by proteolytic enzymes such as trypsin and proteinase K. Dissection of arterioles reduces the background activity of the FRET by protecting it from cleavage through other enzymes however, there are no publications of using FRET probes *in vivo*. Common strategies to reduce the background of FRET probes is to remove single amino acids in the FRET probe peptide sequence without affecting the enzyme of interest. Due to the translucent nature of larval zebrafish, there is potential scope for imaging renin release *in vivo* in larval zebrafish.

1.16 Solid Phase Peptide Synthesis

Solid-phase peptide synthesis (SPPS) is the most commonly used strategy to build short peptides synthetically [131, 132]. Most biological regulatory processes are dependent on peptides and proteins deriving from α-amino acids, and hence there was a need to develop a simple lab-based technique to produce pure peptides. Amino acids are organic compounds that contain two key functional groups, a carboxylic acid (–COOH) and an amine (–NH2) and SPPS is a step-by-step construction of a peptide built on a solid support (Figure 1.7).

Although peptide synthesis in solution is possible, it requires lengthy recovery and purification of the product after every addition of a new amino acid [131]. The solid support in SPPS permits wash out of unreacted reagents without loss of the actual product. SPPS depends on the covalent attachment of a protected amino acid to a solid support and uses either a Boc (tert-butyloxycarbonyl) or Fmoc (9-fluorenylmethoxycarbony) strategy as the protection group for the reactive amino group of the amino acid. The two strategies differ mainly in the deprotection conditions. Fmoc is a more refined and requires moderate bases for deprotection compared to the acid-liable Boc protecting group. In a first step, a Fmoc protected amino acid is covalently bound to a solid support. Removal of the Fmoc protecting group permits a further Fmoc protected amino acid to react only with its carboxylic acid group to the free amine group of the covalently bound amino acid, preventing side reactions. Amino acids with side protecting groups have these deprotected during the final cleavage step of removing the final peptide from the solid support.

1.17 VAST Imaging System

Zebrafish is an ideal model for various diseases. Their *in vitro* development, translucent nature and small size allow for using microscopy to investigate organ and tissue function at high spatial resolution. A significant drawback of using microscopy systems is the time-consuming nature of mounting single fish in a correct orientation for reproducible images while minimising damage to permit recovery and re-imaging of the same fish [133]. First attempts at developing an automated zebrafish imaging system used simple capillary tubes and a fluidics system, which allowed the loading of larval zebrafish into a glass capillary, which was mounted under a microscope and was attached to rotary segments for proper orientation of

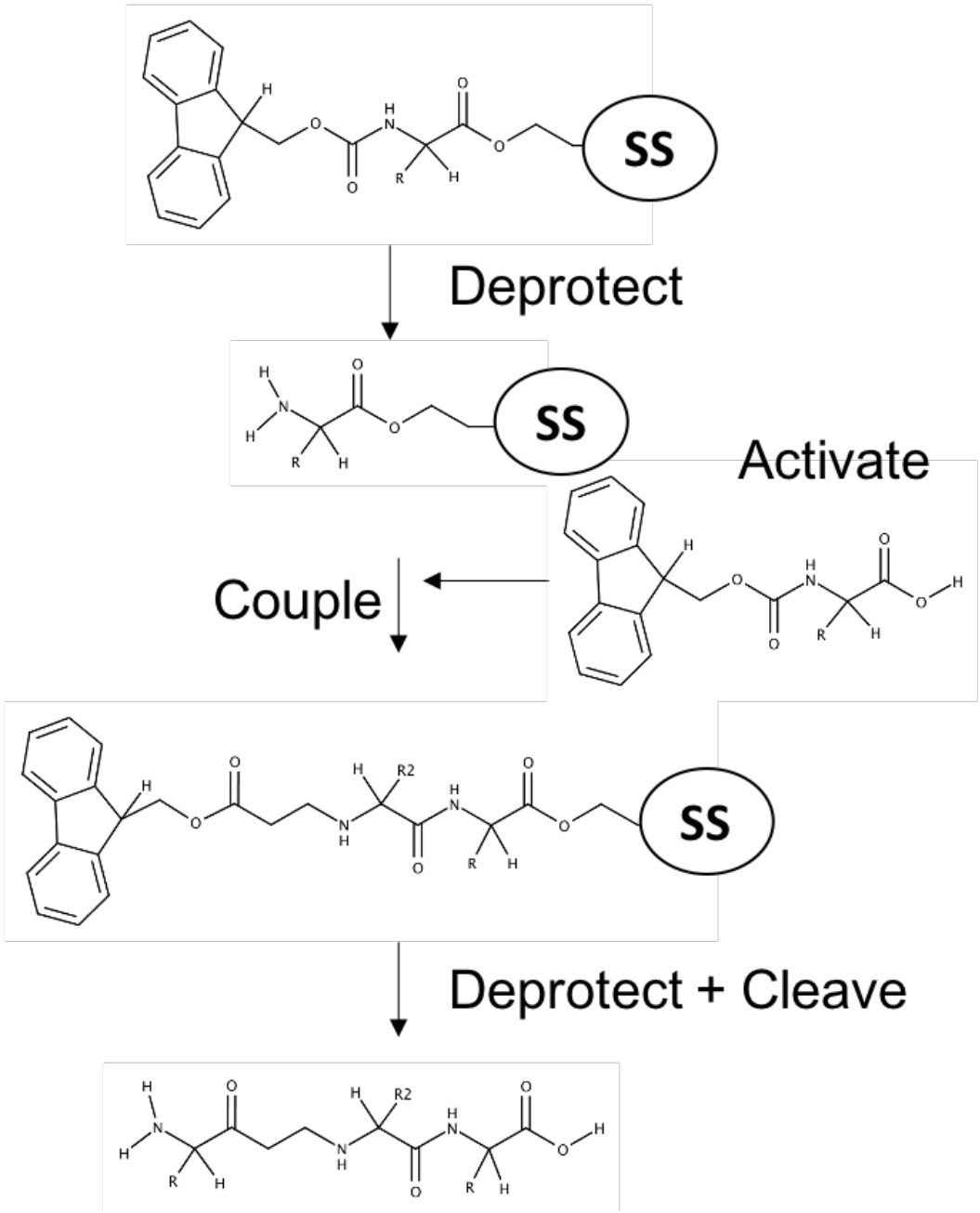

Figure 1.7 | **Fmoc-Chemistry for peptide synthesis** An Fmoc protected amino acid is coupled onto a solid support (SS). Deprotection removes the Fmoc protecting group, exposing an amino reactive group which can be coupled with an activated, further Fmoc protected amino acid. The Fmoc protection ensures that only the carboxyl group can react with the amine group of the deprotected amino acid. Cleavage of the final peptide from the solid support results in complete deprotection.

the fish [134, 135]. This system was further developed into the Vertebrate Automated Screening Technology (VAST) system. The VAST system contains a Large Particle sampler (LP sampler) which gently aspirates larvae from multi-well plates, transporting these to a rotary glass capillary (Figure 1.8).

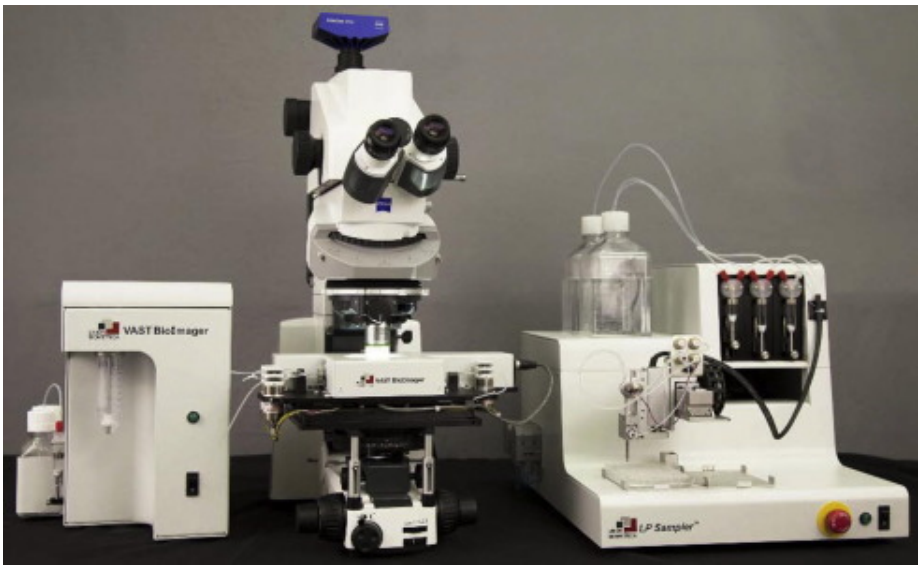

Figure 1.8 | **Vertebrate Automated Screening Technology (VAST) system** Photo of the VAST system linked to the Large Particle (LP) sampler. The LP sampler is connected to the VAST by plastic capillary tubing. Pumps operate the LP sampler, enabling suction of fish into the plastic tubing. Fish are transported to the microscope where a rotatable glass capillary is mounted. The fish is arrested in the glass capillary and a live image permits correct orientation of the fish. After imaging the fish is returned to the LP sampler and with fresh medium placed in the same well on a new multi-well plate. Image taken from Pulak *et al.* [135].

The glass capillary is held in place between two rotating components, capable of rotating the fish by 360°. Installed software recognises the fish entering the capillary and can orientate the fish with highly reproducible accuracy every time. The LP sampler system is then able to return the fish to a separate multi-well plate into the equivalent well, thereby retaining the identity of the fish for future imaging. This automation and handling of larvae permit for high-throughput phenotypic screening and generation of large dataset images. It also minimises the number of fish lost, and the potential damage caused to the fish by manual manipulation of fish orientation.

1.18 Bioluminescent Reporters

Bioluminescence and fluorescence differ in that fluorescence is a type of light stemming from a fluorophore, which is a molecule that is excited by the energy from an external light source. In an excited state, the fluorophore releases energy in the form of light at a different wavelength to the excitation wavelength. Contrary, bioluminescence is not dependent on an external light source and requires excitation from an enzymatic reaction. Both bioluminescence and fluorescence are commonly used in scientific research and their different properties have advantages and disadvantages. Bioluminescence is known to have a highly sensitive detection capacity, and the lack of an external light source eliminates autofluorescence during imaging. The light produced from the bioluminescent reaction is very faint and hence it is not suitable for high-resolution imaging, however higher sensitivity cameras have recently been developed enabling high-resolution bioluminescence microscopy. Luciferase has no post-translational modification and is well-suited as a real-time reporter for gene expression analysis. For the bioluminescent reaction to occur two agents are required: the enzyme luciferase and its substrate luciferin. The oxidative decarboxylation of the luciferin in the presence of oxygen yields energy in form of light which can be measured and imaged (Figure 1.9).

Depending on the luciferase enzyme used, different wavelengths of light and length of light emission can be achieved. When luciferase is expressed its activity can be assayed by addition of the substrate and measuring its light-producing activity using a plate reader or a highly sensitive CCD camera capable of detecting photons. The photon signal can then be superimposed onto a brightfield image in order to localise the source of the signal. Addition of the luciferin can be performed by injection into the fish or addition to the water. Luciferase-based imaging has been widely used in mice for monitoring cell expression and migration [136]. Although less common, the luciferase system has also been used to study various systems in the zebrafish [137, 138, 139, 140, 141]. However, previous zebrafish luciferase work was predominately focused on larval zebrafish, such as the study by Chen *et al.* used bioluminescent imaging systems to investigate heart regeneration in adult zebrafish [140]. There are currently no reports of the luciferase system being used to investigate renal function in zebrafish.

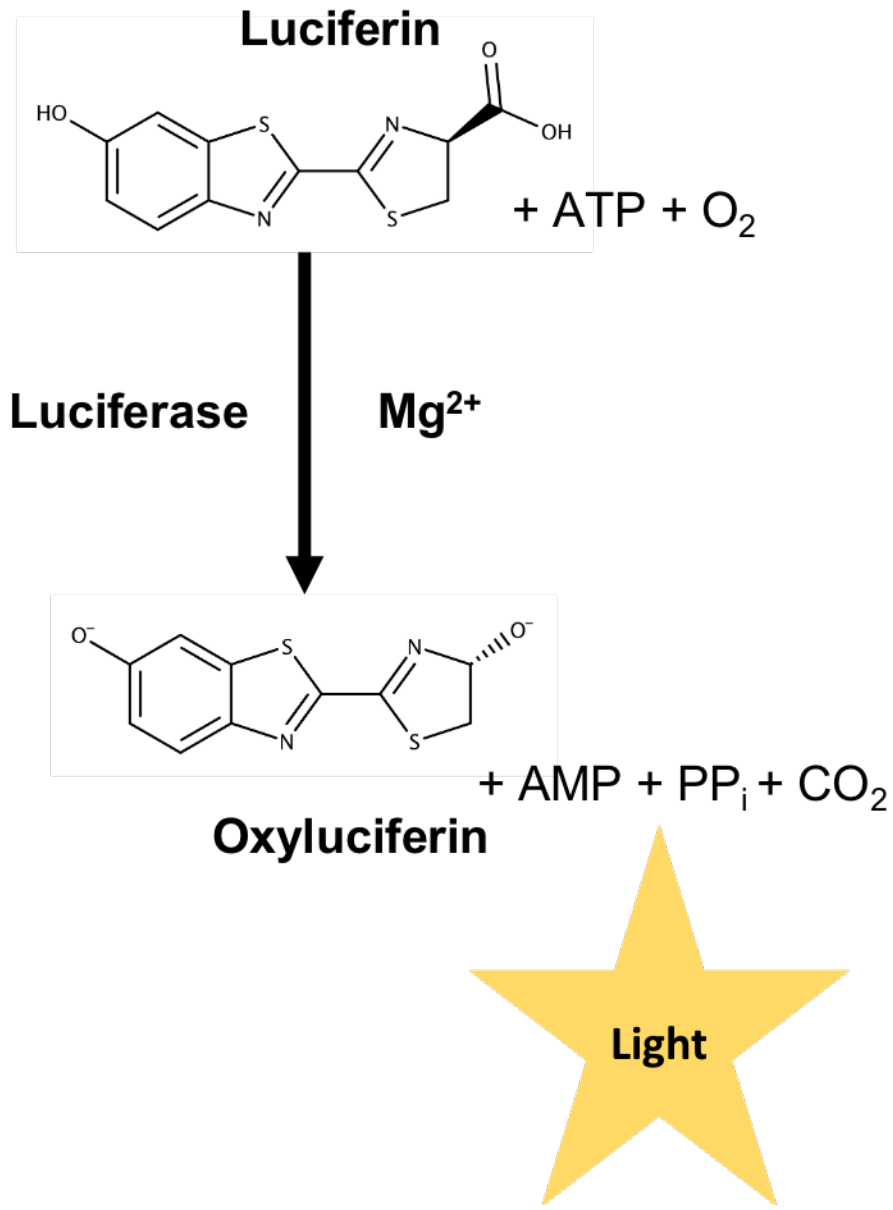

Figure 1.9 | **Bioluminescent reaction** Bioluminescent reaction catalysed by firefly luciferase breakdown of luciferin, producing oxyluciferin and light.

1.19 Aims

Although the zebrafish is a highly valuable model for investigating renin and the RAS, many questions remain unanswered, in particular the role of renin in the zebrafish. Previous studies have demonstrated the spatial expression of renin in the pronephric and mesonephric zebrafish kidneys. However, there is a lack of understanding of the temporal renin gene expression and the renin protein activity in zebrafish due to a lack of tools to permit investigation of these.

I aim to develop a novel bioluminescent renin reporter zebrafish in order to establish a real-time reporter of renin transcription. I hypothesise that the bioluminescent reporter luciferase will faithfully report for renin gene expression within the zebrafish. This novel renin reporter will be validated by a plate-based assay for the quantitative measurement of renin expression as well as bioluminescent microscopy to validate *bona fide* expression of the bioluminescent signal. Current zebrafish renin reporters allow to investigate the spatial distribution of renin expressing cells however, investigating renin gene expression is limited to time consuming assessment of mRNA concentration. Furthermore, the small number of renin expressing cells during early development requires multiple larval fish in order to have high enough mRNA concentration for accurate quantification. A bioluminescent reporter is expected to overcome these limitations due to highly sensitive nature of the bioluminescent assay.

Furthermore, I will identify and synthesise the zebrafish AngI and AngII peptides by SPPS. In collaboration with Attoquant Diagnostics, a mass spectrometry assay will be developed to accurately measure the concentrations of AngI and AngII in adult zebrafish serum and kidney from fish treated with the ACE inhibitor Captopril, and compare it to untreated controls. This will allow to observe a dynamic change in the concentrations of AngI and AngII and demonstrate the effectiveness of Captopril in zebrafish. I will also design a novel zebrafish renin FRET probe using SPPS. I hypothesise that the renin FRET probe will permit accurate measurements of renin activity in zebrafish. There is a lack of antibodies that permit the quantification and visualisation of zebrafish renin. By synthesising the 14-amino acid sequence renin recognises and cleaves, and attaching a fluorophore and quencher to the N- and C- terminal ends of the peptide, the probe will be fluorescently inactive. When zebrafish renin cleaves the probe the fluorescent signal will be recovered and renin activity will be quantifiable. Probe activity will be validated and compared in *mib*$^{-/-}$ and *ren*$^{-/-}$ zebrafish, both lacking active renin

and compared to *mib*$^{+/+}$ and *ren*$^{+/+}$ zebrafish. Moreover, assays will be designed to show an increase of renin activity throughout zebrafish development, indicative of the specificity of the FRET probe.

In order to measure renin enzyme kinetics, recombinant zebrafish renin will be generated in cell based protein expression systems and purified. Western blot analysis and using the FRET probe designed in this thesis, the protein activity will be validated.

During this thesis, the first *ren*$^{-/-}$ zebrafish was generated by CrispRCas9 gene editing. I will use various methods to characterise the *ren*$^{-/-}$ zebrafish line. Histological examination of the adult zebrafish kidney will reveal changes to the kidney morphology. I will also use the VAST system to identify any changes in zebrafish development due to the absence of active renin. I hypothesise that renin is crucial for development, and zebrafish lacking renin will have severe vascular and renal defects. The fish will be exposed to low salt water concentrations to investigate their ability of salt handling in the absence of a functional RAS. I will also use high resolution microscopy imaging on the *ren*$^{-/-}$ zebrafish crossed to existing transgenic zebrafish lines to visualise the cellular changes to renin-expressing cells and possible changes to the pronephric and mesonephric renal vasculature. I hypothesise that the lack of renin will dramatically

Lastly, the crossing of *ren*$^{-/-}$ to the tg(*ren*:RFP-LifeAct) and tg(*acta2*:EGFP) and the development of a FAC sorting protocol has permitted the recovery of *ren*- and *acta2*-expressing cells from *ren*$^{-/-}$ zebrafish kidneys. This permitted further quantification of the number of *ren*- and *acta2*-expressing cells in the metanephros of *ren*$^{-/-}$ and *ren*$^{+/+}$ zebrafish.

This thesis and the tools that will be developed throughout this research will further the understanding and permit future studies using the zebrafish as a model organism for studying renin and the RAS.

Chapter 2

Materials & Methods

2.1 Standard Solutions

A list of standard solutions and their recipes can be found in Table 2.1.

Medium Type	Recipe
1×PBS	10 tablets, 1l ddH_2O
0.5M EDTA	93.05 g EDTA in 500 ml H_2O, pH 8
50×TAE	242 g Tris-base in 700 ml, 57.1 ml acetic acid, 100 ml 0.5 M EDTA
1M Tris	121.14 g Tris base and adjusted to pH 8 using concentrated HCl
4% PFA	4% w/v paraformaldehyde in PBS and used 1M NaOH used to adjust to pH 7.2
Conditioned Water (CW)	6 mg/l marine salts, pH 7.4
1/20 CW	3 mg/l marine salts, pH 7.4
E3 Medium	34.8 g NaCl, 1.6 g KCl, 5.8 g $CaCl_2 \cdot 2\,H_2O$, 9.78 g $MgCl_2 \cdot 6\,H_2O$
10×TBS	24.2 g TRIS Base, 80 g NaCl, pH 7.6
1×TBST	50 ml 10x TBS, 450 ml H_2O 500 µl Tween 20
1×TBST + Milk	5 g Semi skimmed dried milk, 100 ml 1×TBST

Table 2.1 | **Reagent recipes** Table containing names and recipes of all reagents used.

2.2 Zebrafish Procedures

2.2.1 Zebrafish Husbandry

Experiments were approved by the local ethics committee and conducted in accordance with the Animals (Scientific Procedures) Act 1986 in a United Kingdom Home Office-approved establishment. All zebrafish home office regulated work was conducted under the Home office project licence 70/8886 and carried out by myself, unless stated otherwise. Zebrafish were maintained in aquarium system water at a constant water temperature of 28.5 °C on a 14 hour light/10 hour dark cycle.

2.2.2 Zebrafish Pair Mating

Zebrafish pair mating was performed in breeding tanks consisting of a 500 ml main tank containing an insert with small gaps, through which eggs can fall through to prevent the fish from eating them. A male and female fish are placed in the breeding tank in the evening and usually breed first thing in the morning. For time sensitive breeding and to allow control over the egg age, a plastic insert can be added keeping the male and female apart and is removed in the morning. Eggs were collected mid-day by pouring contents of the tank through a sieve. Eggs were washed with system water, mixed with methylene blue to prevent fungal growth and kept in an incubator at 28.5 °C

2.2.3 Zebrafish Breeding by Marbling

For large fish egg numbers, marble boxes were placed directly into the fish tanks. The marble boxes consist of two boxes placed within each other. The internal tank contains a mesh bottom allowing for the eggs to fall through into the external tank to prevent the fish from eating them. The internal tank contains several marbles to encourage fish breeding. The marble box was placed in the fish tank in the late afternoon for fish to breed the subsequent morning. Eggs were collected as described in Section 2.2.2.

2.2.4 Schedule 1

Fish were sacrificed by overdose of anaesthetic. Adult fish were placed in Tricaine solution (MS–222, 4 mg/ml) until cessation of gill movement was observed and there was no reaction to touch. Destruction of the brain was used as the secondary method for the confirmation of death

2.2.5 N-phenylthiourea

N-phenylthiourea (PTU(Sigma Aldrich, P7629)) was used to inhibit the zebrafish from developing pigment. Especially for visualising cells along the anterior mesenteric artery it is essential that the fish are PTU treated. At 4dpf and 5dpf the pigmentation prohibits the anterior mesenteric artery from being imaged accurately. A non toxic option would be to breed the fish on a nacre or casper background, however these are difficult to breed and have been avoided throughout this project. 3 mg/ml PTU was dissolved in Hank's Balanced salt solution by heating the mix to 65 °C. The stock solution was kept for 1 month at 28.5 °C to avoid re-crystallisation and precipitation. PTU was added to the petri dishes for a final concentration of 0.003% w/v. PTU was added approximately 6 hours post fertilisation (hpf) on the same day of egg collection. PTU was changed with water everyday and left in the petri-dishes with the eggs until imaging. Due to the toxic developmental effects of PTU, all treated fish were terminated at 5dpf.

2.2.6 Zebrafish Strains

WIK was the only strain of wild-type zebrafish used in this project and was maintained by the BVS Aquatics Unit housed in the multi-centred Queen's Medical Research Institute in Edinburgh. Transgenic zebrafish used in this study which have not been generated as part of this project have been outlined in Table 2.2.

Strain	Origin	Reference
ren:RFP-LifeAct	Dr Sebastien Rider	Rider *et al.* [47]
acta2:EGFP	Prof. Didier Stainier	Whitesell *et al.* [142]
wt1b:EGFP	BVS Facility	Perner *et al.* [143]
flk:mCherry	BVS Facility	Choi *et al.* [100]
WIK	BVS Facility	Rauch *et al.* [144]

Table 2.2 | **Table listing zebrafish lines used** Origin and reference of the zebrafish lines used throughout this thesis. All transgenic fish are on a WIK background.

2.2.7 Dechorionating Zebrafish Embryos

Chorions were removed at 24hpf using two forceps. Using forceps the chorion was held in place whilst using the an additional pair of forceps to tear the chorion open. The embryo is gently pushed through the opening. Any damaged embryos were discarded.

2.2.8 Zebrafish Anaesthesia

Zebrafish were placed under short-term anaesthesia for fin clipping and imaging purposes. Anaesthetic comprised of 0.04 mg/L tricane diluted aquarium system water.

2.2.9 Genotyping Fin Clip DNA Extraction

Zebrafish were genotyped from caudal fin clips of on fish aged 23dpf or adults (>3 months old). Clipped fins were placed directly in eppendorf tubes containing 200 µl 50mM NaOH and kept on ice until DNA extraction or stored in the freezer at $-20\,^{\circ}$C. Crude DNA extraction was performed by heating the samples in NaOH to $95\,^{\circ}$C in a heat block for 10 minutes with occasional shaking of the tubes to disrupt the tissue. Samples were subsequently cooled to $4\,^{\circ}$C by placing them on ice and adding 1/10th of the original NaOH volume of 1M Tris (pH=8) to neutralise the NaOH. Samples were spun at maximum speed in a centrifuge to pellet the debris.

Supernatant was transferred to a fresh 1.5 ml eppendorf tube and diluted 1:10 for subsequent PCR reactions.

2.2.10 Genotyping PCR Reaction

DNA was extracted as described in Section 2.2.9. For the genotyping PCR Q5 High-Fidelity DNA polymerase (NEB, M0491) was used. The protocol was adapted to minimise the use of the polymerase for one reaction. 3 µl of Q5 buffer was added, 0.3 µl of 10mM dNTP mix, 0.75 µl of forward and reverse primer at a concentration of 10 µM was added respectively. Lastly, 0.075 µl of Q5 polymerase was added resulting in 14.5 µl of reaction volume per tube. 0.5 µl of the fin clip DNA were added and the PCR was run in a thermocycler (Applied Biosciences, Veriti 96-well) on the program (Table 2.3).

Temperature	**Time**	**Cycles**
98 °C	3 seconds	1×
98 °C	5 seconds	30×
68 °C	15 seconds	
72 °C	20 seconds	
72 °C	7 minutes	1×
4 °C	2 minutes	∞

Table 2.3 | **PCR temperature and cycles for genotyping zebrafish** Genotyping of zebrafish with DNA extracted from fin clips.

2.3 Plasmid Generation

2.3.1 Restriction Enzyme Digest

All restriction enzyme digests were performed using restriction enzymes supplied by NewEngland Biolabs. 1 µg of DNA and for the restriction enzyme appropriate 10× buffer were combined and diluted to 19.5 µl using water. 0.5 µl of the restriction enzyme was added to the mixture. The mixture was left at 37 °C for 2 hours

Gene	Direction (5' - 3')	Sequence	Product Size (Bp)
Luciferase	F	AGGTGGACATCACTTACGCT	472
	R	GGCAGACCAGTAGATCCAGA	
GFP	F	GTTAGCGGCTGAAGCACTGC	346
	R	CGAACAGAAACACTGCAGAC	
Renin	F	TCCCCTTCTTGCTCCAAACCTG	467
	R	ACATCTGAGCTGGTGAACCAATGC	

Table 2.4 | ***ren*:LUC genotyping primers** Table containing genotyping primer sequences and their amplicon product size.

before placing on ice. The resulting DNA products were analysed by DNA gel electrophoresis (Section 2.3.2).

2.3.2 Agarose Gel Electrophoresis

For DNA product size determination or investigation of RNA quality an agarose electrophoresis gel was used. The gel constituted of 0.8% agarose, and gel red to stain nucleic acid. Unless stated otherwise the the agarose was dissolved in $1\times$TAE buffer. Gel was run in electrophoresis tanks at 80 V for 1.5 hours.

2.3.3 Vector Amplification

All vectors used in this project were amplified using One Shot^{TM} TOP10 Chemically Competent E. Coli (Invitrogen^{TM}). E. Coli were grown on luria broth (LB) plates containing an antibiotic for selection, dependent on the plasmids antibiotic resistance. Glycerol stocks of all vectors were kept in 5% glycerol at $-80\,^{\circ}$C.

2.3.4 Plasmid and PCR Sequencing

DNA sequencing was performed by DNA Sequencing & Services (MRC I PPU, School of Life Sciences, University of Dundee, Scotland, www.dnaseq.co.uk) using

Applied Biosystems Big-Dye Ver 3.1 chemistry on an Applied Biosystems model 3730 automated capillary DNA sequencer.

2.3.5 Gateway Cloning

All transgenic fish were injected with plasmids generated via the gateway cloning method [91]. Plasmids not generated in house were obtained from sources detailed in Table 2.5.

Plasmid	Origin
p5E-6.4kb-renin	Dr Sebastien Rider
p5E-Luciferase	Dr Calum A. MacRae
p5E-LuciferaseNoStop	Dr Calum A. MacRae
p3E-2A-mcherryp2A	Addgene
p3E-polyA	Addgene
pDestTol2CG2	Addgene
pDestTol2pACryCFP	Addgene
pCS2FA-transposase	Addgene

Table 2.5 | **List of Plasmids** List of entry clones and destination vectors used to build expression vectors.

2.3.6 Generation of *ren*:LUC

The plasmid to create the tg(*ren*:LUC) zebrafish was generated using the following 3 entry clones and destination vector:

- 5' entry clone: p5E-6.4kb-renin
- Middle entry clone: p5E-Luciferase
- 3' entry clone: p3E-polyA
- Destination vector: pDestTol2CG2

All entry clones and the destination vector were validated by restriction digest (Section 2.3.1). In a 1.5 ml eppendorf tube all entry clones (20 fmol) were combined with the destination vector (20 fmol) and TE buffer (4 µl). Gateway™LR Clonase™II Enzyme Mix was thawed on ice and added to the mixture (2 µl). The reaction was incubated at 25 °C for 26 hours. The reaction was stopped by addition of proteinase K (2 µg and incubation at 37 °C for 10 minutes. The reaction was then transformed into Top 10 One Shot E. Coli cells and amplified as described in Section 2.3.3 and verified by DNA sequencing and extensive restriction digest and DNA electrophoresis.

2.3.7 Generation of *ren*:LUC-2A-mCherry

The plasmid to create the tg(*ren*:LUC-2A-mCherry) zebrafish was generated the following 3 entry clones and destination vector:

- 5'-entry clone: p5E-6.4kb-renin
- Middle entry clone: p5E-LuciferaseNoStop
- 3'-entry clone: p3E-2A-mcherryp2A
- Destination vector: pDestTol2pACryCFP

The 'p5E-LuciferaseNoStop' plasmid was generated by TOPO cloning and removing the stop codon from the previous p5E-Luciferase clone using the PCR product using the primers outlined in Table 2.6. All entry clones and the destination vector were validated by restriction digest (Section 2.3.1). In a 1.5 ml eppendorf tube all entry clones (20 fmol) were combined with the destination vector (20 fmol) and TE buffer (4 µl). Gateway™LR Clonase™II Enzyme Mix was thawed on ice and added to the mixture (2 µl). The reaction was incubated at 25 °C for 26 hours. The reaction was stopped by addition of proteinase K (2 µg and incubation at 37 °C for 10 minutes. The reaction was then transformed into Top 10 One Shot E. Coli cells and amplified as described in Section 2.3.3 and verified by DNA sequencing and extensive restriction digest and DNA electrophoresis.

Target Gene	Direction (5' - 3')	Sequence	Product Size (Bp)
Luciferase No Stop	F	ATGGAAGACGCCAAAAA	472
	R	ACACGGCATCTTTCCG	

Table 2.6 | **Luciferase no stop cloning primers** Primers used for the generation of the luciferase gene cassette without the stop codon.

2.3.8 Transposase

Tol2 transposase mRNA for co-injection with the transgenic plasmid DNA was generated from the PCS2FA-transposase plasmid. The vector containing an ampicillin resistance cassette was amplified by the vector amplification method in Section 2.3.3. The plasmid PCS2FA-transposase was digested with NotI and purified by phenol:chloroform extraction and ethanol precipitation. DNA was extracted and processed into mRNA using the Invitrogen™ mMESSAGE mMACHINE™ SP6 Transcription Kit (Invitrogen™ AM1340). The synthesised mRNA was purified with the RNA purification kit (Qiagen, 70042). The RNA precipitate was suspended in distilled water and frozen at $-80\,^{\circ}$C.

2.3.9 Prorenin-Psec2C

For the expression of recombinant renin, the Gibco ExpiCHO Expression System (ThermoFisher™, A29133) was used. The pSecTag2c mammalian expression vector was used as a receiving vector of the renin gene cassette. The vector contains a large cloning site. Upstream of the cloning site, the vector contains a cytomegalovirus (CMV) promoter for high-level constitutive expression. Downstream of the cloning site is a sequence coding for the c-terminal polyhistidine ($6\times$His) tag for rapid purification with nickel-chelating resin and detection with an Anti-His (C-terminal) antibody. The prorenin coding sequence (Appendix A) was synthesised by DC BIOSCIENCES Ltd. with a 5' EcoRI and C-terminal TEV protease site followed by a 3' XhoI restriction site. The TEV protease side enabled removal of the $6\times$His tag if it were to interfere with the protein activity. The EcoRI and XhoI restriction sites permit cloning by restriction digest while maintaining the reading frame. The carrier vector of the renin coding sequence, as well as the

pSecTag2c vector were digested using a double restriction enzyme digestion with the restriction enzymes EcoRI and XhoI. The DNA fragments were separated by DNA gel electrophoresis and extracted from the agarose gel. DNA was recovered from the gel using the Macherey-Nagel™ NucleoSpin™ Gel and PCR Clean-up Kit (Macherey-Nagel, 12303368). Ligation of the the renin coding sequence into the pSecTag2c expression vector was performed using a 1:3 expression vector (50 ng) to renin coding sequence ratio (35 ng) and combining this with the Quickligase (Quick Ligation™ Kit, NEB, M2200S). The mixture was left at 24 °C for 1 hour. After ligation the resulting plasmid was transformed and amplified. Restriction digest analysis with subsequent DNA electrophoresis confirmed successful ligation and maintenance of the reading frame was validated by DNA sequencing.

2.3.10 Renin-Psec2c

The renin-Psec2c plasmid was generated as described in Section 2.3.9. The prorenin coding sequence (Appendix B) was synthesised by DC BIOSCIENCES Ltd. with a 5' EcoRI and C-terminal TEV protease site followed by a 3' XhoI restriction site. The EcoRI and XhoI restriction sites permit cloning by restriction digest while maintaining the reading frame.

2.3.11 Injection Needles

Injection needles were pulled from filament-less glass capillaries (TW100-4, World Precision Instruments (WPI), Sarasota FL, USA) using a Micropipette puller (P-97, Sutter Instrument, Novato CA, USA). The needles were pulled using the following settings: heat 450, pull 85, velocity 55 and time 150. The needles were loaded using Eppendorf™ Microloader™ Pipette Tips (Eppendorf™, 5242956003) and mounted onto a (YS-PV820 Pneumatic PicoPump). The needles were broken using fine forceps closest to the sealed end. Once it was possible to eject liquid from the needle, a calibration injection into mineral oil placed over a graticule was performed allowing the measurement of the diameter of the liquid sphere from which the injection volume could be calculated. The micro manipulator was adjusted to reach an injection volume of 5 nl.

2.3.12 Plasmid Injection

Plasmids were injected into WIK derived eggs unless stated otherwise. WIK eggs were collected using the mass egg production system (MEPS) which was set up in the morning to ensure control over the stage of egg development. For the injection the eggs were required to be collected and injected at the one cell stage to ensure the transgene to be present in all subsequent cells. Injection needles were loaded with 3 µl of 1:1 linearised plasmid DNA (50 ng/ml) and transposase mRNA (50 ng/ml) by using Eppendorf™ Microloader™ Pipette Tips (Eppendorf™, 5242956003). Collected MEPS eggs were placed onto 2% agarose with grooves and water was extracted for the duration of the injections. Once injected, the eggs were transferred into a petri dish and left in the incubator at 28.5 °C. Approximately 6 hours after the injections, the dishes were cleaned and dead eggs and debris were removed.

2.4 *In Vivo* Luciferase Assay

Injected fish eggs were kept at 28.5 °C in for 4 days before being tested for luciferase expression. Fish were washed using embryonic media (E3) twice before transferring single fish into a black 96-well plate. For accurate and even water distribution between wells, the pipette tip was cut off and the fish were placed into the wells with E3 media. A stock solution of luciferin was prepared in E3 (100mM) and added directly into the wells for a final concentration of 10mM. The plate was kept in the dark and left for 5 minutes in order for the fish to take up the luciferin. The plate was placed in a preheated (28.5 °C) bioluminescence plate reader (Victor 3X). Each well was read for 30 seconds in order to maximise light detection.

2.5 Ribonucleic Acid Extraction

1 metal bead was placed into a 2 ml eppendorf tube containing the tissue sample alongside 1 ml lysis reagent (QIAzol Lysis Reagent, Qiagen, 79306). Tissue was homogenised using a tissue lyser (TissueLyser II, Qiagen, 85300) at 30 Hz for 1 minute. Next, the tissue was left to incubate in the lysis reagent at room temperature for 15 minutes before centrifuging at maximum speed for 15 minutes at 4 °C. The supernatant was transferred into heavy phase lock tubes (5PRIME

Phase Lock Gel™, Quantabio, 2302830) for phase separation and 200 µl of bromo-3-chloropropane was added. Tubes were shaken for 10 seconds and left to incubate on bench at room temperature before spinning again at maximum speed for 15 minutes at 4 °C. The aqueous phase containing ribonucleic acid (RNA) was collected and washed with an equal volume of 70% ethanol. The aqueous phase and ethanol mix was then transferred into Qiagen RNeasy Mini Kit (Qiagen, 74106) columns for further cleaning up following the manufacturer's protocol. After the first cleaning step in the Qiagen protocol, DNAse (Ambion – AM1906) was added to remove any gDNA contamination and the column was incubated at 37 °C for 15 minutes before continuing with the provided Quiagen protocol.

Adult Kidney RNA Extraction

Adult kidneys were extracted as described in Section 2.6.1 and a single kidney was placed inside a 2 ml eppendorf tube on and kept cold on dry ice. The RNA extraction was then performed according to the description in Section 2.5.

Whole Embryo RNA Extraction

For larval zebrafish RNA extraction 10 fish were pooled together as one sample to ensure enough RNA was extracted. If the embryos were <3dpf, chorion was removed prior to collection as described in Section 2.2.7. Zebrafish were placed in 2 ml eppendorf tubes and frozen by placing the tubes directly on dry ice. Samples were either processed immediately as described in Section 2.5 or stored at −80 °C.

RNA Quantification

The RNA was eluted from the columns using 42 µl of RNAse free water and 2 µl were used on a NanoDrop (ThermoFisher™NanoDrop 1000 Spectrophotometer) to determine RNA concentration and the absorption ratios at 260nm/280nm and 260nm/230nm ratios indicating possible protein or carbohydrate contaminants, respectively. If the absorption ratio at 260nm and 280nm was approximately 2, a 1% agarose gel was made up using 1×TAE. 500 µg of RNA were loaded on the gel. Gel electrophoresis at 80 V for 1.5 hours was performed to investigate the quality of the RNA. When clear separation of the visible 28 s and 18 s bands could be seen the RNA was regarded as stable and used for downstream applications.

2.5.1 RNA Reverse Transcription

RNA was reverse transcribed to produce cDNA using the High–Capacity cDNA Reverse Transcription Kit (Applied Biosystems™, 4387406). In accordance with the manufacturer's guidelines, a 2×RT Master Mix was prepared and 10 µl of the Master Mix were combined with 10 µl RNA (0.5 µg). The samples included a RNA sample without the Multiscribe enzyme which was included in the subsequent, quantitative polymerase chain reaction (QPCR) assay, to ensure no DNA contaminated the RNA samples. The reverse transcription was performed in a thermocycler (Applied Biosciences, Veriti 96-well) on the program outlined in Table 2.7.

Steps	Time	Temperature
Step 1	10 minutes	25 °C
Step 2	120 minutes	37 °C
Step 3	5 minutes	85 °C
Step 4	∞	4 °C

Table 2.7 | **Reverse transcription cycle conditions** Thermal cycler conditions for the reverse transcription of RNA to cDNA.

2.5.2 Quantitative Polymerase Chain Reaction

Quantitative polymerase chain reaction (QPCR) was performed using the Roche LightCycler® 480 system. cDNA used was generated as described in Section 2.5.1 and diluted 1:40 for further use. All standards and samples were run in triplicates and the average concentration was selected for the analysis. The probes from the Universal Probe Library (UPL, Roche Diagnostics Ltd., UK) used are outlined together with the selected primer sequences in Table 2.8.

One reaction contained 8 µl Perfecta® QPCR FastMix® II (Quantabio, 733-2108) made up according to the manufacturers guidelines containing; 100 nM probe, 20 µM forward and reverse primer, and 2.8 µl nuclease free water. The reactions were plated onto 384 well plates (LightCycler® 480 Multiwell Plate 384, white) and sealed with LightCycler® 480 sealing foil to prevent evaporation. The plates were prepared in a clean fume cabinet and on ice. Prior to loading the plates into the Roche LightCycler® 480 system they were briefly centrifuged to ensure all the sam-

Target Gene	Direction (5' - 3')	Sequence	Probe
clocka	F	CCACACACAGGCACAGAC	#3
	R	AGCTGGGTAGACTGGTTGCTA	
bmal1	F	GGAAAGATTGGACGCATGAT	#6
	R	GGAGCCTCTGATTCTCTGGA	
per2	F	ATGGAGCATTCAGAGCATCAG	#16
	R	CTTGTCTGTGGGGATTCTGG	
cry1a	F	GAGGAGGGCATGAAGGTG	#4
	R	AAGAAGGAGCTGCAGGACAG	
ren	F	CCTTTATACACAGCCTGCTTCA	#43
	R	CCCGGACATTTCCAGAAG	
ef1a	F	CCTTCGTCCCAATTTCAGG	#67
	R	CCTTGAACCAGCCCATGTT	
rsp18	F	GATGGGAAATACAGCCAGGTC	#41
	R	CCAGAAGTGACGGAGACCAC	

Table 2.8 | **QPCR primers** Primer sequences and Roche UPL probe numbers for QPCR analysis.

ples and cDNA were at the bottom of the well. The reactions were run on a Fam-Hydrolysis program outlined in Table 2.9.

Triplicates were analysed and any samples with a standard deviation of the triplicate Cp value higher than 0.5 was excluded. Furthermore, the standard curve was analysed for error and efficiency, where <0.05 and 1.9 to 2.1, respectively was acceptable. Gene concentrations were normalised to the concentration of the selected housekeeper gene.

Temperature	Time	Cycles
95 °C	5 minutes	1
95 °C	10 seconds	50
60 °C	30 seconds	
72 °C	1 seconds	
40 °C	30 seconds	1

Table 2.9 | **Fam-hydrolysis cycle conditions** Fam-hydrolysis method used on the Roche LightCycler® 480 system.

2.6 Cell and Tissue Culturing

2.6.1 Kidney Extraction

Zebrafish were sacrificed as described in Section 2.2.4. The fish were wiped with an ethanol soaked cloth to prevent contamination during extraction. Using spring dissection scissors (World Precision Instruments, WPI, 15906) the body of the fish was opened by performing a long ventral incision from head to the base of the caudal fin. The insides of the fish were removed by a single motion, removing the swim bladder from the posterior to the anterior ends of the fish. Removal of the swim bladder generally results in a successful removal of all internal organs and exposes the kidney. The kidney can be identified by its faint pink colour and presence of pigments. The kidney is gently removed from the the spine and collected in tissue collection medium (Table 2.10).

Medium Type	Recipe
Digestion Buffer	5 mM $CaCl_2$, 10 mg/ml Bacillus Licheniformis protease and 125 U/ml DNAse in PBS
Culture Medium	Leibowitz-15, 10% FCS, 100 U/ml penicillin 100 µg/ml penicillin and 50 µM 2–mercaptoethanol
FACS Buffer	Leibowitz-15, 2% FCS, 100 U/ml penicillin 100 µg/ml penicillin
Tissue Collection Medium	Leibowitz-15, 2% FCS, 100 U/ml penicillin 100 µg/ml penicillin

Table 2.10 | **Cell culturing media** Media containing all the cell culture media and buffers.

2.6.2 Mesonephric Kidney Dissociation

Adult zebrafish kidneys were extracted as described in Section 2.6.1. Two kidneys were placed in tissue collection media (Table 2.10) and kept on ice. Extracted kidneys were processed in a clean tissue culture hood to avoid contamination. Kidneys were washed 3× in collection medium to clear of any contaminants and were placed in 100 µl of digestion buffer (Table 2.10). Kidneys were dissociated in digestion buffer at 6 °C in a thermocycler for 15 minutes and triturated using a P200 Gilson pipette every 2 minutes. Next, the dissociated kidneys were passed through a 40 µm cell strainer to remove undigested lumps and collected in a 50 ml falcon tube. The cell strainer is washed with a further 2 ml of FACS buffer (Table 2.10). The falcon tube containing the cells is spun at 400 g for 5 minutes to pellet the cells. The cells are then resuspended in either 750 µl FACS buffer if taking them for cell sorting or in 1 ml culture medium (Table 2.10) if to be seeded directly on in a culturing plate, as described in Section 2.6.3).

2.6.3 Kidney Cell Culturing

Zebrafish kidney cells were cultured in 96-well plates coated with fibronectin (5 µg/cm^2). 50 µl of fibronectin for a 96-well plate were placed inside the well and left for 24 hours on a rocker. Fibronectin was removed right before seeding the wells with cells. Cells were incubated at 28.5 °C in an CO_2 incubator. The Culture Medium (Table2.10) was changed daily and the wells were inspected for any infections.

2.7 Imaging Modalities

Different imaging modalities were used depending on the level of resolution and quality of images required. With different imaging systems the mounting of the samples varies.

Imaging Zebrafish Mesonephros

Zebrafish kidney was extracted as described in Section 2.6.1 and placed onto a microscopy slide (Thermo Scientific, 11819022). A drop of PBS was added to the kidney from drying out during imaging and a coverslip was applied on top and pressure was applied to spread the kidney under the coverslip. Edges were sealed with nail polish and the slide was imaged the same day using the Leica TCS SP8 confocal laser scanning microscope.

Epifluorescence Microscopy

All screening of zebrafish, injection of larval zebrafish and imaging that did not require high resolution microscopy was performed on a Leica MZ16F stereomicroscope with top lighting. Prior to imaging, zebrafish were anaesthetised as described in Section 2.2.8.

Bioluminescence Microscopy

Bioluminescence images were acquired using the Hamamatsu ORCA II BT 1024 mono-chrome camera (C4742-98-26-KWG2). The camera enables the detection of luminescence signals at 16 bit depth and super cooling the detector to -75 °C allows to acquire images without binning and maximising the signal to noise ratio.

Images were sampled using the Hamamatsu Wasabi Software. Integration varied between 12 and 20 minutes depending on signal strength. Larval zebrafish were anaesthetised using Tricane (MS-222) before mounting them in agarose. 10mM luciferin was added on top of the agarose 15 minutes prior to imaging, to permit absorption by the agarose. Fluorescence images were acquired using the Leica MZ16F stereomicroscope with a dipper lens and top lightning. The exposure time was kept the same across different images when comparing fluorescence intensity.

Confocal Laser Scanning Microscopy

High resolution microscopy was performed on a Leica TCS SP8 confocal laser scanning microscope using two highly sensitive HyD detectors. The microscope was controlled via the Leica LAS X software.

2.8 Peptide Synthesis

2.8.1 Synthesis of Dde-OH

Dimedone (21.2 g, 151 mmol, 1 eq), DMAP (29 g, 156 mmol, 1 eq) and EDC hydrochloride (29.1 g, 152 mmol, 1 eq) were dissolved in DMF (400 ml). Acetic acid (1.59 mmol, 1 eq) was added and the mixture was stirred overnight at room temperature until fully dissolved. The solvent was removed *in vacuo*. The resulting oily substance was dissolved in ethyl acetate (200 ml) and washed with 1M HCl (2$\times$200 ml) until fully dissolved, yielding crude Dde-OH. The crude substance was analysed by TLC (ethyl acetate + 0.1% acetic acid). Purification was performed by column chromatography (eluting with DCM) and the product analysed by analytical HPLC.

2.8.2 Fmoc-Lys(Dde)-OH Synthesis

Fmoc-Lys-OH.HCL (14.12 g, 1 eq), with Dde-OH (9.52 g, 1 eq) was dissolved in 250 ml MeOH. DIPEA (8 ml) was added and using a stirrer the mixture was gently agitated for 60 hours. The solvent was removed *in vacuo* and the crude product was dissolved in ethyl acetate and washed twice with 1M $KHSO_4$. The organic layer was dried, filtered and concentrated yielding crude Fmoc-Lys(Dde)-OH. The product was analysed TLC (ethyl acetate + 0.1% acetic acid) showing that it was

not pure. The crude product was purified by column chromatography (eluting with ethyl acetate + 0.1% acetic acid). Pure fractions were collected and analysed by HPLC. The solvent was removed *in vacuo* and the product was recrystallised using ethyl acetate/hexane. This resulted in crystalline Fmoc-Lys(Dde)-OH.

2.8.3 Rink Linker Polystyrene Resin

For all FRET probes, an aminomethyl polystyrene resin with a loading of 0.745 mmol/g was used. Poly-styrene resin (200 mg, 0.149 mmol, 1 eq) was swollen with DCM for 30 minutes. Fmoc-Rink amide linker (241.19 mg, 0.447 mmol, 3 eq) was dissolved in DMF. Oxyma (63.52 mg, 0.447 mmol, 3 eq) was added and the reaction mixture was gently agitated for 10 minutes before DIC (69.21 µl, 0.447 mmol, 3 eq) was added and agitated for a further 5 minutes. The mixture was added to the pre-swollen polystyrene resin. This reaction mixture was gently agitated at room temperature for 50 minutes. Using the vacuum manifold, the supernatant was removed and the resin was washed 3$\times$ with DMF, followed by 3$\times$DCM and 3$\times$MeOH. Quantitative ninhydrin tests were performed to confirm the lack of free amines.

2.8.4 2-Chlorotrityl Linker Polystyrene Resin

For other peptides, the 2-chlorotrityl chloride resin with a loading of 1 mmol/g was used. 2-chlorotrityl chloride resin (200 mg, 0.2 mmol, 1 eq) was washed and swollen with dry DCM for 30 minutes. To the pre-swollen resin, $SOCl_2$ (35 µl, 0.5mmol, 2.5 eq) dissolved in DCM was added with DIPEA (209.03 µl, 1.2 mmol, 6 eq). The reaction mixture was gently agitated using a stirrer at room temperature for 1 hour. Supernatant was expelled using the vacuum manifold and the resin was washed with dry DMF. A mixture of DCM:MeOH:DIPEA (80:10:10) was added twice for 10 minutes each to cap all reactive groups. The resin was washed with DMF.

2.8.5 Dde Deprotection

Removal of the Dde protection group was performed with 2% hydrazine in DMF. 2% hydrazine was added to the resin 5 $\times$ 2 minutes and between each addition, the

resin was thoroughly washed with DMF. Ninhydrin test was performed to confirm the presence of free amine groups as described in Section 2.8.14.

2.8.6 Fmoc Deprotection

20% piperidine in DMF was added to the pre-swollen resin to remove the Fmoc protecting group. The mixture was agitated for 10 minutes before removing the supernatant using the vacuum manifold. Under vacuum the resin was washed 3× with DMF, 3× with DCM before adding a further 20% piperidine in DMF and agitating for a further 10 minutes. Supernatant was removed using the vacuum manifold and the resin was washed using 3×DMF, 3×DCM and 3×MeOH. The quantitative ninhydrin test was used to confirm the presence of free primary amine groups. For secondary amine groups the chloranil test was performed.

2.8.7 Amino Acid Addition

For all the peptides synthesised in this thesis, Fmoc protected amino acids were used. Fmoc protected amino acids (3 eq) were dissolved in DMF. Oxyma (3 eq) was added to the mixture and the solution was agitated for 10 minutes. DIC (3 eq) was added and the mixture was agitated for a further 5 minutes. The resin was swollen with DCM and the mixture was added and agitated for 1 hour to permit binding of the amino acid to the free amine groups. After 1 hour the resin was washed with 3×DMF, 3×DCM and 3×MeOH using the vacuum manifold. A quantitative ninhydrin test was performed to confirm the lack of free amine groups. If the ninhydrin test indicated free amine groups the reaction was repeated.

2.8.8 Methyl Red Addition

Methyl red coupling was performed as described in Section 2.8.7. The ninhydrin test was used to confirm the lack of free amine groups.

2.8.9 5(6)-Carboxyfluorescein Addition

Addition of the fluorophore 5(6)-carboxyfluorescein was performed as described in Section 2.8.7. The ninhydrin test was used to confirm the lack of free amine groups.

2.8.10 Peptide Cleavage from Resin

Resin was swollen in DCM and a mixture of TFA/TIS/DCM was added at a ratio 9:5:5, respectively. The cartridge with the resin and cleavage mixture was sealed with parafilm as pressure buildup during the reaction can lead to leakage. The mixture was shaken for a minimum of 3 hours to ensure that all side protecting groups were also removed during this step and the peptide was collected via precipitation into cold ether. For determination of successful deprotection of all side protecting groups, the final product was analysed by analytical HPLC described in Section 2.8.13.

2.8.11 Probe Purification and Characterisation

All FRET probes synthesised were purified by semi-preparative HPLC and characterised by analytical HPLC and MALDI mass spectrometry.

2.8.12 Matrix Assisted Laser Desorption Ionisation

Sample was prepared by dissolving the sample in 1 µl of 20 mg/ml sinapinic acid. This was directly mixed on a 100 well gold Voyager™ matrix assisted laser desorption ionisation (MALDI) sample plate. MALDI time of flight (TOF) was measured on a Voyager™ DE-STR MALDI-TOF (Applied Biosystems) mass spectrometer with the laser scanning across the entire sample. Laser power was dependant on the final sample concentration.

2.8.13 Analytical HPLC

Analytical high pressure liquid chromatography (HPLC) was performed on an Agilent 1100 coupled with a Polymer Lab PL-ELS 100 Evaporative Light Scattering detector (ELSD). The ELSD had UV and also detection at 220, 254, 260, 282 and 450 nm. The column used was a Spelco's Discovery C18 (50 mm $\times$ 2.1 mm $\times$ 5 µm). Samples were dissolved in 1 ml 1:1 HPLC-grade MeCN:H_2O. Elution was performed with HPLC-grade deionised water with 0.1% formic acid and HPLC-grade methanol with 0.1% formic acid at 1 ml/min with a gradient of 5% to 95% over 3 minutes, followed by 1 minute isocratic, 1 minute to 5% HPLC-grade methanol with 0.1% formic acid and 1 minute isocratic.

2.8.14 Ninhydrin Test

- Reagent A: 430 mmol of phenol dissolved in absolute ethanol
- Reagent B: 14 mmol ninhydrin dissolved in absolute ethanol

In order to determine the presence or absence of primary amine groups a ninhydrin test was conducted. A small number of resin beads were placed in a glass vial and reagent A was added to reagent B in a 1:3 ratio. The mixture is placed in heating block pre-warmed to a 100 °C for 2 minutes. A blue colour indicates primary free amine groups and a yellow test is indicative of protected or lack of primary amine groups.

2.8.15 Chloranil Test

- Reagent A: 2% acetaldehyde in dimethylformamide (DMF)
- Reagent B: 2% chloranil in DMF

In order to test for secondary amine groups such as on proline, a chloranil test was performed. Small number of beads were collected in a glass vial and solution A and solution B were added to the beads at a ratio of 1:1. The mixture was briefly mixed and left at room temperature for 1 minute. If the resin beads turned blue, it indicated the presence of secondary amine groups and a negative test showed no colour change and the beads remained yellow.

2.8.16 *In Vitro* FRET Assay

10 fish embryos or 1 zebrafish kidney were placed in a 2 ml eppendorf tube with 1 metal bead (Stainless Steel Beads, Quiagen, 69889) and 1M Tris-Buffer, and were homogenised using a tissue lyser (TissueLyser II, Qiagen, 85300) for 1 minute at 30 Hz. Protein concentration was determined by BCA assay (Pierce™ BCA Protein Assay Kit, ThermoFisher, 23227). 50 µl of tissue homogenate was mixed with 50 µl of FRET probe (10 µM) for a final concentration of 5 µM in a single well of a black 96-well plate (Nunchuck's-Immuno™, Merck, P8741). After 1 minute of incubation, the fluorescence intensity was analysed using a plate reader (VICTOR Multilabel Plate Reader, PerkinElmer, 2030-0050). Wells were excited at a wavelength of 480 nm for 1 second and emission fluorescence intensity was measured at 520 nm from the top of the well. All measurements were conducted in triplicates.

2.8.17 Western Blotting

Western blot analysis was performed to analyse recombinant proteins. 5 µg of protein sample were denatured in SDS sample buffer on a heat block for 5 minutes at 90 °C before adding to a well of a 4-12% Bis-Tris gel (Bolt™, Invitrogen, NW04120) and subjected to electrophoresis at 110 V for 2 hours to separate depending on their molecular weights. The separated proteins were transferred by semi-wet transfer onto a nitrocellulose membrane. Successful transfer of the protein was observed by staining the membrane with Ponceau Red, a protein detection dye. The membrane was blocked with 1×TBST + 5% Milk at 4 °C for 1 hour. After blocking, the membrane was washed 3× in 1×TBST. The membrane was incubated overnight at 4 °C with primary mouse anti 6×His antibody (Anti-6×His tag, Abcam, ab18184), diluted 1:2000 in 1×TBST + 5% Milk. The membrane was then washed 3× in 1×TBST before application of the secondary fluorescent goat anti mouse antibody (Goat Anti-Mouse IgG Alexa Fluor 488, Abcam, ab150113) for 1 hour. The membrane was then washed again 3× in 1×TBST before analysis using the Licor Odyssey CLx imaging system (Odyssey CLx, Licor).

2.9 Data Analysis and Statistics

For analysis of two groups and continuous data the students t-test was used. Comparison of 3 or more samples was performed by 1-way ANOVA. All data analysis was performed using GraphPad Prism 8 for MacOSX. All data are represented as mean ± SD with $p < 0.05$ considered to be statistically significant.

Chapter 3

Development of a Transgenic Renin Luciferase Zebrafish

3.1 Introduction

The fluorescent zebrafish renin reporter line, established by Rider *et al.*, permits studies of the spatial distribution of renin-expression cells and their morphology. To date it has been shown, using these reporter fish, that zebrafish renin can be modulated by RAS inhibition and sodium challenges [45,47]. However these reporter fish are not suitable for highly sensitive dynamic investigation of renin gene expression *in vivo*, or studies of the response of the RAS to environmental challenges in real-time. Like many fluorescent proteins, the RFP-LifeAct reporter for renin expression used by Rider *et al.*, undergoes many lengthy post translational modifications before they can be detected. This causes a significant lag from the initial gene expression to being able to detect the functional fluorescent reporter protein, and does not permit investigation of changes in gene expression in real-time. However, firefly luciferase is a monomer which does not require any post-translational modifications and becomes a functional mature enzyme after translation of its mRNA [145]. The use of a luciferase renin reporter would enable the investigation of the renin transcription in 'real-time', with the advantage of providing data on gene expression dynamics and spatial information of gene expression. Luciferase generates bioluminescence through an oxygen- and ATP-dependant reaction, in which the substrate luciferin is catalysed by luciferase, producing oxyluciferin and a photon as a side product (see Figure 1.9). The sensitive and quantitative output of luciferase as a surrogate reporter for renin transcription, combined with the use of pharmacological tools for the RAS, would allow the investigation of new regulatory pathways and studies of the role of the RAS in early development. In this chapter I will present the generation and validation of a renin-luciferase transgene, the design of a high-throughput bioluminescence assay, and the use of bioluminescence imaging to determine the origin of reporter expression.

3.2 Results

3.2.1 Circadian Rhythm Regulating Renin Expression

Most mammals show a steep rise in blood pressure at the start of their active period, i.e. daytime for humans and night time for rodents, where an increase in plasma renin activity (PRA) and ultimately blood pressure increase is observed. Although zebrafish have a low blood pressure system [146], they have a resting phase during the dark cycle and an active phase during the light cycle [147]. In order to determine the activity of clock genes in the zebrafish kidney, adult kidneys were extracted early in the morning after the lights came on (9AM, n=7), the middle of the light cycle (3PM, n=5), immediately after lights went out (12AM, n=11), and middle of the night (5AM, n=5). RNA from the kidneys was extracted and subsequently reverse transcribed into cDNA and QPCR analysis was performed (Figure 3.1). Bmal1 was significantly upregulated in the early afternoon compared to all other time points. Clock1a, which is typically expressed in parallel with Bmal1 showed highest expression in the early morning. Clock1a was significantly lower at all other time points, suggesting a delay in expression compared to mammalian Clock expression. Cry1a, which is typically highly expressed in the evening and lowest in the morning showed up-regulation throughout the day, with a significant increase in expression between 12AM and 5AM (p=0.0009). Expression of Per2 was consistent with previous studies [148, 149], and was found to be lowest towards the end of the dark cycle (5AM) and significantly higher at all other time points. These data confirm activity of clock genes in the kidney and their 24 hour cycles. However, the large gaps between the time-points and delay of gene expression of genes which are usually expressed in parallel suggest that more time points or a more sensitive assay should be proposed. In contrast, the expression of zebrafish renin showed a trend similar to that of its mammalian counterpart, with peak expression at 9AM and reduced expression throughout the day. This trend did not reach significance and these data do not suggest that renin is regulated by the circadian rhythm. The relative renin gene expression data has a large spread suggesting that individual fish might experience a delay in the regulation of renin expression. The QPCR analysis is restrictive to a single time point and labour intensive. Hence, to investigate more closely the dynamic renin expression in the pronephric and mesonephric kidneys zebrafish, a more sensitive and more accessible assay for transcriptional regulation is required.

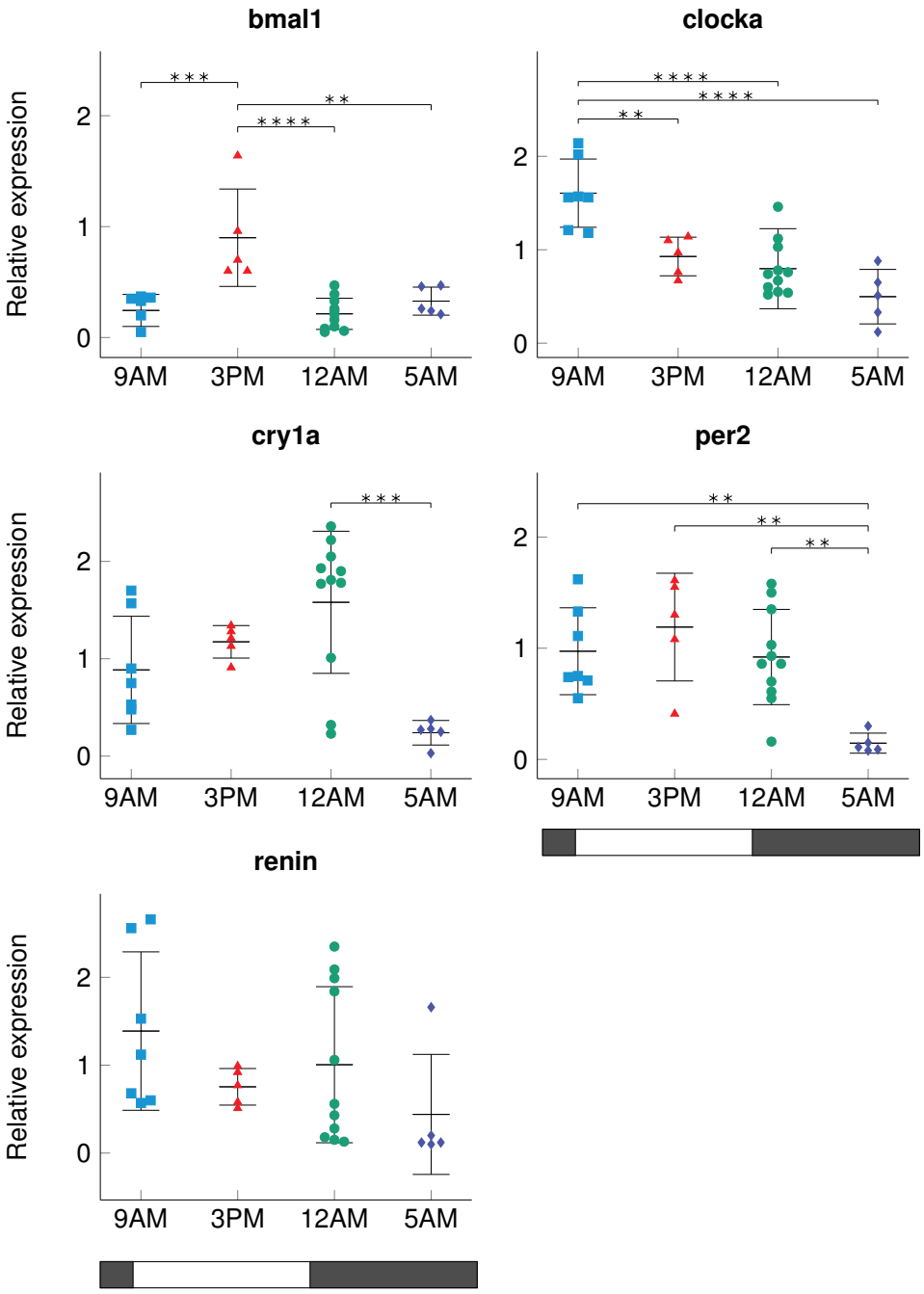

Figure 3.1 | **QPCR analysis of clock gene expression and renin at varying time points** 9AM (n=7), 3PM (n=5), 12AM (n=11), 5AM (n=5). X-axis represents the light/dark cycle in the zebrafish facility. Data normalised to housekeeper genes (rsp18 and elfa). ANOVA with Bonferroni's multiple comparisons test. Data are mean ± SD.*=p<0.05, **=p<0.01, ***=p<0.001, ****=p<0.0001.

3.2.2 Generation of a Novel Dynamic Renin Luciferase Reporter Fish

In order to investigate whether renin expression is more transcriptional subtle than that suggested by the previous experiments, I decided to use a luciferase reporter as a surrogate readout for renin expression. The luciferase reaction is highly sensitive and occurs almost instantaneously when luciferase breaks down the substrate luciferin, which can be detected shortly after initial gene expression. One of the side products emitted from this reaction is light, thereby permitting the detection and quantification of the reaction [139, 150, 151]. Furthermore, in order to detect the light, no external light source is required, eliminating autofluorescence.

For the design of the expression plasmid, the gateway cloning strategy was chosen. Gateway cloning depends on the development of 3 individual plasmids knows as 3', middle, and 5' entry clones [92]. These plasmids contain DNA cassettes with a promoter, reporter and a polyA tail, respectively. Each DNA expression cassette is flanked by specialised recombination sites, which will be recombined in a single reaction into a destination vector while maintaining the reading frame. The chosen destination vector was pDestTol2CG2, which contains the zebrafish *cmlc2* promoter driving EGFP in cardiomyocytes of the heart, and is commonly used as a marker of successful transgenesis in zebrafish [152]. A map of the final entry clone can be seen in Figure 3.2. The destination vector contains tol2 sites. Transposase mRNA, which is co-injected with the plasmid, recognises the tol2 sites and integrates the plasmid into the chromosome. The transposon shows no specific integration site, meaning that the plasmid can translocate anywhere on the chromosome [90].

The 3' entry clone, consisting of the 6.4kb renin promoter, had previously been published Rider *et al.* [47]. To verify the plasmid, diagnostic NcoI and PstI restriction enzyme digests were performed and analysed by DNA electrophoresis. The predicted 9106bp fragment (representing the linearised plasmid) was observed following digestion by NcoI, whilst 7009bp and 2097bp fragments were obtained following digestion with PstI (Figure 3.3B). The commercially available pDestTOl2CG2 destination vector (7796bp) was also analysed by restriction digest and DNA electrophoresis (Figure 3.3C).

The middle entry clone, containing the firefly luciferase coding sequence, was kindly provided by the MacRae Laboratory (Harvard) and restriction digestion with ApaLI confirmed the correct size of the plasmid (3892bp) (Figure 3.3D). Lastly the final insert, the polyA tail was used to fill for the 5' entry clone which was also assessed using a single restriction digest by EcoRI generating two fragments (1911bp, 927bp).

All three entry clones were recombined with the destination vector using LR-clonase. The reaction was left for 24 hours overnight and the product used for transformation into E.coli bacteria generating 26 ampicillin-resistant colonies. Five colonies were chosen and DNA was extracted and processed for extensive restriction digest analysis. Only 1 colony gave the expected DNA fragment sizes (EcoRI=12752bp; PSTI=5152bp, 4743bp, 4622bp; NCOI=11312bp, 3096bp; NHEI =14508bp). The colony was selected and a final restriction analysis was performed followed by DNA sequencing (Figure 3.4). The plasmid was then co-injected into the single cell-stage WIK eggs with transposase mRNA. After 24 hours EGFP expression was observed in the larval zebrafish hearts, indicating successful expression of the *cmlc2*:EGFP transgene.

Mosaic expression is commonly seen in the F0 founders and is suggestive of not all cells containing a copy of the transgene. In order to ensure expression in all cells of interest, transgenic fish are outcrossed to a non-transgenic WIK fish once sexual maturity is reached. This step is also necessary to determine if F0 animals are capable of transgenic germline transmission. An illustration of the breeding strategy to generate a stable transgenic line can be seen in Section 3.5.

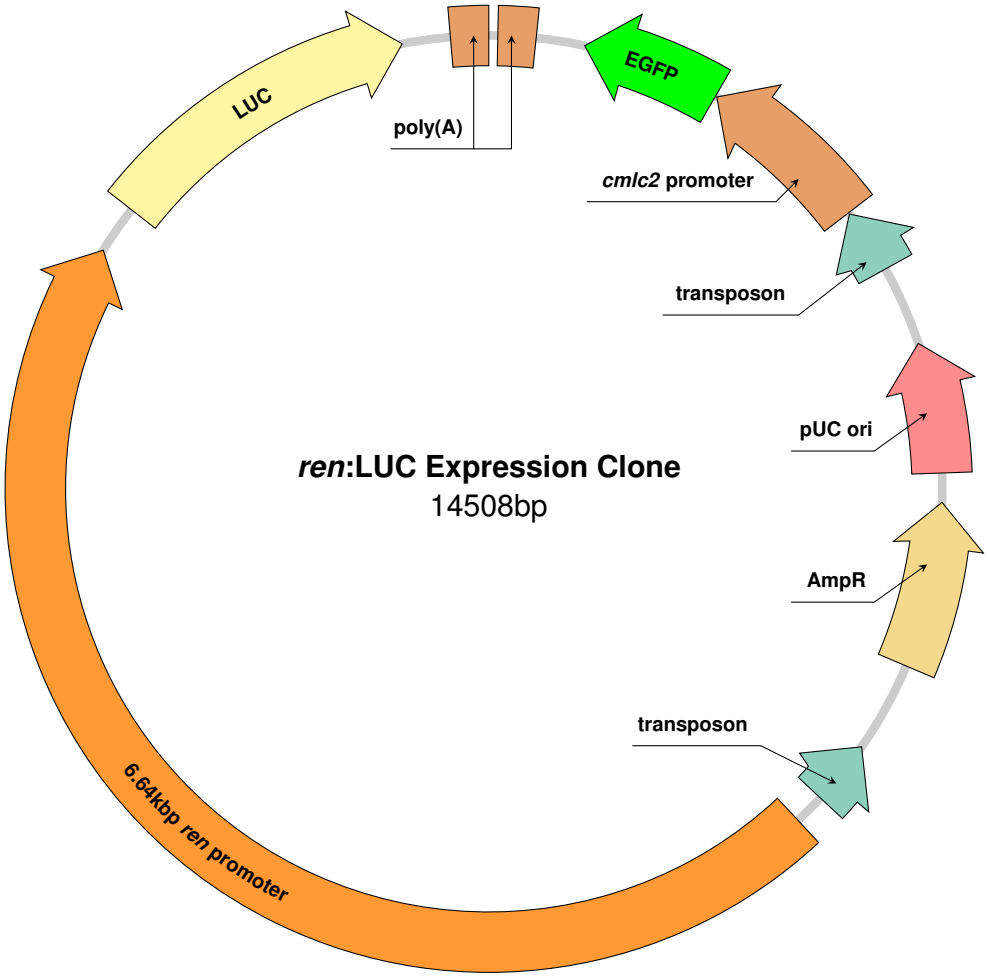

Figure 3.2 | **Plasmid map for the *ren*:LUC expression clone** A previously published 6.64kb renin promoter drives luciferase expression. To improve selection for successful integration of the transgene, the backbone consists of a *cmlc2* promoter driving the fluorescent protein EGFP in the opposite direction.

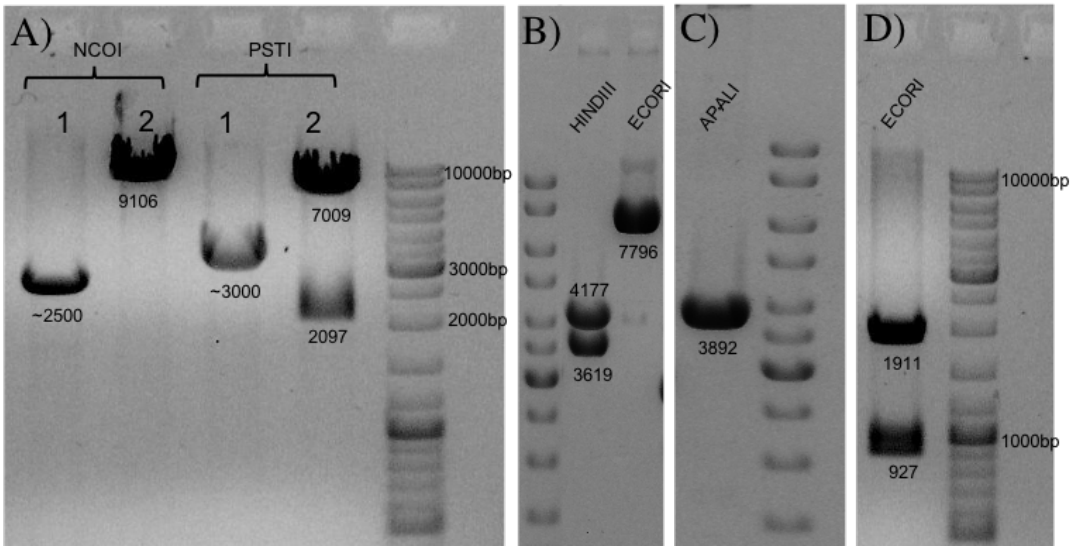

Figure 3.3 | **Restriction enzyme verification of entry clones used for the construction of the *ren*:LUC expression vector** Restriction enzyme digestion and and subsequent gel electrophoresis of entry entry clones. A) 6.64kb renin promoter entry clones digested with restriction enzymes NcoI and PstI. Lane 1 and 2 represent analysis of two different clones. B) pDestTol2CG2 destination vector digest with EcoRI and HindIII, yielding the correct fragment sizes. C) Middle entry clone luciferase reporter digested with ApaI1 restriction enzyme D) Restriction enzyme digest of polyA, 5' entry clone with EcoRI.

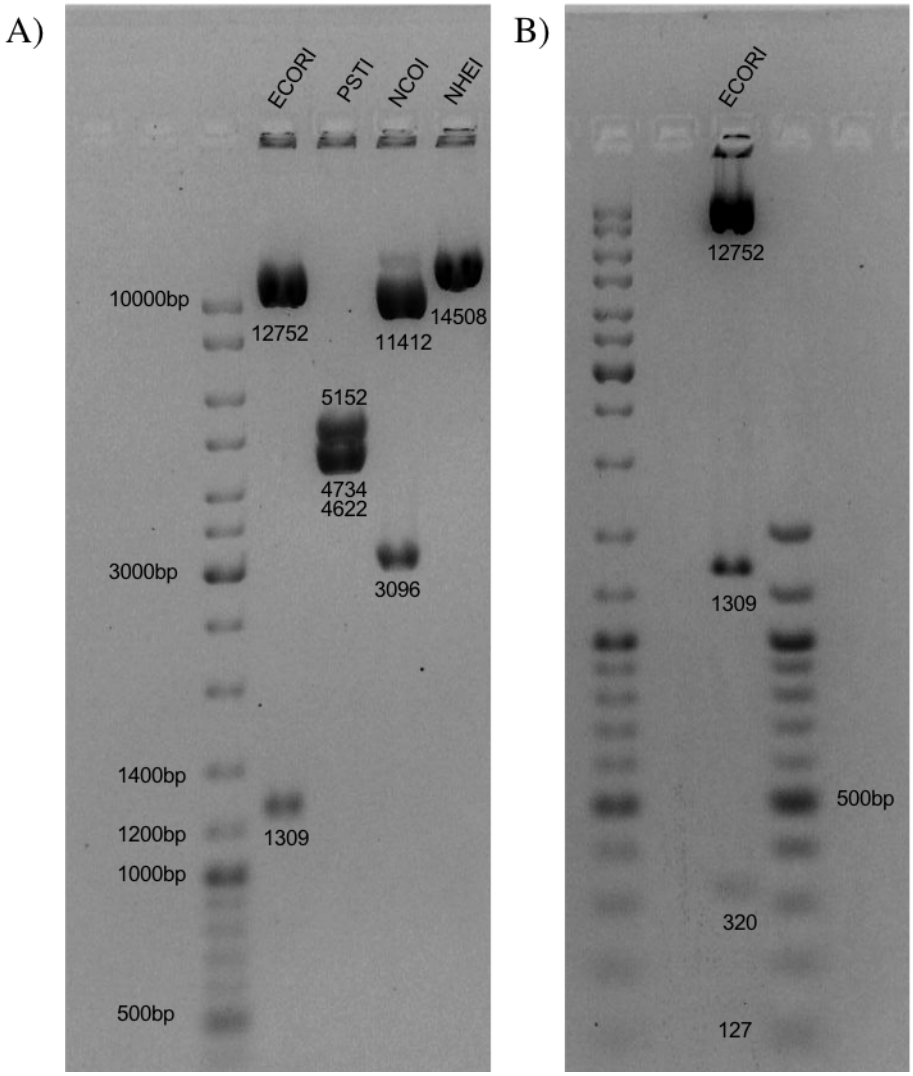

Figure 3.4 | **Restriction enzyme digest and subsequent gel electrophoresis of the *ren*:LUC entry clone** A) 1% agarose gel DNA electrophoresis with restriction enzyme digest analysis of expression clone. Restriction enzymes used were: NheI, NcoI, PstI, and EcoRI. B) 2% agarose gel DNA electrophoresis to visualise the small DNA fragments from the EcoRI restriction digest.

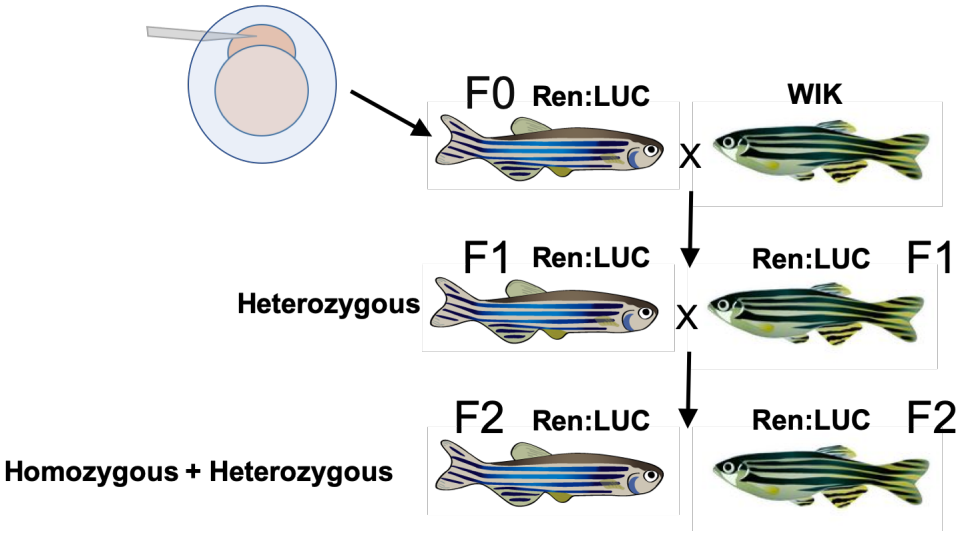

Figure 3.5 | **Breeding strategy for the novel *ren*:LUC line** Plasmid is injected into WIK eggs at the one cell stage. To determine if the transgene has gone germline, fish are outcrossed to the wild-type WIK. F1 progeny is selected by the transgenic *cmlc2*:EGFP reporter and incrossed to generate the F2 generation of homozygous and heterozygous fish.

3.2.3 Luciferase Assay Development

In vitro studies have shown that in the presence of high concentrations of the luciferase substrate, firefly luciferase is strongly inhibited after an initial flash, persisting less than a second, due to the accumulation of inhibitory oxyluciferin. The inhibition is also dependant on the luciferin used and the purity of the substrate. In order to establish the ideal concentration of the luciferin to be used in *in vivo* zebrafish experiments, an *in vitro* titration experiment with 1 µg pure recombinant luciferase was conducted (Figure 3.6). A significant reduction of signal was seen at luciferin concentrations of 100 mM, 50 mM and 25 mM. No significant change in signal was observed at concentrations from 0.5 mM to 10 mM, although the highest signal was seen at 1 mM. Physiological barriers of zebrafish will reduce the concentration of luciferin ultimately reaching the cells expressing luciferase, hence a higher concentration of 10 mM was used.

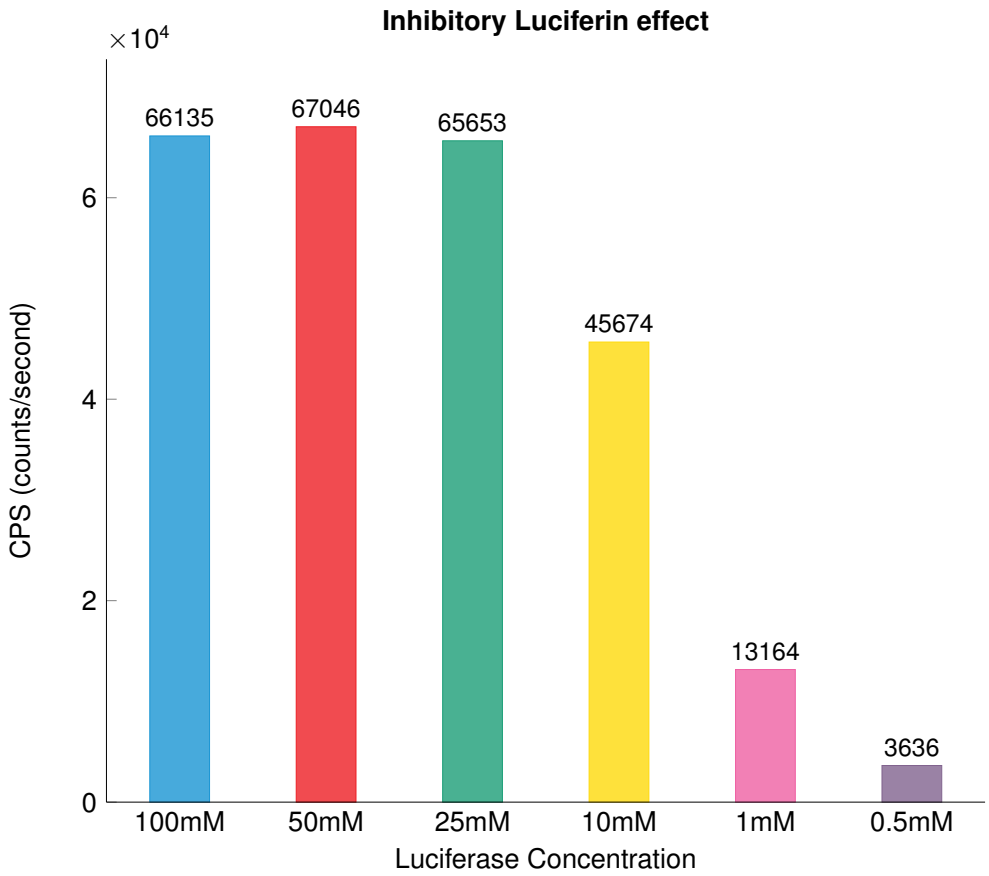

Figure 3.6 | **Luciferase signal at high luciferin concentrations** Measuring luciferase signal at different luciferin concentrations using 1 µg recombinant luciferase. Measurements were performed in triplicates.

3.2.4 *ren*:LUC Founder Selection

Cmlc2:EGFP is an ideal marker for transgenesis since the fish do not require complicated mounting and high resolution microscopy for detection of the EGFP in the zebrafish heart. The *cmlc2* promoter is known to be strongly expressed, independently of the site of integration. However, renin expression is highly dependant on regulatory elements found upstream of the site of integration and it is essential to determine strong transgene expressing founder fish early in development of the transgenic line. F0 injected fish were first selected for EGFP expression with minimal mosaic expression and were subsequently screened using the luciferase assay for luciferase signal strength, presuming a high luciferase signal indicates a good integration site of the plasmid. Single fish were placed into a well of a 96-well plate at 4dpf, since this was the ideal developmental stage for imaging tg(*ren*:RFP-

LifeAct) larval zebrafish [47]. Luciferin was added at a final concentration of 10 mM in the water and fish were left for 5 minutes to allow absorption of the substrate. Measurements of luciferase expression varied significantly from very high expression (>1500 CPS 2.1%) to medium expression (>100 CPS, 19%) from one round of injections (See Figure 3.7). Any fish expressing lower than 100CPS were discarded.

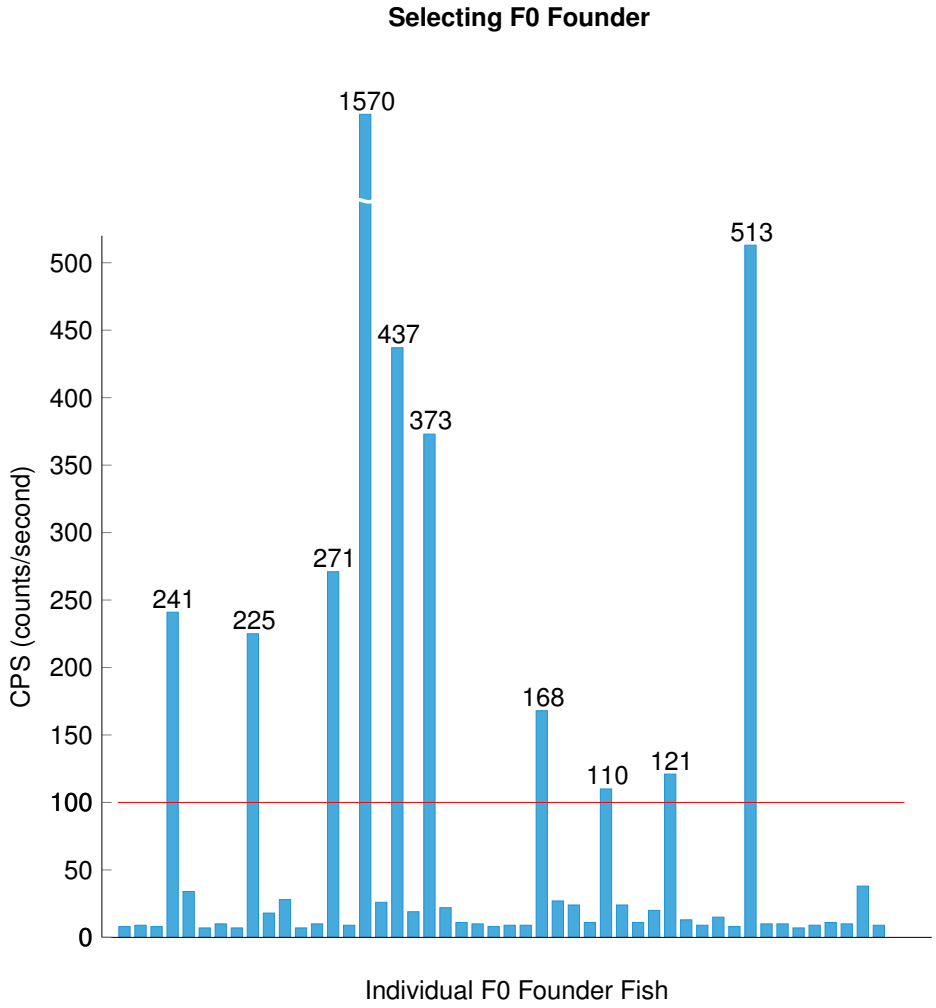

Figure 3.7 | **Selecting injected fish according to the luciferase signal** Injected zebrafish were selected at 24hpf by the EGFP expression driven by the the *cmlc2* promoter. All strong expressing EGFP fish were placed in a single well and luciferin was added to determine the luciferase signal strength in each individual fish. High expressing luciferase fish (CPS>100) were selected and kept for further breeding and establishment of the F1 line.

3.2.5 Breeding of the F0 Founder Fish

Once the F0 fish reached sexual maturity, they were outcrossed to wild-type WIK fish in order to determine successful transgenic germline transmission and to generate the heterozygous F1 line. In cases where a successful germline transgenic adult was identified, the progeny were investigated for the ratio of EGFP expressing fish to non-expressing fish. A 50/50 ratio suggests a single insertion site whereas a higher ratio suggests multiple insertion sites. Furthermore, F1 progeny were investigated for luciferase expression in order to only take forward the highest expressing luciferase fish. High variability in reporter signal intensity was previously also noted in the tg(*ren*:RFP-LifeAct) fish, which utilised the same promoter sequence as the *ren*:LUC construct. Surprisingly, no detectable luciferase signal was seen in the progeny of any high EGFP-expressing F0 fish. By increasing the detection time, to permit more photons to be counted, a low signal was detectable. However, a side by side comparison between a commonly occurring high-expressing F0 and F1 progeny showed that there was a more than a 400-fold reduction in signal in F1 progeny (Figure 3.8). This reduction and loss of signal was seen in all progeny of all founders, independent on their original expression level. F1 progeny were selected according to the luciferase signal compared to background noise from non-bioluminescent age matched wild-type control WIK fish (Figure 3.9).

3.2.6 Genotyping of *ren*:LUC Fish

To validate F1 transgenic progeny transgene-specific primers for EGFP and luciferase were designed (see Table 2.4). DNA extraction was performed on 5dpf larval fish and PCR was performed using WIK fish as negative controls since neither EGFP or luciferase are expressed in wild-type zebrafish. PCR result can be seen in Figure 3.10. The PCR results suggest that the genes coding for EGFP and Luciferase are both present *ren*:LUC zebrafish.

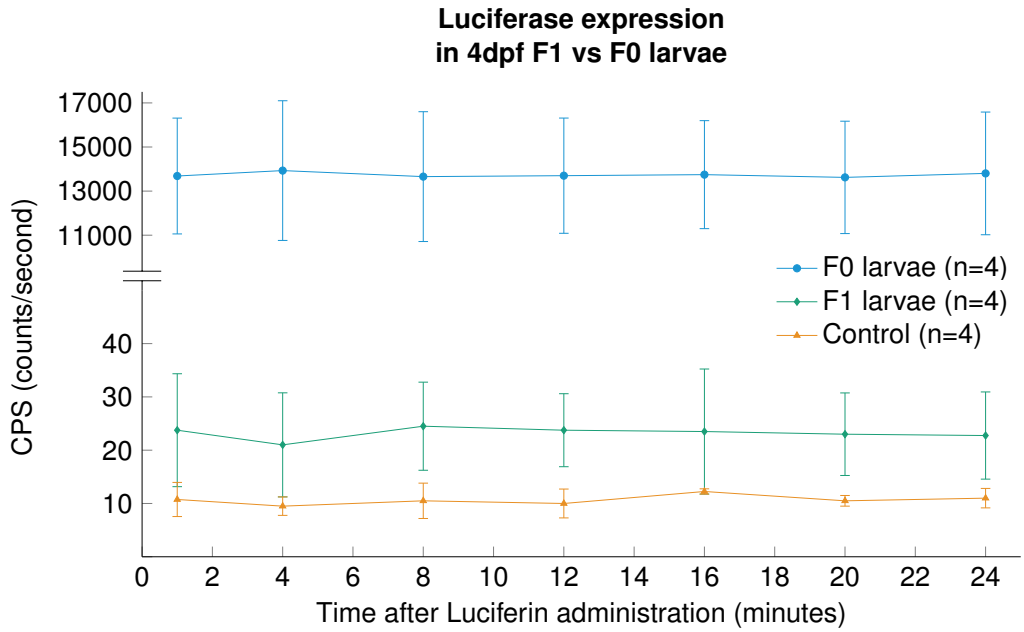

Figure 3.8 | **Luciferase expression comparison between F1 larvae** Luciferase expression at 4dpf in single F0 and F1 larvae over time.

3.2.7 Primary Imaging of Luciferase Expression

In order to determine the origin of the strong signal in F0 founders and whether the weak signal in F1 progeny was stemming from the AMA, a bioluminescence imaging system was required. The major limitation of bioluminescence imaging is that the amount of photons released from the luciferase reaction is very small and highly sensitive, supercooled detectors are required for its detection. One of these systems is the In Vivo Imaging System (IVIS). IVIS generates a brightfield image prior to measuring bioluminescence by a long time exposure. The two separate images were then overlaid. However, the IVIS is optimised for the imaging of rodents and not larval zebrafish, and the spatial resolution is not ideal. 4dpf F1 and F0 larval fish were selected using the plate detecting the luciferase signal and the highest expressers were selected for future breeding (Figure 3.11). Fish were mounted in agarose and 10 mM luciferin was applied to diffuse through the agarose. The identity of each fish from the plate reader was preserved by marking the wells and recording their mounting position in the 6-well plate. The IVIS acquired a bioluminescent image via an 18 minutes exposure and overlaid the signal as a heat map corresponding to the intensity and origin of the luciferase signal. All F0 founders had detectable luminescence in the IVIS (A=1263, B=786, C=290, D=189, E=218,

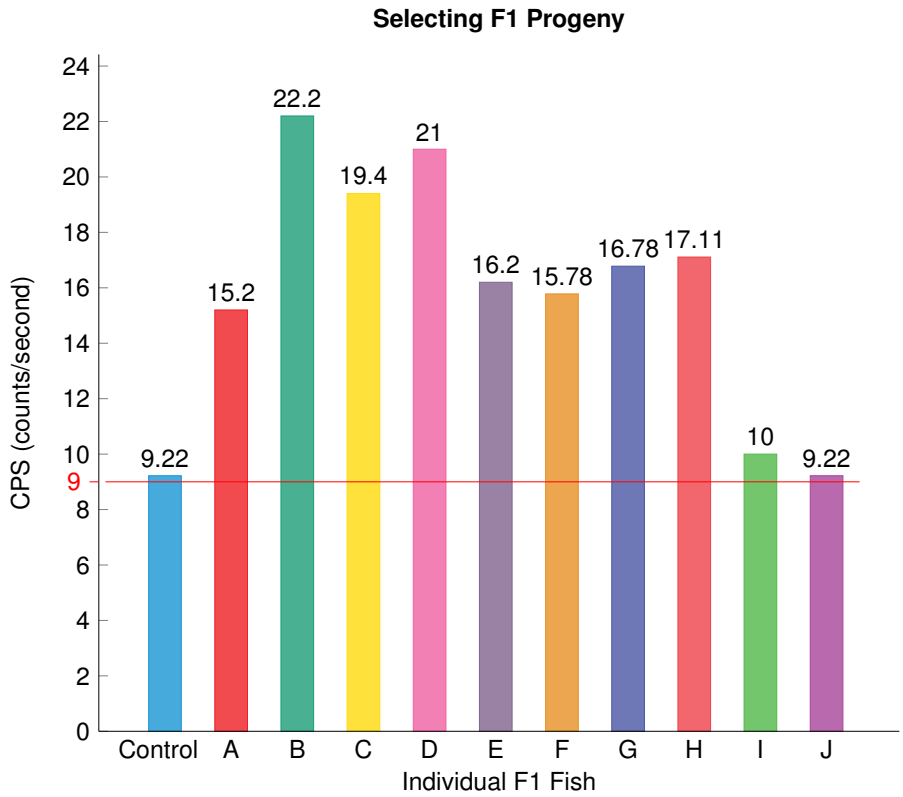

Figure 3.9 | **Luciferase expression of F1 larvae** Luciferase expression at 4dpf in single F1 *ren*:LUC larvae over time from previously high expressing F0 founder fish. Any fish with a luciferase signal below the background signal from a wild-type control (red line) were discarded.

F=569, G=268), however the signal from F1 progeny was not strong enough to be detected (H=35, I=39, J=19, K=24). Imaging of F0 larval fish produced a bullseye signal, with red in the middle indicating the highest signal and blue, on the outside most ring, indicating the lowest signal. A major limitation however, was the size of the signal indicator produced by the IVIS and overlaid onto the black and white image, preventing accurate localisation of the signal origin.

3.2.8 Ectopic Luciferase Expression in the Yolk Sac

To achieve higher spatial resolution, localise the source of the luciferase signal, and investigate whether it originated from the AMA, a bioluminescence microscope imaging system was required. The challenging issue with bioluminescence imaging is the need for highly sensitive sensors that are capable of capturing the small

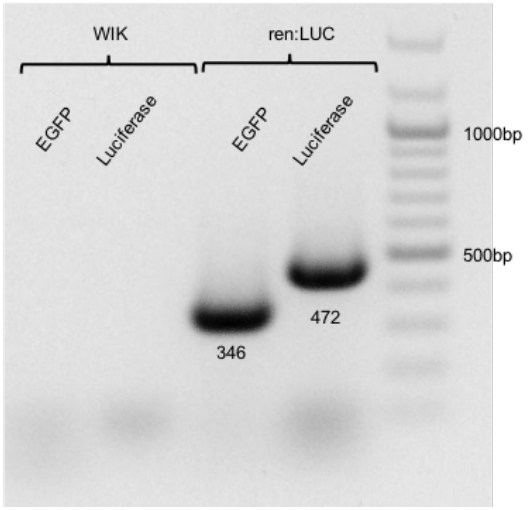

Figure 3.10 | ***ren*:LUC PCR genotyping** PCR and subsequent DNA electrophoresis of PCR product. Genotyping of *ren*:LUC fish to validate the presence of the complete transgene in F1 progeny. WIK fish were used as negative control as EGFP and Luciferase encoding genes are not present in wild-type (WIK) zebrafish.

number of photons emitted by the 5-10 renin cells at the AMA. A supercooled camera mounted on a microscope that was placed within a blacked out room was utilised. Prior to the bioluminescence imaging the fish were selected by the luciferase plate reader assay and only the highest luciferase expressing fish were chosen. The fish were mounted in 1% LMP agarose as described in Chapter 2.7 and exposed for 12 minutes. The bright-field image was acquired using a handheld torch since no source of light was present within the blackout room. In Figure 3.12, a WIK and tg(*ren*:LUC) fish are shown side-by-side. No signal was captured from the wild-type fish however there was a clear signal from the yolk sac of the *ren*:LUC fish. Furthermore, in addition to the yolk sac expression there was no expression where the AMA would be expected (Figure 3.12). A further image was acquired of a high expressing zebrafish to investigate the expression pattern in the yolk sac (Figure 3.13). None of the F1 fish had a signal high enough that permitted imaging. This suggests that all the founder fish previously selected on the high luciferase signal had had ectopic expression stemming from the yolk sac and the fish were not selected for the renin promoter driven luciferase signal. Fish with a low signal (<500 CPS) were not able to be imaged limiting the validation of the expression in founders.

(a) **IVIS imaging**

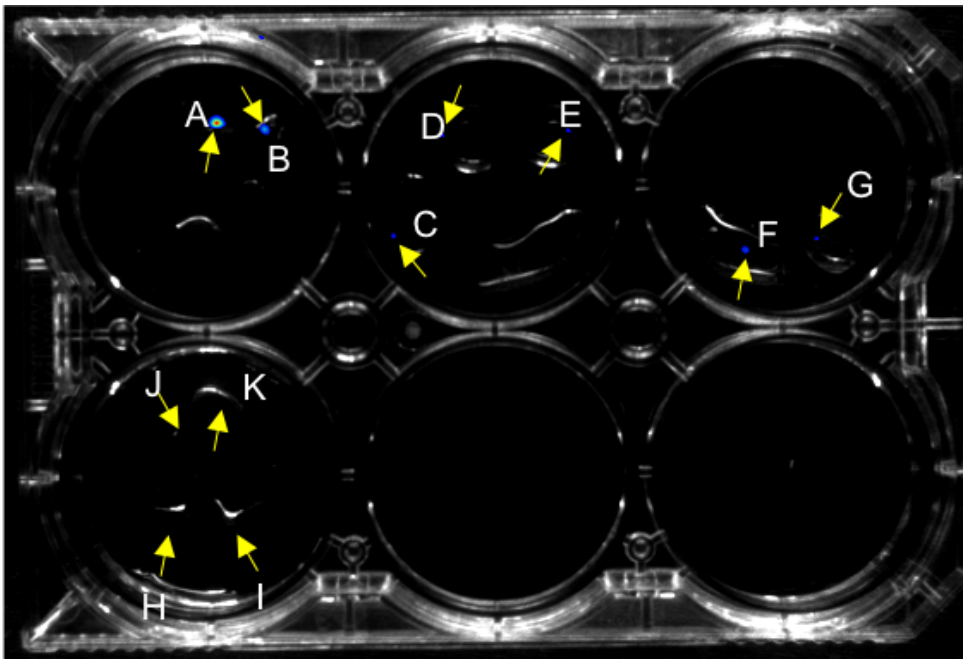

Luciferase expression

(b) F0 tg(*ren*:LUC)

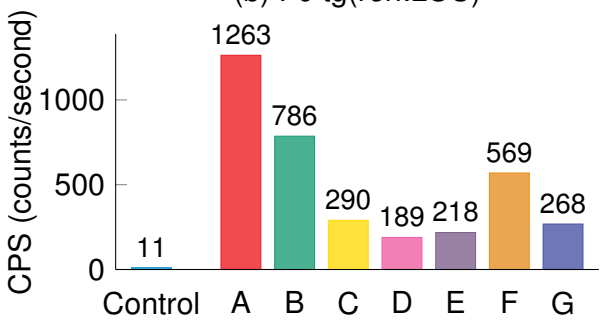

(c) F1 tg(*ren*:LUC)

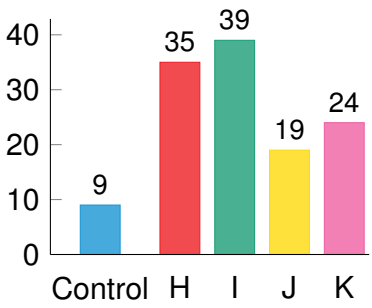

Figure 3.11 | **IVIS imaging luciferase expressing F0 and F1 larval zebrafish** Brightfield image of the 6-well plate containing mounted zebrafish, superimposed with the bioluminescent luciferase signal. Bioluminescent signal strength is represented as, red=1000+ CPS, yellow=500+ CPS, blue=100+ CPS. Fish were mounted on 1% LMP agarose. IVIS system recorded luciferase signal for 18minutes. Yellow arrows point to mounted zebrafish and corresponding letters to the luciferase expression results from the plate reader. (B) Highest expressing F0 fish, each bar represents 1 fish. Control is non luciferase expressing WIK fish. (C) F1 progeny selection for IVIS imaging.

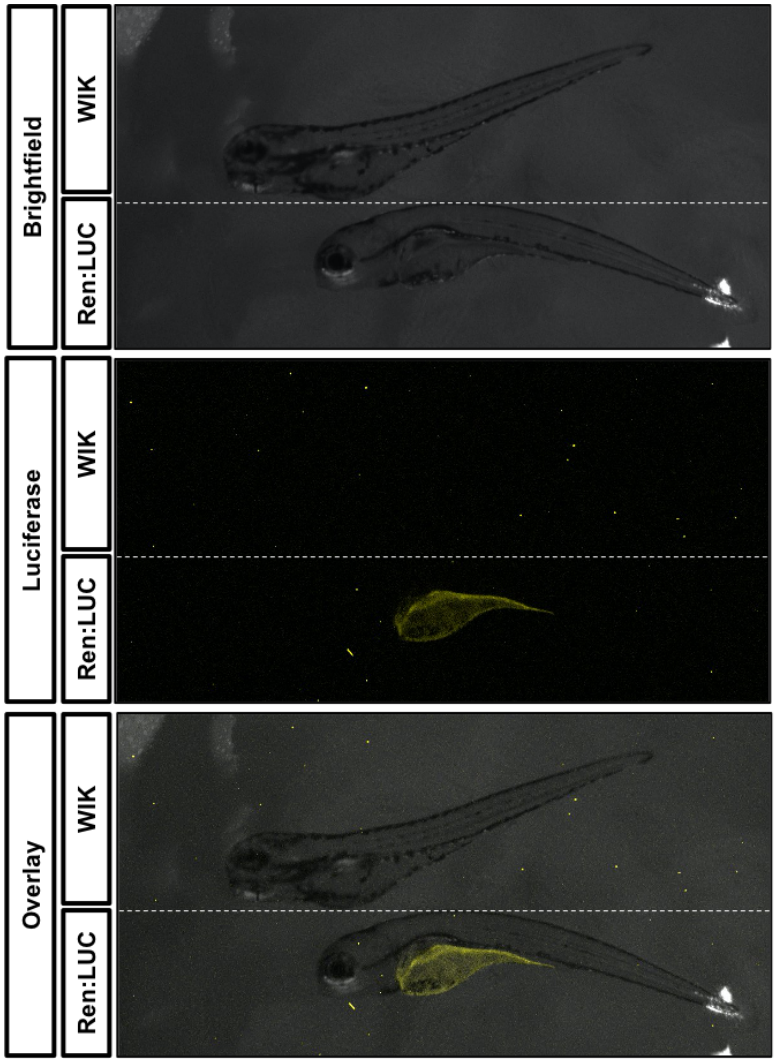

Figure 3.12 | **Luciferase expression in the yolk sac of F0 *ren*:LUC zebrafish** 4dpf WIK and F0, *ren*:LUC zebrafish mounted on 1% LMP agarose. Luciferin was applied and left to dissolve into agarose. Images acquired with 12 minutes exposure. 4dpf F0 larval fish were selected for high luciferase prior to imaging using a plate reader.

3.2.9 EGFP Expression in the Yolk Sac of F0 *ren*:LUC Zebrafish

Following the bioluminescence imaging, the founder F0 larval zebrafish were investigated for EGFP expression in the yolk sac. This was to determine whether the yolk sac expression of a transgene was a characteristic phenomenon when generating novel transgenic animals, which had not previously been noticed in F0 zebrafish.

Upon further characterisation, *cmcl2* driven EGFP expression was clearly visible in the yolk sac zebrafish with EGFP+ hearts (Figure 3.14). The EGFP expression intensity in the yolk sac varied suggesting that the luciferase signal strength should also change and be directly correlated to the EGFP signal strength. Yolk sac EGFP expression was assessed by fluorescence imaging and subsequent image analysis measuring fluorescence intensity. After imaging of the yolk sacs, the luciferase signal strength was then measured in these fish using the plate based luciferase assay. This allowed to directly investigate the correlation between the two reporters in individual fish (Figure 3.15).

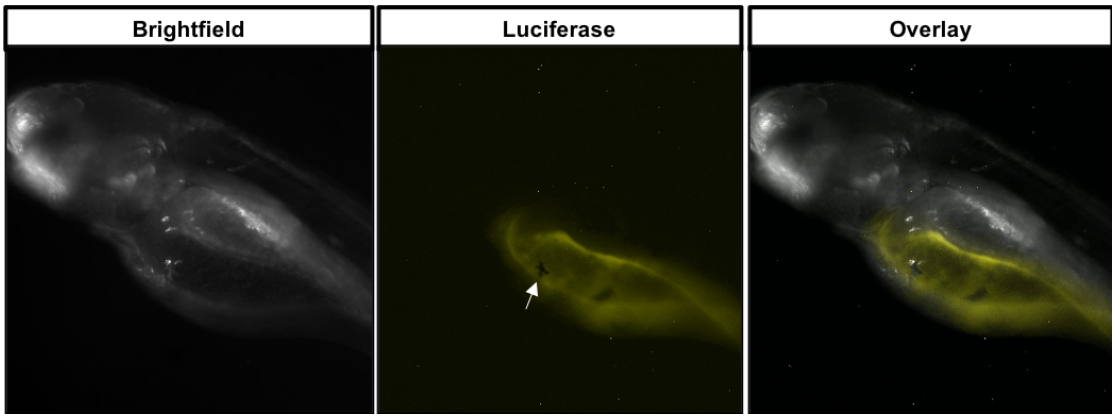

Figure 3.13 | **High magnification bioluminescent image** 10x bioluminescent image with 12 minutes exposure of single 4dpf *ren*:LUC zebrafish. No expression at AMA and expression restricted to yolk sac.

The correlation between the luciferase signal and EGFP signal was positive (R^2=0.599). However, due to the auto-fluorescence in the zebrafish larvae yolk sac, EGFP-negative yolk sacs appear positive in the assay. Visually the EGFP signal in the yolk sac is very distinctive to the autofluorescent signal (Figure 3.14). EGFP signal in the yolk sac was observable from 24hpf and up to 5dpf.

To establish whether EGFP+ yolk sac expression could be used to select against fish expressing luciferase in the yolk sac, larval F0 zebrafish were sorted for EGFP positive and EGFP negative yolk sacs. A luciferase assay was performed on single fish and the data was separated accordingly (Figure 3.16). All F0 zebrafish with positive EGFP expression in the yolk sac had a high luciferase signal. Only one F0 zebrafish with no apparent EGFP expression in the yolk sac had a high luciferase signal (556 CPS), suggesting a potential founder with high luciferase expression stemming from renin expressing cells.

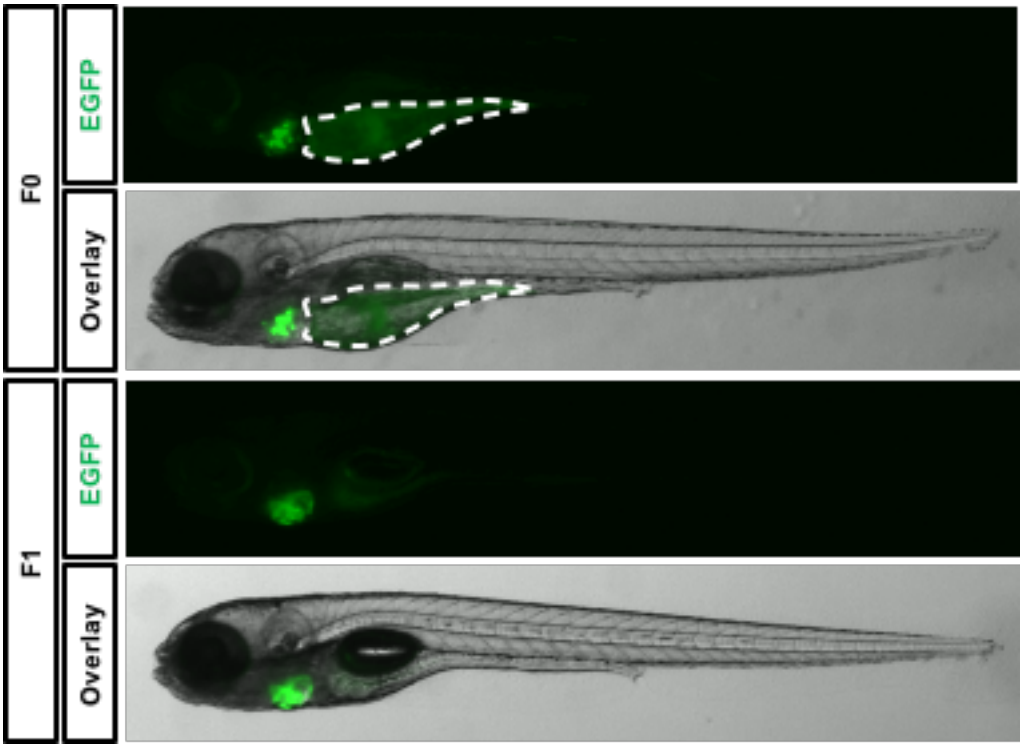

Figure 3.14 | **Yolk sac EGFP expression in larval transgenic zebrafish** Side by side comparison of 5dpf larval F0 and F1 zebrafish. Image was acquired with same gain and exposure settings. Top panel, F1 zebrafish with no mosaic EGFP expression in the heart and no visible EGFP expression in the yolk sac. Bottom panel showing mosaic expression in the heart and clear EGFP expression in the yolk sac. Yolk sac outlined by dashed white line.

3.2.10 Luciferase Expression in Adult F1 and F0 *ren*:LUC Zebrafish Tissue

The luciferase expression in F1 progeny was low at baseline and assays such as investigating the down regulation of renin were not possible in larval zebrafish. In order to determine whether the luciferase expression was low due to the limited number of renin cells during early development (<10 cells at 4dpf), a selection of adult organs were excised, homogenised and analysed using the luciferase assay. Heart, muscle and kidney of previously low-expressing F1 zebrafish were collected, analysed, and compared to equivalent organs harvested from WIK fish and F0 adults (Figure 3.17). Surprisingly, highest luciferase signal was seen in the heart of F0 fish (n=3, mean CPS=124.6) compared to F1 hearts (n=3, mean CPS=57.3) and controls (n=3, mean CPS=4.6). Kidney expression was significantly lower in

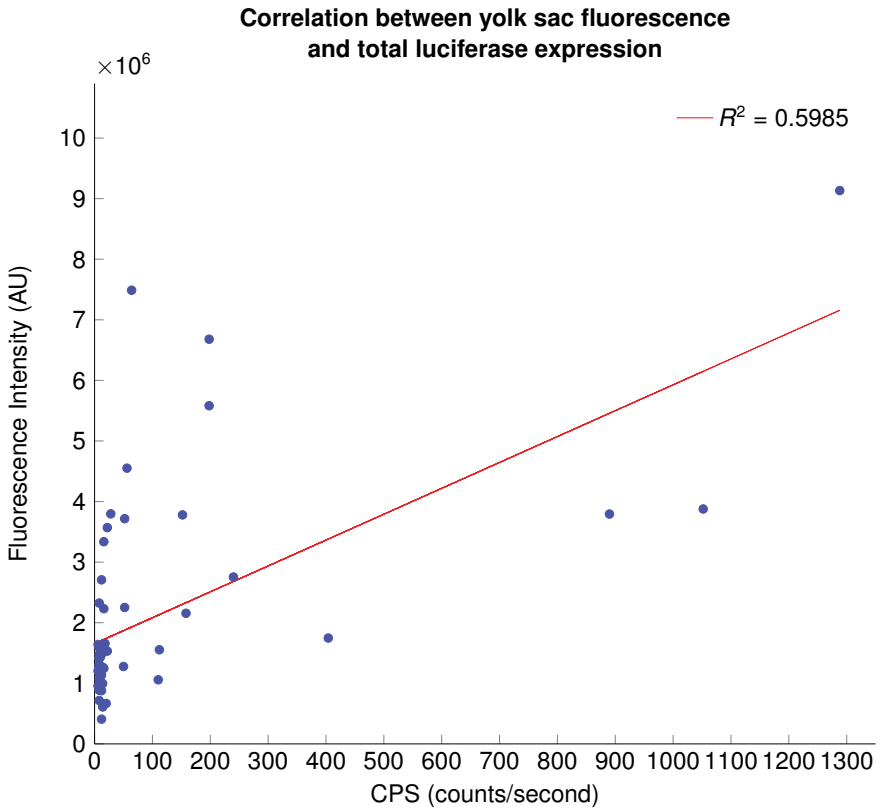

Figure 3.15 | **Luciferase expression comparison between F1 larvae** Each dot represents the measured EGFP and luciferase expression in the yolk sac of visually EGFP+ selected zebrafish (n=63). Pearsons correlation R^2=0.5985.

F0 kidney than F0 heart (n=3, CPS mean=14.6, p=<0.0001) whereas there was no significant change in the signal between the F1 heart and F1 kidney (n=3, CPS mean=48.6, p=0.9987). Luciferase in the muscle was not significantly higher in F0 (n=3, mean CPS=6) and F1 muscle (n=3, mean CPS=8) compared to WIK control (n=3, mean CPS=6). Variability in expression of the same organ of the same group was high. However, overall expression was low in all organs.

Due to the low signal in F1 progeny, which was not strong enough to be imaged, expression was investigated using RAS inhibiting compounds known to increase renin transcription. 0.1 mM of the ACE inhibitor Captopril was administered to a group of 24hpf fish (n=20). A further group received conditioned water (CW) (n=20). The fish were left in the treatment until 4dpf. There was a significant increase in renin expression in the Captopril treated group (Figure 3.18), suggesting that the luciferase signal is representative of renin gene expression.

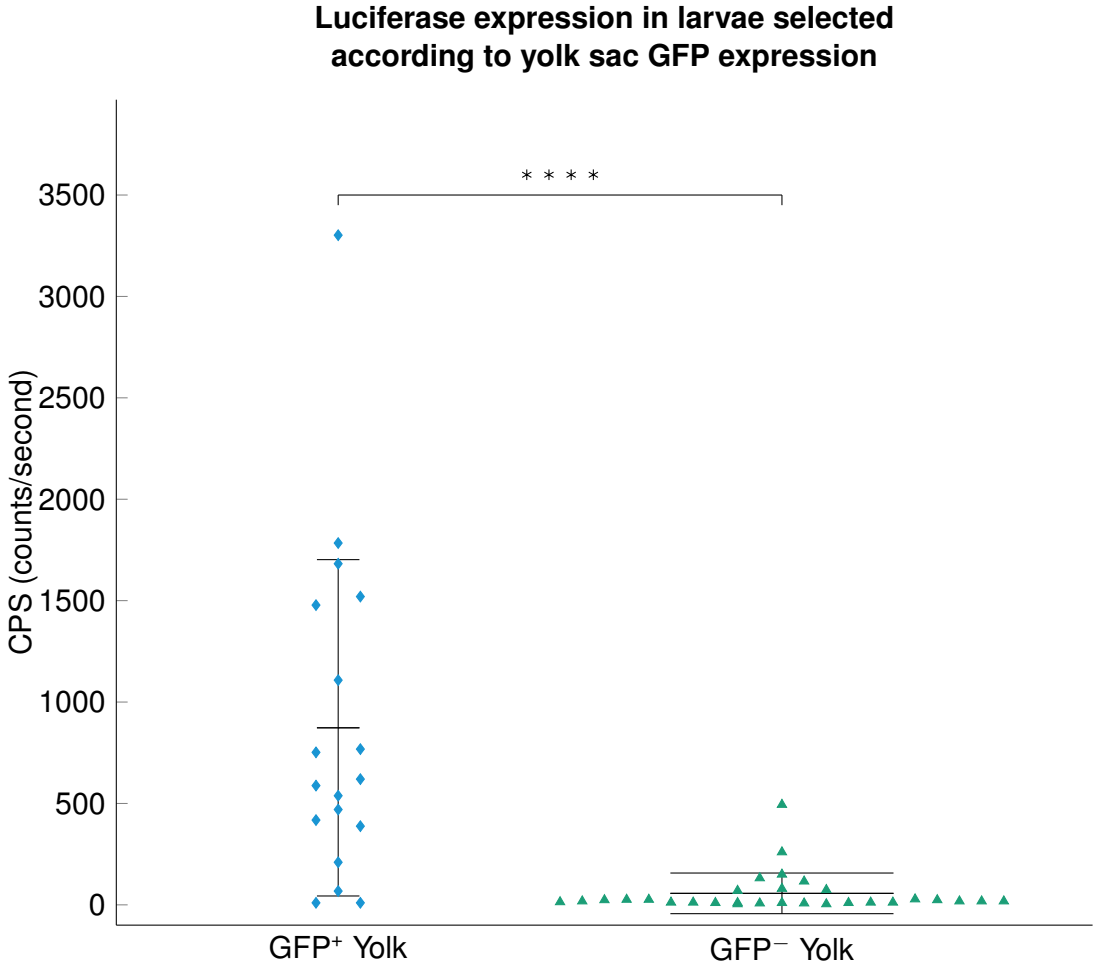

Figure 3.16 | **Whole larval luciferase expression in EGFP+ yolk sac larvae** Larvae grouped on yolk sac EGFP expression prior to luciferase assay to determine whether EGFP yolk sac expression can be used for selecting ectopic expression. Yolk sac EGFP expression group n=18 and group without GFP expression in yolk sac n=30. Data are mean ± SD. Student's t-test, ****=p<0.0001.

3.2.11 *ren*:LUC-2A-mCherry

The selection of transgenic zebrafish with strong luciferase expression in renin expressing cells had proven difficult due to the ectopic luciferase and EGFP expression in the yolk sac. The yolk sac expression signal strength masked the renin cell specific expression and prevented identification of non ectopic, strong expressing transgenic animals. In order to overcome this problem, a new zebrafish renin reporter was proposed using two, reporters for the same promoter. The two reporters were luciferase and a fluorescent reporter, to allow selection of transgenic fish using fluorescent microscopy, similarly as previously performed by Rider *et al.*. The

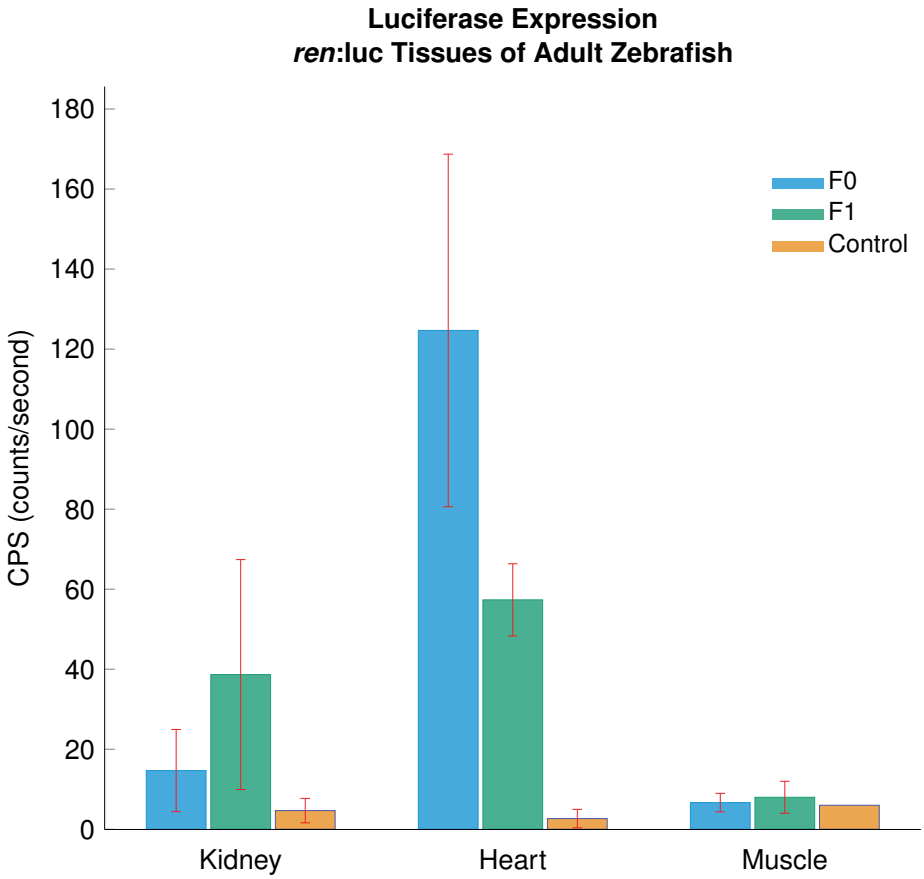

Figure 3.17 | **Luciferase expression in *ex vivo* adult organs** Adult organs were homogenised and luciferin added. 10 one second reads were recorded and the average photon count represented. Each organ n=3 from F1 *ren*:LUC fish selected for previously high luciferase expression.

plasmid was designed to have the two reporter genes separated by a 2A sequence. The 2A sequence encodes a self-cleaving peptide, which cleaves post translation, by a break of the peptide bond between the proline and glycine in the C-terminal of the 2A peptide. Similarly to the *ren*:LUC expression described above, the 6.4kb renin promoter published by Rider *et al.*, was used to drive the expression of luciferase and 2A-mCherry reporters (Figure 3.19).

For the middle entry clone the same luciferase gene cassette that was utilised in Section 3.2.2 was used. However, it was required that the stop codon was removed to permit continuous reading into a 2A-mCherry gene cassette. The stop codon was removed using a PCR cloning strategy as described in the methods in Section 2.3.7. The validity of the middle entry clone with the removal of the stop

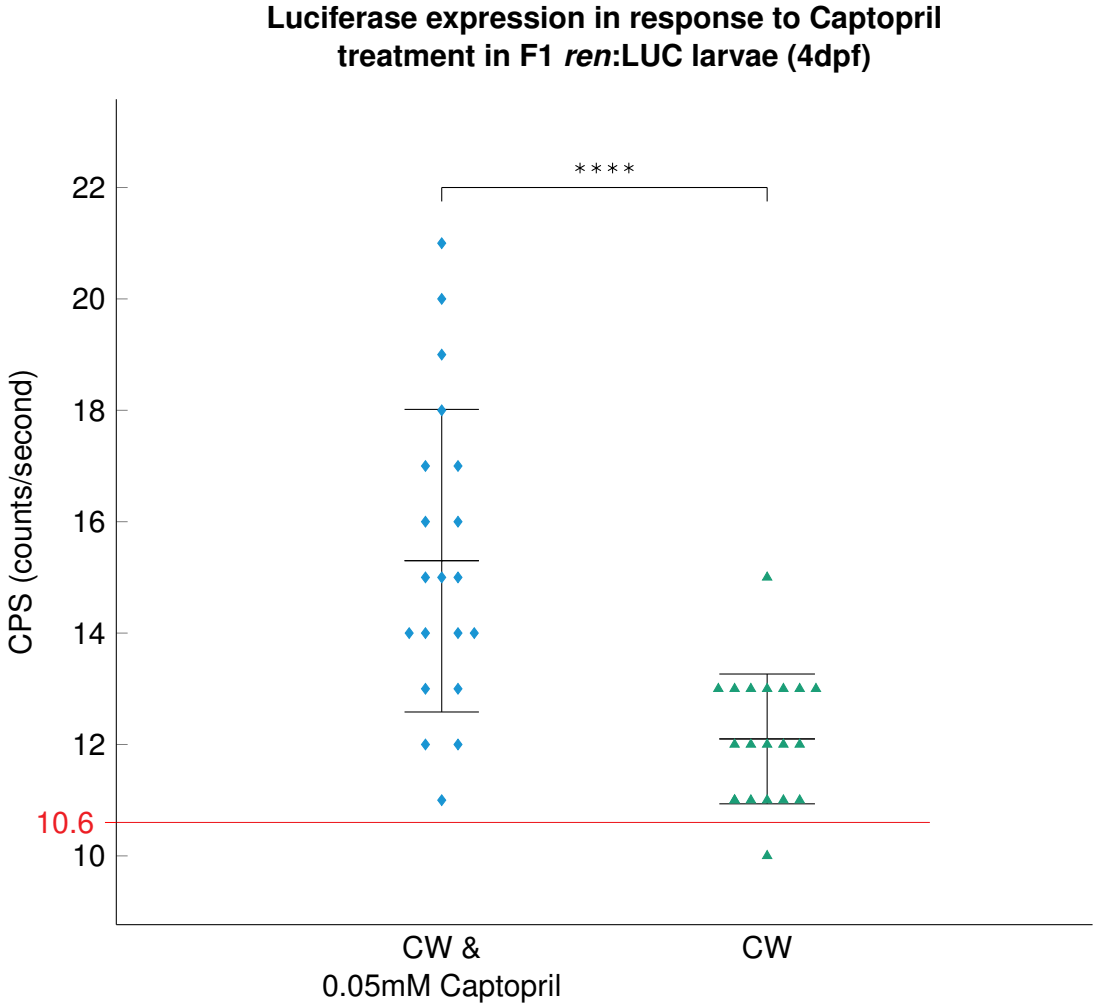

Figure 3.18 | **Luciferase expression in response to Captopril treatment in F1 *ren*:LUC larvae (4dpf)** F1 fish from the same founder were grouped into Captopril treated group (n=20) and conditioned water group (n=20). Treatment was administered 24hpf and luciferase expression was measured 4dpf. Control is CW with Captopril to ensure no bioluminescent background activity of Captopril. Data are mean ± SD. Student's t-test ****=p<0.0001.

codon was performed by restriction digest and subsequent DNA electrophoresis (Figure 3.20). Only clones 1 and 5 showed correct band sizes and clone 1 was taken forward as the final middle entry clone.

The 3' p3E-2A-mCherrypA was acquired through Addgene. Although the pDest-Tol2CG2 destination vector has many advantages, the intensity of the EGFP signal from the heart can interfere with high-resolution imaging of the zebrafish kidney. A new destination vector was chosen avoid this issue. The pDestTol2pACryCFP uses the zebrafish crystallin beta B promoter, which is expressed in the eye of zebrafish,

driving the ECFP as a marker for successful transgenesis. Using the 3' entry clone p3E-2A-mCherrypA, the 5' 4.6kb *ren* promoter, and the luciferase gene cassette as middle entry clone and the pDestTol2pACryCFP destination vector, LR recombination was performed from which six resultant clones were randomly picked and analysed by restriction digest (Figure 3.21). Only clones 1 and 4 gave the correct fragment sizes (HindIII=12470, 2020, 789; EcoRV=10670, 4609; NCOI=13457, 1822; NOTI=15279) and clone 1 was selected to be injected, together with transposase mRNA, to generate the new transgenic zebrafish line.

Despite verification of the plasmid and successful expression of the transgenesis marker, no mCherry expression was seen along the AMA in any fish. MCherry and ECFP were visible in the yolk sac and luciferase expression was also detectable. Despite several rounds of injections no expression could be seen at the AMA. However, the continuous expression of mCherry and ECFP in the yolk sac of F0 larval fish further suggest that ectopic expression in the yolk sac is a phenomenon occurring when generating novel transgenic zebrafish (Figure 3.22). This is unreported and may influence various studies performing experiments of F0 fish. This chapter demonstrated that it is crucial to not disregard this phenomenon and consider it when planning the generation of any future novel transgenic zebrafish lines.

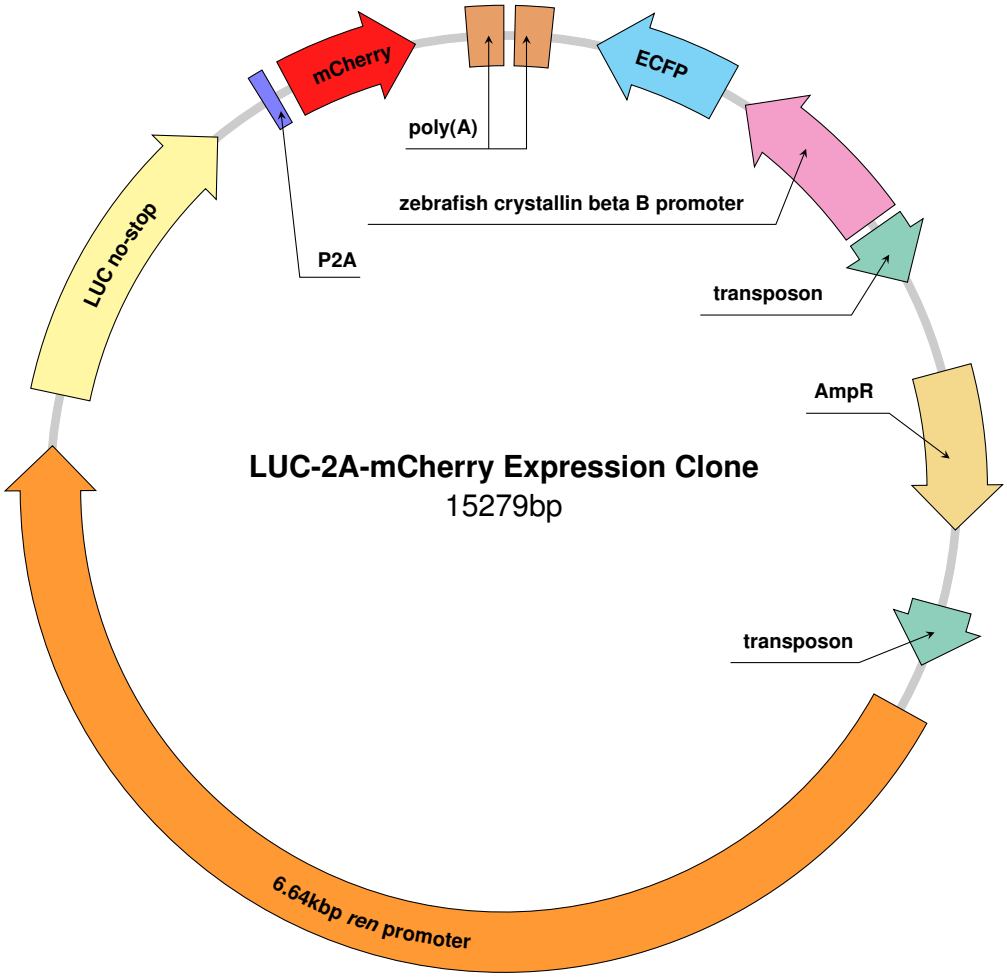

Figure 3.19 | **Plasmid map of the luciferase-2A-mCherry expression clone** Luciferase-2a-mCherry expression clone 15279bp in size. Previously published 6.64kb *ren* promoter driving luciferase with removed stop codon to allow continuous reading over the P2A into the fluorescent mCherry reporter. The backbone contains a zebrafish crystallin beta promoter driving ECFP as a fluorescent eye marker for transgenesis.

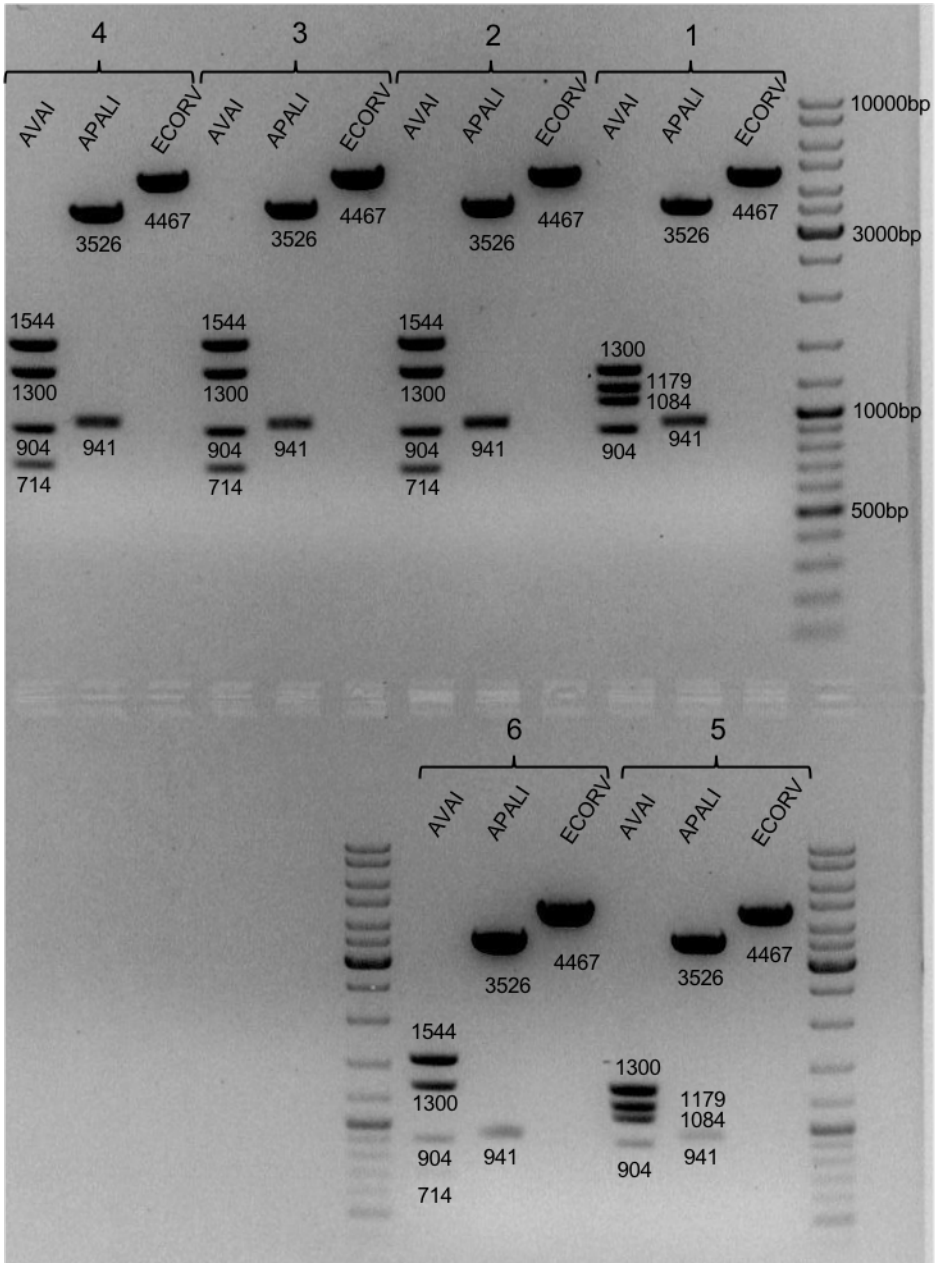

Figure 3.20 | **Restriction digest analysis of the pETR-Luciferase-NoStop clone** Restriction enzyme digest and subsequen DNA gel electrophoresis of the pETR-Luciferase-NoStop clone. 6 clones were selected and DNA extracted. Plasmid DNA was analysed by restriction enzyme digestion using the restriction enzymes PstI, NcoI, and BsaI.

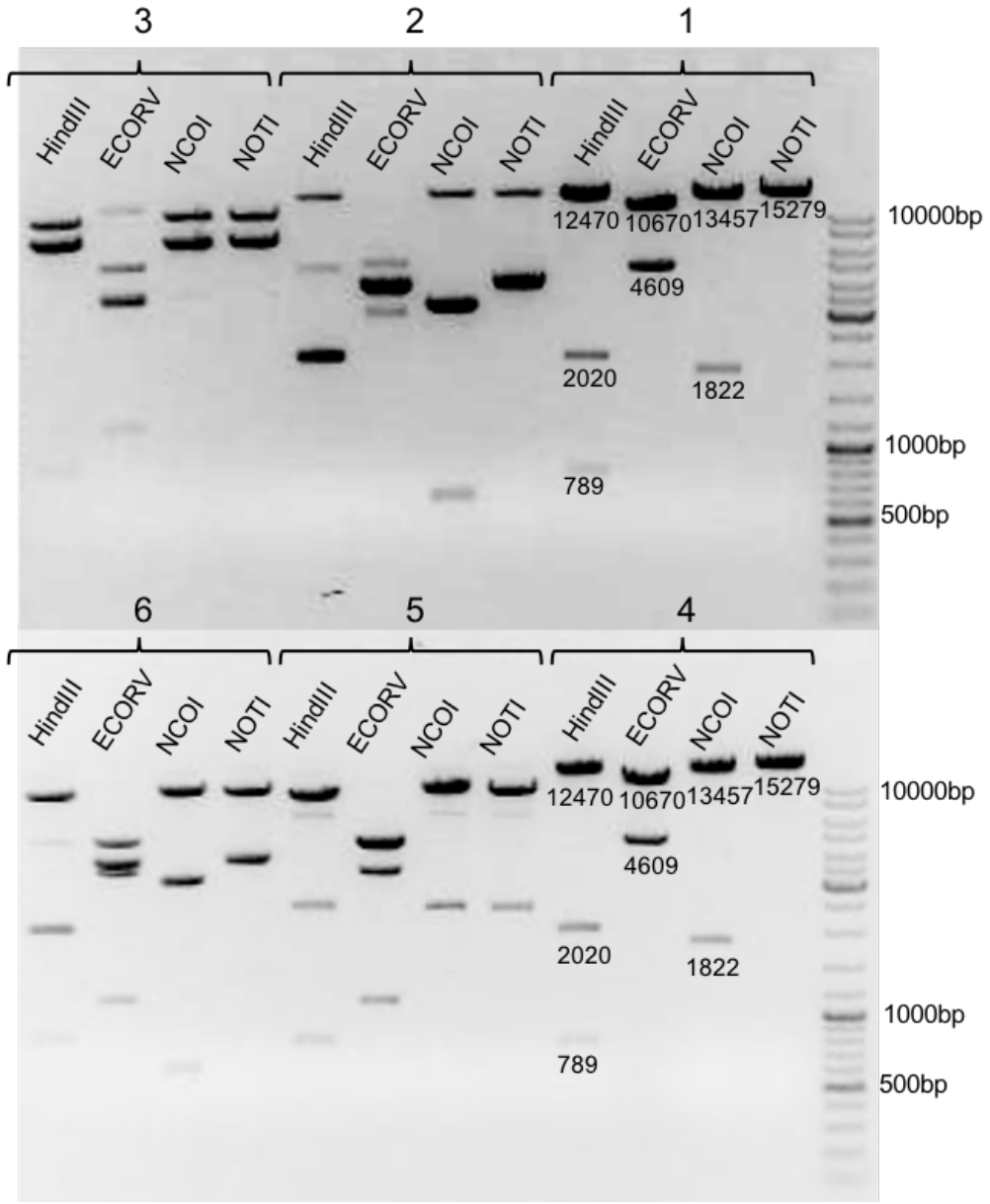

Figure 3.21 | **Restriction digest analysis of the *ren*:LUC-2A-mCherry entry clone** Restriction enzyme digestion and subsequent DNA gel electrophoresis of 6 single transformed colonies post LR reaction. DNA from all colonies was digested with the following restriction enzymes: NotI, NcoI, EcoRV, and HindIII. Expected band sizes are labelled below the bands of clones 1 and 4, which gave the correct sizes.

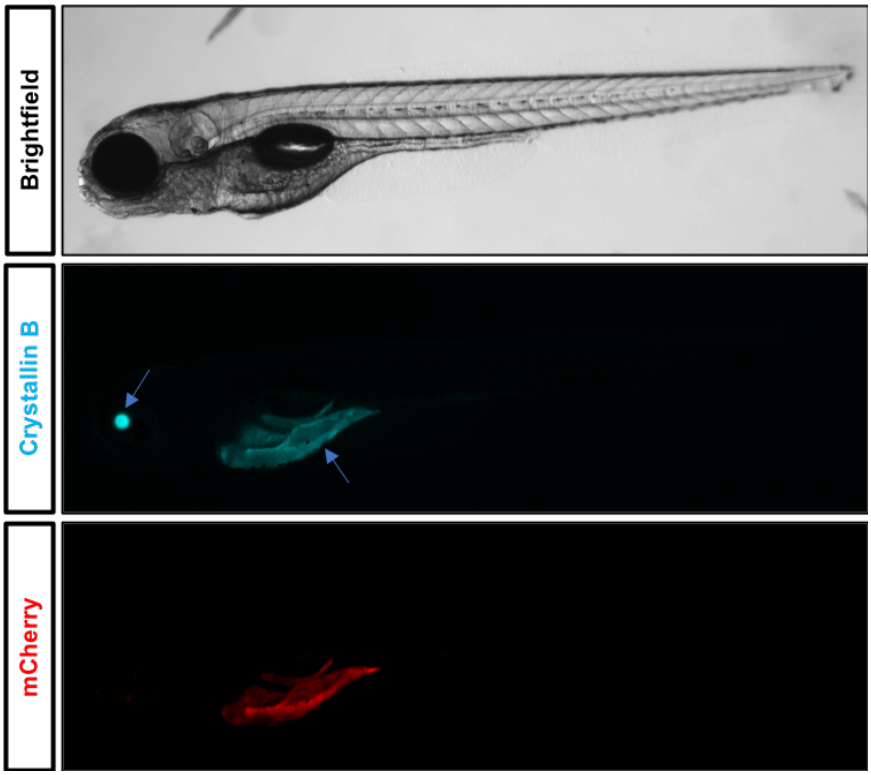

Figure 3.22 | **Ectopic yolk sac expression of *ren*:LUC-2A-mCherry** Ectopic expression of crystallin B and renin reporter fluorophores in the yolk sac of an F0 *ren*:LUC-2A-mCherry zebrafish. Crystallin blue was also expressed in the eye as a transgenic marker. No mCherry expression was visible at the AMA.

3.3 Discussion

In this chapter, I describe the generation of novel zebrafish renin reporter lines. The bioluminescent reporter, firefly luciferase was used as a surrogate marker for renin expression. Compared to fluorescent reporters, luciferase has a short half-life allowing detection of rapid changes in gene expression. Furthermore, it has a high sensitivity, permitting for accurate quantitative studies of gene expression. The novel transgenic lines were designed using a previously characterised renin promoter sequence driving the reporter gene coding for the bioluminescent reporter, firefly luciferase.

3.3.1 Circadian Control of Renin

Circadian rhythm studies in zebrafish have predominantly focused on the characterisation of behavioural and physiological rhythms and the expression patterns of the zebrafish homologous clock genes [153]. The genetic approach to elucidating circadian clock mechanisms have been particularly successful in zebrafish [154]. These studies have demonstrated the presence of clock genes within the zebrafish kidney. However, no previous attempts have been made trying to elucidate whether zebrafish renin is controlled by a circadian rhythm. Whole kidneys were excised from adult zebrafish at 4 different time points corresponding to early morning, midday, evening and middle of the night. Subsequent RNA extraction and QPCR analysis was performed to investigate the relative gene expression of the clock genes and whether renin expression varied throughout 24 hours. Zebrafish undergo a resting phase during the dark-cycle and if zebrafish renin is regulated by a circadian rhythm, a similar pattern to that observed in diurnal mammals was expected [155, 156]. Although the expression levels of the circadian clock genes in the kidney were conformant with previous studies [125, 157], no significant differences were seen in renin expression. However, renin expression at all time points, apart from 3PM, had large variation. Overall, renin expression appeared to have a negative trend with highest expression at 9AM and lowest at 5AM. The QPCR analysis, alongside the time points were not sensitive enough to permit observation of these differences. Hence, the generation of a novel transgenic renin zebrafish line, using a highly-sensitive, real-time time bioluminescent reporter was proposed. Furthermore, the bioluminescent zebrafish reporter would permit investigation of renin expression dynamics and earlier temporal expression than the

previous tg(*ren*:RFP-LifeAct) zebrafish line and further the research on renin and the RAS in zebrafish.

3.3.2 Selecting F0 Founder Fish

Founder fish are commonly selected by choosing fish with the highest reporter expression [152]. This is generally indicative that the transgene has integrated into a permissive site in the genome. However, it is important to remember that the transposase can continuously integrate the tol2 containing transgene causing multiple insertion sites. Luciferase expression in F0 founders was highly variable, which was conformant with reports previously made by Rider *et al.*, using the same renin promoter sequence for the generation of the tg(*ren*:RFP-LifeAct) transgenic zebrafish line. 20% of all injected fish expressed EGFP and luciferase >100 CPS, which is the expected success rate of the tol2 system. Hence, all fish with a signal higher than 100CPS were selected as founder fish. In order to identify whether transgenic animals have multiple insertion sites, and are capable of gremline transmission of the transgene, they are outcrossed to wild-type zebrafish. Progeny from the outcross are analysed for mendelian ratio according to the *cmlc2* driven EGFP expression in the heart.

3.3.3 F1 Progeny Luciferase Expression

Luciferase screening of progeny from previously highly expressing founder demonstrated a dramatic loss of luciferase signal, with no change in EGFP expression in the heart. Germline transmission of the transgene was validated by PCR, demonstrating the presence of both reporter genes in the F1 generation. As the luciferase assay is essentially an output of photons counted over a set time, acquisition time was increased to permit detection of low luciferase signals. Although just above background (>10CPS), a positive signal was detectable in F1 progeny earliest at 4dpf. This was surprising as renin gene expression is reported to commence as early as 24hpf and compared to fluorescent proteins, luciferase has been shown to be an active enzyme after translation of its mRNA, not requiring any lengthy protein folding and should be detectable sooner. To demonstrate that the luciferase expression was reporting for renin promoter activity in the F1 progeny, Captopril was administered to larval zebrafish. Administration of Captopril has been previously shown to increase renin gene expression and a significant difference was

observed when comparing luciferase signals from Captopril versus non Captopril treated controls [47, 64]. However, the expression was still very low, potentially limiting studying compounds that have a negative regulatory role on renin expression. In order to increase the sensitivity of the assay, Nanoluc luciferase could have been used instead of firefly luciferase. Nanoluc luciferase recognises a structurally enhanced substrate, furimazine, which produces a signal lasting for up to two hours with a luminescence 100 fold brighter compared to the commonly used firefly luciferase [158].

3.3.4 Yolk Sac Luciferase Expression

To determine the origin of the strong luciferase signal in the F0 founder fish and the signal in the F1 progeny, bioluminescence imaging techniques were applied. The bioluminescent reaction produces are very small amount of light, which requires highly sensitive supercooled cameras to permit detection. The IVIS is specialised for imaging rodents, by aquiring a black and white image prior to a long-time exposure to detect the luciferase signal. The luciferase signal is then superimposed on to the black and white image, permitting localisation of the signal. However, the spatial resolution is limited. The IVIS demonstrated that the F1 progeny, with luciferase signals ranging between 19-39 CPS, are unsuitable for bioluminescence imaging. F0 founders however, had a strong signal but the localisation was not possible due to the low spatial resolution. Hence, F0 with a luciferase signal higher than 1000 CPS were selected and a house-build bioluminescent microscopy system was utilised, permitting a higher spatial resolution. The imaging revealed luciferase expression in the yolk sac of all luciferase expressing F0 fish. Furthermore, upon closer investigation, EGFP was also expressed in the yolk sac of zebrafish. *Cmlc2* and renin are both not expressed in the cells of the yolk sac and hence the origin of this is believed to be ectopic. Moreover, this suggests that generation of transgenic zebrafish leads to ectopic expression of the reporters in the yolk sac. This phenomenon is unreported. In fact only one previous study has described this phenomenon, by investigating whether the injection volume used for transgene injection was the cause for the transient yolk sac expression [159]. Although demonstrating that the injection volume did not affect the transgene expression in the cells of the yolk sac, it was demonstrated that the the high transgene expression is located in the yolk syncytial layer (YSL), containing large polyploid nuclei. The YSL is a peripheral cellular syncytium, surrounding the lipid and protein rich

yolk sac core. The main function of the YSL is to export amino acids and hydrolyse lipids as well as synthesise lipoproteins to transport lipids to the embryo until it is able to feed independently [160].

3.3.5 *ren*:LUC-2A-mCherry

As the strong luciferase signal from the yolk sac masks potential signals stemming from renin cells, a new transgene was generated using two reporters, driven by the same 6.4kb renin promoter sequence. The two reporters are separated by the '2A' self cleaving peptide sequence. The novel transgenic zebrafish line permitted selection of tg(*ren*:LUC-2A-mCherry) fish visually for the strongest mCherry signal originating from renin expressing cells. After several rounds of breeding and establishing a homozygous, stable transgenic zebrafish line, quantitative renin gene expression analysis could then be performed without interference from ectopic transgene expression. Interestingly, confirming the above mentioned observations, all three reporters were expressed in the yolk sac of larval zebrafish. However, despite *crystallinB*:ECFP transgene expression in the eyes of zebrafish, no transgene expression was observed in renin expressing cells. Further DNA sequencing validated the injected plasmid as well as genotyping did not indicate any abnormalities. Successful co-expression and functionality two reporter proteins was demonstrated by the expression of mCherry as well as luciferase in the yolk sac of F0 founder fish. Studies have shown that the 2A system is the ideal strategy for co-expressing multiple reporter proteins *in vivo*. There have however, been reports of fluorescent proteins such as EGFP interfering with the 2A cleavage mechanism [161]. Although this has not been investigated with reporter proteins such as luciferase or mCherry, if luciferase were to interfere with the 2A skipping mechanism, the amount of fluorescent protein generated in renin expressing cells in larval fish may not be sufficient to be detected. Unfortunately, adult tg(*ren*:LUC-2A-mCherry) fish were not investigated due to the lack of signal in larval zebrafish which were subsequently terminated.

3.3.6 Luciferase Expression in Adult Tissues

The chapter predominantly focuses on investigating luciferase expression in larval zebrafish. Zebrafish commence self-feeding after 5dpf, at which point the yolk sac has been fully metabolised. To determine whether adult zebrafish, which were

perviously wrongfully selected for yolk sac expression had luciferase expression in the kidney, the kidney alongside several control organs (heart and muscle) were excised from adult zebrafish (>3 months of age) and luciferase expression was compared to wild-type equivalent control organs. Higher luciferase expression was observed in the F1 kidneys compared to kidneys from F0 founder fish. Founder fish are commonly subject to mosaic expression, where not all cells contain a copy of the transgene. This can result in not all renin expressing cells expressing the transgene and may explain the lower, more varied luciferase expression. Most surprisingly was the high luciferase expression measured in the heart of both, F1 and F0 tg(*ren*:LUC) zebrafish. Although generally low expressing, compared to the yolk sac signal from F0 fish, a significant difference is observed compared to the wild-type control. Studies have demonstrated that renin mRNA is expressed in the heart at low levels, however most cardiac renin is believed have derived from the kidney [162,163,164]. Further, highly sensitive studies are required to validate and elucidate the luciferase signal in the heart.

Although the main aim of this chapter, to generate a luciferase renin reporter zebrafish line was not achieved, the chapter has highlighted crucial points which have to be regarded when generating a novel transgenic zebrafish line. Generation of novel transgenic reporters transiently express fluorescent reporters in the yolk sac, which can have potential misleading effects this could have on quantitative comparative analyses. This is observation will have a crucial impact on the generation of future transgenic lines utilising quantitative reporters such as luciferase.

Chapter 4

Design of a Zebrafish Renin FRET Probe

4.1 Introduction

The first quenched FRET probe to investigate the dynamics of enzymatic activity was a fluorescently quenched peptide substrate for ACE [165]. However, the FRET probe showed poor sensitivity and high background fluorescence *in vitro* when used on human plasma. More promising FRET probes were developed subsequently by Chagas *et al.* which permitted the study of various endopeptidases, including human renin *in vitro* [166, 167]. Imaging FRET probes to study the activity of renin was performed by Peti-Peterdi *et al.*, who have developed a dissection and perfusion technique of glomeruli to image the real-time release of renin using commercially available FRET probes [129, 168].

The basis of designing a FRET probe for zebrafish renin is understanding the substrate, angiotensinogen, which renin recognises and cleaves. The amino acid sequence for zebrafish angiotensinogen is known, however there have been no reports of measuring angiotensinogen and its derivatives, AngI and AngII in zebrafish tissues. By comparing the zebrafish angiotensinogen amino acid sequence with the well annotated mammalian sequences, I was able to determine the renin cleavage site on zebrafish angiotensinogen and the resulting amino acid sequence for AngI resulting from the cleavage. Removal of 2 amino acids from the N-terminus of AngI results in the 8 amino acid, AngII sequence. The amino acids sequences for AngI and AngII are short and the peptides are known not to contain any complicated secondary structures making it possible to synthesise these peptides by SPPS.

In collaboration with Attoquant Diagnostics, which specialises in the measurement of angiotensins in various species using mass spectrometry, we designed an experiment that could measure concentrations of AngI and AngII in the zebrafish kidney and serum. The mass spectrometry assay run by Attoquant Diagnostics requires the mass spectrometry detectors to be primed with exogenous pure peptide, which is to be measured. The assay was used to measure the AngI and AngII concentrations in serum and kidney of zebrafish treated with Captopril against an untreated control group. By priming the mass spectrometers with the synthesised AngI and AngII peptides and observing a dynamic change of AngII in the zebrafish tissues in response to Captopril, the assay would further validate the the identified sequences for AngI and AngII.

Having identified the substrate for zebrafish renin permitted development of a molecular probe to measure and image renin activity in the zebrafish, real-time and

in vivo. A fluorescein derivative, namely 5(6)-carboxyfluorescein was attached to the amino-terminus of the synthesised tetradecapeptide amino acid angiotensinonogen sequence. A for, 5(6)-carboxyfluorescein commonly used quencher, Methyl Red was attached to the C-terminus of the renin substrate, inactivating fluorescent signals from the un-cleaved probe. In this chapter I will be discussing the synthesis of the probe, and verification of its specificity using various zebrafish models. Furthermore I will be discussing the design and expression of a plasmid to produce the first recombinant zebrafish renin.

4.2 Results

4.2.1 Zebrafish Ang1-14

The zebrafish angiotensinogen sequence shares a low amino acid sequence homology to that of mouse (28.4%), rat (29%) and human (28.1%) [169]. Previous reports have defined the mammalian tetradeca-peptide sequence and recognised that the His-Pro-Phe motif on the N-terminal side of angiotensinogen is a crucial determinant of renin substrate specificity [37,170]. By comparing the angiotensinogen protein sequences of mouse, rat and human to that of the zebrafish, the tetradeca-peptide sequence is identifiable (Figure 4.1). The zebrafish tetradeca-peptide sequence only shares 50% identity with that of humans, rats and mice. Most notable are the differences of the 9th and 11th amino acid, however there is conservation of the His-Pro-Phe sequence. In the angiotensinogen amino acid sequence, renin cleaves angiotensinogen between the 10th (Leu) and 11th (Phe) amino acid generating the decapeptide AngI, which is further cleaved between the 8th (The) and 9th (Asn) amino acid by ACE. From the sequence alignment, the 10 amino acids on the N-terminus of the tetradecapeptide form AngI and the 8 amino acids on the N-terminus form AngII. These sequences were synthesised using SPPS.

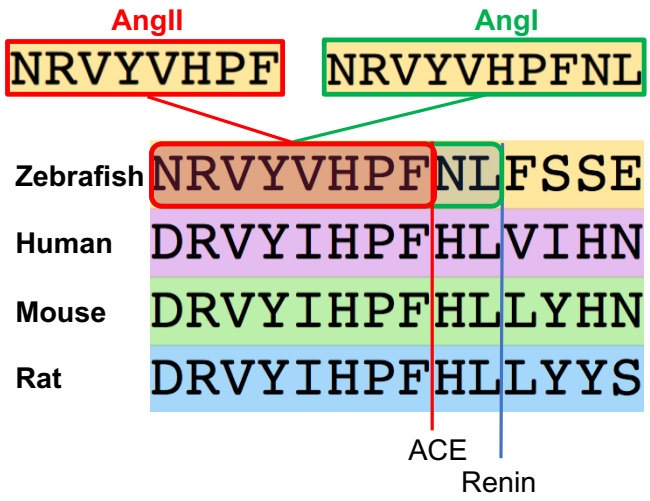

Figure 4.1 | **Renin substrate sequence homology** Comparison of the tetradeca angiotensinogen sequence recognised and cleaved by renin with highlighted, AngI and AngII sequence homology renin cleavage and ACE cleavage site of AngI in Human, Rat and Mice and the predicted renin cleavage site in Zebrafish.

4.2.2 AngI Synthesis

AngI was synthesised using the 10 amino acid sequence defined in Section 4.2.1. AngI is the product of the renin cleavage of the N-terminus of angiotensinogen. AngI is biologically inactive and acts as a substrate for ACE. The peptide was synthesised using SPPS on a Chloro-(2'-chloro)trityl polystyrene resin (Figure 4.2). The AngI peptide was purified using reverse phase HPLC and analysed using analytical HPLC and MALDI-TOF MS (Figure 4.3 & 4.4). Calculated mass for the peptide was 1258.45 Da and after reverse phase HPLC a single peptide was detected using the ELS detector by analytical HPLC, indicating a pure compound.

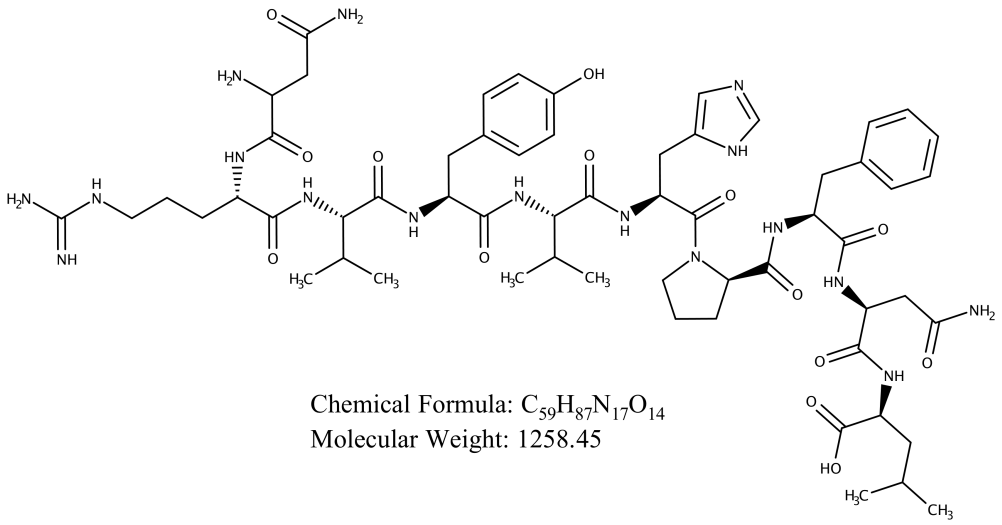

Figure 4.2 | **AngI structure** Structure of the synthesised AngI peptide.

4.2.3 AngII Synthesis

AngII was synthesised from the identified 8 amino acid sequence in Section 4.2.1. AngI is the product of the ACE cleavage of the N-terminus of AngII. The peptide was synthesised on a Chloro-(2'-chloro)trityl polystyrene resin (Figure 4.5). The AngII peptide was purified using reverse phase HPLC and analysed using analytical HPLC and MALDI-TOF MS (Figure 4.6 & 4.7).

4.2.4 Mass Spectrometry Calibration

The synthesis of AngI and AngII permitted calibration of mass spectrometers to identify and measure the concentration of the endogenous AngI and AngII in ze-

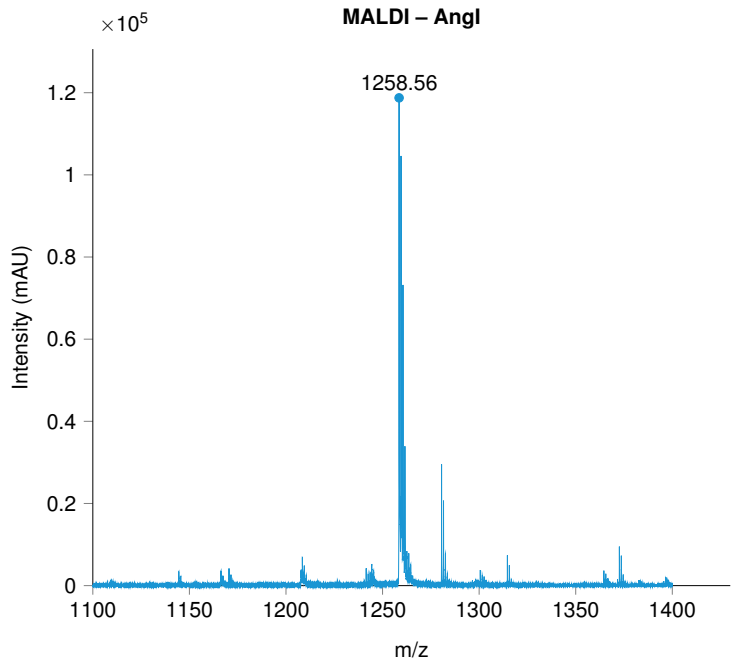

Figure 4.3 | **AngI Peptide Synthesis** MALDI MS trace and mass calculated for $C_{59}H_{87}N_{17}O_{14}$ 1258.5, found 1258.56.

brafish tissues. Attoquant Diagnostics GmbH provides a service to measure angiotensins within tissues using a mass spectrometry assay. To ensure specific detection of the compounds of interest, the synthesised peptides are titrated in the mass spectrometry buffer and subsequently measured (Figures 4.8 & 4.9) (Mass Spectrometry Data Provided by Attoquant Diagnostics).

4.2.5 AngI and AngII Measurement in Zebrafish Kidney Tissue

375 adult fish were treated with 0.05 mM Captopril over 7 days to block the ACE mediated conversion of AngI to AngII. As a control 300 fish were housed in conditioned water (CW) for 7 days without Captopril. After 7 days of treatment, fish kidneys and serum were extracted. The mass spectrometry assay required 100 µl of serum and 50 mg tissue to permit accurate measurements. The number of fish used, allowed for 5 AngI and AngII measurements in kidney tissue and 3 measurements in serum. The mean AngI concentration in kidney tissue of CW fish was 17.4 ng/g (n=5) and was non-significantly reduced (p=0.0768) in Captopril treated fish (6.996 ng/g, n=5), which was surprising as commonly an increase in AngI is observed in response to ACE inhibition (Figure 4.10). However, a dramatic de-

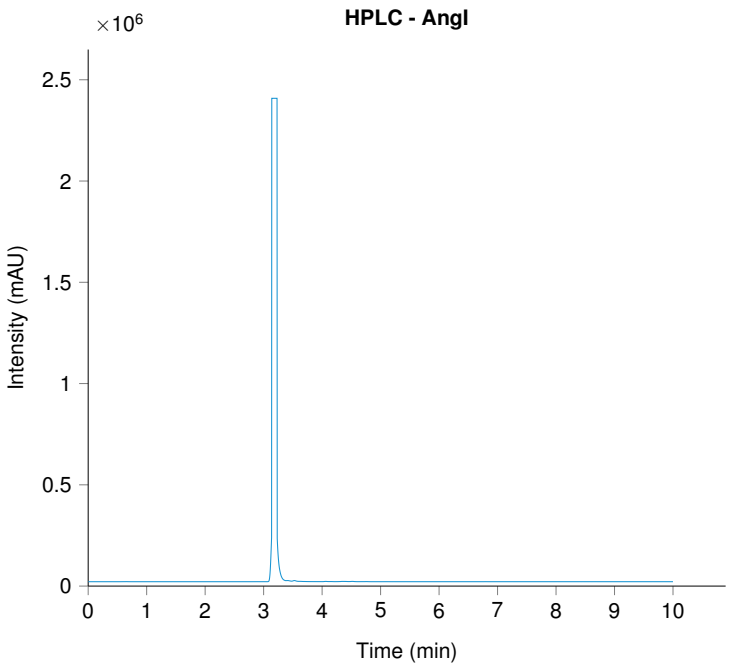

Figure 4.4 | **Analytical HPLC of AngI** Analytical HPLC trace of AngI with a single signal at 3.1 minutes.

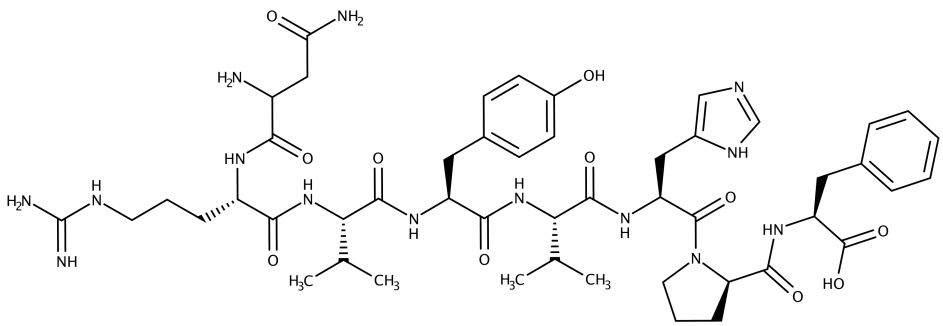

Chemical Formula: $C_{49}H_{70}N_{14}O_{11}$
Molecular Weight: 1031.19

Figure 4.5 | **AngII structure** Structure of the by solid phase peptide synthesis synthesised AngII peptide.

crease of AngII concentration was seen in zebrafish kidney tissue from 330.62 pg/g to 5.56 pg/g in the Captopril treated group ($p<0.0001$), suggesting Captopril being highly effective in inhibiting zebrafish ACE.

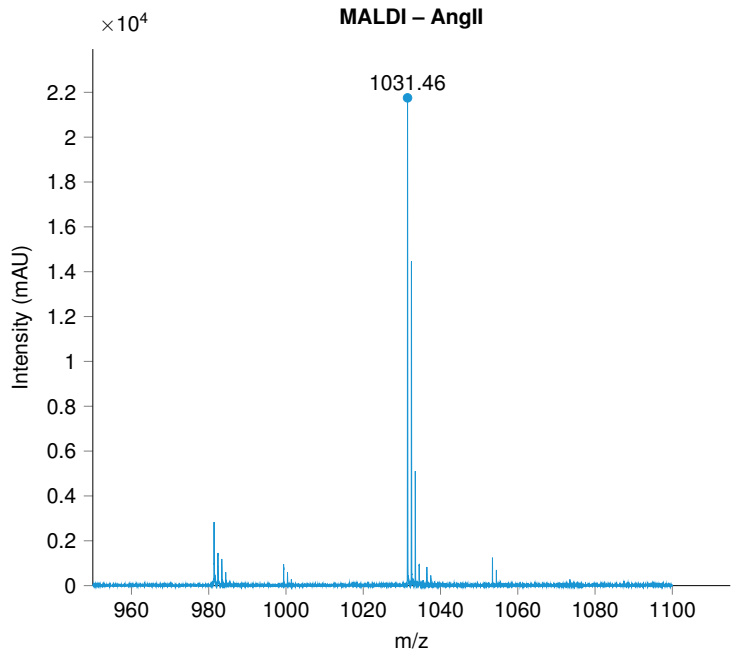

Figure 4.6 | **AngII Peptide Synthesis** MALDI MS trace for AngI, mass calculated for $C_{49}H_{70}N_{14}O_{11}$ 1031.2, found 1031.46.

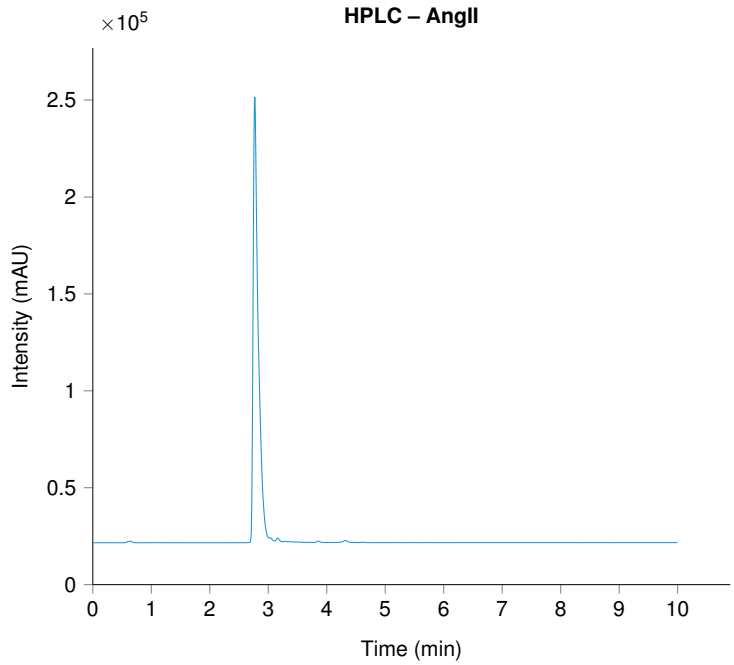

Figure 4.7 | **Analytical HPLC of AngII** Analytical HPLC trace of AngII with a single signal at 2.9 minutes.

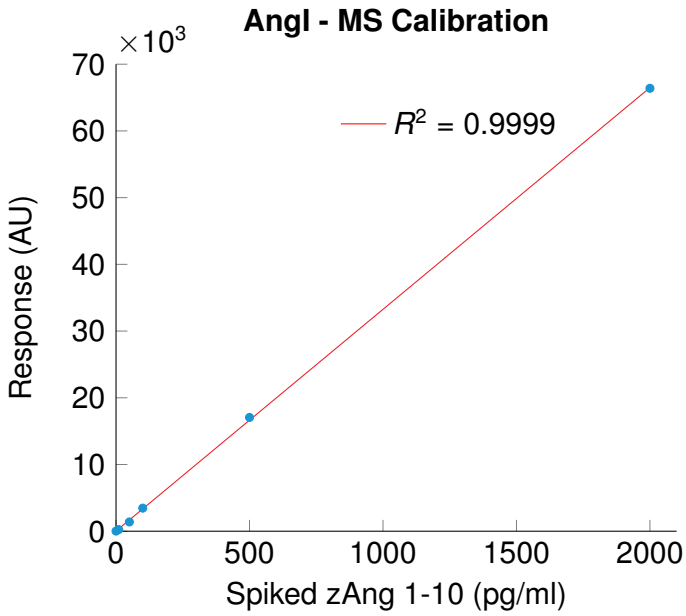

Figure 4.8 | **AngI mass spectrometry calibration** Calibration of mass spectrometer using synthesised AngI in mass spectrometry assay buffer. R^2=0.9999.

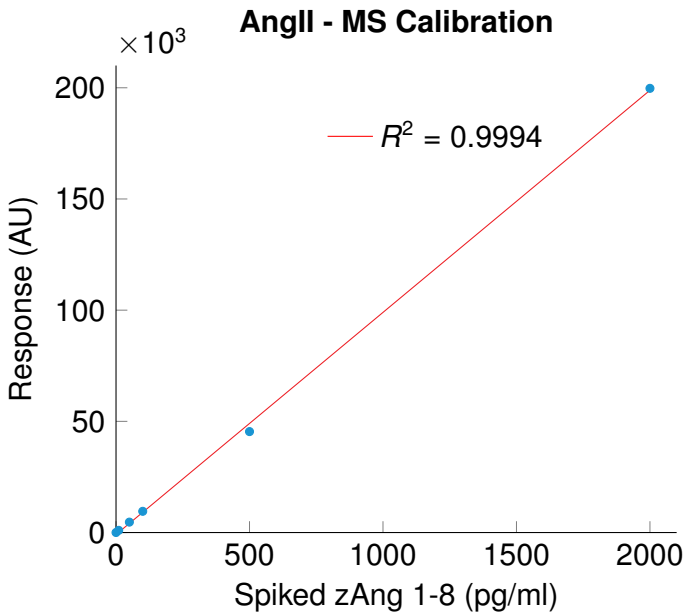

Figure 4.9 | **AngII mass spectrometry calibration** Calibration of mass spectrometer using synthesised AngII in mass spectrometry assay buffer. R^2=0.9994.

4.2.6 AngI and AngII Measurement in Zebrafish Serum

In serum, contrary to the kidney tissue results, a non significant increase (p=0.1271) in AngI concentration was observed in the Captopril treated group

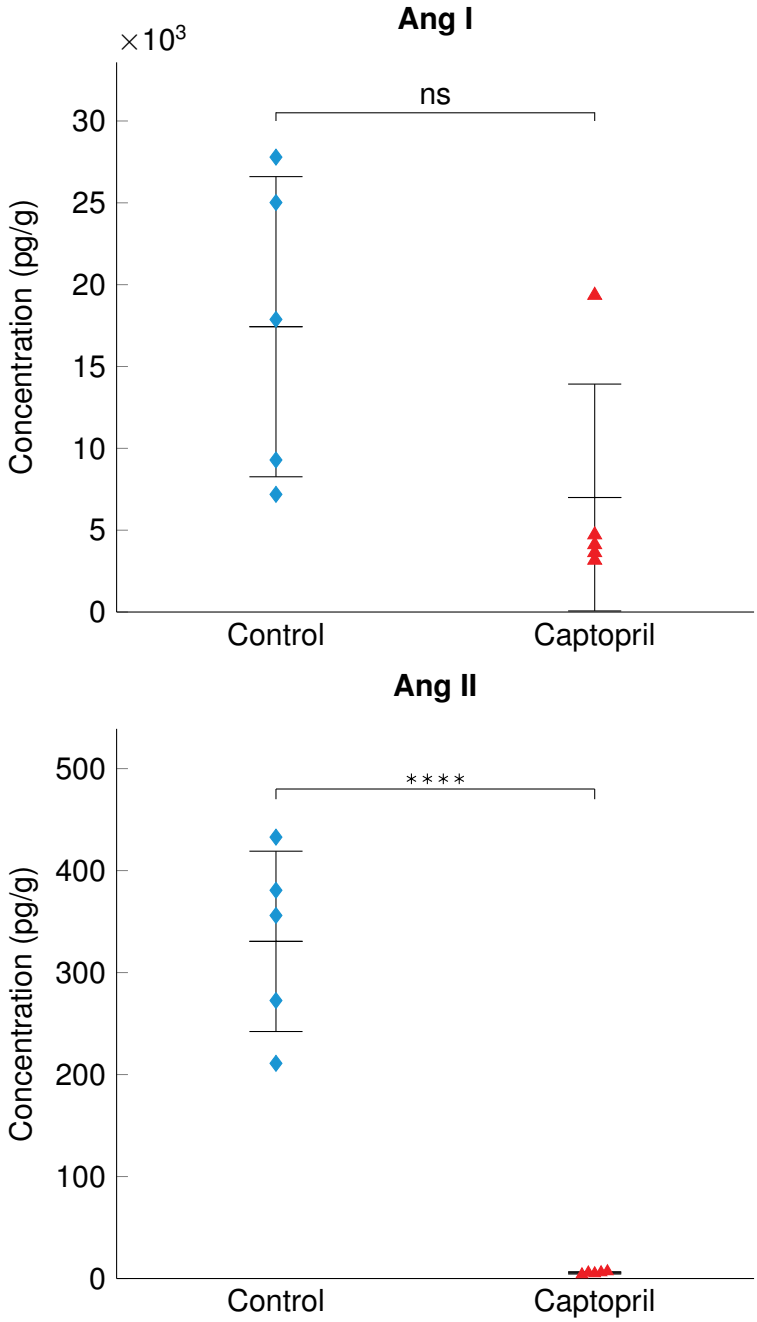

Figure 4.10 | **Measurment of Ang I and Ang II in whole adult mesonephric kidney tissue** Concentrations of Ang I and Ang II were measured in adult whole zebrafish kidney tissue in response to a 7 day 0.05 mM Captopril treatment. Ang I n=5, p=0.0768; Ang II n=5, p<0.0001. Each point represents a mass spectrometry measurement of a collective 75 mesonephric zebrafish kidneys. Data are mean ± SD. Student's t-test, ****=p<0.0001.

(n=5, mean=195.2 pg/g) compared to control group without Captopril treatment (n=5, mean=93.7 pg/g) (Figure 4.11). AngII was reduced in the Captopril treated group (n=5, mean=87.77 pg/g) compared to the untreated group (mean=182.6 pg/g), however, the difference was not significant (p=0.4670).

4.2.7 Synthesis of RenP1

There is a lack of tools that permit investigation of active zebrafish renin. Various tools have been developed that allow investigation of mammalian renin. Most interestingly is the use of FRET probes which can be designed to fluoresce upon interaction with renin. Thus FRET probes were designed using the tetradecapeptide sequence discussed in Section 4.2.1. The RenP1 FRET probe was developed using the zebrafish tetradecapeptide sequence (NRVYVHPFNLFSSE) and the 5(6)-carboxyfluorescein to allow simple quantification and visualisation. The peptide sequence was synthesised using SPPS on a polystyrene resin. On the N-terminus, 5(6)-carboxyfluorescein was attached, which was quenched by the addition of Methyl Red on the C-terminus of the peptide sequence (Figure 4.12). Quenching of 5(6)-carboxyfluorescein by Methyl Red has been commonly used and has also been visualised using a spectrometer (Figure 4.13). Furthermore, successful quenching was demonstrated by measuring the fluorescence intensity of 5(6)-carboxyfluorescein attached to the tetradecapepeptide sequence with and without Methyl Red (Figure 4.14). The probe was purified using semi-preparative HPLC and structure was verified using MALDI-TOF MS (Figure 4.15) and analytical HPLC (Figure 4.25). The presence of 5(6)-carboxyfluorescein permitted analytical HPLC analysis by ELS and detection at 490 nm.

4.2.8 RenP1 Activity at Different Stages of Development

RenP1 activity was assessed in homogenate from 3dpf (n=5), 4dpf (n=5) and 5dpf (n=5) zebrafish using a micro-plate fluorescence assay. All larval zebrafish used in this experiment originated from the same cutch and were measured on the same plate. Briefly, 25 fish were collected at 3-, 4- and 5dpf. For each measurement, 5 fish were homogenised and the homogenate was placed in a well of a 96-well plate. RenP1 (10 µl) was added to the homogenate and fluorescence intensity was measured at 520 nm after 0.1 second excitation at 480 nm. An increase in fluorescence intensity was observed from 3dpf to 4dpf ($p<0.0001$) and from 3dpf

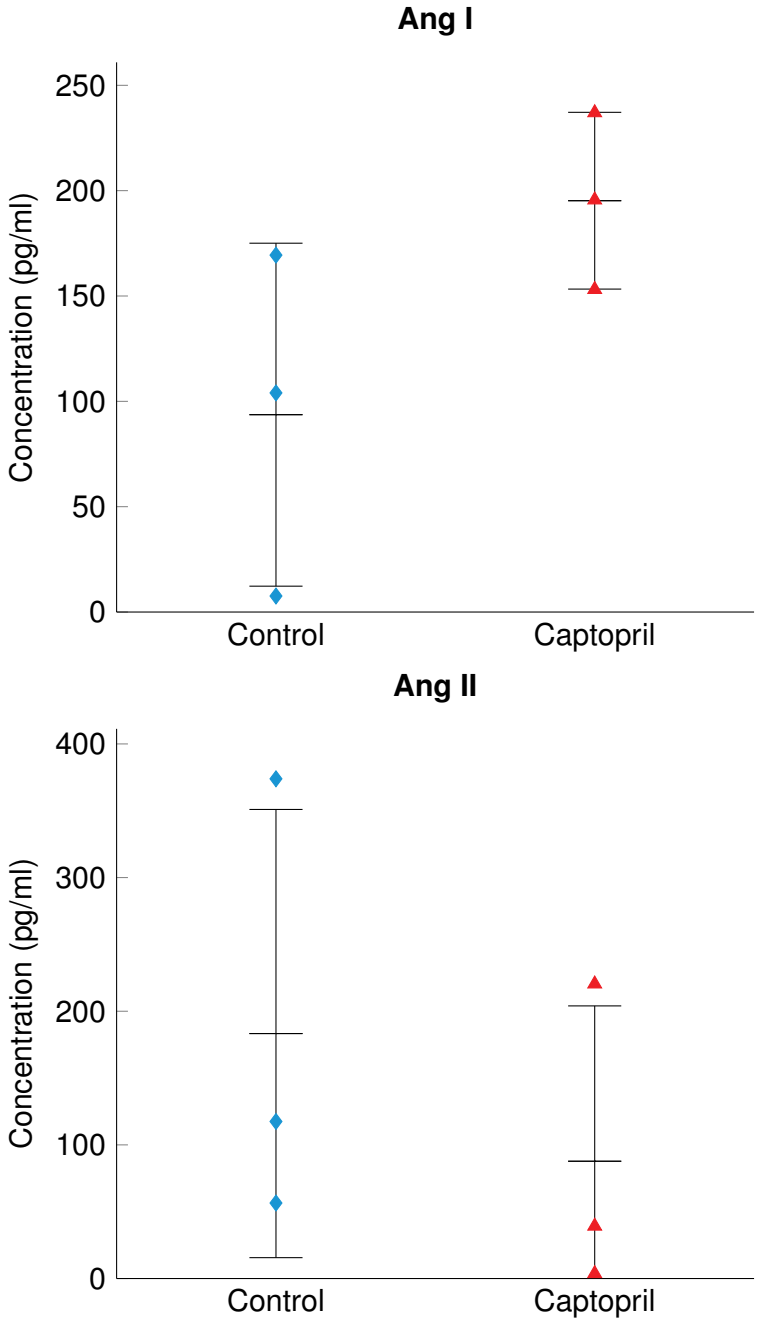

Figure 4.11 | **Measurment of Ang I and Ang II in adult zebrafish serum** Concentrations of Ang I and Ang II were measured in adult zebrafish serum of zebrafish after 7 day 0.05 mM Captopril treatment or conditioned water (CW) control. Ang I n=3, p=0.1271; Ang II n=3, p=0.4670. Each point on the graph represents one mass spectrometry assay from serum from 120 adult zebrafish. Data are mean ± SD. Student's t-test was performed.

Figure 4.12 | **RenP1 FRET Probe** Structure of the RenP1 FRET probe. 5(6)-Carboxyfluorescein as fluorophore attached to the N-terminus and Methyl Red to the C-terminus acting as the quencher. Calculated mass: 2445.68.

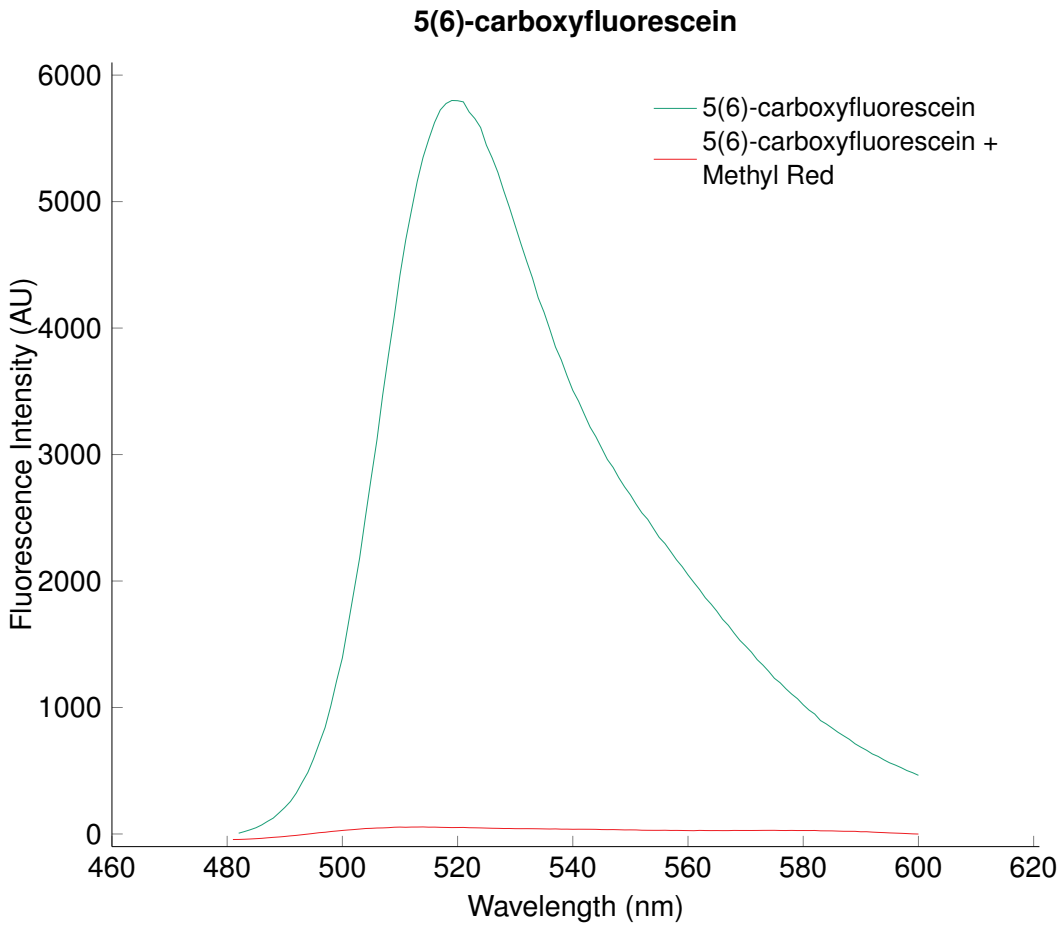

Figure 4.13 | **Emission spectra of 5(6)-carboxyfluorescein** Green: Emission spectra of 5(6)-carboxyfluorescein by excitation at 480 nm and emission curve peak at 520 nm. Red: Emission spectra of 5(6)-carboxyfluorescein in the presence of Methyl Red, by excitation at 480 nm and no detectable emission peak.

to 5dpf ($p<0.0001$) (Figure 4.17). However, no significant increase was observed between 4dpf and 5dpf ($p<0.0001$).

4.2.9 RenP1 Activity in Captopril Treated Larval Zebrafish

The ACE inhibitor Captopril, which has been demonstrated to be highly effective in zebrafish in Section 4.2.5, upregulates renin mRNA and ultimately circulating renin concentration [64, 171]. In order to have a better understanding of the specificity of renin on the FRET probe, larval zebrafish were treated with Captopril and RenP1 activity was compared to untreated (CW), age matched larval zebrafish. Five fish were collected and homogenised for each measurement. RenP1 was added to the

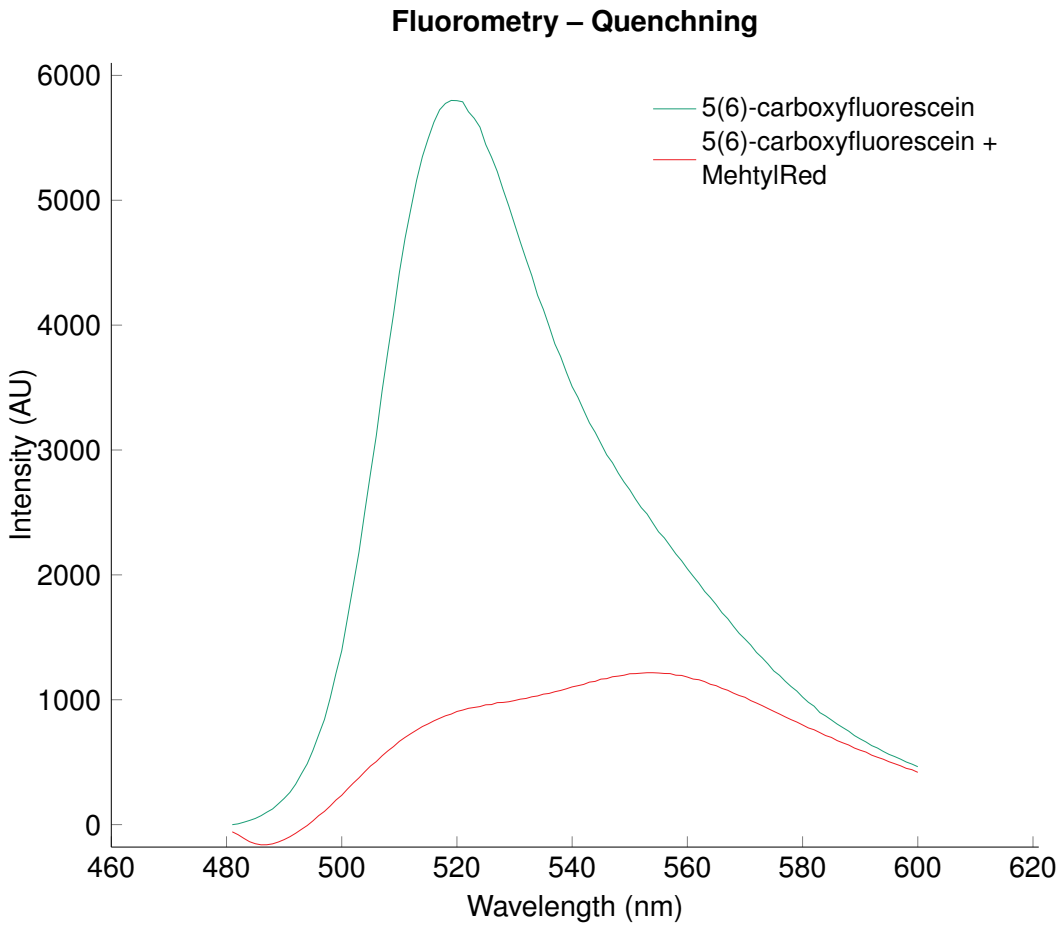

Figure 4.14 | **Emission spectra of RenP1** Green: Emission spectra of RenP1 without quecheing by Methyl Red by excitation at 480 nm and emission curve peak at 520 nm. Red: Emission spectra of quenched RenP1 by Methyl Red, by excitation at 480 nm

homogenate and fluorescence intensity at was measured at 520 nm by excitation at 480 nm over 1 hour. (Figure 4.18). A significant difference in fluorescence intensity was observed at all time points between the Captopril treated and CW group.

4.2.10 RenP1 Activity in Adult Zebrafish Plasma

Captopril was also used to assess the RenP1 activity in adult zebrafish serum from zebrafish treated with 0.05 mM Captopril (n=3) or left in CW (n=3) for 7 days prior to serum extraction. Blood was collected and serum extracted. Each measurement required pooled blood from 125 fish. The RenP1 FRET probe was directly added to the serum and fluorescence intensity was measured over 2 hours (Figure 4.19).

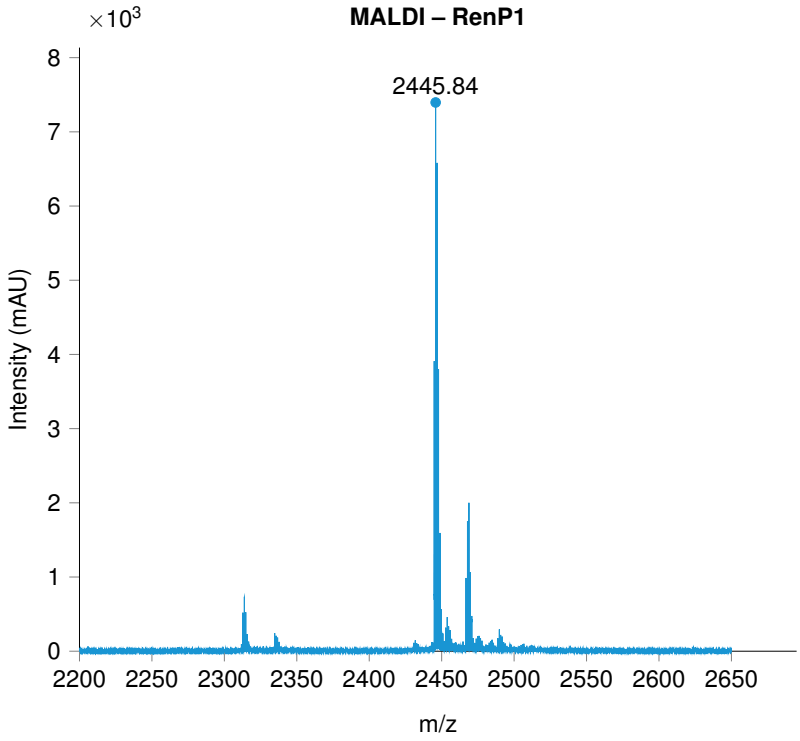

Figure 4.15 | **RenP1 MALDI analysis** MALDI MS of RenP1, mass calculated for $C_{121}H_{149}N_{27}O_{29}$ 2445.68, found 2446.21.

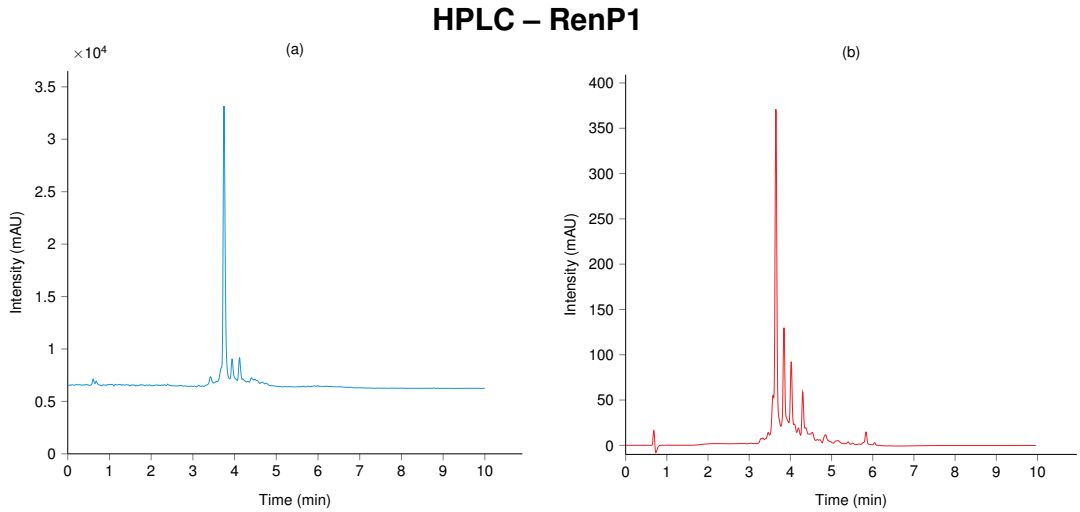

Figure 4.16 | **Analytical HPLC - RenP1** Analytical HPLC trace after semi-preparative HPLC column. (a) HPLC ELSD trace of RenP1 (b) HPLC trace with detection at 490 nm.

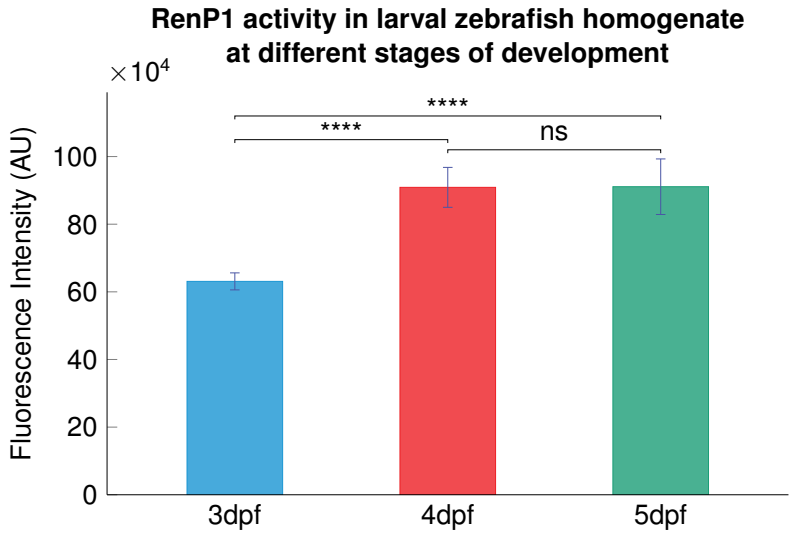

Figure 4.17 | **RenP1 fluorescence intensity in homogenate of larval zebrafish** RenP1 fluorescence intensity measured in homogenate of larval zebrafish at 3dpf (n=5), 4dpf (n=5), 5dpf (n=5). Every biological replicate constitutes of the homogenate of 5 age matched zebrafish. Fluorescence intensity was measured after 1 hour of adding the RenP1 Fret probe to the homogenate. Data are mean ± SD. ANOVA, ****=p<0.0001.

Fluorescence intensity only increased slowly, suggesting a low concentration of enzymes activating the FRET probe. Higher fluorescence intensity was measured over 1 hour in plasma from Captopril treated fish.

4.2.11 RenP1 Activity in Mib$^{ta52b(-/-)}$ Zebrafish Mutants

RenP1 activity was assessed in Notch signalling impaired mib^{ta52b} mutants. Mib^{ta52b} zebrafish mutants do not express Notch 3 due to lack of the ubiquitin ligase mib, which is required for the delta-mediated activation of the Notch receptor in target cells. Mib$^{ta52b(-/-)}$ zebrafish mutants do not to express renin mRNA at any stage of development [47, 172]. Fluorescence intensity was compared to age matched wild-type zebrafish. There was a significant decrease in fluorescence intensity in mib^{ta52b} mutants compared to wild-type zebrafish at 5dpf (p=<0.0001) at every 5 minutes measurement over 1 hour (Figure 4.20).

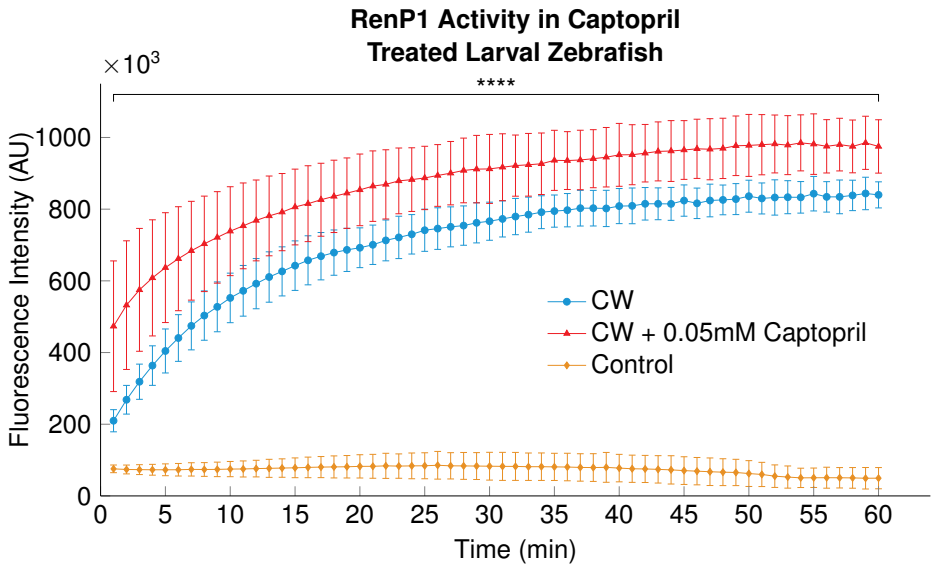

Figure 4.18 | **RenP1 Activity in 0.05 mM Captopril treated 5dpf larval Zebrafish** RenP1 fluorescence intensity was measured every minute for 1 hour in homogenate of 5dpf larval zebrafish. Fish were either left to develop in normal water (CW) or conditioned water with 0.05 mM Captopril (CW + 0.05 mM Captopril). Each biological replicate consisted of 10 homogenised larval zebrafish. Control is probe with CW. Data are ± SD. ANOVA with Bonferroni's multiple comparisons test, ****=p<0.0001.

4.2.12 RenP1 Activity in *ren*$^{-/-}$ Larval Zebrafish

The specificity of the probe was assessed using CRISPR/Cas9 mediated *ren*$^{-/-}$ zebrafish, developed in our laboratory and characterised in chapter 5. Change in RenP1 fluorescence intensity was assessed in 5dpf *ren*$^{-/-}$ larval zebrafish (n=5) against age matched *ren*$^{+/+}$ (n=5) whole zebrafish. The fish were left to develop in conditioned system water for 5dpf. For each assay measurement, 5 fish were pooled together, homogenised and placed in a well of a 96-well plate and RenP1 was added. The plate was left for 24 hours and fluorescence intensity was measured using a fluorescent microplate reader. No difference in fluorescence intensity was observed in *ren*$^{-/-}$ zebrafish (p=0.4972) (Figure 4.21).

4.2.13 RenP1 Activity in *ren*$^{-/-}$ Adult Zebrafish

RenP1 fluorescence activity was measured in homogenised kidney and muscle tissue excised from *ren*$^{-/-}$ and *ren*$^{+/+}$ adult zebrafish. The muscle tissue was used as a control tissue. A significantly higher fluorescence intensity was measured in

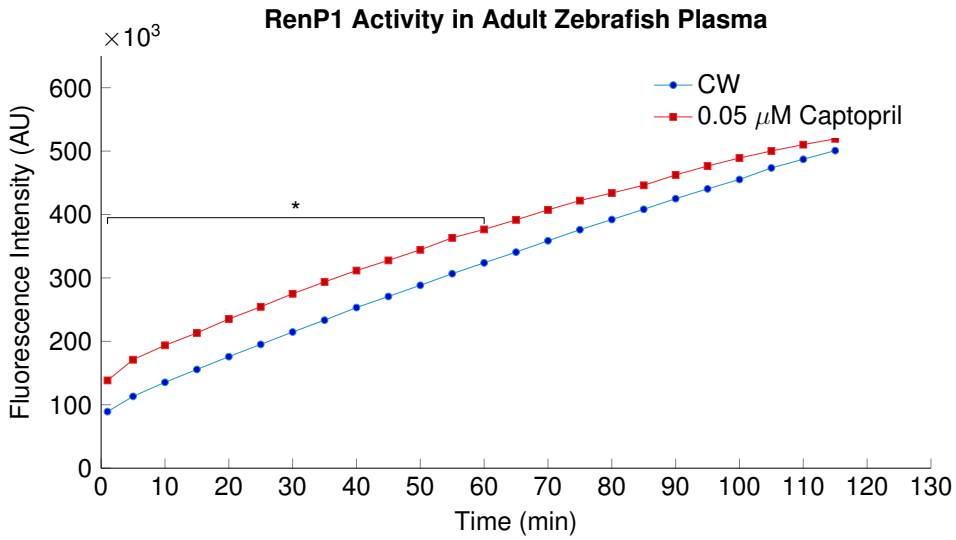

Figure 4.19 | **RenP1 Activity in Adult Plasma of Captopril Treated Zebrafish** RenP1 fluorescence intensity was measured in plasma collected from adult zebrafish after 7 days in conditioned water (CW) (n=3) and 0.05 mM Captopril (n=3). Each biological replicate is the plasma from 120 adult zebrafish. Fluorescence intensity was measured every 5 minutes over 2 hours. Data are mean ± SD. ANOVA (p=0.056) with Bonferroni's multiple comparisons test *=p<0.05.

homogenate from kidneys excised from *ren*$^{+/+}$ (n=5) compared to and *ren*$^{-/-}$ zebrafish (p=.0.0052) (Figure 4.22). No significant difference in fluorescence intensity could be observed in the muscle tissue between *ren*$^{+/+}$ and *ren*$^{-/-}$ zebrafish (p=0.6561). The fluorescence intensity of *ren*$^{+/+}$ and *ren*$^{-/-}$ muscle to kidney tissue was significantly higher, respectively (p<0.0001).

Breeding the *ren*$^{-/-}$ zebrafish with tg(*ren*:RFP-LifeAct) and tg(*acta2*:EGFP) zebrafish lines and the development of a FAC sorting protocol, allowed FAC sorting for renin expressing cells and vascular renal cells from *ren*$^{+/+}$ and *ren*$^{-/-}$ zebrafish. The sorted cells were seeded onto fibronectin coated plates and cultured. Cell media was collected after 2 days of cell culture and assessed using the FRET probe plate based assay. The experiment was repeated 3 times from culture media from the same cells (Figure 4.23). A significant difference in fluorescence intensity was observed in cell media from *ren*$^{+/+}$ and *ren*$^{-/-}$ RFP-LifeAct positive cells (p<0.0001). No difference in fluorescence intensity was observed between fresh culture media and media taken from *ren*$^{+/+}$ cells RFP-LifeAct positive cells (p=0.1268).

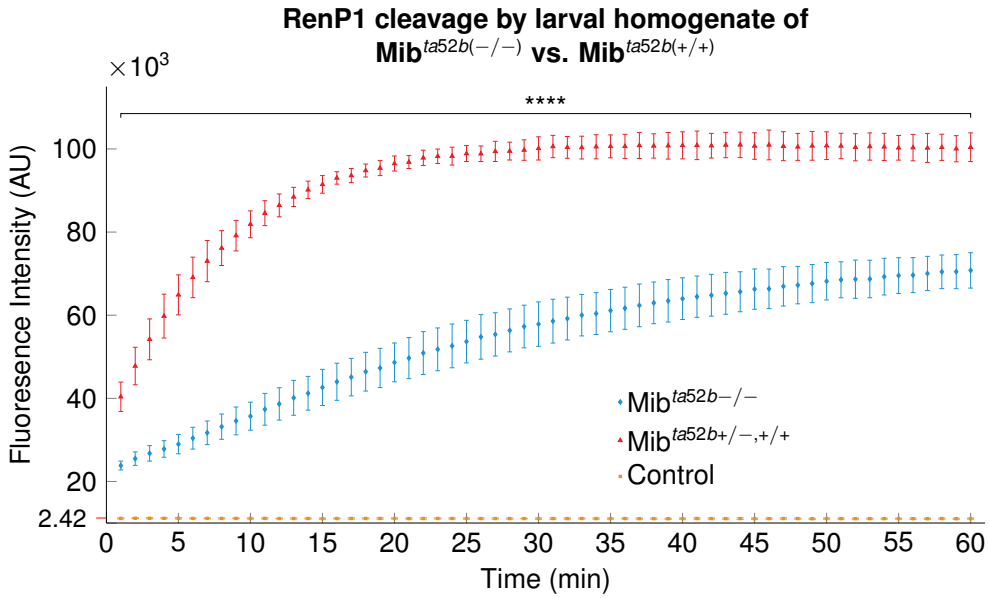

Figure 4.20 | **RenP1 cleavage by homogenised larval Mib$^{ta52b(-/-)}$ and Mib$^{ta52b(+/+)}$ zebrafish** RenP1 cleavage by homogenised larval Mib$^{ta52b(-/-)}$ n=8 and Mib$^{ta52b(+/+)}$ n=8 zebrafish. Each biological replicate constitutes of the homogenate of 10, 5dpf larval zebrafish. Fluorescence intensity of the 5(6)-carboxyfluoresein was measured every minute for 1 hour. Control is the RenP1 FRET probe without any homogenate. Data are mean ± SD. ANOVA with Bonferroni's multiple comparisons test ****=p<0.0001.

4.2.14 Probe Specificity

Proteinase K has been identified as a protease that can cleave the FRET probe. Proteinase K is a serine protease and has a broad cleave specificity [173]. The protease predominantly cleaves peptides at peptide bonds adjacent to the carboxyl group of aromatic amino acids with a blocked amino group.

A further non-renin cleavage of the probe was assessed using trypsin. Trypsin, similarly to proteinase K is also a serine protease and is commonly found in the digestive system of many vertebrates [174]. Trypsin is known to cleave peptide chains predominantly at the carboxyl site of the amino acids lysine and arginine [175]. In the RenP1 FRET probe such sites are Arg^2 and Lysine^{15}.

4.2.15 Synthesis of RenP1-D

In order to increase the specificity of the probe, single amino acids in the FRET probe are removed or changed in order to prevent contaminating enzymes cleav-

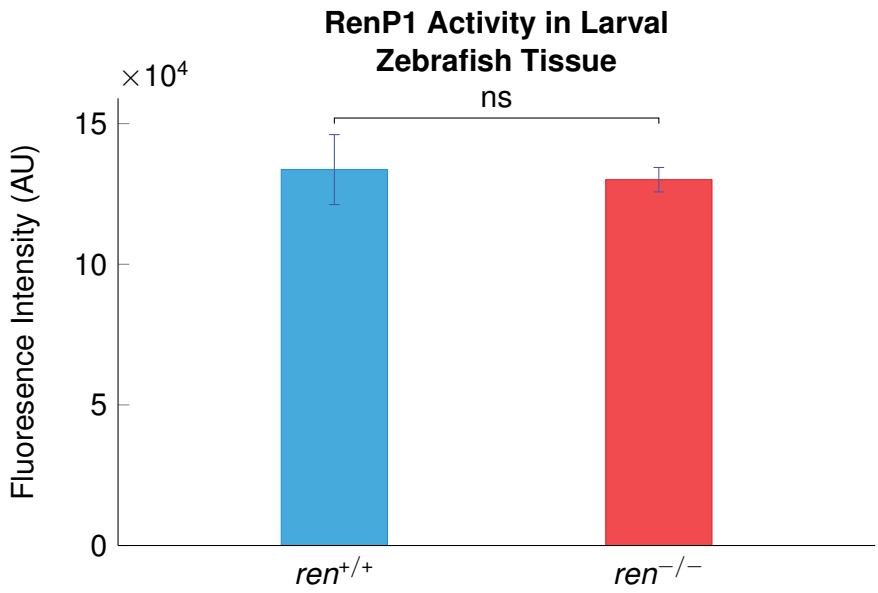

Figure 4.21 | **Fluorescence intensity of RenP1 in *ren*$^{+/+}$ and *ren*$^{-/-}$ larval tissue** Fluorescence intensity increase of RenP1 was assessed 24 hours after adding RenP1 to homogenised, *ren*$^{+/+}$ or *ren*$^{-/-}$ larval fish (n=5). Each biological replicate consists of 5 homogenised larval fish. Data are mean ± SD. Student's t-test, ns=not significant.

ing the probe. However, changes in amino acids may affect the enzyme substrate interaction. Due to lack of pure renin, testing the affinity of zebrafish renin to the substrate was not possible. A new probe was designed to prevent cleavage by trypsin and proteinase K. Proteases are chiral and can distinguish between L- and D-enantiomeric substrates and D-peptides are capable of resisting cleavage by many proteases [176, 177] The new RenP1-D FRET probe design was based on the tetradeca-peptide sequenced synthesied for RenP1. Amino acids Glu^{2}-Ser^{3} and Phe^{8}-Asn^{15} were exchanged for D-amino acids which should reduce background activity by becoming unsuitable for enzymatic degradation by trypsin and proteinase K without influencing renin. The FRET probe was also synthesised by solid phase peptide synthesis. A C-terminus Lysine-Dde amino acid was used for elective deprotection and attachment of the MR quenching the N-terminus attached 5(6)-carboxyfluoroscein. The peptide was analysed using analytical HPLC and MALDI and purified using a semi-preparative HPLC column.

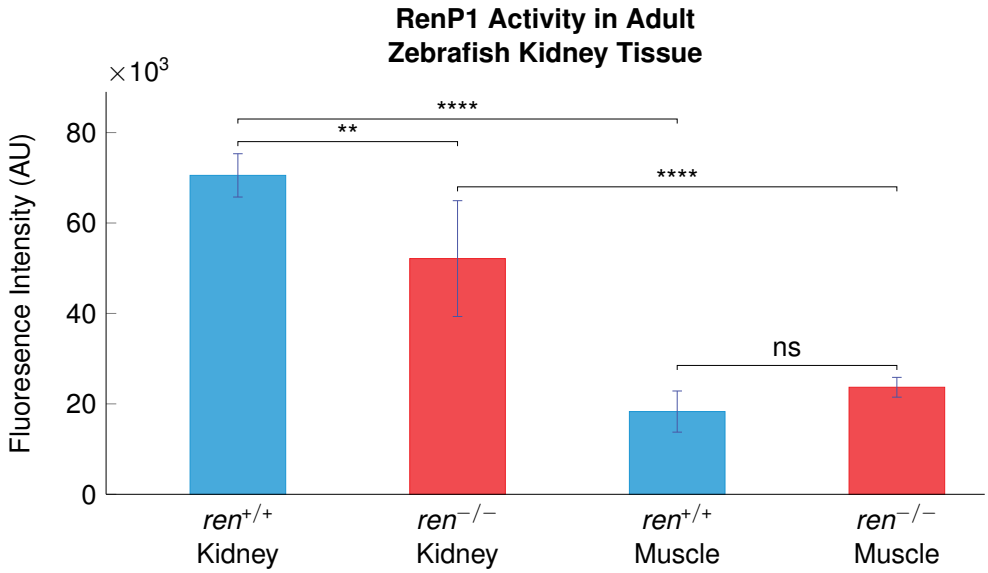

Figure 4.22 | **Fluorescence intensity of RenP1 in *ren*$^{+/+}$ and *ren*$^{-/-}$ zebrafish kidney and muscle tissue** Fluorescence intensity increase of RenP1 was assessed 24 hours after adding RenP1 to homogenised, *ren*$^{+/+}$ or *ren*$^{-/-}$ muscle (n=5) and kidney tissue (n=5). Data are mean ± SD. ANOVA ($p<0.0001$) with Bonferroni's multiple comparisons test, **=$p<0.01$, ***=$p<0.001$, ****=$p<0.0001$.

4.2.16 Testing RenP1-D

Trypsin cleavage of RenP1-D was assessed and compared to RenP1. Fluorescence intensity was measured every minute over 1 hour (Figure 4.26). No difference of fluorescence was observed between RenP1 and RenP1-D, suggesting no difference of trypsin cleavage of RenP1-D compared to RenP1.

Cleavage kinetics of RenP1-D by proteinase K were assessed and fluorescence was measured every 5 minutes over 1 hour and compared to RenP1-D. (Figure 4.27). There was an increase in fluorescence compared to RenP1-D suggesting that the D-amino acids hinder proteinase K cleavage of RenP1-D.

To investigate whether RenP1-D influenced the ability of renin cleavage and whether the reduced activity of proteinase K reduced background activity several assays in adult and larval fish were performed. Fluorescence activity was measured in homogenised kidney and muscle tissue excised from *ren*$^{-/-}$ and *ren*$^{+/+}$ zebrafish. The muscle tissue was used as a control tissue as zebrafish musculature contains no renin expressing cells. A significantly higher fluorescence intensity was measured in homogenate from kidneys excised from *ren*$^{+/+}$ (n=5) compared

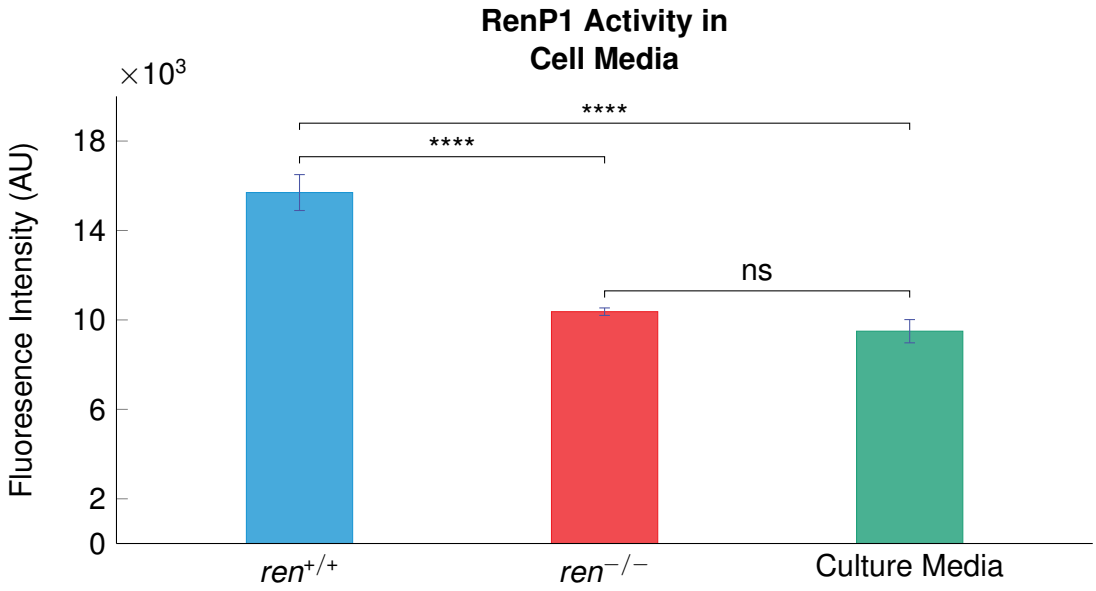

Figure 4.23 | **Fluorescence intensity of RenP1 in cell media from cultured zebrafish *ren* and *acta2* expressing cells from *ren*$^{+/+}$ and *ren*$^{-/-}$ zebrafish** Fluorescence intensity increase of RenP1 was assessed 24 hours after adding RenP1 to cell media from cultured RFP-LifeAct and EGFP expressing cells collected from tg(*ren*:RFP-LifeAct; *acta2*:EGFP) *ren*$^{+/+}$ or tg(*ren*:RFP-LifeAct; *acta2*:EGFP) *ren*$^{-/-}$ zebrafish fish (n=3). Data are mean $\pm$ SD. ANOVA (p<0.0001) with Bonferroni's multiple comparisons test ****=p<0.0001.

to and *ren*$^{-/-}$ zebrafish (p=0.0052) (Figure 4.22). No significant difference in fluorescence intensity could be observed in the muscle tissue between *ren*$^{+/+}$ and *ren*$^{-/-}$ zebrafish (p=0.6561). However, the fluorescence intensity of *ren*$^{+/+}$ and *ren*$^{-/-}$ muscle to kidney tissue was significantly higher, respectively (p<0.0001, p<0.0001). The results did not differ or improve the assay compared to the results seen in Section 4.2.13.

Change in RenP1-D fluorescence intensity was assessed in 5dpf *ren*$^{-/-}$ larval zebrafish (n=5) against age matched *ren*$^{+/+}$ (n=5) whole zebrafish. The fish were left to develop in conditioned system water for 5 days. For each assay measurement, 5 fish were pooled together, homogenised and placed in a well of a 96-well plate and RenP1-D was added. The plate was left for 24 hours and fluorescence intensity was measured using a fluorescent microplate reader. No difference in fluorescence intensity was observed between *ren*$^{+/+}$ and *ren*$^{-/-}$ larval zebrafish (p=0.4972) (Figure 4.21).

RenP1-D activity was assessed in cell media from *ren*$^{+/+}$ and *ren*$^{-/-}$ RFP-

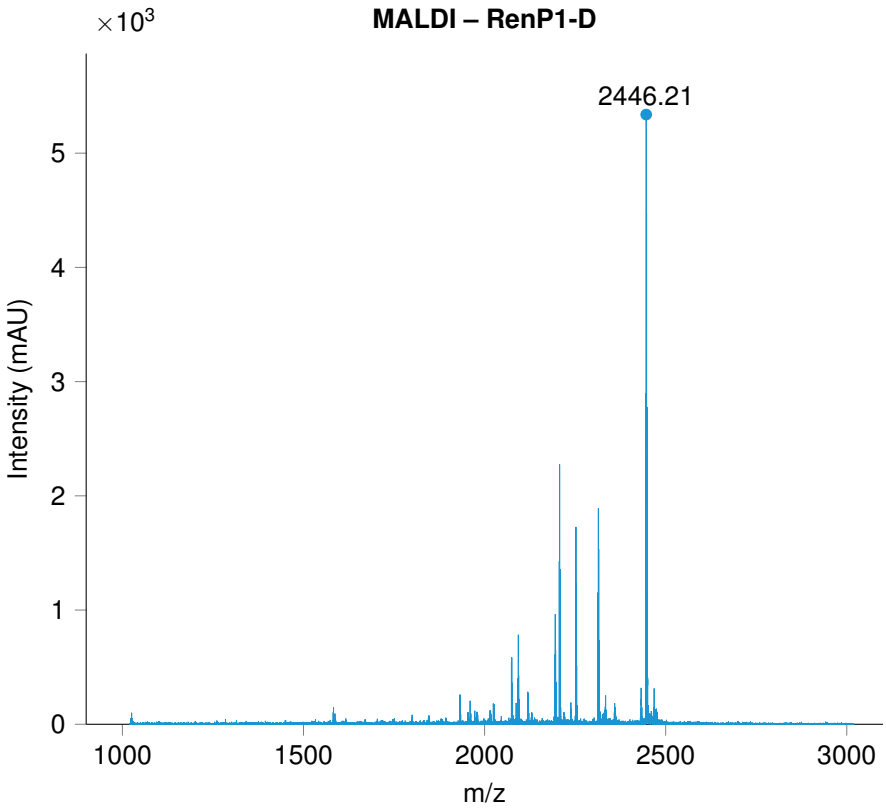

Figure 4.24 | **RenP1-D MALDI analysis** MALDI MS of RenP1-D, mass calculated for $C_{121}H_{149}N_{27}O_{29}$ 2445.68, found 2446.21.

LifeAct positive was cells, collected after 2 days of cell culture The experiment was repeated 3 times from culture media from the same cells (Figure 4.23). No difference in fluorescence intensity was observed of the FRET probe in media from *ren*$^{+/+}$ and *ren*$^{-/-}$ RFP-LifeAct positive cells (p=0.1500). Furthermore, No difference in fluorescence intensity was observed between fresh culture media and media taken from *ren*$^{+/+}$ cells RFP-LifeAct positive cells (p=0.8545).

4.2.17 Recombinant Prorenin Synthesis

Throughout this chapter the probe was tested on various different zebrafish models that either have an increase or decrease in active zebrafish renin. However, the specificity and enzyme kinetics of renin cleavage of RenP1 has not been assessed. There is no commercially available recombinant zebrafish renin. Recombinant mammalian renin is commonly expressed in mammalian cell expression

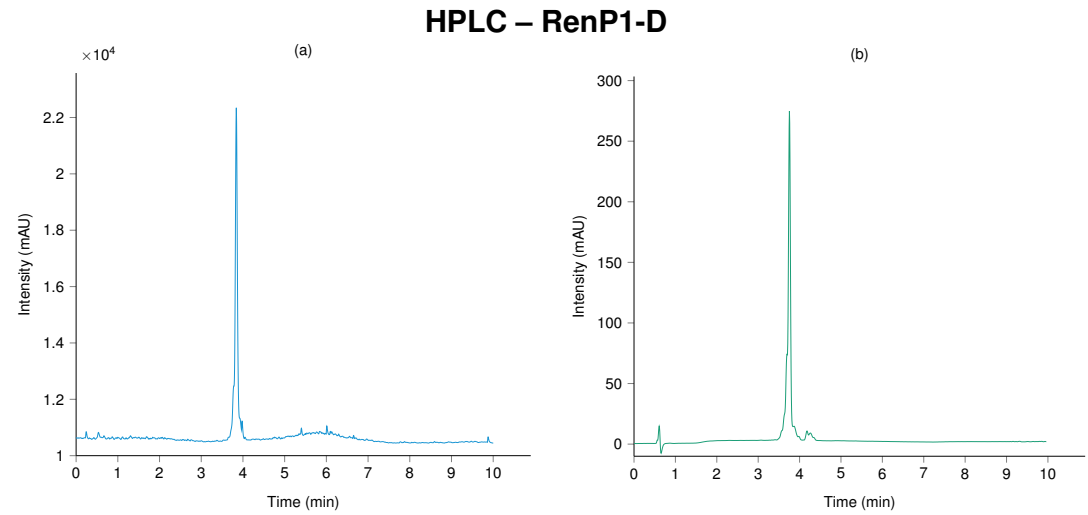

Figure 4.25 | **Analytical HPLC - RenP1-D** Analytical HPLC trace after semi-preparative HPLC column. (a) HPLC ELSD trace of RenP1-D (b) HPLC trace with detection at 490 nm.

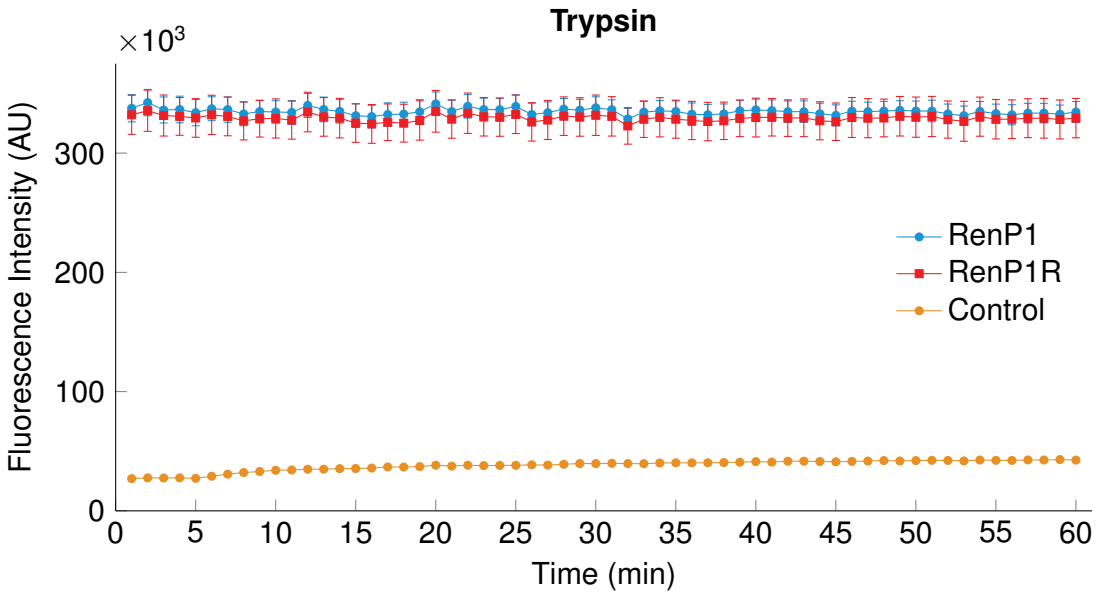

Figure 4.26 | **Cleavage kinetics of Trypsin on RenP1R** Cleavage kinetics of trypsin on RenP1R were measured and assessed versus RenP1. Fluorescence intensity was measured every minute for 1 hour. Control is average of both FRET probes background fluorescence.

systems, as prorenin and subsequently activated by removal of the pro-segment by partial trypsin digestion [178]. To express recombinant prorenin, the coding sequence for prorenin was synthesised by DC BIOSCIENCES Ltd.. The sequence

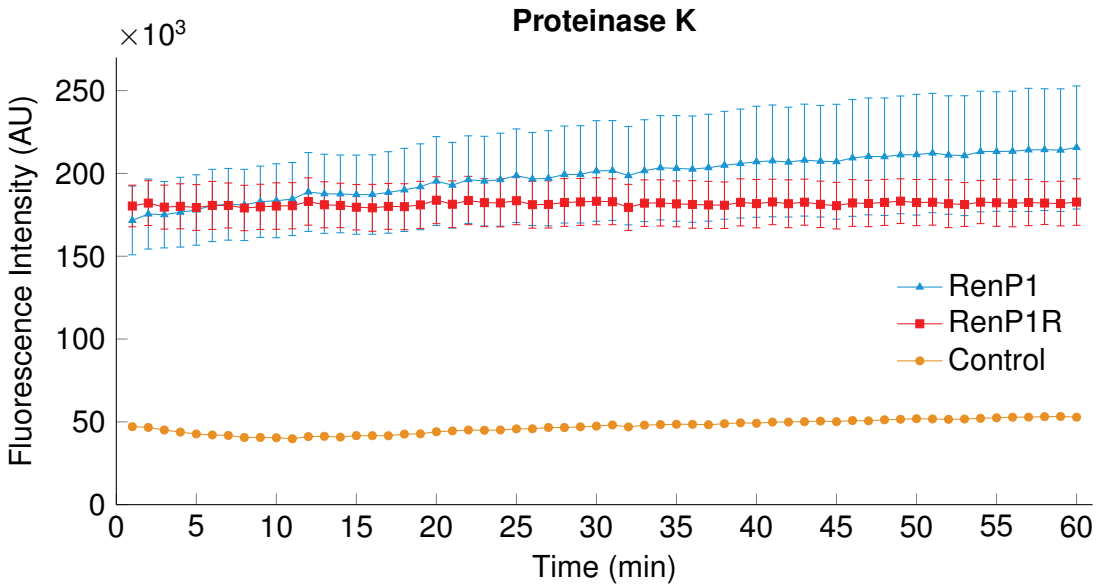

Figure 4.27 | **Cleavage kinetics of Proteinase K on RenP1R** Cleavage kinetics of Proteinase K on RenP1R were measured and assessed versus RenP1. Fluorescence intensity was measured every minute for 1 hour. Control is average of both FRET probes background fluorescence.

was designed to incorporate a 5' EcoRI and a 3' XhoI restriction enzyme cut site (see Appendix A). These permit for simple restriction digest and subsequent ligation for plasmid cloning. The synthesised prorenin coding sequence, shipped in a cloning vector, was excised by restriction digest by EcoRI and XhoI alongside the destination vector (psec2c). The different sized bands were separated by gel electrophoresis (Figure 4.31). The prorenin coding sequence band (1160bp) was extracted from the agarose gel alongside the digested psec2c vector and ligated. The resulting plasmid was analysed by restriction digest with APAL1 and MSC1 restriction enzymes and gel electrophoresis (Figure 4.33). The plasmid was further verified by DNA sequencing.

4.2.18 Recombinant Renin Synthesis

Prorenin is the inactive from of renin. The endogenous enzyme responsible for renin activation is still unknown. Commonly trypsin has been shown to cleave the 43 amino acid pro-segment and is able to activate renin *in vitro*. Using trypsin to activate the recombinant zebrafish renin, could lead to trypsin contamination in the final product. In an attempt to avoid trypsin contamination, the coding se-

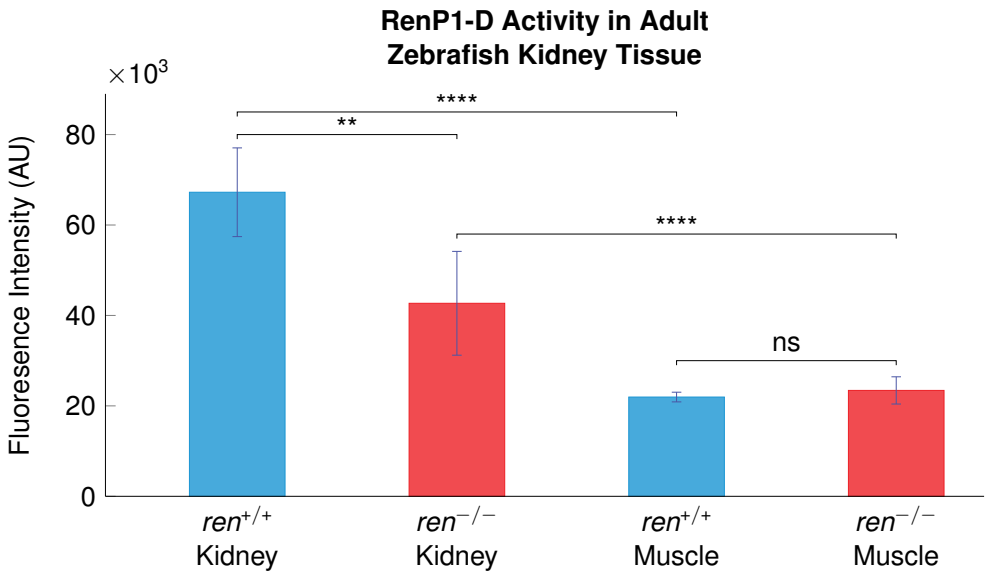

Figure 4.28 | **Fluorescence intensity of RenP1 in *ren*$^{+/+}$ and *ren*$^{-/-}$ zebrafish kidney and muscle tissue** Fluorescence intensity increase of RenP1 was assessed 24hrs after adding RenP1 to homogenised, *ren*$^{+/+}$ or *ren*$^{-/-}$ muscle (n=5) and kidney tissue (n=5). Data are mean $\pm$ SD. ANOVA (p<0.0001) with Bonferroni's multiple comparisons test**=p<0.01, ***=p<0.001, ****=p<0.0001.

quence for renin, without the coding sequence for the pro-segment was synthesised by DC BIOSCIENCES Ltd.. However, renin has been commonly synthesised as prorenin and activity of renin by synthesis without the pro-signal has not been previously demonstrated. The sequence, similarly to the prorenin sequence, was designed to incorporate a 5' EcoRI and a 3' XhoI restriction enzyme cut site (see Appendix B). These permit for simple restriction digest and subsequent ligation for plasmid cloning. The synthesised renin coding sequence, shipped in a cloning vector, was excised by restriction digest by EcoRI and XhoI alongside the destination vector (psec2c) the different sized bands were separated by DNA gel electrophoresis (Figure 4.31). The renin coding sequence band (1060bp) was extracted from the agarose gel alongside the digested psec2c vector and ligated. The resulting plasmid was analysed by restriction digest with APAL1 and MSC1 restriction enzymes and gel electrophoresis (Figure 4.35). From 6 selected plasmid clones all appeared to have the correct band sizes. The plasmid further verified by DNA sequencing.

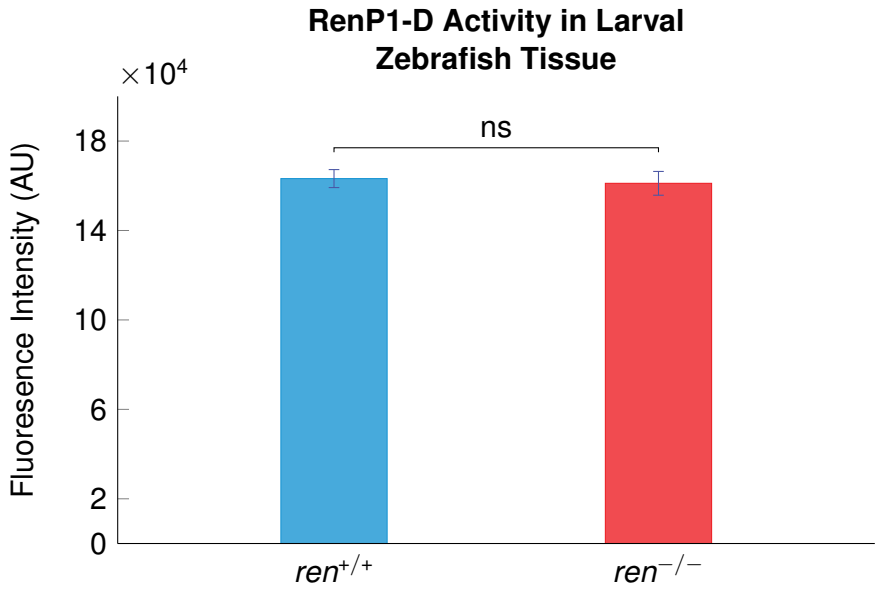

Figure 4.29 | **Fluorescence intensity of RenP1-D in *ren*$^{+/+}$ and *ren*$^{-/-}$ larval tissue** Fluorescence intensity increase of RenP1-D was assessed 24 hours after adding RenP1-D to homogenised, *ren*$^{+/+}$ or *ren*$^{-/-}$ larval fish (n=5). Each biological replicate consists of 5 homogenised larval fish. Data are mean ± SD. Student's t-test, ns=not significant.

4.2.19 Recombinant Renin Cell Expression

The renin-psec2c and prorenin-psec2c plasmids were transfected to Chinese Ovarian Hamster (CHO) cells using the Expi-system, and left for 5 days. The ExpiCHO system plasmids are designed to secrete the protein of interest into the cells media due to the secretion signal from the V-J20C region of the mouse Ig kappa chain. After 5 days of culture, cells transfected with renin-psec2c and cells transfected with prorenin-psec2c were harvested alongside the cell media. Expression of the protein was verified by western blot, using a mouse anti 6×His antibody. The protein was visualised by Alexa 488 goat anti mouse secondary antibody and scanning of the protein containing membrane (Figure 4.36). No protein expression could be seen in the cell media and cell lysate from cells transfected with the renin-psec2c plasmid. Furthermore, there was no secretion of recombinant prorenin from cells transfected with prorenin-psec2c. Only the cell lysate contained a His-tagged protein that was over expressed (Figure 4.36).

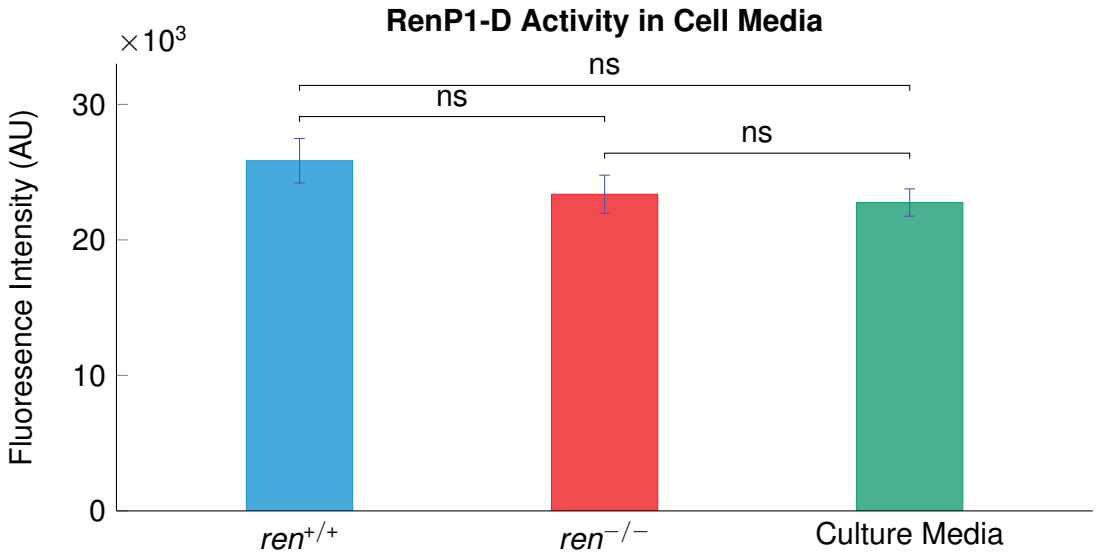

Figure 4.30 | **Fluorescence intensity of RenP1-D in cell media from cultured zebrafish *ren* and *acta2* expressing cells from *ren*$^{+/+}$ and *ren*$^{-/-}$ zebrafish** Fluorescence intensity increase of RenP1-D was assessed 24 hours after adding RenP1-D to cell media from cultured LifeActRFP and EGFP expressing cells collected from tg(*ren*:RFP-LifeAct; *acta2*:EGFP) *ren*$^{+/+}$ or tg(*ren*:RFP-LifeAct; *acta2*:EGFP) *ren*$^{-/-}$ zebrafish (n=3). Data are mean ± SD. ANOVA (p=0.5593) with Bonferroni's multiple comparisons test, ns=p>0.05.

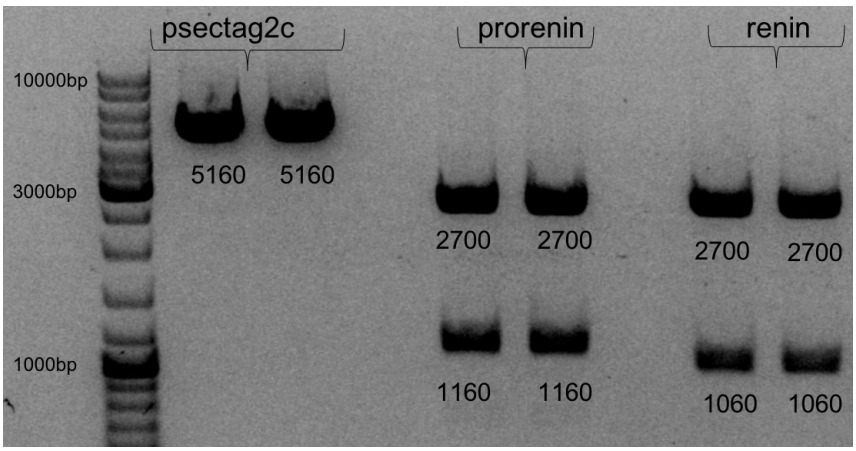

Figure 4.31 | **Gel electrophoresis of restriction enzyme digest of psectag2c vector and prorenin and renin carrier vectors** Gel electrophoresis of restriction enzyme digest of psectag2c vector and prorenin and renin carrier vectors by EcoRI and XhoI and 10kb ladder.

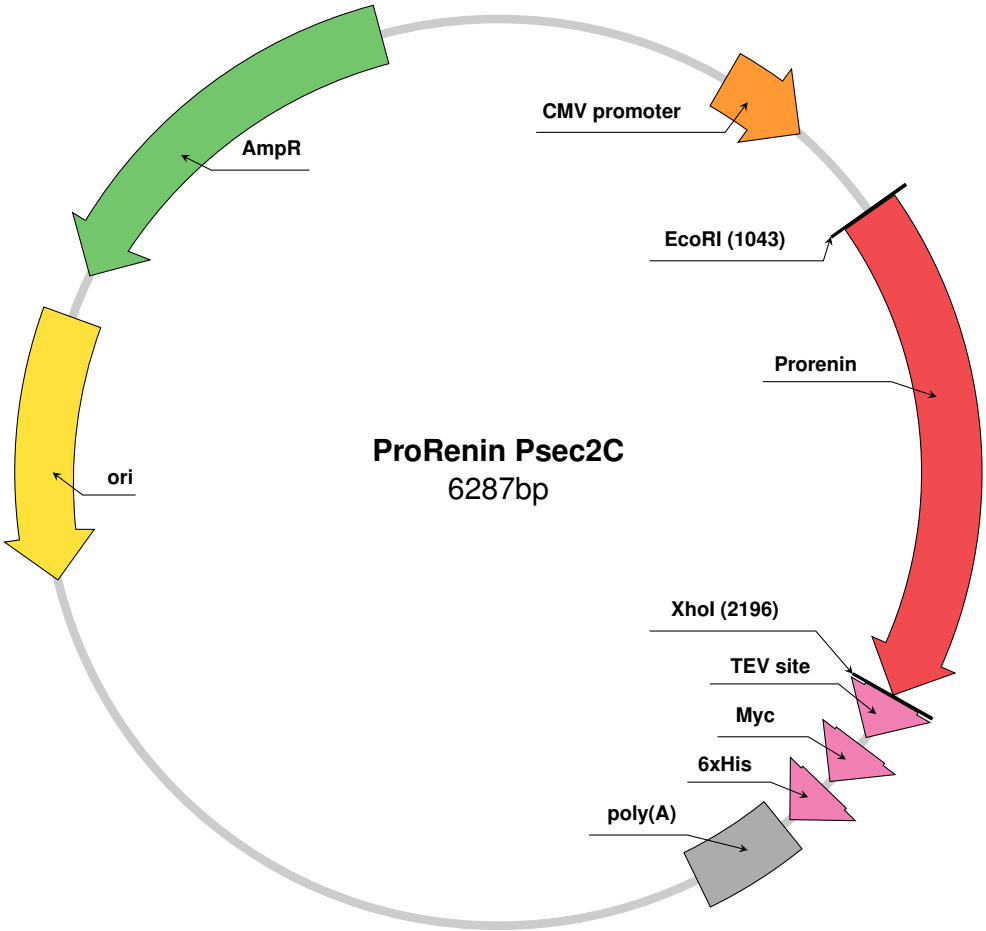

Figure 4.32 | **Prorenin Psec2c Plasmid Map** Plasmid map of the PSec2C vector containing the zebrafish prorenin coding sequence placed downstream of the CMV promoter. Plasmid contains the AmpR casette for antibiotic plasmid selectivity. Downstream of the prorenin coding sequence is a TEV restriction site and a 6×His signal for purification and identification purposes.

4.2.20 Prorenin Activation

The protein collected from the cell lysate was purified by using His-tag capturing columns. Activation by removal of the pro segment from the prorenin was performed using immobilised trypsin, to prevent trypsin contamination in the final product. Trypsin was left to cleave prorenin for 15 minutes before washing and eluting the product. The eluted, trypsin activated protein was identified by western blot (Figure 4.37). No protein was detected using western blot analysis and subsequent visualisation of the protein using fluorescent tagged antibodies. The partial trypsin digest caused dilution of the protein. The product was too dilute for west-

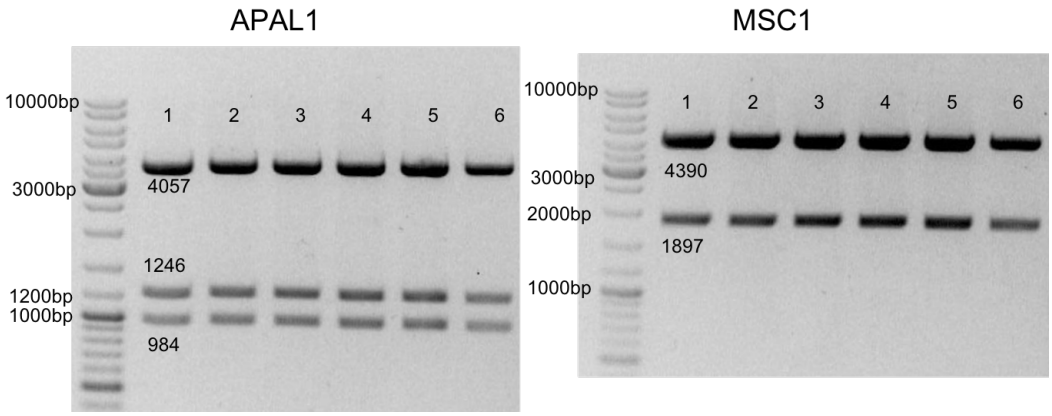

Figure 4.33 | **Gel electrophoresis of restriction enzyme digest of prorenin psectag2c vector** Gel electrophoresis of restriction enzyme digest of prorenin psectag2c by APAL1 and MSC1. First lane contains 10kb ladder followed by 6 selected clones and their DNA analysed by restriction digest by APAL1 and MSC1 and gel electrophoresis.

ern blotting analysis to identify the protein. RenP1 activity was determined in the elution media containing the activated prorenin. No difference in cleavage kinetics of RenP1 was observed between prorenin and activated prorenin (Figure 4.38).

Further attempts at recombinant renin expression were made by the Max-Delbrück-Centrum (MDC) for Molecular Medicine. Similar expression plasmids were designed for protein expression in HEK293 cells and for bacterial protein expression. However, no protein expression could be observed after multiple over-expression attempts, suggesting that the higher temperature of mammalian based protein expressing cell systems might interfere with correct expression of zebrafish recombinant proteins.

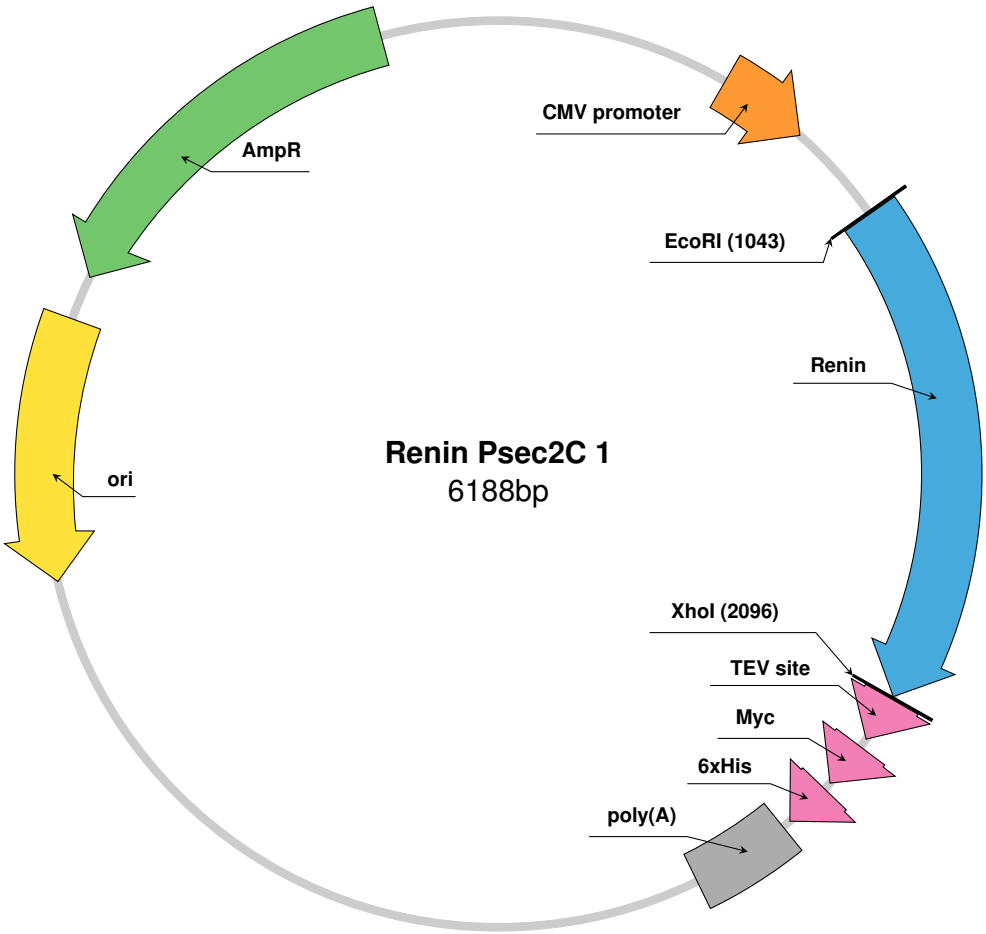

Figure 4.34 | **Renin Psec2c Plasmid Map** Plasmid map of the PSec2C vector containing the zebrafish renin coding sequence placed downstream of the CMV promoter. Plasmid contains the AmpR cassette for antibiotic plasmid selectivity. Downstream of the renin coding sequence is a TEV restriction site and a 6×His signal for purification and identification purposes.

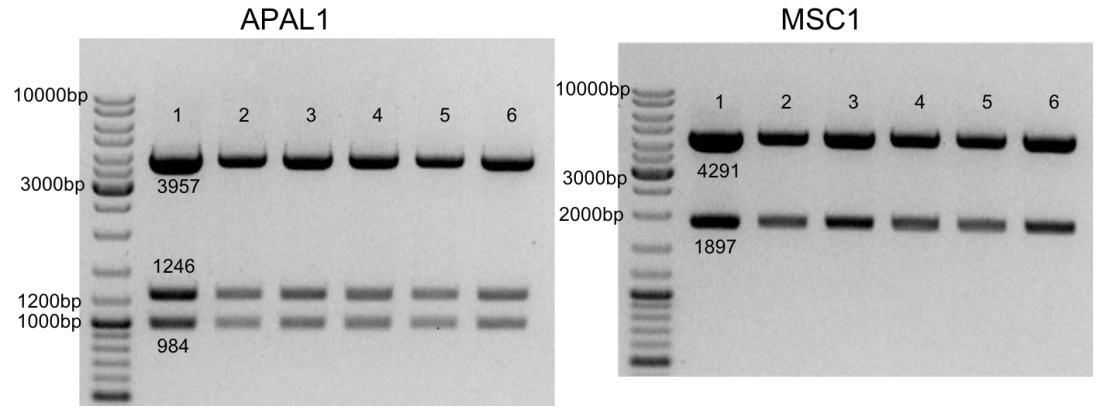

Figure 4.35 | **DNA gel electrophoresis of restriction enzyme digest of prorenin psectag2c vector** Gel electrophoresis of restriction enzyme digest of renin psectag2c by APAL1 and MSC1. First lane contains 10kb ladder followed by 6 selected clones and their DNA analysed by restriction digest by APAL1 and MSC1 and gel electrophoresis.

Figure 4.36 | **Western Blot analysis of the recombinant renin and prorenin expression from CHO cells** Cell media and cell lysate were run on a 4-12% gradient gel under non denaturing conditions. After transfer to 0.45 µm nitrocellulose the blotted bands were immunodetected with a specific mouse anti 6×His and subsequently visualized with Alexa 488 goat anti-mouse IgG antibodies. Lane: MW marker, lane 1: Renin cell media 2: Renin Cell lystate 3: Prorenin cell media 4: Prorenin cell Lysate 5: His-tagged positive control protein.

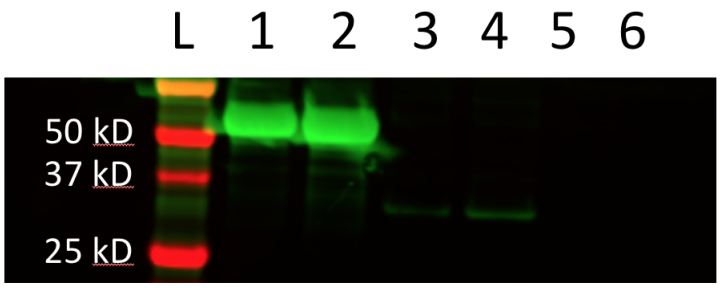

Figure 4.37 | **Western Blot analysis of the trypsin activation of recombinant zebrafish prorenin** Cell media and cell lysate were run on 4-12% gradient gels under non-denaturating conditions. After transfer to 0.45 µm nitrocellulose the blotted bands were immunodetected with a specific mouse anti 6×His and subsequently visualized with alexa 488 goat anti-mouse IgG antibodies. L: MW marker, lane 1: 5 µg His-tagged positive control protein 2: 10 µg His-tagged positive control protein 3: 5 µg Recombinant Prorenin 4: 10 µg Recombinant Prorenin 5: 5 µg Recombinant Renin 6: 10 µg Recombinant Renin.

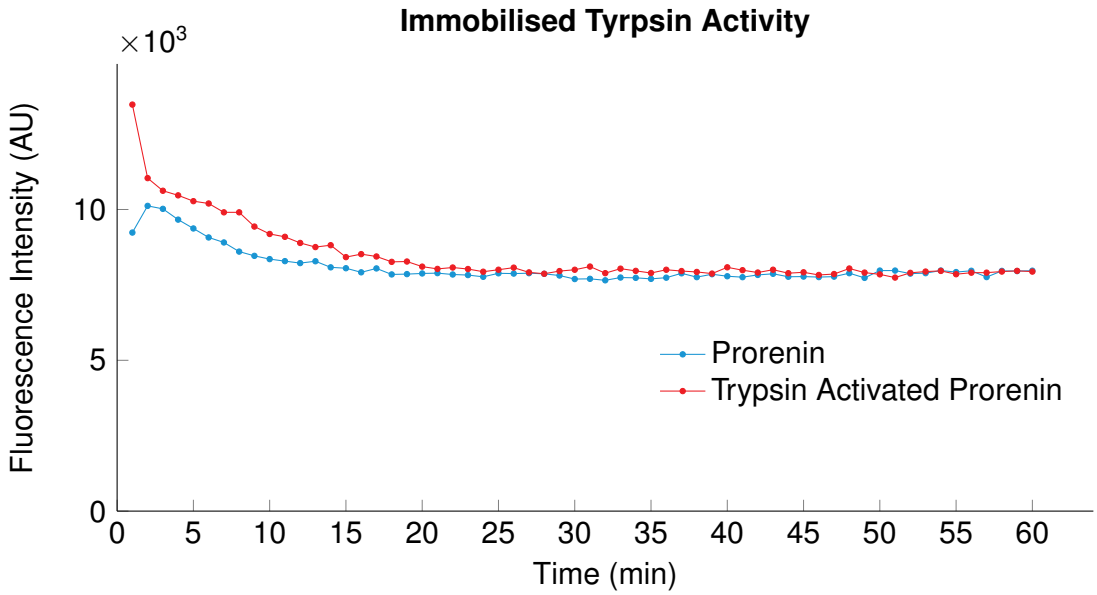

Figure 4.38 | **Testing activity of recombinant zebrafish prorenin** Testing activity of recombinant prorenin and trypsin activated prorenin with the RenP1 probe.

4.3 Discussion

In this chapter I synthesised zebrafish AngI and AngII by SPPS. In collaboration with Attoquant diagnostics, we were able to use the synthetic AngI and AngII to calibrate an MS assay to detect AngI and AngII concentrations in kidneys of adult zebrafish. The AngI and AngI concentrations were measured in kidneys from zebrafish treated with the ACE inhibitor Captopril and the measurements were compared to untreated controls. Furthermore, this chapter describes the synthesis and validation of the first renin zebrafish FRET probe. Although, lacking recombinant renin to investigate enzyme kinetics, first results suggest successful cleavage of the probe in larval and adult zebrafish assays.

Lastly, several attempts have been made in expressing recombinant renin. Although these have been unsuccessful they gave an understanding of the possible difficulties of expressing zebrafish proteins in mammalian protein expression systems.

4.3.1 Zebrafish Angiotensinogen Tetradecapeptide Sequence

The sequences for AngI and AngII were identified by comparison of the zebrafish angiotensinogen amino acid sequence to its mammalian counterparts. Structural and biochemical studies on the interaction of renin and angiotensinogen have shown that renin recognises a tetradecapeptide amino acid sequence at the N-terminal of angiotensinogen and is the only known substrate [179]. The well annotated mammalian sequences permit identification of the tetradeca-peptide sequence in the zebrafish sequence and the potential renin cleavage site. The renin cleavage of angiotensinogen has been shown to exhibit species specificity by demonstrating that human angiotensinogen cannot be readily cleaved by mouse renin [180]. Although only 50% sequence homology between zebrafish and its mammalian counterparts can be seen, the eight amino acids encoding AngII are highly conserved across a wide range of species. Paritcularly striking is the preservation of the His-Pro-Phe amino acid sequence which is crucial for the cleavage of the substrate by renin [37].

4.3.2 AngI and AngII Synthesis

Both peptides were synthesised using SPPS, which showed promising yields of product. Peptide concentration was 120 mg and 114 mg, for AngI and AngII, respectively after purification by HPLC column. Purification of the compound suggested 99% purity and should permit using the peptides for injecting into zebrafish for further experiments. Using SPPS many simple zebrafish peptides can be synthesised.

4.3.3 AngI and AngII measurement in Zebrafish Tissues

The synthesis of Zebrafish AngI and AngII permitted identification and measurement of AngI and AngII concentrations in the zebrafish kidney and serum. In order to provoke a dynamic change of expression of AngII and possibly AngI, zebrafish were treated with the ACE inhibitor Captopril. ACE is a metalloenzyme that cleaves a dipeptide from the C-terminus of the decapeptide AngI to form the vasopressor Ang II [181]. Captopril has been previously shown to be effective in zebrafish by studies investigating the zebrafish responsiveness to different salt concentrations. The measurement of AngII in the zebrafish tissue showed that Captopril is highly effective in the zebrafish as there was a complete lack of renal AngII in adult zebrafish that were Captopril treated for 7 days. Surprisingly there was no decrease in the AngI concentration measured in the kidney tissue. Previous *in vitro* and *in vivo* studies have shown that ACE inhibitors increase AngI [182, 183]. A possible explanation for the decrease seen in the zebrafish renal tissue is that the renal renin stores might be exhausted following the increased secretion in order to compensate for the complete lack of AngII. The serum results showed high variability for both the AngI and AngII measurements and suggest low reproducibility. A possibly cause for this might be the serum preparation and the half life of AngI and AngII.

The MS assay is highly accurate in measuring AngI and AngII concentrations, however, requires a large number of fish to have sufficient material to permit the measurement. An increased sensitivity and optimisation of the assay would hopefully reduce the number of fish needed and allow for more measurements to be performed.

4.3.4 Reduced Activity in Mib Mutants

The notch signalling pathway is a highly evolutionary conserved signalling pathway involved in the the pattern formation and cell fate determination by cell to cell interactions [184]. Mind Bomb is a ubiquitin ligase required for the activation of the Notch receptor in target cells [172]. Zebrafish mind bomb (mib) mutants have a compromised notch signalling pathway which leads to the premature differentiation of neural progenitors causing severe neurogenic phenotypes and a range of developmental defects due to the failure to develop proper somites, neural crest and vasculature. Interestingly it has been shown that renin cells express high levels of Notch3 and that mib^{ta52b} mutant fish do not express renin mRNA at any stage of development suggesting that a proper notch signalling pathway is required for larval ren expression [47, 185]. Prior to the generation of the first renin knockout-fish the mib^{ta52b} mutant presented the best opportunity of a renin like knockout zebrafish mutant in order to test the specificity of the RenP1 FRET probe. Although a significant difference can be observed in the RenP1 fluorescence activity, suggesting the lack of renin causes a reduction in the fluorescence signal. However, the mib^{ta52b} mutant has been characterised with many major developmental phenotypes which may also lead to an impaired development of the digestive system. This could ultimately lead to the lack of development of digestive enzymes and lead to a decrease in cleavage kinetics of the probe observer with the mib^{ta52b} mutants.

4.3.5 RenP1 in Larval Zebrafish

Due to the lack of recombinant renin the RenP1 probe specificity was assessed by RAS altered zebrafish. Renin is first expressed in the zebrafish at 24hpf. Renin cell area at the AMA was previously assessed using a transgenic zebrafish line expressing RFP-LifeAct under a renin promoter, expressing RFP in renin expressing cells [47]. Investigating the fluorescent signal stemming from the renin cells at the AMA suggested an increased renin cell area. If zebrafish secret functional renin at this stage of development and the probe is renin specific a steady increase should be seen in the RenP1 activity at different days of development. RenP1 activity in homogenate larval fish at 3dpf, 4dpf and 5dpf suggested that there was increased activity of RenP1 from 3dpf to 4- and 5dpf however, not between 4- and 5dpf. This suggests that at 3dpf, with the commencement of the pronephric filtration, there is an increase in active renin. RenP1 activity was not assessed prior to 3dpf. At

2dpf the larval zebrafish are still enveloped in their protective chorion and express chorion digesting enzymes that might interfere with RenP1 activity. It would be interesting to investigate RenP1 activity throughout the first 2 weeks of zebrafish development and investigate whether an increase of renin can be observed with the formation of mesonephros which occurs at 14dpf.

RenP1 activity was also assed in zebrafish treated with the ACE inhibitor Captopril. Fish were left in Captopril from 24hpf to 5dpf, washed and homogenised prior to the RenP1 micro-plate assay. A clear increase in RenP1 fluorescence intensity was observed in fish treated with Captopril. This observation concours with previous studies showing that animals treated with Captopril show renin cell recruitment along renal arterioles, and have a higher PRA. [47, 79, 186].

4.3.6 RenP1 in Adult Zebrafish

RenP1 activity was also assessed in adult zebrafish. Similarly as in larval zebrafish, RenP1 activity was assessed in RAS modulated adult zebrafish treated with the ACE inhibitor Captopril. Furthermore, the previously discussed MS assay revealed high effectiveness of Captopril on zebrafish ACE, which should diminish the AngII mediated negative feedback and an increase in renin transcription and secretion. RenP1 activity in zebrafish plasma of Captopril treated fish revealed higher cleavage kinetic activity within the first hour of the assay. Although this change is not as dramatic as observed in the larval fish, the assaying of zebrafish plasma has proven difficult in the MS assay. ReninP1 activity in the kidneys of Captopril treated adult zebrafish was not assessed. It would be interesting to see whether RenP1 activity would complement the MS data.

4.3.7 *ren*$^{-/-}$ Larval Zebrafish

The *ren*$^{-/-}$ zebrafish, developed in our laboratory is the ideal model to test the probe on zebrafish lacking active renin. This model was developed after the testing with the mib^{ta52b} mutants, showing a decrease of probe activity in homogenised larval zebrafish. RenP1 activity was assessed in 5dpf homogenised *ren*$^{-/-}$ larval zebrafish and compared to age matched wild-type zebrafish. Surprisingly, no change change in RenP1 activity was observed. However, previously data has suggested that there was a difference in RenP1 activity between Captopril and non-Captopril treated fish. The data suggests that the effectiveness of Captopril

might cause a dramatic increase in active renin present, which is identifiable using the RenP1 probe. However, potentially the early larval renin activity is low and the difference between *ren*$^{-/-}$ and *ren*$^{+/+}$ larval zebrafish requires a more sensitive assay, with a more specific probe.

4.3.8 *ren*$^{-/-}$ Adult Fish

Despite the lack of change in RenP1 activity in the larval zebrafish, RenP1 activity was assessed in the adult kidney of *ren*$^{-/-}$ zebrafish and compared to *ren*$^{+/+}$, wild-type controls. Furthermore, zebrafish muscle tissue was used as a control as no renin activity is expected in muscle tissues. There was a significant increase in fluorescence intensity measured in *ren*$^{+/+}$ compared to *ren*$^{-/-}$ zebrafish. Furthermore, there was no difference in the muscle tissue. This experiment suggests successful cleavage of the probe, however the lack of dramatic difference suggests that the lack of specificity and high background activity interferes with the probe.

Due to the lack of sensitivity of the probe in larval *ren*$^{-/-}$ and *ren*$^{+/+}$ zebrafish, it would be interesting to assess at what time point during zebrafish development, enough renin is present to detect a significant difference.

4.3.9 Probe Specificity

Due to lack of recombinant renin, the Km value of zebrafish renin and the probe specificity could not be assessed. However, the above mentioned assays were able to show dynamic changes in the cleavage kinetics of RenP1 in models that are expected to have higher or lower concentrations of renin. A further difficulty is the lack of a zebrafish renin inhibitor. Despite a long history of development of renin inhibitors, the only successful renin inhibitor currently available is Aliskiren, Aliskiren is a non-peptide renin inhibitor as is currently successfully used as a hypertension mono-therapy. Aliskiren is highly specific to human renin and has not been tested in this project. Despite the evidence that renin activity is measurable in larval and adult zebrafish, it would be interesting to investigate whether a dynamic change as well as a dose response could be measured using Aliskiren in zebrafish. However, aliskiren effectiveness would have to be assessed first as-well as a drug repose curve.

To increase the probe sensitivity, a new RenP1-D FRET probe was successfully synthesised. RenP1-D was identified to be cleaved by trypsin and proteinase K.

Studies have shown that most proteases are chiral and that they can distinguish between L- and D-enantiomeric substrates and that D-peptides are capable of resisting cleavage by many proteases [176, 177]. Despite successful synthesis no difference could be seen in cleaving kinetics between RenP1-D and RenP1 when exposed to trypsin. Although not significant, there was an ultimately higher fluorescent signal from the RenP1 probe compared to the RenP1-D probe when exposed to proteinase K. Assays to test the probe were designed to test whether the probe specificity was increased and whether potential cleavage by renin was influenced. No differences in the assays could be observed, apart from when measuring activity in the cell media from *ren*$^{-/-}$ and *ren*$^{+/+}$ cells from tg(*ren*:RFP-LifeAct) and tg(*acta2*:EGFP) zebrafish.

Further testing would have to be conducted. It is crucial to assess a possible change in affinity of renin to the substrate containing D-amino acids. Although the 4 amino acids directly at the peptide cleavage were not changed (Ser^{9}-Asn^{12}), the amino acids crucial for renin cleavage (His^{6}, Pro^{7}, Phe^{8}) were replaced with their enantiomeric form,

4.3.10 Recombinant Renin

The FRET probe specificity was a major issue during the development of the zebrafish renin FRET probe. In order to increase the specificity, the pure enzyme is required. The development of an recombinant protein turned out to be difficult due to the different temperatures at which zebrafish proteins are folded. If there was a pure protein this would allow to develop various new probes with single amino acids changed that would inhibit trypsin from cleaving the probe however the recombinant renin would be required to be able to assess how the single amino acid change effected renin from cleaving the probe.

Several different methods were employed to develop recombinant renin; however, most were unsuccessful. Mammalian renin was previously successfully expressed as the inactive renin form, prorenin, in CHO and HEK293 cells [187, 188]. In this thesis, zebrafish renin was attempted to be expressed in CHO cells and HEK293 cells. HEK293 yielded no protein and CHO cells protein over expression was observed, however the protein was trapped within inclusion bodies and required additional purification steps. Western blot analysis demonstrated that the protein was of the wrong molecular size to the expected zebrafish prorenin or renin and inactive.

In collaboration to the work performed in the thesis, attempts were made by the MDC in Berlin, which specialises in the expression of recombinant proteins, to express zebrafish renin in bacterial and mammalian cells, which were also unsuccessful. Expression of zebrafish proteins has previously been performed in bacterial cells [189]. The temperature at which the mammalian cells are maintained (37 °C) at, might be the problem causing factor of the expression of more complex zebrafish proteins.

Chapter 5

Characterisation of a Renin Knockout Zebrafish

5.1 Introduction

To deepen our understanding of the role of renin and the RAS in zebrafish, a CRISPR/CAS9 induced renin knockout zebrafish was generated. Zebrafish renin specific gRNAs were designed to target CRISPR-Cas9 to renin exon 2, resulting in an 8bp deletion. The targeted knockout was identified by sequencing.

This chapter focuses on the phenotypic characterisation of the *ren*$^{-/-}$ zebrafish line using different methodologies, including the high-throughput VAST system. The VAST system allowed for a large number of age matched fish to be imaged and downstream image analysis identified morphological differences between *ren*$^{-/-}$ and *ren*$^{+/+}$ fish. During early development a noticeable delay in swim bladder inflation and body length was observed and was suggestive of renin playing an important role during early zebrafish development.

To assess morphological differences at a cellular level, the *ren*$^{-/-}$ knockout fish were crossed to existing transgenic lines to assess kidney development, renal vasculature and morphology of juxtaglomerular cells in the absence of renin. A cross of the *ren*$^{-/-}$ fish to the tg(*wt1b*:EGFP) transgenic fish, enabled the visualisation of glomerular and tubular structures of the pronephros during early kidney development. For a better understanding of JG cell morphology, the *ren*$^{-/-}$ fish were crossed to the tg(*ren*:RFP; *acta2*:EGFP) double transgenic line. Although no difference in cell morphology, between the *ren*$^{-/-}$ and *ren*$^{+/+}$ was noticeable in the pronephric kidney, high resolution imaging of *ex vivo* zebrafish mesonephric kidneys revealed a dramatic increase of renin-expressing cells along the renal arterioles. This phenotype was further quantified using FACS to sort for red (*ren*:LifeAct-RFP) and green (*acta2*:EGFP) positive cells. In this chapter I will characterise the various phenotypes of the first renin knockout zebrafish and discuss possible roles of renin during early development in the pronephric and its possible roles in the mesonephric zebrafish kidney.

5.2 Results

The *ren*$^{-/-}$ zebrafish strain, was generated in our laboratory by Linda Mullins and Sebastien Rider and has a deletion of 8 bp in renin exon 2, causing a truncation of the mRNA between nucleotides 1388 and 1380, resulting in a frameshift mutation and premature truncation of the normal open reading frame after codon 75 (Figure 5.1). I was given the opportunity to phenotypically characterise the breeding *ren*$^{-/-}$ zebrafish line using different molecular techniques.

5.2.1 Viability

Phenotypic observations were performed on PCR-validated *ren*$^{-/-}$ larval fish and compared to age-matched *ren*$^{+/+}$ (WIK) fish. *Ren*$^{-/-}$ showed no loss in viability during the first 5dpf in an normal salt environment (CW) (Figure 5.2). A previous study showed that zebrafish exposed to Captopril in combination with low salt (1/20 CW) results in a 97% loss of viability at 4dpf [47]. The lack of renin in *ren*$^{-/-}$ fish will result in the loss of production of AngI, and therefore the absence of AngII, leading to an inability to handle low a salt concentration environment. Viability was not reduced in *ren*$^{-/-}$ fish exposed to 1/20 CW. Exposing *ren*$^{-/-}$ fish to 0.05 mM Captopril in CW, which has previously been demonstrated to be the highest concentration without any toxic effect [47], reduced viability by only 5% (n=42) and had no effect on viability in *ren*$^{+/+}$ fish during early development. The combination of Captopril with dilute medium (1/20 CW) resulted in 0% viability in *ren*$^{-/-}$ and 12.5% in *ren*$^{+/+}$ fish, however surviving wild type fish showed severe pericardial and yolk sac oedema at 5dpf.

5.2.2 Hatching

A delay in hatching of the *ren*$^{-/-}$ fish larval fish from the protective chorion was observed. The hatching period in zebrafish occurs between 48-72hpf and individual fish from the same clutch will hatch sporadically throughout the third day [190]. The number of hatched fish was assessed at the end of the third day of development in *ren*$^{-/-}$ and age matched *ren*$^{+/+}$ control (Figure 5.3). Only 43.75% of *ren*$^{-/-}$ had hatched by the end of the third day compared to 73.33% of *ren*$^{+/+}$ fish (p=0.0207). Exposing the fish to 1/20 CW caused a even more dramatic decrease of hatched fish at 3dpf. Only 7.6% of *ren*$^{-/-}$ hatched compared to 68.74% (p=0.0003).

Figure 5.1 | **Sequencing data from *ren*$^{-/-}$ and *ren*$^{+/+}$ fish** Sequencing data confirming the deletion of 8bp in the *ren*$^{-/-}$ zebrafish and the premature stop codon at the beginning of exon 3 coming into frame, leading to a premature truncation of renin protein. **A** Normal DNA sequence of zebrafish renin, with the 8bp deletion site highlighted. **B** Sequencing data from a *ren*$^{-/-}$ zebrafish with the 8bp deletion. **C** Renin coding sequence with the deletion site indicated leading to early termination of translation at the beginning of exon 3.

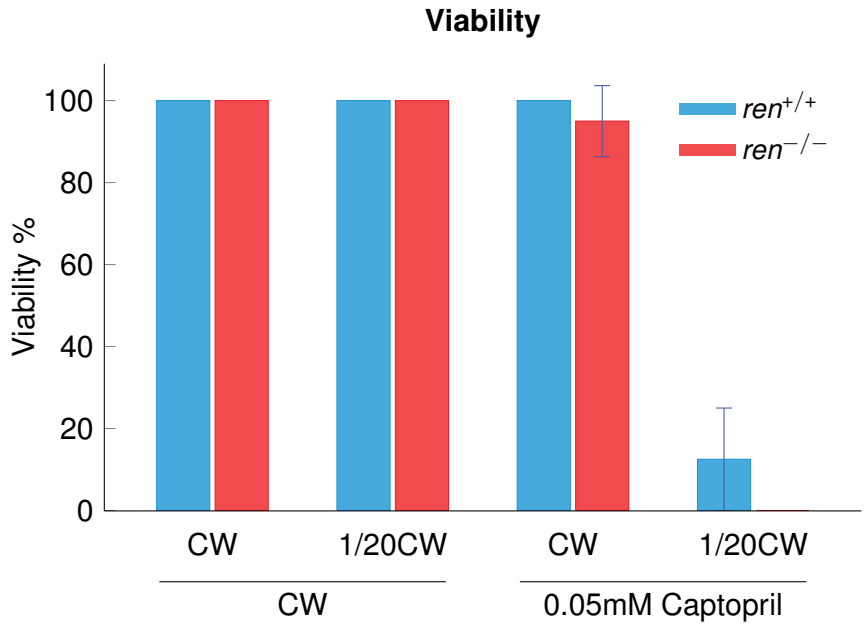

Figure 5.2 | **Viability of *ren*$^{-/-}$ fish** Viability of *ren*$^{+/+}$ (n=48) versus *ren*$^{-/-}$ (n=48) fish was assessed at 5dpf. 100% viability was seen in *ren*$^{+/+}$ and *ren*$^{-/-}$ in normal salinity (CW) and dilute medium (1/20 CW). Addition of 0.05 mM of the angiotensin-converting enzyme inhibitor Captopril to CW reduced the viability of *ren*$^{-/-}$ fish by 5% (n=42). Addition of Captopril to 1/20 CW reduced viability of *ren*$^{+/+}$ fish by 87.5% (n=48) and no *ren*$^{-/-}$ fish survived to 5dpf (n=48).

To determine if a functional RAS was required for hatching of fish, Captopril was administered to fish in CW and 1/20 CW. Administration of Captopril, similarly to 1/20 CW without Captopril, reduced the number of hatched *ren*$^{-/-}$ fish by 91.7% and *ren*$^{+/+}$ by 30.75% (p=0.0024). Combination 1/20 CW and Captopril reduced the number of hatched *ren*$^{+/+}$ and *ren*$^{-/-}$ fish by 43.75% and 84.25%, respectively (p=0.0225). However, the final number of hatched fish was strongly influenced by the low viability of these fish in the Captopril and 1/20 CW.

5.2.3 Oedema During Early Larval Development

Oedema is suggestive of the inability of proper osmoregulation and specifically pericardial and yolk sac oedema is a sign of developmental toxicity in the larval zebrafish [191]. To assess at which stage of development the phenotypic differences arise between the *ren*$^{-/-}$ and *ren*$^{+/+}$ larvae, larval *ren*$^{-/-}$ and *ren*$^{+/+}$ zebrafish were placed in CW or 1/20 CW and oedema occurrences were recorded (0-5dpf).

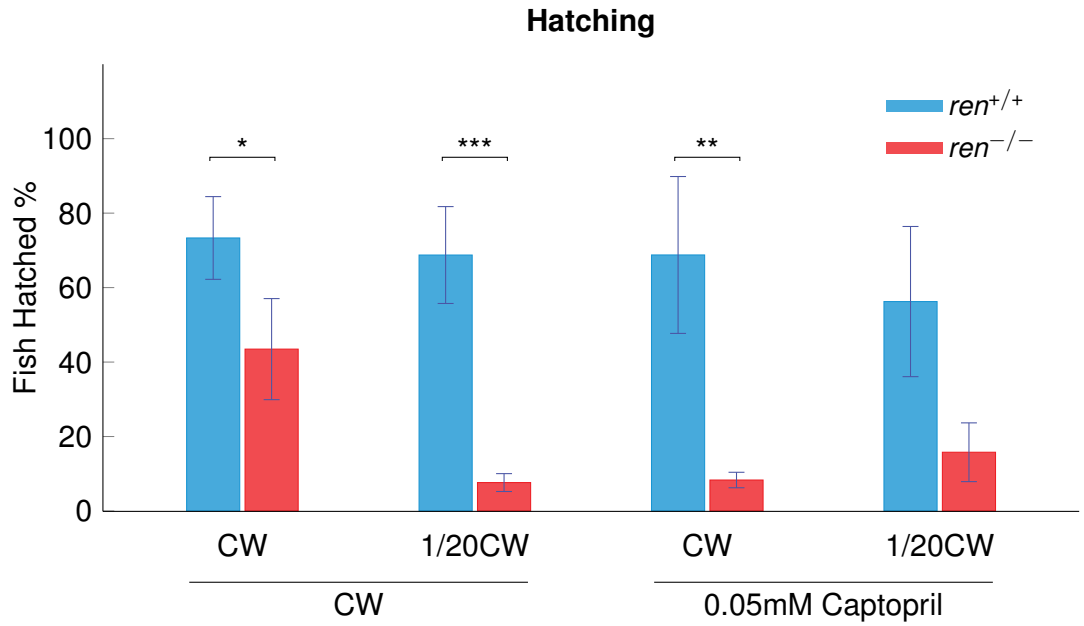

Figure 5.3 | **Quantity of *ren*$^{+/+}$ and *ren*$^{-/-}$ zebrafish hatched at 3dpf** The number of hatched *ren*$^{+/+}$ versus *ren*$^{-/-}$ fish was assessed at 72hpf. In normal salinity (CW) 73.3% of *ren*$^{+/+}$ (n=3) and only 43.48% of *ren*$^{-/-}$ (n=3, p=0.0207) had hatched. Low salinity (1/20 CW) reduced number of hatched *ren*$^{+/+}$ to 68.8% (n=3) and *ren*$^{-/-}$ fish to 7.6% of (n=3, p=0.0003). Addition of 0.05 mM Captopril to CW reduced the number of *ren*$^{+/+}$ fish hatched to 68.8% (n=3) and 8.3% in *ren*$^{-/-}$ fish (n=3, p=0.0024). 1/20CW and Captopril reduced hatching to 56.3% and 15.9% of *ren*$^{+/+}$ (n=3) and *ren*$^{-/-}$ fish (n=3), respectively (p=0.0225). Data are mean $\pm$ SD.*=p<0.05, **=p<0.01, ***=p<0.001.

Oedema was defined as the presence of any pericardial effusion and or a cranial haemorrhage. In CW, *ren*$^{+/+}$ fish did not develop any oedema (Figure 5.4). A small subset of *ren*$^{-/-}$ fish developed oedemas at 5dpf (8.7%). In 1/20 CW, 12.5% of *ren*$^{-/-}$ fish developed pericardial oedema and 4% of *ren*$^{+/+}$ developed oedemas. No oedema were noted prior to 2dpf and there was also no increase after 3dpf suggesting normal salinity is crucial between 2 and 3dpf of development, the time at which filtration in the zebrafish pronephros is first observed [103].

5.2.4 Oedema in Response to Captopril

Although viability did not significantly decrease in *ren*$^{-/-}$ fish exposed to 0.05 mM Captopril (Figure 5.2), 30% of the fish developed oedema by 4dpf (Figure 5.5). No oedema was seen in *ren*$^{+/+}$ fish during the first 5 days of development. In 1/20

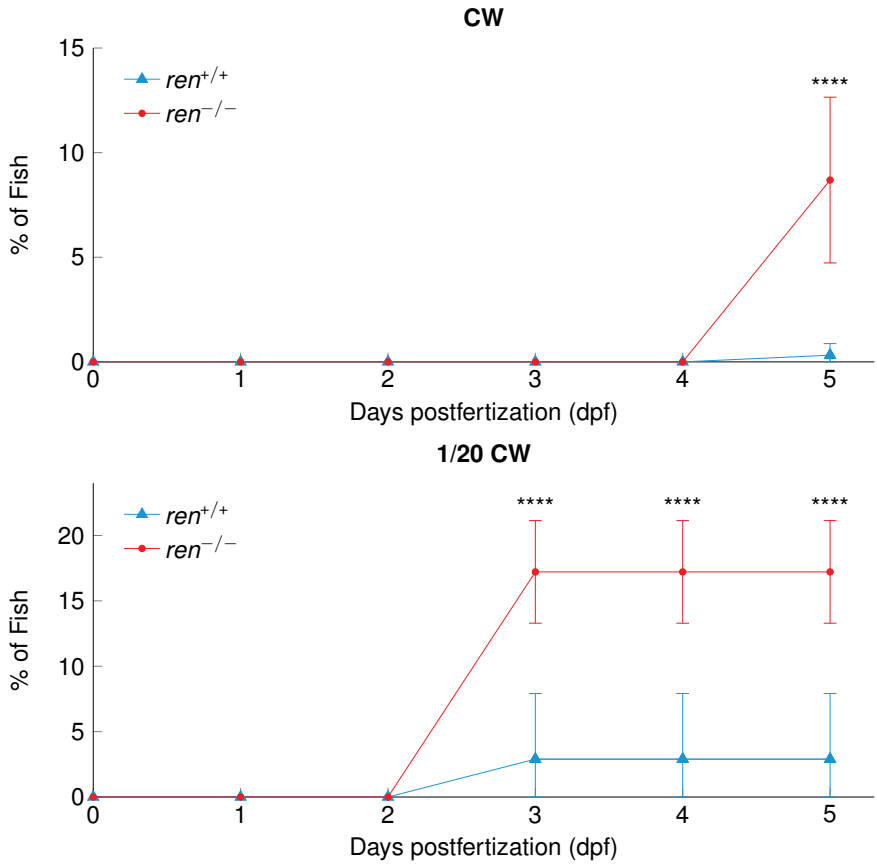

Figure 5.4 | **Occurrence of oedema during early development** Occurrences of pericardial and yolk sac oedemas during the first 5 days of *ren*$^{+/+}$ and *ren*$^{-/-}$ fish during development in normal salinity (CW) and low salt (1/20 CW). Data are mean $\pm$ SD. ****=p<0.0001.

CW and Captopril, oedemas were noted as early as 24hpf in *ren*$^{+/+}$ and 48hpf in *ren*$^{-/-}$. No *ren*$^{-/-}$ and *ren*$^{+/+}$ fish survived past 3dpf and 4dpf, respectively. This was suggests that despite the lack of renin in *ren*$^{-/-}$ fish, inhibition of ACE reduces viability suggesting that ACE might be implicated in other pathways.

5.2.5 Delay in Swim Bladder Inflation

In zebrafish the swim bladder develops at 4-5dpf and is directly correlated to the fish length, an indicator of overall fish development. A preliminary experiment investigated the swim bladder size in *ren*$^{-/-}$ at 5dpf against age-matched *ren*$^{+/+}$ fish (Figure 5.6). There was a significant difference in swim bladder size in *ren*$^{-/-}$ fish at 5dpf (p=<0.0001, n=9). Interestingly, when fish were grown in 1/20 CW, no sig-

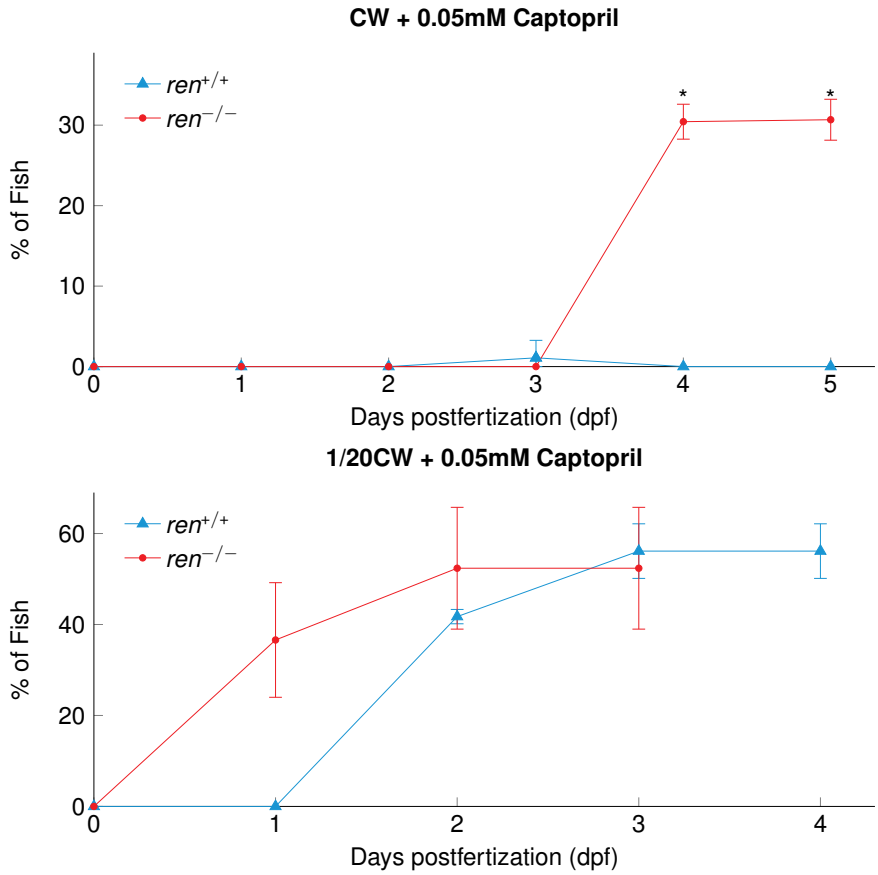

Figure 5.5 | **Occurrence of oedema during early development of zebrafish exposed to** 0.05 mM **Captopril** Incidence of pericardial and yolk sac oedema in *ren*$^{+/+}$ and *ren*$^{-/-}$ fish during first 5 days of development, when exposed to 0.05 mM Captopril in normal salt (CW) and low salt (1/20 CW). Data are mean ± SD.*=p<0.05.

nificant difference in swim bladder size was observed (p=0.5705, n=9). In line with previous observations, there was a reduction of swim bladder size of *ren*$^{+/+}$ fish in CW compared to *ren*$^{+/+}$ in 1/20 CW (p<0.0001) [43]. The high variability in *ren*$^{+/+}$ fish in 1/20 CW suggests that not all fish are capable of handling low salt equally.

5.2.6 Swim Bladder and Length Measurement up to 5 Days of Development

The VAST system allows a large number of fish to be imaged with highly reproducible accuracy. Furthermore, the fish are anaesthetised and collected from a 96-well plate and returned following the image acquisition to the same well. The

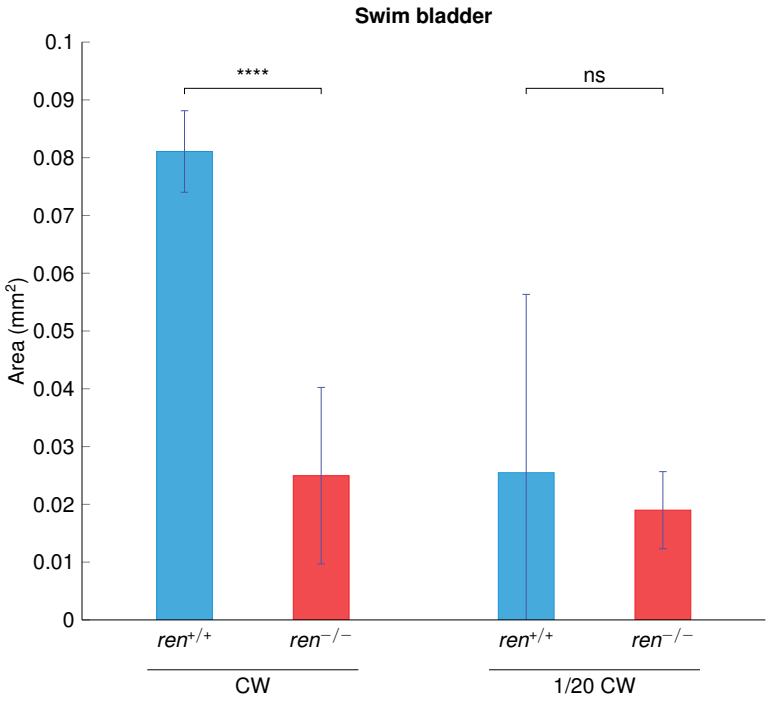

Figure 5.6 | **Swim bladder size of *ren*$^{+/+}$ and *ren*$^{-/-}$ at 5dpf** Swim bladder area was assessed at 5dpf in *ren*$^{+/+}$ (n=9) and *ren*$^{-/-}$ (n=9) zebrafish, from acquired lateral brightfield images. Swim bladder size was reduced in *ren*$^{-/-}$ fish in normal salt water (CW) (p<0.0001). No significant difference in swim bladder size was observed in low salt water (1/20 CW), *ren*$^{+/+}$ (n=9) *ren*$^{-/-}$ (n=8), p=0.5705). Swim bladder size of *ren*$^{+/+}$ fish was reduced in 1/20 CW. Data are mean $\pm$ SD. ****=p<0.0001.

absence of mounting medium and minimal exposure to anaesthetic enables the same fish to be tracked for several days during development. However, during the imaging and transfer of the fish, approximately 10% of the fish are injured and lost after every imaging session. To reduce the number of fish lost and allow statistically significant and reproducible data to be collected, the measurements were restricted to 3 time points. The preliminary data for swim bladder inflation suggested delayed development in *ren*$^{-/-}$ fish at 5dpf. The VAST was used to image fish at 3dpf, 4dpf and 5dpf to determine whether the delay in development occurs before 5dpf. Lateral images were acquired and the size of the swim bladder as well as the length of the fish were assessed (Figure 5.7). Fish with no visible swim bladder were recorded to have a swim bladder area of 0 mm^2. Although the VAST imaging systems ensures reproducible images, the tail region is commonly excluded from the image. In these instances the length was not recorded. There

was no difference in fish length at 3dpf between *ren*$^{-/-}$ (n=38, length=3.43 mm) and *ren*$^{+/+}$ (n=37, length=3.36 mm) fish and a lack of inflated swim bladders in both *ren*$^{-/-}$ (n=47, area=0 mm^2) and *ren*$^{+/+}$ (n=48, area=0 mm^2) fish (Figure 5.8). An increased size and more fish with inflated swim bladders were observed at 4dpf in *ren*$^{+/+}$ (n=20, length=3.7 mm; n=46, area=29.26 mm^2) fish compared to *ren*$^{-/-}$ (n=30, length=3.54 mm; n=43, area=7.87 mm^2) fish, and the latter had a significant reduction in length (p=0.0156). This phenotype was more dramatic at 5dpf with all *ren*$^{+/+}$ (n=44, area=117.46 mm^2) having inflated swim bladders of various sizes however, many *ren*$^{-/-}$ (n=41, area=48.26 mm^2) fish lacked or had small swim bladders. Furthermore, there was a significant difference in fish length (*ren*$^{+/+}$: n=15, length=3.89 mm; *ren*$^{-/-}$: n=28, length=3.69 mm) at 5dpf between the two genotypes (p=0.0063).

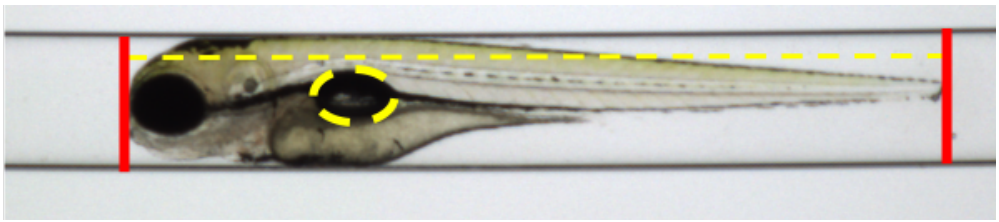

Figure 5.7 | **VAST system measurements** Lateral larval zebrafish image acquired using the VAST system. The fish is held in place in a rotatable capillary. Yellow dotted circular line indicates the area determined for the swim bladder area measurements. Red lines and dotted yellow line in-between indicate an example measurement of the length of a zebrafish.

5.2.7 Swim Bladder and Length Measurement up to 8 Days of Development

The VAST is optimised for larval zebrafish and the width of the capillary transporting the fish to the imaging system limits the fish to a maximum age of 8dpf. Since the most significant phenotype in developmental delay appears to be at 5dpf, I was interested to determine whether the phenotype persisted past 5 days of development. New images using the VAST brightfield system were acquired at 3 different time points (4dpf, 5dpf, and 8dpf) (Figure 5.9). Surprsingly, swim bladder size was not significantly different in size at 4dpf (*ren*$^{+/+}$: n=46, area=0.046 mm^2; *ren*$^{-/-}$: n=46, area=0.045 mm^2; p=0.9793), which might be due to measurements

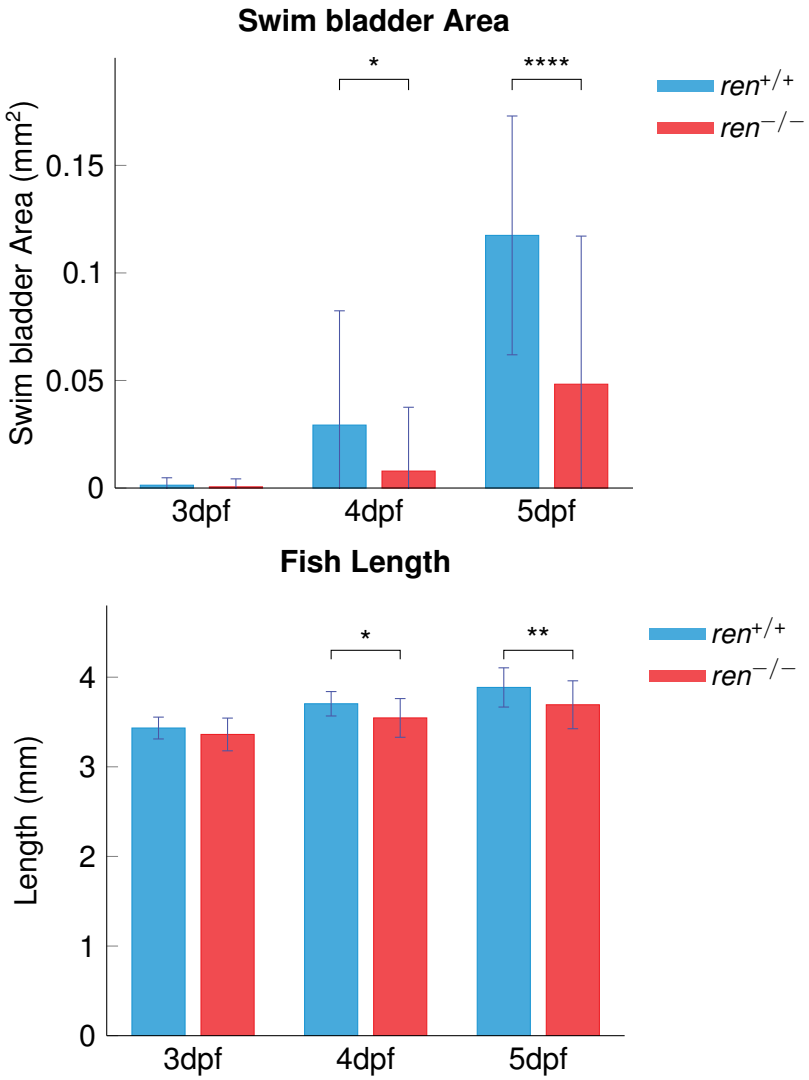

Figure 5.8 | **Swim bladder area and fish length during early development** Ren$^{+/+}$ and *ren*$^{-/-}$ zebrafish larvae were imaged at 3dpf, 4dpf and 5dpf using the VAST brightfield imaging system and fish length and swim bladder size were assessed. Swim bladder size was reduced in *ren*$^{-/-}$ at 4dpf (p=0.0358, n=47), and 5dpf (p=<0.0001, n=44). Significant differences in fish length were seen at 4dpf (p<0.0156, n=30) and 5dpf (p=0.063, n=28) although no significant differences were observed at 3dpf (p=0.2970, n=37). Data are mean ± SD. *=p<0.05, **=p<0.01, ****=p<0.0001.

occurring earlier in than in the previous experiment. However, swim bladder was significantly different at 5dpf (*ren*$^{+/+}$: n=38, area=0.115 mm^2; *ren*$^{-/-}$: n=40, area=0.0574 mm^2; p<0.0001). Interestingly no significant difference of swim bladder area was observable at 8dpf (*ren*$^{+/+}$: n=40, area=0.255 mm^2; *ren*$^{-/-}$: n=41,

area=0.224 mm^2; p=0.1594). The growth retardation at 4dpf (*ren*$^{+/+}$: n=40, length=3.79 mm; *ren*$^{-/-}$: n=38, length=3.58 mm; p<0.0001) and 5dpf (*ren*$^{+/+}$: n=30, length=3.88 mm; *ren*$^{-/-}$: n=29, length=3.76 mm; p=0.0107), was no longer evident by 8dpf (*ren*$^{+/+}$: n=19, length=3.9 mm; *ren*$^{-/-}$: n=21, length=3.87 mm; p=0.8653) suggesting that the fish were capable of reversing the phenotype seen during early development with pathways overcoming the lack of renin from 5dpf.

5.2.8 Pronephric Development

Many components of the RAS are expressed in the developing kidney suggesting an involvement in renal development [192]. The translucent nature of the larval zebrafish allows for renal development to be investigated *in-vivo*, by using transgenic zebrafish lines such as the tg(*wt1b*:EGFP). *Wt1b* is localised in the pronephric proximal tubule and glomerulus in the developing nephron [98]. Confocal imaging of the tg(*wt1b*:EGFP) permits visualisation of the pronephric kidney structures and downstream image analysis allows for measurement of the pronephric structures. Unpublished work in our laboratory showed that fish with an impaired RAS develop asymmetrically sized glomeruli at the pronephric stage and experience a delay in glomerular fusion. I measured the glomerular distance, neck width and glomerular area in 3dpf, 4dpf and 5dpf *ren*$^{-/-}$ and aged matched *ren*$^{+/+}$ zebrafish (Figure 5.10). No difference between the left and right glomerulus was observed in *ren*$^{-/-}$ and *ren*$^{+/+}$ fish at any of the 3 stages of development (Figure 5.11). However, when measuring the anterior and posterior distance between the fusing glomeruli in the pronephric zebrafish kidney, there was a significant delay in fusion of the glomerulus at all stages of development (Figure 5.12). Pronephric neck length was decreased at 3dpf and 4dpf in both the left and right neck regions (Figure 1.13). At 5dpf neck width of the left tubule was significantly different (Figure 5.14). This suggests that renin renin is required for proper development of the zebrafish pronephros and the lack of renin leads to delay of pronephric glomerular fusion.

5.2.9 Renin Cell Morphology in the Pronephric Kidney

In normal salinity RAS blockade in the zebrafish has been shown to increase mural *ren*:LifeAct-RFP expression at the AMA [47] and this is consistent with the RAS-mediated negative feedback on renin expression. To test whether such a feedback

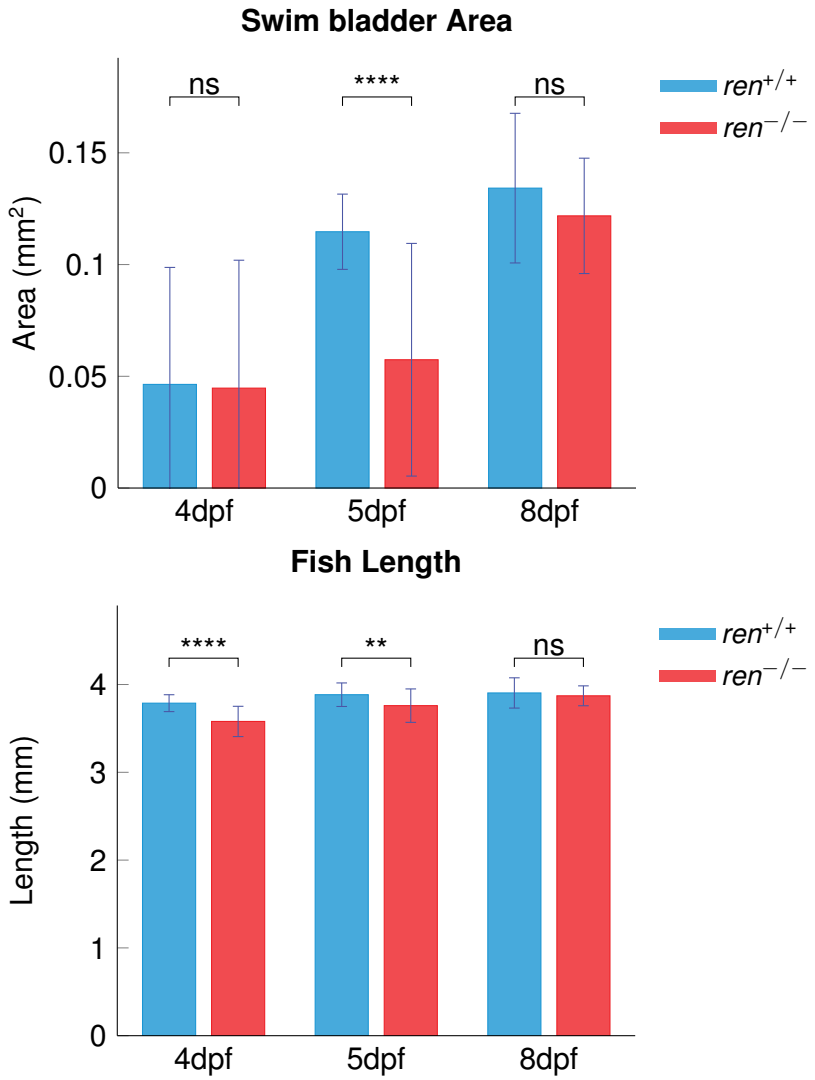

Figure 5.9 | **Swim bladder size and length of *ren*$^{-/-}$ fish** *ren*$^{+/+}$ and *ren*$^{-/-}$ zebrafish larvae were imaged at 3 developmental time points (4dpf, 5dpf and 8dpf) using the VAST birghtfield imaging system and fish length and swim bladder size were assessed. Swim bladder development is was delayed in *ren*$^{-/-}$ at 5dpf ($p<0.0001$, n=37), however no difference was seen at 8dpf. Significant differences in fish length were seen at 4dpf ($p<0.0001$, n=29) and 5dpf ($p=0.0119$, n=29) although no significant difference was observed at 8dpf ($p=0.8478$, n=22). Data are mean $\pm$ SD. **=$p<0.01$, ****=$p<0.0001$.

mechanism existed in the *ren*$^{-/-}$ fish, the extent of mural cell *ren*:LifeAct-RFP expression at the AMA was determined in *ren*$^{+/+}$ and *ren*$^{-/-}$ carrying the *ren*:LifeAct-RFP transgene using the SPIM microscopy system. No significant change at 5dpf in the *ren*:LifeAct-RFP cell expressing coverage at the AMA could be observed

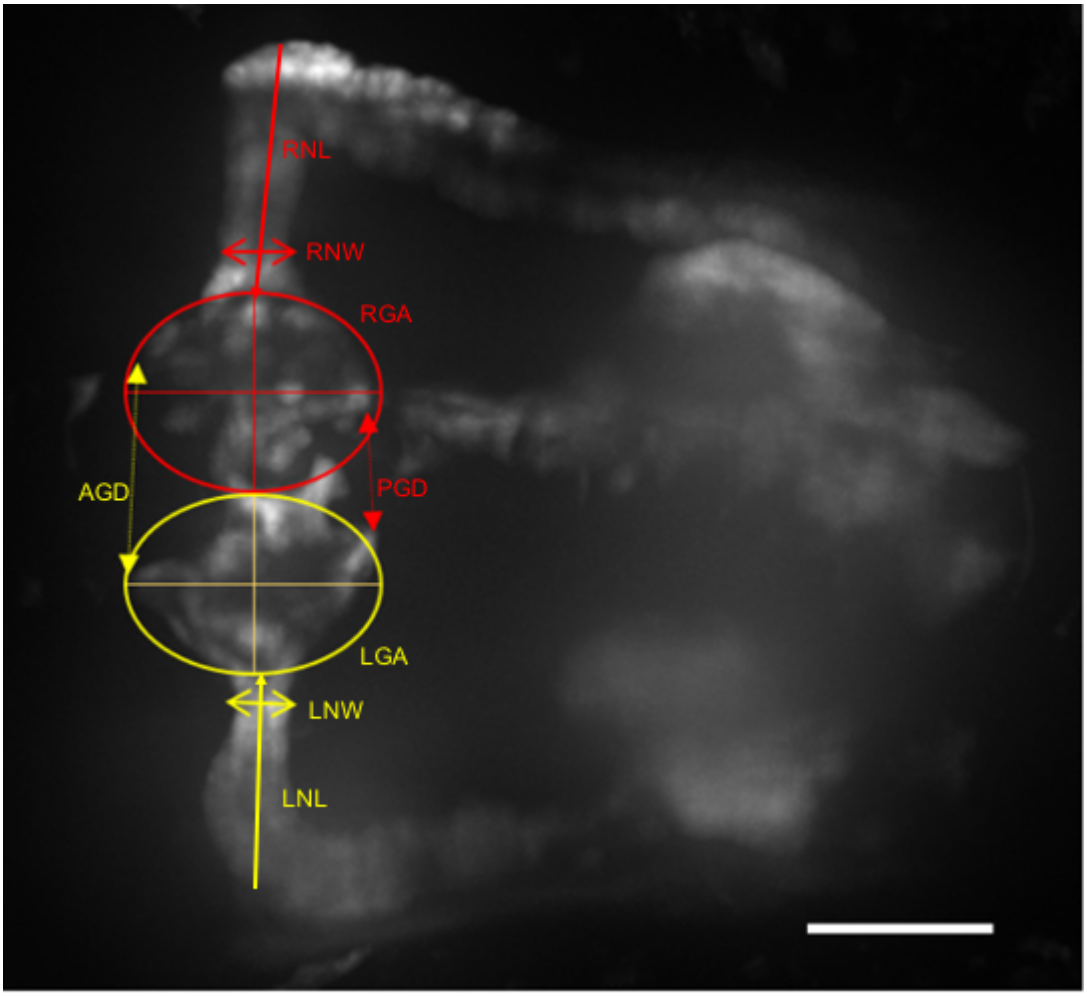

Figure 5.10 | **Fluorescent dorsal image of the pronephros of the tg(*wt1b*:EGFP) transgenic line** Fluorescent image of the pronephros of a Tg(*wt1b*:EGFP) on a *ren*$^{-/-}$ background acquired using the VAST confocal system. The VAST imaging system ensured accurate reproducible orientation of every imaged fish. Yellow oval indicates the measurement for the left glomerular area (LGA), yellow double sided arrow indicates the left neck width (LNW), dotted line with double sided yellow arrows indicates the anterior glomerular distance (AGD), yellow arrow indicates left neck length (LNL). Red oval is an example measurement for the right glomerular area (RGA), red double sided arrow the right neck width (RNW) and the red dotted line with double sided arrow indicates the posterior glomerular distance (PGD), and red arrow indicates right neck length (RNL). Scale bar=50 µm.

(Figure 5.15). The lack of increase of *ren*:LifeAct-RFP expressing cells suggest that renin might not be crucial during early development in terms of its role in the RAS cascade.

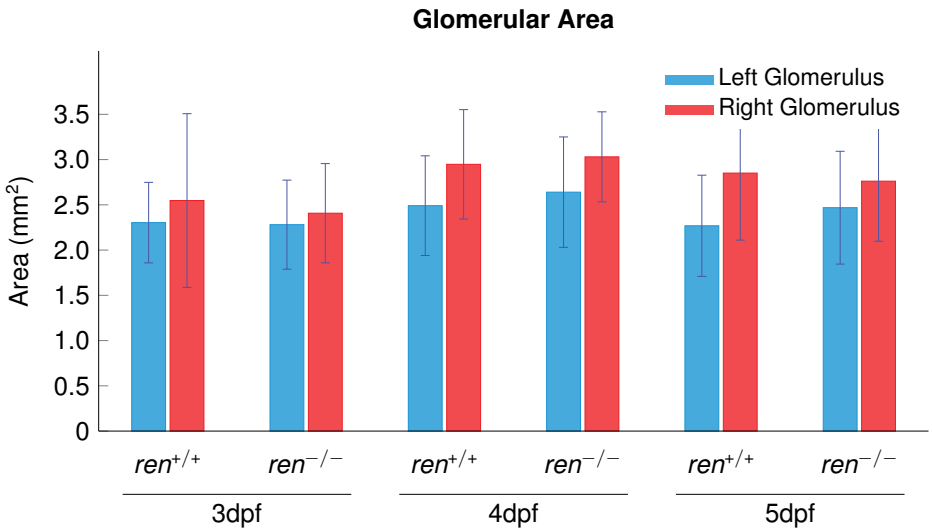

Figure 5.11 | **Comparison of glomerular area between *ren*$^{+/+}$ and *ren*$^{-/-}$ zebrafish at 3dpf, 4dpf and 5dpf** Measurements of glomerular area during pronephric development. Images were acquired using the VAST system to ensure reproducibility. Area of right and left glomerulus were measured using dorsal images of the larval zebrafish (*ren*$^{+/+}$: 3dpf n=43, 4dpf=35, 5dpf=33; *ren*$^{-/-}$: 3dpf n=39, 4dpf=30, 5dpf=29). Data are mean $\pm$ SD.

5.2.10 Renin Cell Morphology in the Mesonephric Kidney

The role of renin in the pronephric kidney might be different to that in the mesonephric kidney, and to investigate this I crossed *ren*$^{-/-}$ and *ren*$^{+/+}$ fish with tg(*ren*:LifeAct-RFP, *acta2*:EGFP) double reporter fish. Renin cells are specialised smooth muscle cells, expressing the smooth muscle marker *acta2*. The double transgenic would visualise smooth muscle cells, renin cells expressing *ren*:LifeAct-RFP, *acta2*:EGFP and potentially permit capture of smooth muscle cells assuming a renin phenotype. Confocal imaging of *ex vivo* mesonephric kidneys of tg(*ren*:LifeAct-RFP, *acta2*:EGFP) revealed a substantial increase of *ren*:LifeAct-RFP expressing cells in the *ren*$^{-/-}$ and fish compared to the *ren*$^{+/+}$ control fish (Figure 5.16). In *ren*$^{+/+}$ mesonephric kidneys, renin expressing cells are located along afferent arterioles but not efferent arterioles [67]. The cells appear in a interchanging pattern with *acta2* expressing smooth muscle cells. In the mesonephric *ren*$^{-/-}$ kidney, smooth muscle cells appear to lose *acta2*:EGFP expression which is replaced by expression of *ren*:LifeAct-RFP, giving the vessels an appearance of continuous renin cell covering the vessel (Figure 5.16).

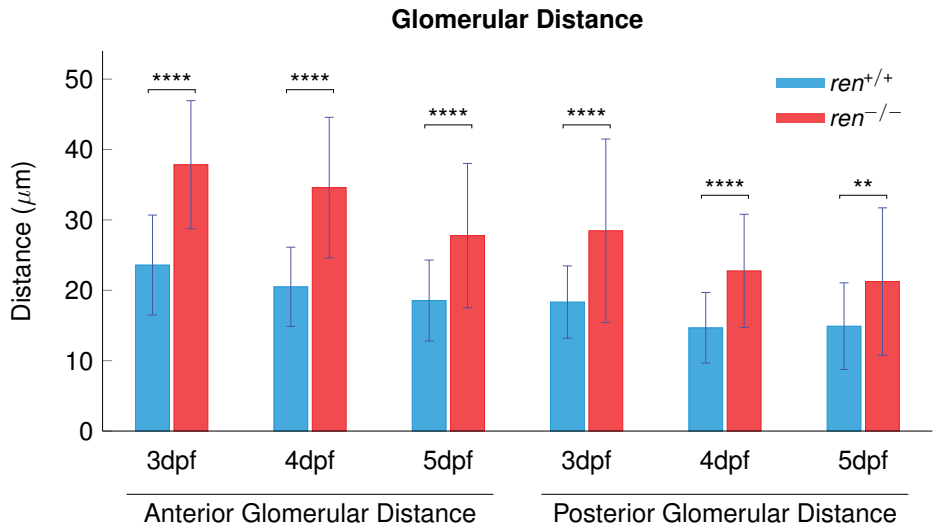

Figure 5.12 | **Comparison of glomerular distance in *ren*$^{+/+}$ and *ren*$^{-/-}$ zebrafish at 3dpf, 4dpf and 5dpf** Measurements of the anterior and posterior glomerular distance to investigate a possible delay in glomerular fusion in *ren*$^{-/-}$ zebrafish. The pronephric images were from age matched *ren*$^{+/+}$ (3dpf n=43, 4dpf=35, 5dpf=33) and *ren*$^{-/-}$ (3dpf n=39, 4dpf=30, 5dpf=29) fish crossed with the transgenic tg(*wt1b*:EGFP), acquired using the spinning disk confocal microscope mounted to the VAST system. Data are mean ± SD. **=p<0.01, ****=p<0.0001.

5.2.11 Mesonephric Kidney Histology

Coronal plane sections of adult *ren*$^{+/+}$ and *ren*$^{-/-}$ zebrafish were taken in a dorsal to ventral orientation. This permitted nearly fully intact 5 µm thick sections of the adult mesonephric zebrafish kidney to be prepared. H&E staining visualised major renal structures (Figure 5.17). Kidneys of *ren*$^{-/-}$ fish showed vacuolation of the proximal tubule (n=3). No vacuolation was observed in the distal tubule and the number of glomeruli appeared unchanged between *ren*$^{+/+}$ and *ren*$^{-/-}$ zebrafish kidneys.

5.2.12 Verification of RFP and EGFP Expression in FAC Sorted Renin and Smooth Muscle Actin Cells

EGFP- and RFP- positive cells were sorted by FACS from kidneys of adult *ren*$^{-/-}$ and *ren*$^{+/+}$ tg(*ren*:LifeAct-RFP, *acta2*:EGFP) fish. The FACS and cell dissociation protocols were carefully optimised to ensure the capture of live cells and to maximise the recovery of the small number of renin expressing cells. The FACS gating

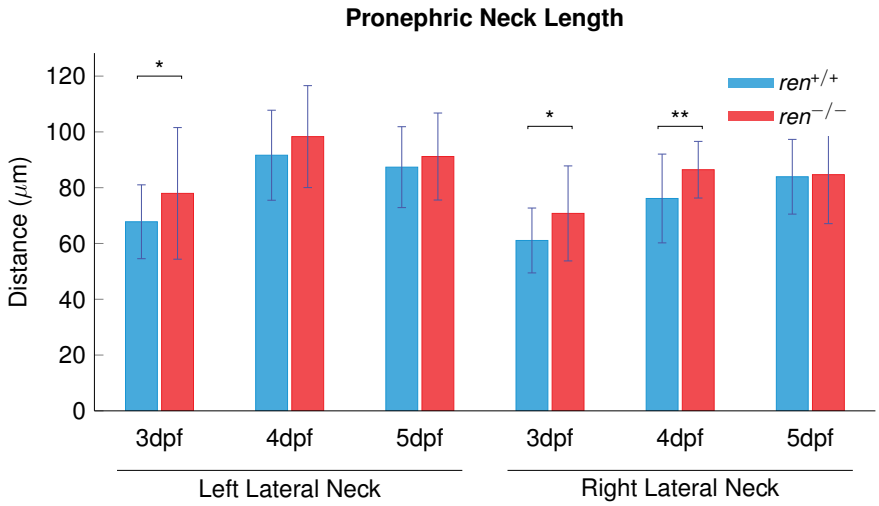

Figure 5.13 | **Comparison of the lateral neck length of the pronephros in *ren*$^{+/+}$ and *ren*$^{-/-}$ zebrafish at 3dpf, 4dpf and 5dpf** Measurements of the lateral neck length to investigate a delay in pronephric development in *ren*$^{-/-}$ fish. The tg(*wt1b*:EGFP) zebrafish on a *ren*$^{+/+}$ and *ren*$^{-/-}$ background were imaged using the VAST confocal system. Downstream image analysis permitted the measurement of the left and right neck length (*ren*$^{+/+}$: 3dpf n=43, 4dpf=35, 5dpf=33; *ren*$^{-/-}$: 3dpf n=39, 4dpf=30, 5dpf=29). Data are mean $\pm$ SD.*=p<0.05, **=p<0.01.

was optimised to capture, separately, RFP- and EGFP-expressing cells, to quantify the number of *ren* and *acta2* expressing cells respectively (Figure 5.18). Further gating of the sorted GFP-positive cells was performed to detect LifeAct-RFP and EGFP double positive cells. The gating also permitted the quantification of EGFP-positive cells with varying LifeAct-RFP brightness allowing me to determine the number of cells transitioning from a smooth muscle to renin expressing cell phenotype.

Following previous experiences in our laboratory, the cells were seeded onto fibronectin-coated, glass-bottom culture dishes. The fibronectin is ideal for JG cell attachment to glass-bottom dishes, which permit light penetration for confocal microscopy imaging. Confocal microscopy was used to image EGFP and RFP expression. The cells fully adhered to the fibronectin-coated dishes and expressed LifeAct-RFP and EGFP (Figure 5.19). The images were acquired using high resolution microscopy to enable visualisation of the cytoskeleton which is revealed by the binding of LifeAct-RFP to intracellular actin. Although the cells settled, no changes in cell morphology or evidence for cell proliferation was observed, and LifeAct-RFP and EGFP fluorescence were no longer visible in cells after 5 days in

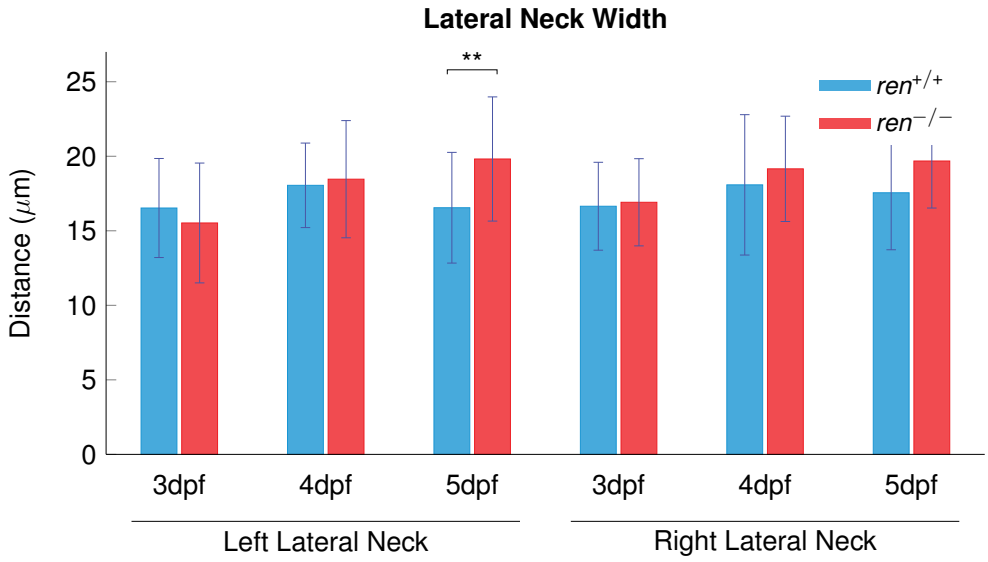

Figure 5.14 | **Comparison of the lateral neck width of the pronephros in zebrafish at 3dpf, 4dpf and 5dpf.** Measurements of the lateral neck width in *ren*$^{+/+}$: 3dpf n=43, 4dpf=35, 5dpf=33; *ren*$^{-/-}$: 3dpf n=39, 4dpf=30, 5dpf=29) to investigate a delay in pronephric development in *ren*$^{-/-}$ fish. The tg(*wt1b*:EGFP) zebrafish on a *ren*$^{+/+}$ and *ren*$^{-/-}$ background were imaged using the VAST system. Data are mean $\pm$ SD. **=p<0.01.

culture, indicating cell de-differentiation or cell death. However, this first demonstrated successful sorting and culturing of renin cells, expressing both *ren*:LifeAct-RFP, *acta2*:EGFP, in line with previous observations by Rider et al. [67].

5.2.13 FAC sorting *ren* and *acta2* Expressing Cells from Mesonephric *ren*$^{+/+}$ and *ren*$^{-/-}$ Zebrafish Kidneys.

FAC sorted EGFP- and LifeAct-RFP-positive cells from the transgenic tg(*ren*:LifeAct-RFP; *acta2*:EGFP) fish on *ren*$^{-/-}$ and *ren*$^{+/+}$ backgrounds were quantified by analysis of the FACS data (Figure 5.18). LifeAct-RFP and EGFP expression were confirmed by high resolution imaging of cells plated on fibronectin-coated culture dishes. The cell sorting quantified the phenotype of the increased number of renin expressing cells observed in Section 5.2.10. The FACS data show that in *ren*$^{+/+}$ fish kidneys, the sorted cells comprised of 78% EGFP-positive cells, 1.5% LifeAct-RFP-positive cells and 20.23% double-positive cells expressing both EGFP- and LifeAct-RFP. In contrast *ren*$^{-/-}$ fish had 64% EGFP-positive cells,

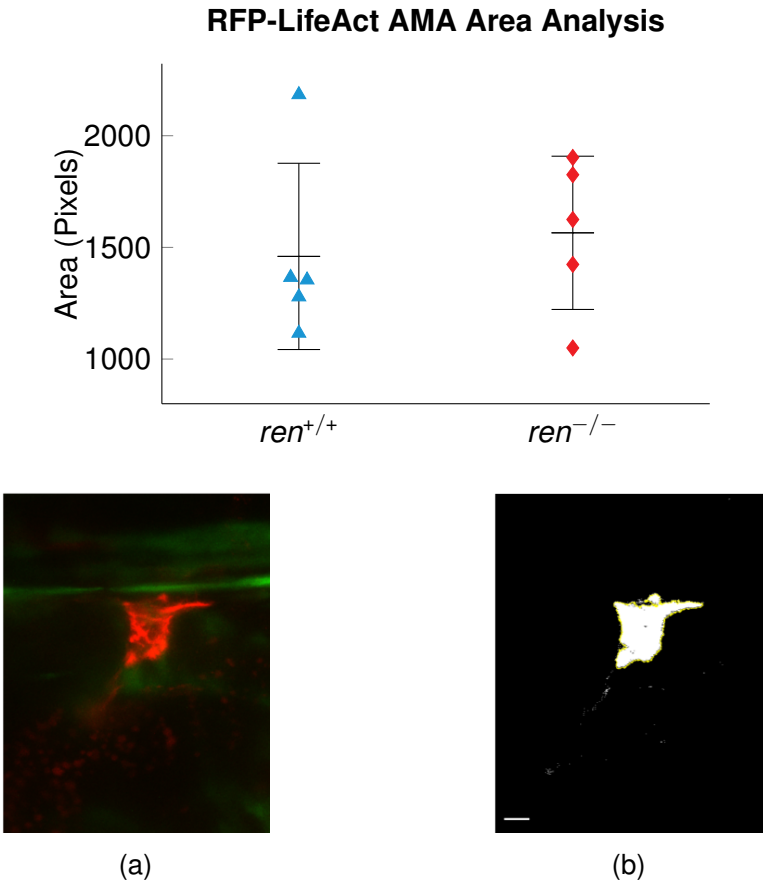

Figure 5.15 | **Evaluation of *ren*:RFP-LifeAct signal at the AMA in tg(*ren*:RFP-LifeAct, *acta2*:EGFP) on a *ren*$^{+/+}$ and *ren*$^{-/-}$ background** (a) Pronephric AMA with red being RFP-LifeAct in *ren* expressing cells and green being EGFP in *acta2* expressing cells. (b) representative greyscale image for mean area analysis . There was no significant difference in the area of RFP-LifeAct along the AMA in *ren*$^{+/+}$ and *ren*$^{-/-}$ 5dpf larval zebrafish.

3% LifeAct-RFP-positive cells and 32% double-positive cells. This suggests that *ren*$^{-/-}$ fish possess twice the number of *ren*-expressing cells, only expressing *ren*:LifeAct-RFP, in the adult mesonephric kidney, and a 60% increase in cells expressing both reporters. This is suggestive of a higher number of cells transitioning from a smooth muscle cell phenotype to a renin-expressing cell.

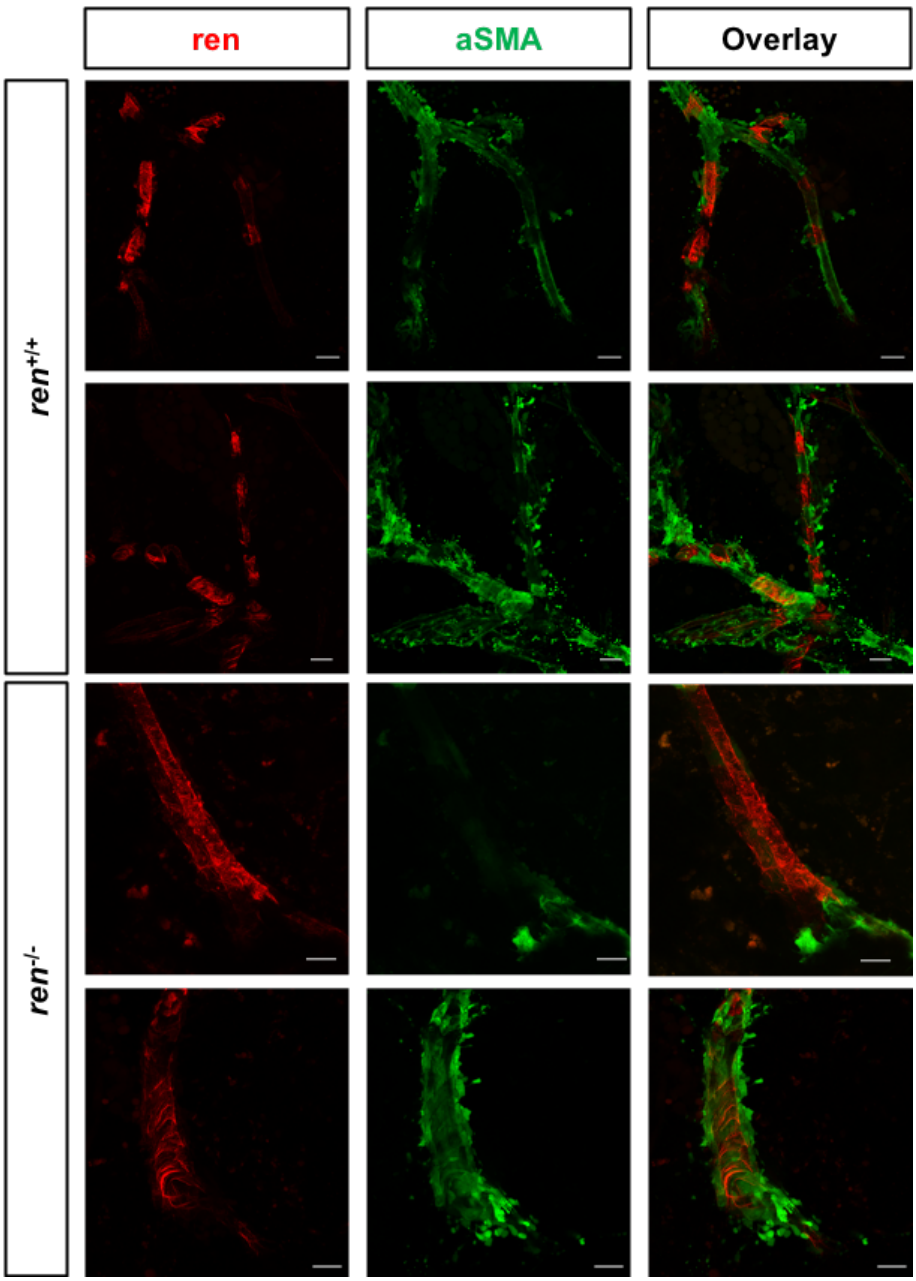

Figure 5.16 | **Expression of renin and smooth muscle markers in the mesonephric kidney in zebrafish on a *ren*$^{+/+}$ and *ren*$^{-/-}$ background** Fluorescent image of tg(*ren*:LifeAct-RFP, *acta2*:EGFP), *ren*$^{+/+}$ and *ren*$^{-/-}$ mesospheric kidney squash. Images of *ren*$^{-/-}$ mesonephros revealed increase of renin expressing cells along renal arterioles. *Ren*$^{-/-}$ renal vasculature looses intermittent pattern of renin and smooth muscle cells. Scale bar=50 µm.

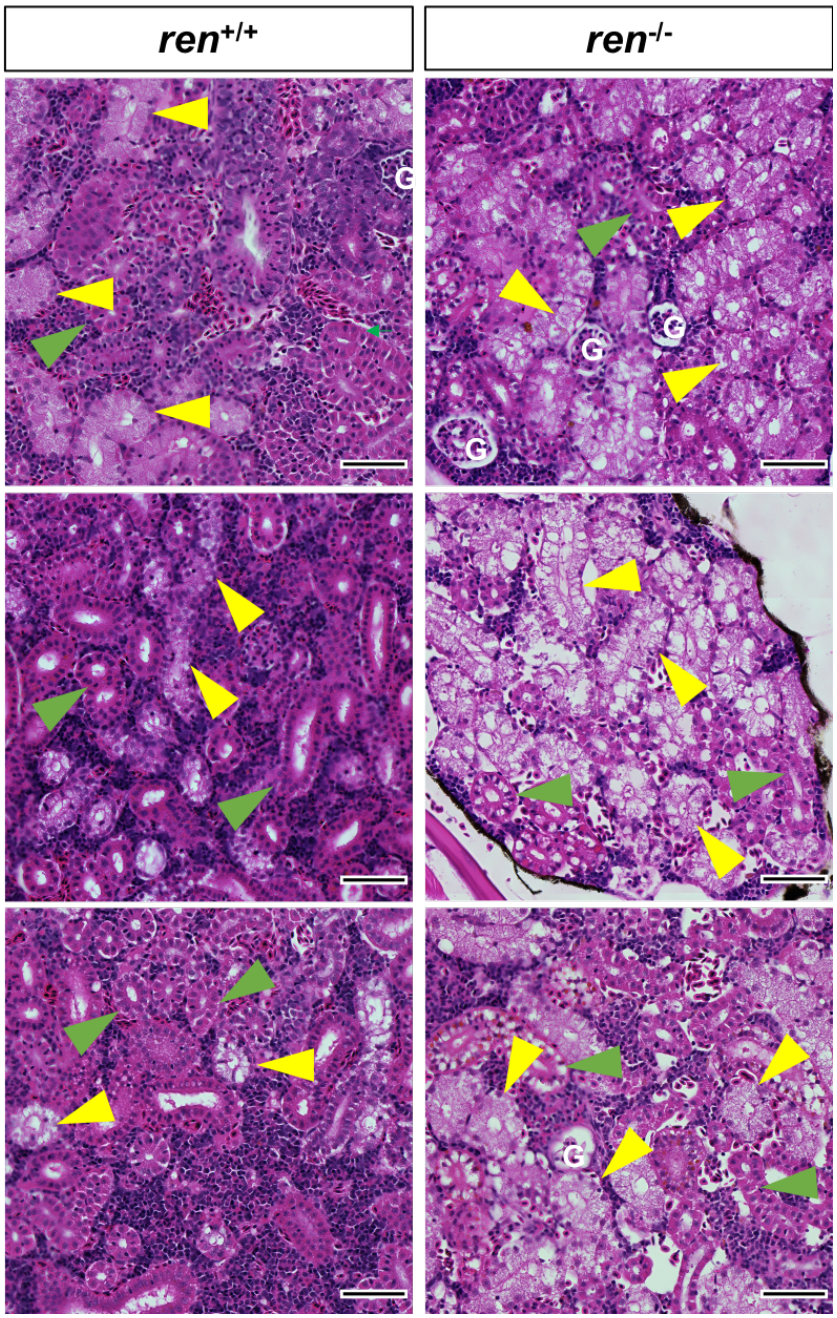

Figure 5.17 | **H&E stain of a *ren*$^{+/+}$ and a *ren*$^{-/-}$ zebrafish mesonephric kidney section** Comparison of H&E stained adult mesonephric kidneys from *ren*$^{-/-}$ and *ren*$^{+/+}$ fish revealed excessive vacuolation of proximal tubule cells (yellow arrows) in the kidney of *ren*$^{-/-}$ fish. Cells of the distal tubule (green arrows) appeared unchanged. G shows the glomeruli in the kidney sections. Scale bar=100 µm.

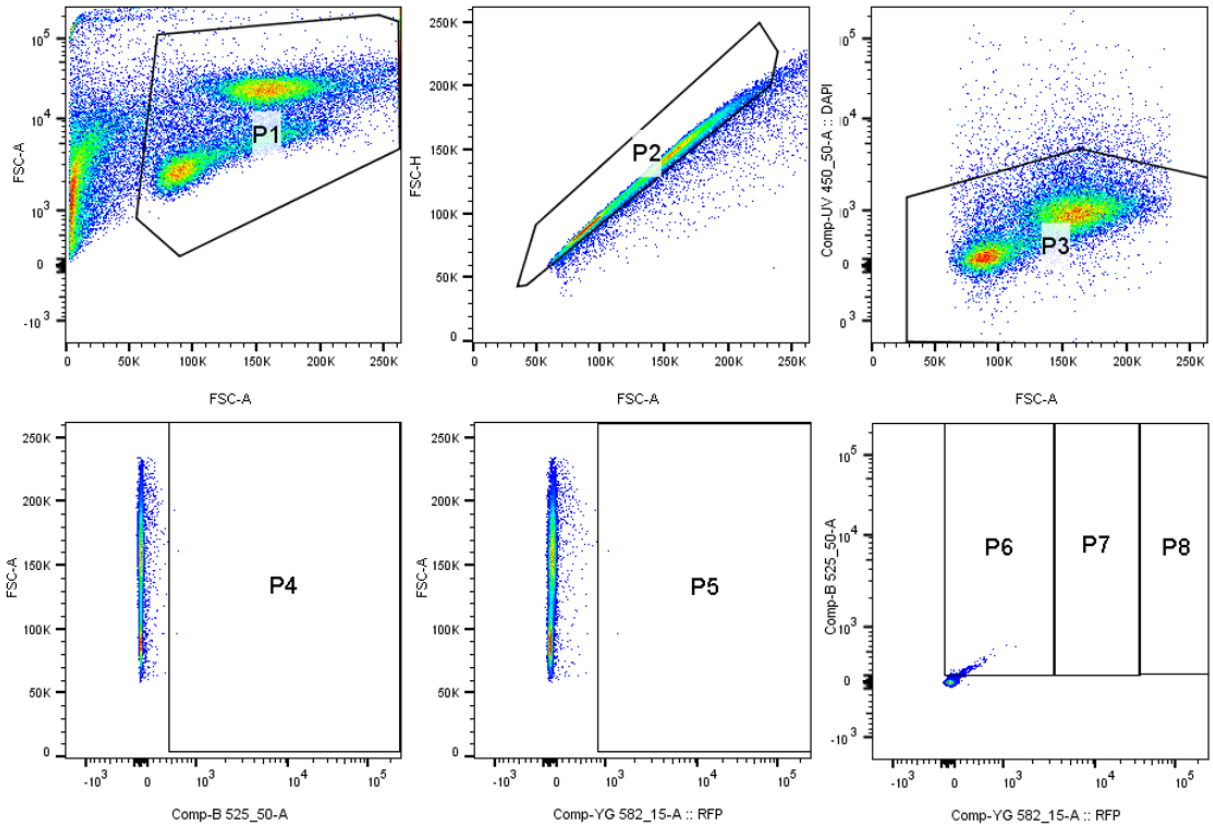

Figure 5.18 | **Gating used for FACS of *ren* and *acta2* expressing cells** Using cells from adult $ren^{+/+}$ and $ren^{-/-}$ tg(*ren*:RFP; *acta2*:EGFP) kidney digests, gating strategy was optimised on non fluorescent WIK mesonephric kidneys. P1, singlet cells were gated on by plotting the side scatter area (SSC-A) against forward scatter height (FSC-H). P2, the population of live, single cells were gated by plotting the FSC-H of the singlet cells against the forward scatter area (FSC-A). P3, Following the previous gating, cells negative for the 'live-dead' marker DAPI were selected. P4 and P5 were gated on the FSC-A against the green (525 nm) or red (582 nm) laser to discriminate between autofluorescence and true signal. P6, P7 and P8 were gated for the green vs red channel and with low, medium, and high RFP signal, respectively.

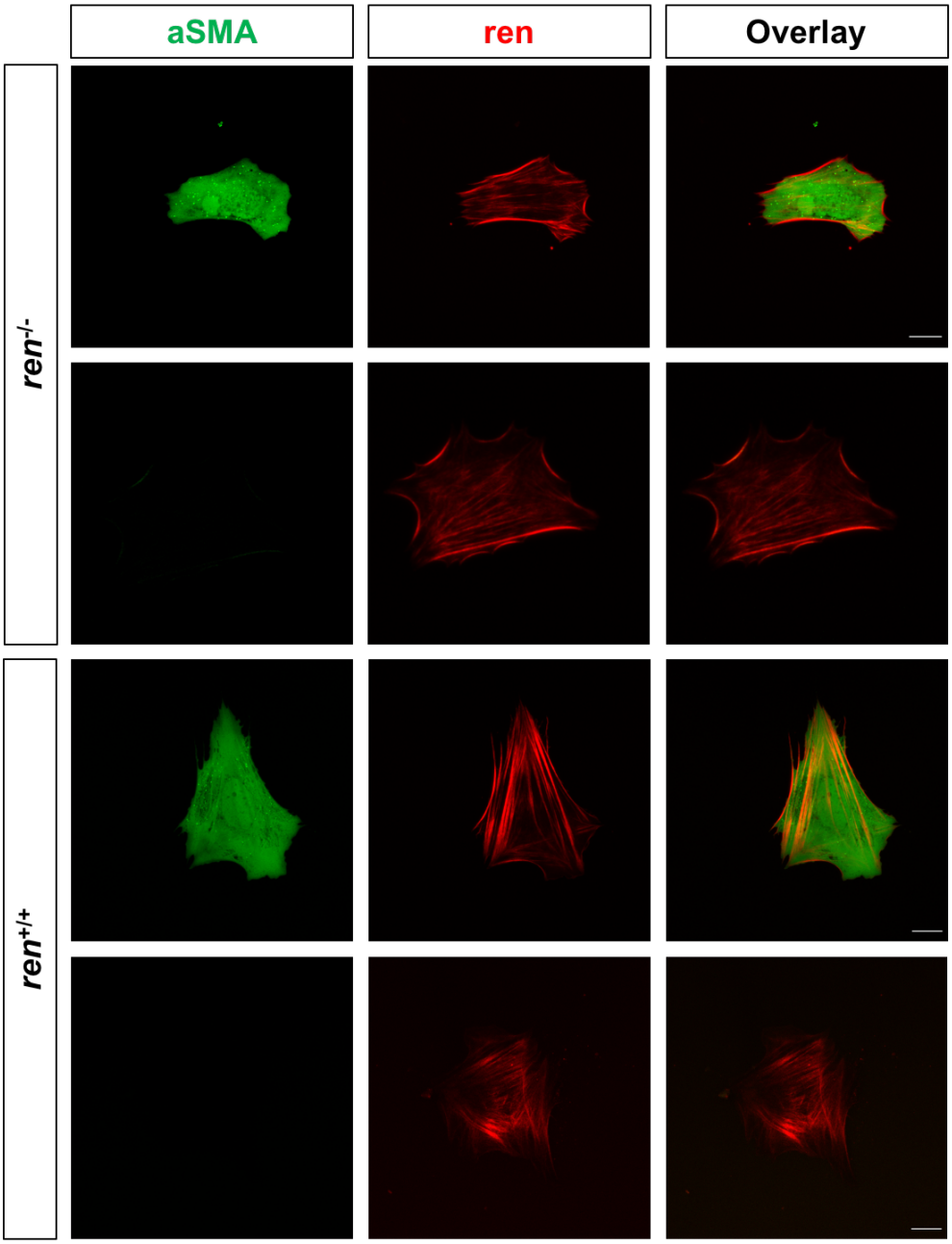

Figure 5.19 | **Confirmation of RFP and EGFP expression in *ren* and *acta2* expressing cells isolated from adult metanephric kidneys** *ren* and *acta2* expressing cells from metanephric tg(*ren*:LifeAct-RFP; *acta2*:EGFP) $ren^{+/+}$ and $ren^{-/-}$ kidneys were FAC sorted on their RFP and EGFP expression and plated on fibronectin-coated (50 µg/ml) dishes. Images were acquired after 48 hours of culture with a confocal microscope and a 60× objective lens. Green: EGFP expression in *acta2* expressing cells, red: LifeAct-RFP expression in *ren* expressing cells. Scale bars=20 µm.

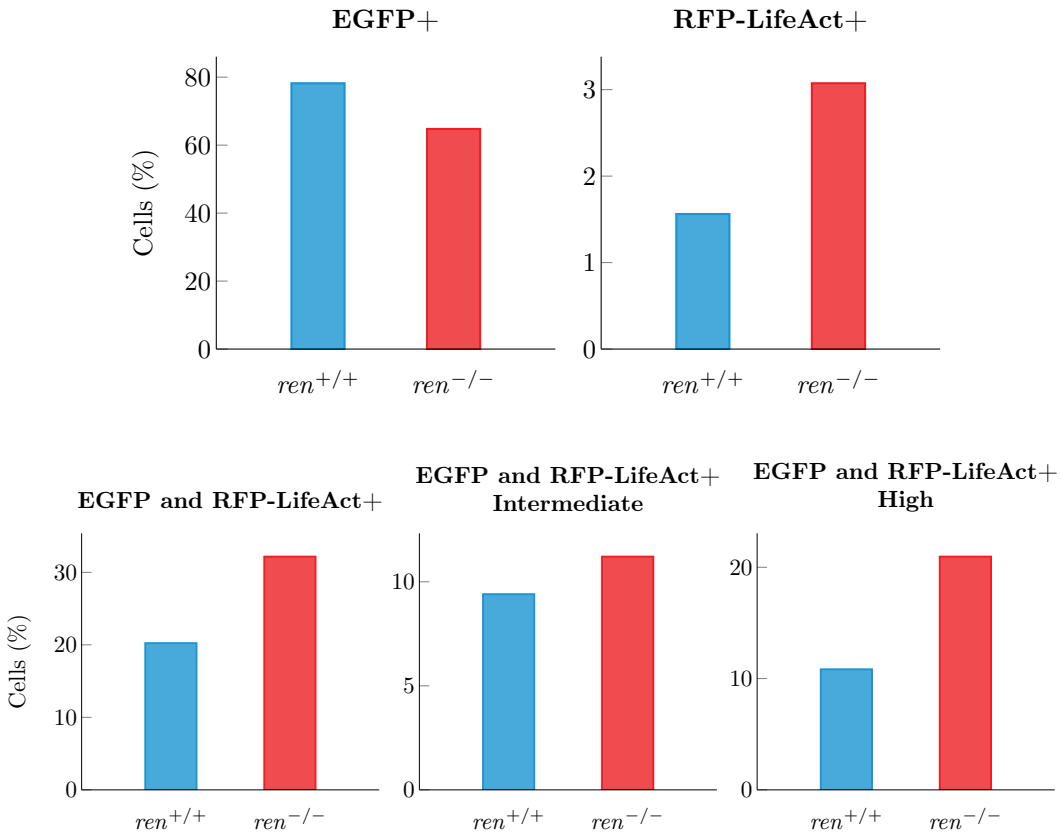

Figure 5.20 | **Quantification of cell sorting data from FAC sorting of adult metanephric tg(*ren*:LifeAct-RFP; *acta2*:EGFP) *ren*$^{+/+}$ and *ren*$^{-/-}$ zebrafish kidneys** Quantified data on *ren*- (LifeAct-RFP) and *acta2*- (EGFP) expressing cells. The cell sorts are from combining 10 *ren*$^{+/+}$ and 10 *ren*$^{-/-}$ zebrafish mesonephric kidneys.

5.3 Discussion

5.3.1 Knockout Validation

This chapter focuses on the characterisation of the first renin null zebrafish strain. Homozygous renin knockout fish were genotyped by PCR amplification of the knockout region with subsequent sequencing of the PCR product verifying the 8bp deletion in renin exon 2. The 8bp deletion causes a frameshift mutation resulting in early termination of renin translation. Knockout animals are commonly validated by confirming the absence of the protein using western blotting. Unfortunately, there is a general lack of zebrafish-specific antibodies and, critically, there is no antibody available that recognises zebrafish renin. Due to the low protein homology between zebrafish and mammalian renin [40], it is highly unlikely that mammalian renin antibodies recognise and bind to the zebrafish renin epitope. Furthermore, mRNA levels were not confirmed in the knockout and compared to wild-type zebrafish. Lack of detectable renin mRNA would suggest a successful knockout, however, previous reports have indicated that not all transcripts with a frameshift mutation are directed to the Nonsense Mediated Decay pathway and might be detectable. Hence, measurement of the renin protein is crucial to fully verify this knockout [193].

AngI and AngII is virtually undetectable in the plasma of *Ren-1^c* mice [62]. It would be interesting to validate this by measuring the absence of AngI and AngII in the plasma and kidney tissue of *ren*$^{-/-}$ zebrafish. The mass spectrometry assay described in chapter 2.0 was shown to be highly accurate and specific to zebrafish AngI and AngII. However, a disadvantage of the mass spectrometry assay is the large quantity of animals required for a single measurement, making it unaffordable for routine analysis.

5.3.2 Viability

Phenotypic observations were carried out during the early stages of development of *ren*$^{-/-}$ zebrafish larvae. There were no obvious behavioural differences, such as swimming action, between *ren*$^{-/-}$ and wild type zebrafish during early development and adulthood. A loss of viability was reported in homozygous *Ren-1^c* mice [62] which require daily administration of saline solution in order to prevent neonatal death, and are polyuric due to their inability to concentrate their urine [62]. In contrast, there was also no reduction in viability in *ren*$^{-/-}$ fish under normal salt

concentrations. The survival of *ren*$^{-/-}$ fish might be due to the differences in environment and water handling, since zebrafish are obviously surrounded by water and dehydration is not an issue. To test the requirement for renin in salt handling in zebrafish, larval *ren*$^{-/-}$ fish were placed in a low salt environment and showed no evidence of reduced viability. The survival of *ren*$^{-/-}$ fish in a low salt environment suggests that alternative pathways can compensate for the lack of renin. Loss of viability of *ren*$^{-/-}$ fish was only observed when the fish were placed in low salt and treated with Captopril and this was in keeping with a previous study by Rider *et al.*, which reported only 3% survival when fish were treated with Captopril and exposed to a low salt environment [47].

In addition to the advantages of their aqueous environment, zebrafish have ionicytes in their gills and their skin during early development, providing alternative routes for salt homeostasis. Salt regulation in fish is performed by a variety of organs, including the kidneys, gills and skin. However, these structures are not fully developed in early embryos. Larval zebrafish rely predominantly on ion pump activity of the ionocytes, which cover the larval fish skin [194]. Furthermore, it has been shown that larval fish become more tolerant of salinity from the blastula and gastrula stages compared to the cleavage stage due advanced osmoregulatory capacities [194]. It would be interesting to see whether the other salt handling mechanisms are upregulated in *ren*$^{-/-}$ zebrafish, in comparison to *ren*$^{-/-}$ controls.

5.3.3 Salt Handling

The physiologically relevance of the RAS in fish, and its involvement in volume control, was first shown by Smith *et al.* [195]. AngII is recognised as the major regulatory hormone for controlling salt reabsorption in the mammalian kidney [7]. Salt and blood pressure regulation by AngII is enabled predominantly through the AT_1 receptor, which is expressed significantly higher in adult mammalian tissues compared to the AT_2 receptor [196]. Tucker *et al.*, first identified the presence of AT_1 receptors in zebrafish [46]. The mechanisms underlying the blood pressure regulation through AngII activity are different across species, however, plasma AngII and renin have both been shown to be transiently or chronically elevated when transferring euryhaline fish species into salt water [195, 197]. Furthermore, Hoshijima and Hirose reported an increase of renin mRNA when exposing zebrafish to $1/20$ salt water [43]. The $1/20$ salt water concentration used in this chapter is based on that

initial experiment [43]. However, whether the RAS is the major mechanism involved in the salt uptake in fresh water fish is still undetermined. Two studies recently suggested that the RAS is crucial for the salt handling in zebrafish in ion poor water, however further studies are required to assess if AngII receptors are expressed in the larval pronephric, as well as the adult mesonephric, kidney [44, 47]. It would be interesting to assess the ion channels in the gills and determine whether there is an increased expression of these in repose to the lack of renin in *ren*$^{-/-}$ zebrafish.

5.3.4 Swim Bladder

Phenotypic observations between *ren*$^{+/+}$ and *ren*$^{-/-}$ fish during early development, showed a delay in swim bladder development and in some fish no obvious swim bladder could be seen. Furthermore, *ren*$^{+/+}$ fish maintained in 1/20CW showed a similar phenotype. A previous study has suggested that lower ionic concentrations have an effect on zebrafish development, however no differences in morphology were reported when fish were placed in high ionic concentrations [43]. The observation that *ren*$^{-/-}$ fish exhibit a similar developmental delay when grown in CW as *ren*$^{+/+}$ fish do in 1/20 CW suggests that *ren*$^{-/-}$ fish appear to struggle with proper salt regulation. Since no significant differences in swim behaviour can be seen in adult *ren*$^{-/-}$, suggesting swim bladder development normalises at a certain time point, swim bladder inflation was traced from 3dpf up to 8dpf. Interestingly, fish length, which is directly correlated to the inflation of the swim bladder, and swim bladder inflation, were most significantly reduced at 5dpf. However, at later stages the phenotype appeared to be normalised since no differences were observed between *ren*$^{+/+}$ and *ren*$^{-/-}$ fish. It would be valuable to understand what mechanisms these fish use between 5- and 8- dpf, which allow them to revert the oedema phenotype caused by the lack of renin.

5.3.5 Mesonephric Kidney Morphology

The lack of a functional renin gene leads to profound changes in kidney morphology. Especially dramatic is the vacuolation of the proximal tubular cells within the mesonephric kidney. Cytoplasmic vacuolation is characterised by the appearance of vacuoles in renal tubules with the lack of any further morphological changes such as renal degeneration [198]. The proximal tubule can be identified by the presence of a brush border which is not present in the distal tubule. Vacuolation

of cells is indicative of an osmotic imbalance and suggests that increased solute transport across these cells increases the internal osmotic pressure. However, at the present time it is not possible to tell whether the morphological changes in the kidney structure are due to the absence of functional renin or whether they are due to the lack of AngII. In mammalian studies it has been shown that blockade of AngII causes changes to the number of glomeruli. It is difficult to assess the number of glomeruli in the zebrafish since the adult kidney, unlike its mammalian counterpart, is not structurally solid compared to the mammalian metanephric kidney. Furthermore the mesonephric zebrafish kidney is known to exhibit age-dependent nephrogenesis, continually growing as the fish increases in length- age- matched control would have to be carefully selected.

5.3.6 Renal Function

In mice and rats the lack of renin has shown to lead to a reduction in blood pressure. As a result it is argued that this also causes the reduction of renal function and a decrease in proteinuria is observed. Glomerular function in the zebrafish can be assessed via the use of dextran-based compounds [103]. Dextrans are complex polysaccharides, consisting of a mixture of glucose polymers [199]. A major advantage of using dextran for assessing the glomerular filtration is the availability of dextran of variable molecular sizes. Dextrans have been shown to be inert and are commonly labelled with fluorescent tags and can be visually detected within the vasculature of zebrafish larvae [104, 105]. By tracing dextran in the zebrafish pronephros, the filtration activity of the pronephros as been shown to commence after 3dpf. In a healthy pronephric kidney a dextran smaller than 10 kDa is filtered by the glomerulus, however dextran of larger molecular weight (>70 kDa) are filtered less efficiently. Hence, the filtration rate and also the glomerular function can be assessed using the injection of low to high molecular weight fluorescent dextran and measurement of the fluorescent intensity in the blood vessels, respectively [104, 105, 200, 201]. Future studies on the *ren*$^{-/-}$ fish should include renal function. Glomerular filtration could be assessed in adult *ren*$^{-/-}$ fish bred on the 'casper' background, allowing the imaging of blood vessels and fluorescent intensity measurements of injected dextran. Alternatively, Rider *et al.*, developed a clearance assay in which they measured excreted dextran rather than residual dextran remaining in the fish, and this method could be adopted [201]. Such studies remain to be undertaken.

5.3.7 Renin Cell Morphology

During early kidney development renin cells are expressed throughout the mammalian renal vasculature, gradually becoming more restricted in their vascular location. Only after birth, do the renin cells become spatially defined to the JGA [202]. However, mammalian renal smooth muscle cells retain the ability to switch to an endocrine renin phenotype in response to a physiological challenge [185, 203, 204, 205]. It is expected that the lack of a functional renin gene would simulate a severe physiological challenge. To assess whether more renin cells are present in the pronephric zebrafish kidney, *ren*$^{+/+}$ fish were crossed to the renin and perivascular double transgenic reporter line tg(*ren*:LifeAct-RFP, *acta2*:EGFP). The RFP-positive area of renin-expressing cells along the AMA in the zebrafish pronephric kidney was not found to be statistically different to that of *ren*$^{+/+}$ fish, suggesting that renin might not exert a crucial regulatory function during early stages of development. However, imaging of the excised mesonephric kidney of the double transgenic line tg(*ren*:LifeAct-RFP, *acta2*:EGFP) on a *ren*$^{-/-}$ background showed a dramatic phenotype and increase of renin cells along the renal vasculature. This was further quantified by the use of FACS, showing double the number of renin expressing cells in the adult mesonephric kidney. Furthermore, there was an increase in cells expressing both, smooth muscle marker *acta2* and *ren*. However, as shown in Figure 5.16, there is a reduction of smooth muscle cells, suggesting that these cells change their phenotype from a smooth muscle phenotype to a renin expressing cell phenotype. This would emphasise that the physiological function of these perivascular renal cells appears to be conserved.

A subset of mammalian metanephric renin cells are granulated [49]. Rider *et al.*, used immuno-gold staining and electron microscopy to visualise granulation in renin-expressing cells in the of the adult kidney zebrafish. There have been no reports of the granulation of renin-expressing cells in the pronephric zebrafish kidney despite EM being used to image glomerular pronephric structures [64].

5.3.8 Investigation of *ren*$^{+/-}$ Zebrafish

Although heterozygous *Ren*-1$^{c+/-}$ mice showed no phenotype (i.e. no difference in kidney development, blood pressure or renin mRNA) compared to WT animals [64], it should not be assumed that heterozygous fish would be entirely normal. Therefore whilst this chapter focused on the phenotypic characterisation of *ren*$^{-/-}$,

it would be of interest in future work to determine whether heterozygous ren$^{+/-}$ zebrafish have any detectable phenotype.

5.3.9 Transcriptional Adaptation

Several adverse *ren*$^{-/-}$ phenotypes have been reported in this chapter. However, compared to mouse and rat renin null models the zebrafish appeared to be able to cope with low salt concentrations and did not show signs of significant architectural kidney abnormalities. An interesting study by Rossi *et al.*, studied the reason for the lack of obvious phenotypes in some gene knockout experiments and proposed 'transcriptional adaptation' as a possible mechanism [206]. According to the concept of transcriptional adaption, transcripts arising from a targeted gene can cause altered transcription of genes, the products of which can compensate for the original loss of gene function. Studies show that the compensatory mechanism is not seen in cases of complete knockout of an entire gene locus, or a promoter region both of which result in the complete loss of gene transcripts [207]. The *ren*$^{-/-}$ knockout fish have a 8bp deletion in exon 2, causing a frameshift mutation and early termination of translation, however the promoter region of gene remains intact. Therefore transcription of the mutated mRNA could, in theory, activate transcriptional adaptation. Although no specific genes are known to be able to complement for the loss of renin, scRNA sequencing data might suggest compensatory genetic pathways to explain the lack of some phenotypes in the *ren*$^{-/-}$ zebrafish strain.

Chapter 6

Discussion

6.1 Summary

In this thesis, I aimed to develop tools to study the function and activity of the RAS and its rate-limiting enzyme renin, in zebrafish.

During the development of a novel renin reporter zebrafish line, using a bioluminescent reporter to permit studying the dynamics of renin expression *in vivo*, I was able to visualise and report on a previously poorly studied phenomenon [159]. During the development of transgenic zebrafish reporter lines using fluorescence or bioluminescence, reporter proteins are transiently expressed in the yolk sac of larval zebrafish. The ectopic expression is not observable in adult zebrafish and subsequent generations. Although the ectopic signal has prevented the establishment of a new renin bioluminescent reporter fish, it has advanced the understanding of generating new transgenic zebrafish lines in our department. It is crucial to have an understanding of this phenomenon since it may influence quantitative studies using genetic reporters due to the expression from the yolk sac and the possibility of masking bone fide transgene expression.

This project also aimed to overcome the limitation of investigating RAS components in the zebrafish due to the lack of tools to study zebrafish RAS proteins. Previous studies enabled the determination of the AngI and AngII peptide sequences, which subsequently were synthesised using SPPS [169]. The synthetic AngI and AngII peptides were then employed to calibrate an MS assay, in collaboration with Attoquant Diagnostics, which enabled the measurement of endogenous zebrafish AngI and AngII in mesonephric kidneys of zebrafish treated with Captopril and compare the results against untreated controls. There was a dramatic lack of AngII in kidneys of Captopril treated fish, suggesting Captopril is highly effective in inhibiting ACE in zebrafish. Furthermore, a zebrafish renin FRET probe was developed by synthesising the 14-amino acid sequence recognised and cleaved by zebrafish renin. Attachment of a non-toxic fluorophore to the N-terminus and a quencher of that fluorophore, to the C-terminus of the peptide sequence, successfully quenched the fluorescent signal. A plate-based assay was designed to assess and validate that cleavage of the peptide resulted in a quantifiable fluorescent signal. Despite several unsuccessful attempts to produce recombinant zebrafish renin, to fully validate and increase the specificity of the probe, an assay was designed that permitted measuring activity of the FRET probe *in vivo*, using larval zebrafish homogenates and tissues from adult zebrafish. Experiments provided evidence that the probe was successfully cleaved by zebrafish renin by using the

probe at different stages of larval development, and the application of pharmacological strategies (i.e. Captopril) and zebrafish mutant lines.

Lastly, chapter 5 describes an extensive characterisation of the first renin knockout zebrafish. Ren KO zebrafish do not show reduced viability unlike renin KO mice which require post-natal injections of saline for survival [62]. However, high-throughput imaging using the VAST system revealed a delay in development, observable by the delay of an inflated swim bladder and reduced fish length when comparing them to age-matched wild-type controls. Furthermore, crossing the *ren*$^{-/-}$ zebrafish line to existing fluorescent reporter lines such as the tg(*wt1b*:EGFP) and subsequent confocal microscopy imaging, suggested a delay in the glomerular fusion of the pronephros. Crossing the *ren*$^{-/-}$ zebrafish to the renin reporter line tg(*ren*:RFP-LifeAct) and the smooth muscle reporter tg(*acta2*:EGFP), revealed a dramatic increase of renin cells in the mesonephros. The high-resolution imaging visualised the change in renin cell morphology compared to *ren*$^{-/-}$ fish. Furthermore, the crossing of *ren*$^{-/-}$ fish to tg(*ren*:RFP-LifeAct) and tg(*acta2*:EGFP) fish facilitated the development of a FAC-sorting protocol which allowed the purification of renin-expressing and smooth muscle actin-expressing cells from *ren*$^{-/-}$ and *ren*$^{-/-}$ zebrafish for imaging, co-culture and the preparation of scRNAseq libraries. Pathological examination of the zebrafish mesonephros revealed vacuolation of cells of the proximal tubule of *ren*$^{-/-}$ zebrafish. Lastly, the FACS protocol has allowed sorting for renin expressing cells of *ren*$^{-/-}$ and *ren*$^{-/-}$ zebrafish and perform scRNAseq and generate a gene expression profile of these cells. Although the first attempts were only partially successful, a gene expression profile for cells deriving from *ren*$^{-/-}$ fish was possible. The preliminary data gave insight into the genes highly expressed in renin expressing cells from *ren*$^{-/-}$ fish, which have been previously reported to be essential for the recruitment of renin cells in response to physiological stresses on the RAS [185, 203, 208]. Although not in the scope of the timeline of this thesis, a successful FACS and subsequent scRNAseq analysis were performed on cells from *ren*$^{-/-}$ and *ren*$^{-/-}$ allowing for a direct comparison between the two.

6.2 Future Directions

6.2.1 Renin FRET Probe

The site of angiotensinogen cleavage by renin has not been directly identified in zebrafish. Mass spectrometry analysis of the cleavage products from the FRET probe designed in this thesis would demonstrate this. The sizes of the cleavage products can be predicted and are identifiable by the N-terminal 5(6)-carboxyfluorescein and the C-terminal Methyl Red. Although attempts have been made in recovering the products from the cleavage reaction of *in vitro* experiments, the zebrafish tissue homogenates have made it difficult to detect the products through the background noise. Pure zebrafish renin would be required to perform this experiment successfully.

Although the FRET probe has shown activity in zebrafish tissues and whole embryo homogenates, only initial attempts have been made to inject the probe into live zebrafish. The main limitation was, predicatably, the mobility of the probe once injected. The development of a membrane-bound FRET probe would potentially allow the detection and localisation of renin activity in real-time. Membrane-bound FRET probes have previously been developed [209, 210, 211]. The addition of a lipid tail to the N-terminus of the FRET probe could lead to the integration of the FRET probe into the cell membranes of endothelial cells when injected. The N-terminal fluorophore would remain anchored within the cell membrane after removal of the N-terminus, containing the quencher, after renin interaction with the FRET probe. An *in vitro* assay to permit imaging of single cells to demonstrate the successful integration of the probe into the cell membrane as well as using renin to demonstrate that the probe can still be cleaved would be required.

Attempts were made to design a probe using a combination of L- and D-peptides. Previous studies have suggested that most proteases are chiral and that they can distinguish between L- and D-enantiomeric substrates and that D-peptides are capable of resisting cleavage by many proteases [176, 177]. Although no change was observed, a panel Ang1-14 peptides with single L-amino acids exchanged for D-amino acids, and subsequent kinematic assays should be performed. This could lead to higher specificity and resistance of the peptide to other proteases without changing the renin cleavage capability of its substrate.

Throughout this project, it has been shown that larval zebrafish are highly autofluorescent. Previous work in our laboratory has described the synthesis of FRET

probes using fluorophore-quencher pairs which emit at near-infrared or ultraviolet. Although these probes do not allow for qualitative imaging of the FRET probe activity, they may enhance the quantitative read-out generated by renin activity on the FRET probe *in vivo*.

6.2.2 Recombinant Renin

Several different methods were employed to develop recombinant renin; however, most were unsuccessful. Mammalian renin was previously successfully expressed as the inactive renin form, pro-renin, in CHO and HEK293 cells [187, 188]. In this thesis, the production and purification of zebrafish renin was attempted using CHO cells and HEK293 cells. HEK293 yielded no protein and although over expression was observed in CHO cells the protein was trapped within inclusion bodies and required additional purification steps. Western blot analysis demonstrated that the protein was of the wrong molecular size to the expected zebrafish pro-renin or renin and inactive.

In collaboration, reseachers at the recombinant protein core facility at the Max-Delbrück-Centrum (MDC) in Berlin attempted to express zebrafish renin in bacterial and mammalian cells, however their efforts were also unsuccessful. Expression of other zebrafish proteins has previously been reported in bacterial cells [189]. The temperature at which the mammalian cells are maintained (37 °C) might be the problem causing factor of the expression of more complex zebrafish proteins.

Recombinant zebrafish renin would allow the assessment of the enzyme kinetics between renin and its substrate without the interference of activity from other proteolytic enzymes. Furthermore, using recombinant renin in *in vivo* FRET probe assays would also allow to accurately assess changes of the ability of renin to cleave the peptide sequence when substituting single bases of the renin FRET probe.

Recombinant renin would also permit the development of a zebrafish renin antibody. There have been reports of using human renin antibodies for the detection of zebrafish renin [44], however, it is not clear how specifically these anti-mammalian renin antibodies recognise the zebrafish renin due to the low amino acid sequence homology between mammalian and zebrafish renins.

The renin knockout zebrafish has revealed some dramatic morphological changes in the mesonephric kidney. However, several questions remain unanswered, such as at what stage does the lack of renin induce these morphological

changes. Recombinant renin would permit administer renin at different stages of zebrafish development and potential observe a reversal of the renin knockout phenotype.

6.2.3 Measuring RAS Peptides

In the FRET probe development chapter, extensive work has gone into the synthesis of zebrafish AngI and AngII. Both peptides were required for the calibration of MS instruments and led to the development of an assay, in collaboration with Attoquant Diagnostics, which permitted the accurate measurements of endogenous AngI and AngII concentrations in zebrafish tissues. The assay demonstrated the effectiveness of Captopril in blocking the conversion of AngI to AngII. Further assays could be designed to validate the renin knockout zebrafish by demonstrating the complete absence of AngI and AngII. However, more interestingly would be to demonstrate the presence, and measure the concentration, of the smaller RAS peptides such as Ang1-7 or Ang1-9. Although studies have failed to identify an analogous protein for the mammalian MAS receptor in zebrafish, there have been reports of an analogue for ACE2, despite no studies further verifying this [41].

6.2.4 *Ren*$^{-/-}$

The majority of physiological phenotypes were assessed in larval *ren*$^{-/-}$ zebrafish. Larval zebrafish, compared to adults have various additional strategies that permit handling of salt, which may explain the loss of viability when exposing larval *ren*$^{-/-}$ zebrafish to water containing 1/20th of the normal concentration of salt [194]. It would be particularly interesting to investigate the physiological effects of low salt on adult zebrafish lacking renin and determine whether zebrafish have other mechanisms permitting salt handling. Furthermore, the pathological and subsequent immunohistochemical examination of the fish gills using ionicyte specific antibodies could reveal possible changes to the fish gills. A possible phenotype could be the increased expression of sodium ion transporters in the gills to overcome the lack of salt handling performed by the kidney of adult zebrafish.

The morphology of the mesonephric zebrafish kidney revealed that the proximal tubules were vacuolated. The vacuolation is comparable to the 'moth eaten' appearance seen in renin null rats [63, 198]. The vacuolation is suggestive of the inability of proper osmoregulation. It would be of interest to perform immunohis-

tochemistry in combination with antibodies specific for sodium transporters in the kidney, to investigate any changes in the density of sodium transporters expressed.

Ren$^{-/-}$ adult zebrafish displayed a dramatic increase in the number of renin cells along the arterioles of the mesonephros, suggesting an increase in renin cell recruitment to overcome the lack of renin. It would be interesting to see if this phenotype could be recreated by using the ACE inhibitor Captopril. Captopril is highly effective in inhibiting zebrafish ACE, causing a lack of AngII and increasing renin transcription [47, 64]. However, the effects of Captopril on renin cell morphology has not been assessed.

Lastly, EM studies have shown that zebrafish renin cells contain large electron-dense granules. Furthermore, using LysoTracker staining, these granules are highly acidic, suggestive of renin processing. Electron microscopy of *ren*$^{-/-}$ transgenic zebrafish would hopefully show the absence of these storage granules in larval as well as adult zebrafish kidneys.

Bibliography

[1] Andrew P. McMahon. Development of the Mammalian Kidney. *Current Topics in Developmental Biology*, 117:31–64, 2016.

[2] Melissa Little, Kylie Georgas, David Pennisi, and Lorine Wilkinson. Kidney development: Two tales of tubulogenesis. *Current Topics in Developmental Biology*, 90(C):193–229, 2010.

[3] John F. Bertram, Rebecca N. Douglas-Denton, Boucar Diouf, Michael D. Hughson, and Wendy E. Hoy. Human nephron number: Implications for health and disease. *Pediatric Nephrology*, 26(9):1529–1533, 2011.

[4] M. Minuth, E. Hackenthal, K. Poulsen, E. Rix, and R. Taugner. Renin immunocytochemistry of the differentiating juxtaglomerular apparatus. *Anatomy and Embryology*, 162(2):173–181, 1981.

[5] L. Morgan, F. Broughton Pipkin, and N. Kalsheker. Angiotensinogen: Molecular biology, biochemistry and physiology. *The International Journal of Biochemistry & Cell Biology*, 28(11):1211–1222, 1996.

[6] Matthew A. Sparks, Steven D. Crowley, Susan B. Gurley, Maria Mirotsou, and Thomas M. Coffman. Classical renin-angiotensin system in kidney physiology. *Comprehensive Physiology*, 4(3):1201–1228, 2014.

[7] Steven D. Crowley and Thomas M. Coffman. Recent advances involving the renin-angiotensin system. *Experimental Cell Research*, 318(9):1049–1056, 2012.

[8] Robert M. Carey, Zhi Qin Wang, and Helmy M. Siragy. Role of the angiotensin type 2 receptor in the regulation of blood pressure and renal function. In *Hypertension*, volume 35, pages 155–163, 2000.

[9] Sadaharu Higuchi, Haruhiko Ohtsu, Hiroyuki Suzuki, Heigoro Shirai, Gerald D. Frank, and Satoru Eguchi. Angiotensin II signal transduction through the AT1 receptor: Novel insights into mechanisms and pathophysiology, 2007.

[10] Z Q Wang, A F Moore, R Ozono, H M Siragy, and R M Carey. Immunolocalization of subtype 2 angiotensin II (AT2) receptor protein in rat heart. *Hypertension*, 32:78–83, 1998.

[11] Catherine A. Lemarié and Ernesto L. Schiffrin. The angiotensin II type 2 receptor in cardiovascular disease. *JRAAS - Journal of the Renin-Angiotensin-Aldosterone System*, 11(1):19–31, 2010.

[12] Helmy M. Siragy, Tadashi Inagami, Toshihiro Ichiki, and Robert M. Carey. Sustained hypersensitivity to angiotensin II and its mechanism in mice lacking the subtype-2 (AT2) angiotensin receptor. *Proceedings of the National Academy of Sciences of the United States of America*, 96(11):6506–6510, 1999.

[13] Lutz Hein, Gregory S. Barsh, Richard E. Pratt, Victor J. Dzau, and Brian K. Kobilka. Behavioural and cardiovascular effects of disrupting the angiotensin II type-2 receptor gene in mice. *Nature*, 377(6551):744–747, 1995.

[14] Melissa N. Barber, Donella B. Sampey, and Robert E. Widdop. AT2 receptor stimulation enhances antihypertensive effect of AT1 receptor antagonist in hypertensive rats. *Hypertension*, 34(5):1112–1116, 1999.

[15] Robert M. Carey. Newly discovered components and actions of the renin-angiotensin system. *Hypertension*, 62(5):818–822, 2013.

[16] Robson A S Santos, Anderson J. Ferreira, Thiago Verano-Braga, and Michael Bader. Angiotensin-converting enzyme 2, angiotensin-(1-7) and Mas: New players of the renin-angiotensin system. *Journal of Endocrinology*, 216(2), 2013.

[17] M. Donoghue, F. Hsieh, E. Baronas, K. Godbout, M. Gosselin, N. Stagliano, M. Donovan, B. Woolf, K. Robison, R. Jeyaseelan, R. E. Breitbart, and S. Acton. A novel angiotensin-converting enzyme-related carboxypeptidase (ACE2) converts angiotensin I to angiotensin 1-9. *Circulation research*, 87(5), 2000.

[18] Jörg Peters and Susanne Clausmeyer. Intracellular sorting of renin: Cell type specific differences and their consequences. *Journal of Molecular and Cellular Cardiology*, 34(12):1561–1568, 2002.

[19] Robert Tigerstedt and P. Q. Bergman. Niere und Kreislauf. *Skandinavisches Archiv Für Physiologie*, 8(1):223–271, 1898.

[20] Jérôme Célérier, Amauri Cruz, Noël Lamandé, Jean Marie Gasc, and Pierre Corvol. Angiotensinogen and its cleaved derivatives inhibit angiogenesis. *Hypertension*, 39(2 I):224–228, 2002.

[21] H. A. Bock, M. Hermle, F. P. Brunner, and G. Thiel. Pressure dependent modulation of renin release in isolated perfused glomeruli. *Kidney International*, 41(2):275–280, 1992.

[22] J. N. Lorenz, H. Weihprecht, X. R. He, O. Skott, J. P. Briggs, and J. Schnermann. Effects of adenosine and angiotensin on macula densa-stimulated renin secretion. *American Journal of Physiology - Renal Fluid and Electrolyte Physiology*, 265(2 34-2), 1993.

[23] Phillip Darwin Bell, Jean Yves Lapointe, Ravshan Sabirov, Seiji Hayashi, Janos Peti-Peterdi, Ken ichi Manabe, Gergely Kovacs, and Yasunobu Okada. Macula densa cell signaling involves ATP release through a maxi anion channel. *Proceedings of the National Academy of Sciences of the United States of America*, 100(7):4322–4327, 2003.

[24] Robert M. Carey, H. Elizabeth McGrath, Ellen S. Pentz, R. Ariel Gomez, and Paula Q. Barrett. Biomechanical coupling in renin-releasing cells. *Journal of Clinical Investigation*, 100(6):1566–1574, 1997.

[25] T. Imai, H. Miyazaki, S. Hirose, H. Hori, T. Hayashi, R. Kageyama, H. Ohkubo, S. Nakanishi, and K. Murakami. Cloning and sequence analysis of cDNA for human renin precursor. *Proceedings of the National Academy of Sciences of the United States of America*, 80(24 I):7405–7409, 1983.

[26] W. A. Hsueh and J. D. Baxter. Human prorenin. *Hypertension*, 17(4):469–479, 1991.

[27] R. E. Pratt, J. E. Carleton, J. P. Richie, C. Heusser, and V. J. Dzau. Human renin biosynthesis and secretion in normal and ischemic kidneys. *Proceedings of the National Academy of Sciences of the United States of America*, 84(22):7837–7840, 1987.

[28] C. D. Sigmund, C. A. Jones, H. J. Jacob, J. Ingelfinger, U. Kim, D. Gamble, V. J. Dzau, and K. W. Gross. Pathophysiology of vascular smooth muscle in renin promoter-T-antigen transgenic mice. *American Journal of Physiology - Renal Fluid and Electrolyte Physiology*, 260(2 29-2), 1991.

[29] Jung J. Kang, Ildikó Toma, Arnold Sipos, Elliott J. Meer, Sarah L. Vargas, and János Peti-Peterdi. The collecting duct is the major source of prorenin in diabetes. *Hypertension*, 51(6):1597–1604, 2008.

[30] A. A.M. Franken, F. H.M. Derkx, A. J. Man In't Veld, W. C.J. Hop, G. H. Van Rens, E. Peperkamp, P. T.V.M. De Jong, and M. A.D.H. Schalekamp. High plasma prorenin in diabetes mellitus and its correlation with some complications. *Journal of Clinical Endocrinology and Metabolism*, 71(4):1008–1015, 1990.

[31] Genevieve Nguyen. Renin, (pro)renin and receptor: An update. *Clinical Science*, 120(5):169–178, 2011.

[32] G. Nguyen. Renin/prorenin receptors. *Kidney International*, 69(9):1503–1506, 2006.

[33] Genevieve Nguyen and Dominik N. Muller. The biology of the (pro)renin receptor. *Journal of the American Society of Nephrology*, 21(1):18–23, 2010.

[34] A. H.Jan Danser and Jasper J. Saris. Prorenin uptake in the heart: A prerequisite for local angiotensin generation? *Journal of Molecular and Cellular Cardiology*, 34(11):1463–1472, 2002.

[35] L. T. Skeggs, K. E. Lentz, A. B. Gould, H. Hochstrasser, and J. R. Kahn. Biochemistry and kinetics of the renin-angiotensin system. *Federation Proceedings*, 26(1):42–47, 1967.

[36] N Nakamura, S Satomura, S Matsuura, and K Murakami. Identification of the active site of human renin with use of new fluorogenic peptides. *Journal of biochemistry*, 109(5):741–5, 1991.

[37] Tsutomu Nakagawa, Jyunji Akaki, Ryousuke Satou, Masatoshi Takaya, Hideyuki Iwata, Akemi Katsurada, Kazuhiro Nishiuchi, Yoshihiro Ohmura, Fumiaki Suzuki, and Yukio Nakamura. The His-Pro-Phe motif of angiotensinogen is a crucial determinant of the substrate specificity of renin. *Biological Chemistry*, 388(2):237–246, 2007.

[38] Jacob Bouhnik, Eric Clauser, Joël Menard, Pierre Corvol, Donny Strosberg, and Jean Pierre Frenoy. Rat Angiotensinogen and Des(angiotensin I)angiotensinogen: Purification, Characterization, and Partial Sequencing. *Biochemistry*, 20(24):7010–7015, 1981.

[39] M J Peach. Renin-angiotensin system: biochemistry and mechanisms of action. *Physiological reviews*, 57(2):313–370, 1977.

[40] P. Liang. Genomic characterization and expression analysis of the first non-mammalian renin genes from zebrafish and pufferfish. *Physiological Genomics*, 16:314–322, 2004.

[41] David Fournier, Friedrich C. Luft, Michael Bader, Detlev Ganten, and Miguel A. Andrade-Navarro. Emergence and evolution of the renin-angiotensin-aldosterone system. *Journal of Molecular Medicine*, 90(5):495–508, 2012.

[42] Paula Armesto, Xavier Cousin, Emilio Salas-Leiton, Esther Asensio, Manuel Manchado, and Carlos Infante. Molecular characterization and transcriptional regulation of the renin–angiotensin system genes in Senegalese sole (Solea senegalensis Kaup, 1858): Differential gene regulation by salinity. *Comparative Biochemistry and Physiology, Part A*, 184:6–19, 2015.

[43] Kazuyuki Hoshijima and Shigehisa Hirose. Expression of endocrine genes in zebrafish larvae in response to environmental salinity. *Journal of Endocrinology*, 193:481–491, 2007.

[44] Yusuke Kumai, Nicholas J. Bernier, and Steve F. Perry. Angiotensin-II promotes Na+ uptake in larval zebrafish, Danio rerio, in acidic and ion-poor water. *Journal of Endocrinology*, 220(3):195–205, 2014.

[45] Yusuke Kumai and Steve F Perry. Mechanisms and regulation of Na+ uptake by freshwater fish. *Respiratory Physiology & Neurobiology*, 184:249–256, 2012.

[46] B. Tucker, C. Hepperle, D. Kortschak, B. Rainbird, S. Wells, A. C. Oates, and M. Lardelli. Zebrafish Angiotensin II Receptor-like 1a (agtrl1a) is expressed in migrating hypoblast, vasculature, and in multiple embryonic epithelia. *Gene Expression Patterns*, 7(3):258–265, 2007.

[47] Sebastien A Rider, Linda J Mullins, Rachel F Verdon, Calum A Macrae, and John J Mullins. Renin expression in developing zebrafish is associated with angiogenesis and requires the Notch pathway and endothelium. *Am J Physiol Renal Physiol*, 309:531–539, 2015.

[48] Julia Riedl, Alvaro H. Crevenna, Kai Kessenbrock, Jerry Haochen Yu, Dorothee Neukirchen, Michal Bista, Frank Bradke, Dieter Jenne, Tad A. Holak, Zena Werb, Michael Sixt, and Roland Wedlich-Soldner. Lifeact: A versatile marker to visualize F-actin. *Nature Methods*, 5(7):605–607, 2008.

[49] Sebastien A. Rider, Helen C. Christian, Linda J. Mullins, Amelia R. Howarth, Calum A. MacRae, and John J. Mullins. Zebrafish mesonephric renin cells are functionally conserved and comprise two distinct morphological populations. *American Journal of Physiology - Renal Physiology*, 312(4):F778–F790, 2017.

[50] Dominik Steppan, Anita Zügner, Reinhard Rachel, and Armin Kurtz. Structural analysis suggests that renin is released by compound exocytosis. *Kidney International*, 83(2):233–241, 2013.

[51] Ying Jey Guh, Chia Hao Lin, and Pung Pung Hwang. Osmoregulation in zebrafish: Ion transport mechanisms and functional regulation. *EXCLI Journal*, 14:627–659, 2015.

[52] F. GARCIAROMEU and J. MAETZ. the Mechanism of Sodium and Chloride Uptake By the Gills of a. *The Journal of general physiology*, 47:1195–1207, 1964.

[53] Pung Pung Hwang and Tsung Han Lee. New insights into fish ion regulation and mitochondrion-rich cells. *Comparative Biochemistry and Physiology - A Molecular and Integrative Physiology*, 148(3):479–497, 2007.

[54] R. Kala, F. Fyhrquist, and A. Eisalo. Diurnal variation of plasma angiotensin II in man. *Scandinavian Journal of Clinical and Laboratory Investigation*, 31(4):363–365, 1973.

[55] Pung Pung Hwang and Ming Yi Chou. Zebrafish as an animal model to study ion homeostasis. *Pflugers Archiv European Journal of Physiology*, 465(9):1233–1247, 2013.

[56] David H. Evans, Peter M. Piermarini, and Keith P. Choe. The multifunctional fish gill: Dominant site of gas exchange, osmoregulation, acid-base regulation, and excretion of nitrogenous waste. *Physiological Reviews*, 85(1):97–177, 2005.

[57] Pung Pung Hwang. Ion uptake and acid secretion in zebrafish (Danio rerio). *Journal of Experimental Biology*, 212(11):1745–1752, 2009.

[58] Murray J. Favus and David Goltzman. Regulation of Calcium and Magnesium. In *Primer on the Metabolic Bone Diseases and Disorders of Mineral Metabolism: Seventh Edition*, pages 103–108. 2009.

[59] Stephen D. McCormick and Don Bradshaw. Hormonal control of salt and water balance in vertebrates. *General and Comparative Endocrinology*, 147(1):3–8, 2006.

[60] Tatsuya Sakamoto and Stephen D. McCormick. Prolactin and growth hormone in fish osmoregulation. *General and Comparative Endocrinology*, 147(1):24–30, 2006.

[61] H. Ruskoaho. Atrial natriuretic peptide: Synthesis, release, and metabolism. *Pharmacological Reviews*, 44(4):481–602, 1992.

[62] Nobuyuki Takahashi, Maria Luisa S.Sequeira Lopez, John E. Cowhig, Melissa A. Taylor, Tomoko Hatada, Emily Riggs, Gene Lee, R. Ariel Gomez, Hyung Suk Kim, and Oliver Smithies. Ren1c homozygous null mice are hypotensive and polyuric, but heterozygotes are indistinguishable from wild-type. *Journal of the American Society of Nephrology*, 16(1):125–132, 2005.

[63] Carol Moreno, Mathew Hoffman, Timothy J. Stodola, Daniela N. Didier, Jozef Lazar, Aron M. Geurts, Paula E. North, Howard J. Jacob, and Andrew S. Greene. Creation and characterization of a renin knockout rat. *Hypertension*, 57(3 PART 2):614–619, 2011.

[64] T Yang, Y Endo, Y G Huang, A Smart, J P Briggs, and J Schnermann. Renin expression in COX-2-knockout mice on normal or low-salt diets. *American journal of physiology. Renal physiology*, 279(5):F819–25, 2000.

[65] L J Field, W M Philbrick, P N Howles, D P Dickinson, R A McGowan, and K W Gross. Expression of tissue-specific Ren-1 and Ren-2 genes of mice: comparative analysis of 5'-proximal flanking regions. *Molecular and Cellular Biology*, 4(11):2321–2331, 1984.

[66] Junji Ishida, Fumihiro Sugiyama, Keiji Tanimoto, Keiko Taniguchi, Mikio Syouji, Eriko Takimoto, Hisashi Horiguchi, Kazuo Murakami, Ken Ichi Yagami, and Akiyoshi Fukamizu. Rescue of angiotensinogen-knockout mice. *Biochemical and Biophysical Research Communications*, 252(3):610–616, nov 1998.

[67] Sebastien A. Rider, Helen C. Christian, Linda J. Mullins, Amelia R. Howarth, Calum A. MacRae, and John J. Mullins. Zebrafish mesonephric renin cells are functionally conserved and comprise two distinct morphological populations. *American Journal of Physiology - Renal Physiology*, 312(4):F778–F790, 2017.

[68] Pontus B. Persson. Renin: Origin, secretion and synthesis. *Journal of Physiology*, 552(3):667–671, 2003.

[69] Maria Luisa S. Sequeira-Lopez, Eugene E. Lin, Minghong Li, Yan Hu, Curt D. Sigmund, and R. Ariel Gomez. The earliest metanephric arteriolar progenitors and their role in kidney vascular development. *American Journal of Physiology - Regulatory Integrative and Comparative Physiology*, 308(2):R138–R149, 2015.

[70] E. E. Lin, M. L.S. Sequeira-Lopez, and R. Ariel Gomez. RBP-J in FOXD1+ renal stromal progenitors is crucial for the proper development and assembly of the kidney vasculature and glomerular mesangial cells. *American Journal of Physiology - Renal Physiology*, 306(2), 2014.

[71] Vasantha Reddi, Alejandro Zaglul, Ellen S. Pentz, and R. Ariel Gomez. Renin-expressing cells are associated with branching of the developing kidney vasculature. *Journal of the American Society of Nephrology*, 9(1):63–71, 1998.

[72] A Sauter, K Machura, B Neubauer, A Kurtz, and C Wagner. Development of renin expression in the mouse kidney. *Kidney International*, 73:43–51, 2008.

[73] Martin R. Yeomans and Emma Coughlan. *Mood-induced eating. Interactive effects of restraint and tendency to overeat*, volume 52. Brooks/Cole, 2009.

[74] Gene Lee, Natalia Makhanova, Kathleen Caron, Maria L. Sequeira Lopez, R. Ariel Gomez, Oliver Smithies, and Hyung Suk Kim. Homeostatic responses in the adrenal cortex to the absence of aldosterone in mice. *Endocrinology*, 146(6):2650–2656, 2005.

[75] Charlotte Starke, Hannah Betz, Linda Hickmann, Peter Lachmann, Björn Neubauer, Jeffrey B. Kopp, Maria Luisa S. Sequeira-Lopez, R. Ariel Gomez, Bernd Hohenstein, Vladimir T. Todorov, and Christian P.M. Hugo. Renin lineage cells repopulate the glomerular mesangium after injury. *Journal of the American Society of Nephrology*, 26(1):48–54, 2015.

[76] Karl F. Hilgers, Vasantha Reddi, John H. Krege, Oliver Smithies, and R. Ariel Gomez. Aberrant renal vascular morphology and renin expression in mutant mice lacking angiotensin-converting enzyme. *Hypertension*, 29(1 II):216–221, 1997.

[77] A. Tufro-McRreddie, L. M. Romano, J. M. Harris, L. Ferder, and R. A. Gomez. Angiotensin II regulates nephrogenesis and renal vascular development. *American Journal of Physiology - Renal Fluid and Electrolyte Physiology*, 269(1 38-1), 1995.

[78] Karl F. Hilgers, Victoria F. Norwood, and R. Ariel Gomez. Angiotensin's role in renal development. *Seminars in Nephrology*, 17(5):492–501, 1997.

[79] Armin Kurtz. Renin Release: Sites, Mechanisms, and Control. *Annu. Rev. Physiol*, 73:377–99, 2011.

[80] Sadayoshi Ito and Keishi Abe. Contractile properties of afferent and efferent arterioles. In *Clinical and Experimental Pharmacology and Physiology*, volume 24, pages 532–535, 1997.

[81] János Peti-Peterdi. Calcium wave of tubuloglomerular feedback. *American Journal of Physiology - Renal Physiology*, 291(2), 2006.

[82] János Peti-Peterdi, Peter Komlosi, Amanda L. Fuson, Youfei Guan, André Schneider, Zhonghua Qi, Reyadh Redha, Laszlo Rosivall, Matthew D. Breyer, and P. Darwin Bell. Luminal NaCl delivery regulates basolateral PGE2 release from macula densa cells. *Journal of Clinical Investigation*, 112(1):76–82, 2003.

[83] Gerald F. DiBona. Neural control of the kidney: Functionally specific renal sympathetic nerve fibers. In *American Journal of Physiology - Regulatory Integrative and Comparative Physiology*, volume 279, 2000.

[84] A. D. Everett, R. M. Carey, R. L. Chevalier, M. J. Peach, and R. A. Gomez. Renin release and gene expression in intact rat kidney microvessels and single cells. *Journal of Clinical Investigation*, 86(1):169–175, 1990.

[85] P. Borensztein, S. Germain, S. Fuchs, J. Philippe, P. Corvol, and F. Pinet. cis-Regulatory elements and trans-acting factors directing basal and cAMP-stimulated human renin gene expression in chorionic cells. *Circulation Research*, 74(5):764–773, 1994.

[86] Syed S. Quadri, Silas A. Culver, Caixia Li, and Helmy M. Siragy. Interaction of the renin angiotensin and COX systems in the kidney. *Frontiers in Bioscience - Scholar*, 8(2):215–226, 2016.

[87] George Streisinger, Charline Walker, Nancy Dower, Donna Knauber, and Fred Singer. Production of clones of homozygous diploid zebra fish (Brachydanio rerio). *Nature*, 291(5813):293–296, 1981.

[88] Charles W. Creaser. The Technic of Handling the Zebra Fish (Brachydanio rerio) for the Production of Eggs Which Are Favorable for Embryological Research and Are Available at Any Specified Time Throughout the Year. *Copeia*, 1934(4):159, 1934.

[89] Kerstin Howe, Matthew D. Clark, Carlos F. Torroja, James Torrance, Camille Berthelot, Matthieu Muffato, John E. Collins, Sean Humphray, Karen McLaren, Lucy Matthews, Stuart McLaren, Ian Sealy, Mario Caccamo, Carol Churcher, Carol Scott, Jeffrey C. Barrett, Romke Koch, Gerd Jörg Rauch, Simon White, William Chow, Britt Kilian, Leonor T. Quintais, José A. Guerra-Assunção, Yi Zhou, Yong Gu, Jennifer Yen, Jan Hinnerk Vogel, Tina Eyre, Seth Redmond, Ruby Banerjee, Jianxiang Chi, Beiyuan Fu, Elizabeth Langley, Sean F. Maguire, Gavin K. Laird, David Lloyd, Emma Kenyon, Sarah Donaldson, Harminder Sehra, Jeff Almeida-King, Jane Loveland, Stephen Trevanion, Matt Jones, Mike Quail, Dave Willey, Adrienne Hunt, John Burton, Sarah Sims, Kirsten McLay, Bob Plumb, Joy Davis, Chris Clee, Karen Oliver, Richard Clark, Clare Riddle, David Eliott, Glen Threadgold, Glenn Harden, Darren Ware, Beverly Mortimer, Giselle Kerry, Paul Heath, Benjamin Phillimore, Alan Tracey, Nicole Corby, Matthew Dunn, Christopher Johnson, Jonathan Wood, Susan Clark, Sarah Pelan, Guy Griffiths, Michelle Smith, Rebecca Glithero, Philip Howden, Nicholas Barker, Christopher Stevens, Joanna Harley, Karen Holt, Georgios Panagiotidis, Jamieson Lovell, Helen Beasley, Carl Henderson, Daria Gordon, Katherine Auger, Deborah Wright, Joanna Collins, Claire Raisen, Lauren Dyer, Kenric Leung, Lauren Robertson, Kirsty Ambridge, Daniel Leongamornlert, Sarah McGuire, Ruth Gilderthorp, Coline Griffiths, Deepa Manthravadi, Sarah Nichol, Gary Barker, Siobhan Whitehead, Michael Kay, Jacqueline Brown, Clare Murnane, Emma Gray, Matthew Humphries, Neil Sycamore, Darren Barker, David Saunders, Justene Wallis, Anne Babbage, Sian Hammond, Maryam Mashreghi-Mohammadi, Lucy Barr, Sancha Martin, Paul Wray, Andrew Ellington, Nicholas Matthews, Matthew Ellwood, Rebecca Woodmansey, Graham Clark, James Cooper, Anthony Tromans, Darren Grafham, Carl Skuce, Richard Pandian, Robert Andrews, Elliot Harrison, Andrew Kimberley, Jane Garnett, Nigel Fosker, Rebekah Hall, Patrick Garner, Daniel Kelly, Christine Bird, Sophie Palmer, Ines Gehring, Andrea Berger, Christopher M. Dooley, Zübeyde Ersan-Ürün, Cigdem Eser, Horst Geiger, Maria Geisler, Lena Karotki, Anette Kirn, Judith Konantz, Martina Konantz, Martina Oberländer, Silke Rudolph-Geiger, Mathias Teucke, Kazutoyo Osoegawa, Baoli Zhu, Amanda Rapp, Sara Widaa, Cordelia Langford, Fengtang Yang, Nigel P. Carter, Jennifer Harrow, Zemin Ning, Javier Herrero, Steve M.J. Searle, Anton Enright, Robert Geisler, Ronald H.A. Plasterk, Charles Lee, Monte Westerfield, Pieter J. De Jong, Leonard I. Zon, John H. Postlethwait, Christiane Nüsslein-Volhard, Tim J.P. Hubbard, Hugues Roest Crollius, Jane Rogers, and Derek L. Stemple. The zebrafish reference genome sequence and its

relationship to the human genome. *Nature*, 496(7446):498–503, 2013.

[90] Karl J. Clark, Mark D. Urban, Kimberly J. Skuster, and Stephen C. Ekker. Transgenic zebrafish using transposable elements. *Methods in Cell Biology*, 104:137–149, 2011.

[91] Kristen M. Kwan, Esther Fujimoto, Clemens Grabher, Benjamin D. Mangum, Melissa E. Hardy, Douglas S. Campbell, John M. Parant, H. Joseph Yost, John P. Kanki, and Chi Bin Chien. The Tol2kit: A multisite gateway-based construction Kit for Tol2 transposon transgenesis constructs. *Developmental Dynamics*, 236(11):3088–3099, nov 2007.

[92] John S. Reece-Hoyes and Albertha J.M. Walhout. Gateway recombinational cloning. *Cold Spring Harbor Protocols*, 2018(1):1–6, 2018.

[93] Roland Taugner, Eberhard Hackenthal, Roland Taugner, and Eberhard Hackenthal. Morphology of the Juxtaglomerular Apparatus. *The Juxtaglomerular Apparatus*, pages 5–43, 1989.

[94] Massimo M. Santoro, Gabriella Pesce, and Didier Y. Stainier. Characterization of vascular mural cells during zebrafish development. *Mechanisms of Development*, 126(8-9):638–649, 2009.

[95] Sunny Hartwig, Jacqueline Ho, Priyanka Pandey, Kenzie MacIsaac, Mary Taglienti, Michael Xiang, Gil Alterovitz, Marco Ramoni, Ernest Fraenkel, and Jordan A. Kreidberg. Genomic characterization of Wilms' tumor suppressor 1 targets in nephron progenitor cells during kidney development. *Development*, 137(7):1189–1203, 2010.

[96] Gregory R. Dressler. The Cellular Basis of Kidney Development. *Annual Review of Cell and Developmental Biology*, 22(1):509–529, 2006.

[97] Frank Bollig, Rebecca Mehringer, Birgit Perner, Christina Hartung, Matthias Schäfer, Manfred Schartl, Jean Nicolas Volff, Christoph Winkler, and Christoph Englert. Identification and comparative expression analysis of a second wt1 gene in zebrafish. *Developmental Dynamics*, 235(2):554–561, 2006.

[98] Birgit Perner, Christoph Englert, and Frank Bollig. The Wilms tumor genes wt1a and wt1b control different steps during formation of the zebrafish pronephros. *Developmental Biology*, 309(1):87–96, 2007.

[99] Hwei Jan Hsu, Guang Lin, and Bon Chu Chung. Parallel early development of zebrafish interrenal glands and pronephros: Differential control by wt1 and ff1b. *Development*, 130(10):2107–2116, 2003.

[100] Jayoung Choi, Linda Dong, Janice Ahn, Diem Dao, Matthias Hammerschmidt, and Jau Nian Chen. FoxH1 negatively modulates flk1 gene expression and vascular formation in zebrafish. *Developmental Biology*, 304(2):735–744, 2007.

[101] Lauri Saxén and Hannu Sariola. Early organogenesis of the kidney. *Pediatric Nephrology*, 1(3):385–392, 1987.

[102] Koichiro Ichimura, Ekaterina Bubenshchikova, Rebecca Powell, Yayoi Fukuyo, Tomomi Nakamura, Uyen Tran, Shoji Oda, Minoru Tanaka, Oliver Wessely, Hidetake Kurihara, Tatsuo Sakai, and Tomoko Obara. A Comparative Analysis of Glomerulus Development in the Pronephros of Medaka and Zebrafish. *PLoS ONE*, 7(9), 2012.

[103] Iain A. Drummond, Arindam Majumdar, Hartmut Hentschel, Marlies Elger, Lila Solnica-Krezel, Alexander F. Schier, Stephan C.F. Neuhauss, Derek L. Stemple, Fried Zwartkruis, Zehava Rangini, Wolfgang Driever, and Mark C. Fishman. Early development of the zebrafish pronephros and analysis of mutations affecting pronephric function. *Development*, 125(23):4655–4667, 1998.

[104] Jane F. Armstrong, Kathryn Pritchard-Jones, Wendy A. Bickmore, Nicholas D. Hastie, and Jonathan B.L. Bard. The expression of the Wilms' tumour gene, WT1, in the developing mammalian embryo. *Mechanisms of Development*, 40(1-2):85–97, 1993.

[105] Albrecht G. Kramer-Zucker, Stephanie Wiessner, Abbie M. Jensen, and Iain A. Drummond. Organization of the pronephric filtration apparatus in zebrafish requires Nephrin, Podocin and the FERM domain protein Mosaic eyes. *Developmental Biology*, 285(2):316–329, sep 2005.

[106] I. A. Drummond and A. J. Davidson. Zebrafish kidney development. *Methods in Cell Biology*, 134:391–429, 2016.

[107] Ra Wingert and Aj Davidson. The zebrafish pronephros: A model to study nephron segmentation. *Kidney International*, 7337:1120–1127, 2008.

[108] Rebecca A. Wingert, Rori Selleck, Jing Yu, Huai Dong Song, Zhu Chen, Anhua Song, Yi Zhou, Bernard Thisse, Christine Thisse, Andrew P. McMahon, and Alan J. Davidson. The cdx genes and retinoic acid control the positioning and segmentation of the zebrafish pronephros. *PLoS Genetics*, 3(10):1922–1938, 2007.

[109] Massimo Nichane, Claude Van Campenhout, Hélène Pendeville, Marianne L. Voz, and Eric J. Bellefroid. The Na+/PO4 cotransporter SLC20A1 gene labels distinct restricted subdomains of the developing pronephros in Xenopus and zebrafish embryos. *Gene Expression Patterns*, 6(7):667–672, 2006.

[110] Goran Ivanis, Marvin Braun, and Steve F Perry. Renal expression and localization of SLC9A3 sodium/hydrogen exchanger and its possible role in acid-base regulation in freshwater rainbow trout (Oncorhynchus mykiss). *American journal of physiology. Regulatory, integrative and comparative physiology*, 295(3):R971–8, 2008.

[111] Yan Ru Su, Charles A. Klanke, Timothy W. Houseal, Stephen C. Linn, Scott E. Burk, Tena S. Varvil, Brith E. Otterud, Gary E. Shull, Mark F. Leppert, and Anil G. Menon. Molecular cloning and physical and genetic mapping of the human anion exchanger isoform 3 (slc2c) gene to chromosome 2q36. *Genomics*, 22(3):605–609, 1994.

[112] Carolyn E. Fisher and Sarah E.M. Howie. The role of megalin (LRP-2/Gp330) during development. *Developmental Biology*, 296(2):279–297, 2006.

[113] Norman D. Rosenblum. Kidney development. In *National Kidney Foundation's Primer on Kidney Diseases, Sixth Edition*, pages 19–25. 2013.

[114] Odyssé Michos. Kidney development: from ureteric bud formation to branching morphogenesis. *Current Opinion in Genetics and Development*, 19(5):484–490, 2009.

[115] Weibin Zhou, Rudrick C. Boucher, Frank Bollig, Christoph Englert, and Friedhelm Hildebrandt. Characterization of mesonephric development and regeneration using transgenic zebrafish. *American Journal of Physiology - Renal Physiology*, 299(5):1040–1047, 2010.

[116] Cuong Q. Diep, Zhenzhen Peng, Tobechukwu K. Ukah, Paul M. Kelly, Renee V. Daigle, and Alan J. Davidson. Development of the zebrafish mesonephros. *Genesis*, 53(3-4):257–269, 2015.

[117] Cuong Q. Diep, Dongdong Ma, Rahul C. Deo, Teresa M. Holm, Richard W. Naylor, Natasha Arora, Rebecca A. Wingert, Frank Bollig, Gordana Djordjevic, Benjamin Lichman, Hao Zhu, Takanori Ikenaga, Fumihito Ono, Christoph Englert, Chad A. Cowan, Neil A. Hukriede, Robert I. Handin, and Alan J. Davidson. Identification of adult nephron progenitors capable of kidney regeneration in zebrafish. *Nature*, 470(7332):95–101, 2011.

[118] Ralph E. Mistlberger. Neurobiology of food anticipatory circadian rhythms. *Physiology and Behavior*, 104(4):535–545, 2011.

[119] R. Orozco-Solis and P. Sassone-Corsi. Epigenetic control and the circadian clock: Linking metabolism to neuronal responses. *Neuroscience*, 264:76–87, 2014.

[120] Joseph S. Takahashi. Transcriptional architecture of the mammalian circadian clock. *Nature Reviews Genetics*, 18(3):164–179, 2017.

[121] Jay C. Dunlap. Molecular bases for circadian clocks. *Cell*, 96(2):271–290, 1999.

[122] Robert S. Modlinger, Kurosh Sharif-Zadeh, Norman H. Ertel, and Michael Gutkin. The circadian rhythm of renin. *Journal of Clinical Endocrinology and Metabolism*, 43(6):1276–1282, 1976.

[123] R. D. Gordon, L. K. Wolfe, D. P. Island, and G. W. Liddle. A diurnal rhythm in plasma renin activity in man. *The Journal of clinical investigation*, 45(10):1587–1592, 1966.

[124] Thomas M. Coffman. Under pressure: The search for the essential mechanisms of hypertension. *Nature Medicine*, 17(11):1402–1409, 2011.

[125] Gregory M. Cahill. Clock mechanisms in zebrafish. *Cell and Tissue Research*, 309(1):27–34, 2002.

[126] Th Förster. Zwischenmolekulare Energiewanderung und Fluoreszenz. *Annalen der Physik*, 437(1-2):55–75, 1948.

[127] Elizabeth A. Jares-Erijman and Thomas M. Jovin. FRET imaging. *Nature Biotechnology*, 21(11):1387–1395, 2003.

[128] Peter L. Choyke, Raphael Alford, Haley M. Simpson, Josh Duberman, G. Craig Hill, Mikako Ogawa, Celeste Regino, and Hisataka Kobayashi. Toxicity of organic fluorophores used in molecular imaging: Literature review. *Molecular Imaging*, 8(6):341–354, nov 2009.

[129] János Peti-Peterdi, Attila Fintha, Amanda L. Fuson, Albert Tousson, and Robert H. Chow. Real-time imaging of renin release in vitro. *American Journal of Physiology - Renal Physiology*, 287(2):56–2, 2004.

[130] Adriana K. Carmona, Maria Aparecida Juliano, and Luiz Juliano. The use of fluorescence resonance energy transfer (FRET) peptides for measurement of clinically important proteolytic enzymes. *Anais da Academia Brasileira de Ciencias*, 81(3):381–392, 2009.

[131] Raymond Behrendt, Peter White, and John Offer. Advances in Fmoc solid-phase peptide synthesis. *Journal of Peptide Science*, 22(1):4–27, 2016.

[132] D.C. Sherrington. Solid Phase Peptide Synthesis — A Practical Approach. *Reactive Polymers*, 12(3):310, 1990.

[133] D. R. Snider and E. D. Clegg. Alteration of phospholipids in porcine spermatozoa during in vivo uterus and oviduct incubation. *Journal of animal science*, 40(2):269–274, 1975.

[134] Tsung Yao Chang, Carlos Pardo-Martin, Amin Allalou, Carolina Wählby, and Mehmet Fatih Yanik. Fully automated cellular-resolution vertebrate screening platform with parallel animal processing. *Lab on a Chip*, 12(4):711–716, 2012.

[135] Rock Pulak. Tools for automating the imaging of zebrafish larvae. *Methods*, 96:118–126, 2016.

[136] Kevin A. Feeney, Marrit Putker, Marco Brancaccio, and John S. O'Neill. In-depth Characterization of Firefly Luciferase as a Reporter of Circadian Gene Expression in Mammalian Cells. *Journal of Biological Rhythms*, 2016.

[137] Meltem Weger, Benjamin D. Weger, Nicolas Diotel, Sepand Rastegar, Tsuyoshi Hirota, Steve A. Kay, Uwe Strähle, and Thomas Dickmeis. Real-time in vivo monitoring of circadian E-box enhancer activity: A robust and sensitive zebrafish reporter line for developmental, chemical and neural biology of the circadian clock. *Developmental Biology*, 380(2):259–273, 2013.

[138] Benjamin D. Weger, Meltem Weger, Nicole Jung, Christin Lederer, Stefan Bräse, and Thomas Dickmeis. A chemical screening procedure for glucocorticoid signaling with a zebrafish larva luciferase reporter system. *Journal of Visualized Experiments*, (79):1–9, 2013.

[139] R Mayerhofer, K Araki, and a a Szalay. Monitoring of spatial expression of firefly luciferase in transformed zebrafish. *Journal of bioluminescence and chemiluminescence*, 10(5):271–5, 1995.

[140] Chen Hui Chen, Ellen Durand, Jinhu Wang, Leonard I. Zon, and Kenneth D. Poss. Zebraflash transgenic lines for in vivo bioluminescence imaging of stem cells and regeneration in adult zebrafish. *Development (Cambridge)*, 140(24):4988–4997, 2013.

[141] Jason R. Becker, Tamara Y. Robinson, Chetana Sachidanandan, Amy E. Kelly, Shannon Coy, Randall T. Peterson, and Calum A. MacRae. In vivo natriuretic peptide reporter assay identifies chemical modifiers of hypertrophic cardiomyopathy signalling. *Cardiovascular Research*, 93(3):463–470, 2012.

[142] Thomas R. Whitesell, Regan M. Kennedy, Alyson D. Carter, Evvi Lynn Rollins, Sonja Georgijevic, Massimo M. Santoro, and Sarah J. Childs. An α-smooth muscle actin (acta2/αsma) zebrafish transgenic line marking vascular mural cells and visceral smooth muscle cells. *PLoS ONE*, 9(3), 2014.

[143] Birgit Perner, Christoph Englert, and Frank Bollig. The Wilms tumor genes wt1a and wt1b control different steps during formation of the zebrafish pronephros. *Developmental Biology*, 309(1):87–96, 2007.

[144] Gerd-Jörg Rauch, Michael Granato, and Pascal Haffter. A polymorphic zebrafish line for genetic mapping using SSLPs on high-percentage agarose gels. *Technical Tips Online*, 2(1):148–150, 1997.

[145] J R de Wet, K V Wood, M Deluca, D R Helinski, and S Subramani. Firefly luciferase gene: structure and expression in mammalian cells. *Mol.Cell Biol.*, 7(0270-7306 (Print)):725–737, 1987.

[146] Norman Hu, H. Joseph Yost, and Edward B. Clark. Cardiac morphology and blood pressure in the adult zebrafish. *Anatomical Record*, 264(1):1–12, 2001.

[147] Amanda Sorribes, Haraldur Porsteinsson, Hrönn Arnardóttir, Ingibjórg P. Jóhannesdóttir, Benjamín Sigurgeirsson, Gonzalo G. de Polavieja, and Kar Karlsson. The ontogeny of sleep-wake cycles in zebrafish: A comparison to humans. *Frontiers in Neural Circuits*, 7(NOV), 2013.

[148] Deng Feng Huang, Ming Yong Wang, Wu U. Yin, Yu Qian Ma, Han A.N. Wang, Tian Xue, Da Long Ren, and Bing Hu. Zebrafish lacking circadian gene per2 exhibit visual function deficiency. *Frontiers in Behavioral Neuroscience*, 12, 2018.

[149] Ying Li, Guang Li, Haifang Wang, Jiulin Du, and Jun Yan. Analysis of a Gene Regulatory Cascade Mediating Circadian Rhythm in Zebrafish. *PLoS Computational Biology*, 9(2), 2013.

[150] Alessandro Rienzo, Amparo Pascual-Ahuir, and Markus Proft. The use of a real-time luciferase assay to quantify gene expression dynamics in the living yeast cell. *Yeast*, 29(6):219–231, 2012.

[151] A. R. Brasier, J. E. Tate, and J. F. Habener. Optimized use of the firefly luciferase assay as a reporter gene in mammalian cell lines. *BioTechniques*, 7(10):1116–1122, 1989.

[152] Xiaowen Chen, Dafne Gays, and Massimo M. Santoro. Transgenic zebrafish. In *Methods in Molecular Biology*. 2016.

[153] David Whitmore, Nicholas S. Foulkes, Uwe Strähle, and Paolo Sassone-Corsi. Zebrafish Clock rhythmic expression reveals independent peripheral circadian oscillators. *Nature Neuroscience*, 1(8):701–707, 1998.

[154] R. Allada, P. Emery, J. S. Takahashi, and M. Rosbash. Stopping time: The genetics of fly and mouse circadian clocks. *Annual Review of Neuroscience*, 24:1091–1119, 2001.

[155] David Duguay and Nicolas Cermakian. The crosstalk between physiology and circadian clock proteins. *Chronobiology International*, 26(8):1479–1513, 2009.

[156] Lisa R. Stow and Michelle L. Gumz. The Circadian Clock in the Kidney. *Journal of the American Society of Nephrology*, 22(4):598–604, 2011.

[157] Jun Hirayama, Maki Kaneko, Luca Cardone, Gregory Cahill, and Paolo Sassone-Corsi. Analysis of circadian rhythms in zebrafish. *Methods in Enzymology*, 393:186–204, 2005.

[158] Christopher G. England, Emily B. Ehlerding, and Weibo Cai. NanoLuc: A Small Luciferase Is Brightening Up the Field of Bioluminescence. *Bioconjugate Chemistry*, 27(5):1175–1187, 2016.

[159] D W Williams, F Müller, F L Lavender, L Orbán, and N Maclean. High transgene activity in the yolk syncytial layer affects quantitative transient expression assays in zebrafish Danio rerio) embryos. *Transgenic research*, 5(6):433–42, 1996.

[160] Charles B. Kimmel and Robert D. Law. Cell lineage of zebrafish blastomeres. III. Clonal analyses of the blastula and gastrula stages. *Developmental Biology*, 108(1):94–101, 1985.

[161] Pablo De Felipe, Garry A. Luke, Jeremy D. Brown, and Martin D. Ryan. Inhibition of 2A-mediated 'cleavage' of certain artificial polyproteins bearing N-terminal signal sequences. *Biotechnology Journal*, 5(2):213–223, 2010.

[162] N. Von Lutterotti, D. F. Catanzaro, J. E. Sealey, and J. H. Laragh. Renin is not synthesized by cardiac and extrarenal vascular tissues: A review of experimental evidence, 1994.

[163] A. H. Jan Danser, Jorge P. Van Kats, Peter J.J. Admiraal, Frans H.M. Derkx, Jos M.J. Lamers, Pieter D. Verdouw, Pramod R. Saxena, and Maarten A.D.H. Schalekamp. Cardiac renin and angiotensins: Uptake from plasma versus in situ synthesis. *Hypertension*, 24(1):37–48, 1994.

[164] A. H. Jan Danser, Catharina A.M. Van Kesteren, Willem A. Bax, Monique Tavenier, Frans H.M. Derkx, Pramod R. Saxena, and Maarten A.D.H. Schalekamp. Prorenin, renin, angiotensinogen, and angiotensin-converting enzyme in normal and failing human hearts: Evidence for renin binding. *Circulation*, 96(1):220–226, 1997.

[165] Amoes CARMEL and Arieh YARON. An Intramolecularly Quenched Fluorescent Tripeptide as a Fluorogenic Substrate of Angiotensin-I-Converting Enzyme and of Bacterial Dipeptidyl Carboxypeptidase. *European Journal of Biochemistry*, 87(2):265–273, 1978.

[166] Maria C.F. Oliveira, Izaura Y. Hirata, Jair R. Chagas, Paulo Boschcov, Roseli A.S. Gomes, Amintas F.S. Figueiredo, and Luiz Juliano. Intramolecularly quenched fluorogenic peptide substrates for human renin. *Analytical Biochemistry*, 203(1):39–46, 1992.

[167] Jair R. Chagas, Luiz Juliano, and Eline S. Prado. Intramolecularly quenched fluorogenic tetrapeptide substrates for tissue and plasma kallikreins. *Analytical Biochemistry*, 192(2):419–425, 1991.

[168] Ildikó Toma, Julie Kang Jung, and János Peti-Peterdi. Imaging renin content and release in the living kidney. *Nephron - Physiology*, 103(2):71–74, 2006.

[169] Yunjie Wang and Hermann Ragg. An unexpected link between angiotensinogen and thrombin. *FEBS Letters*, 585(14):2395–2399, jul 2011.

[170] Hong Lu, Lisa A. Cassis, Craig W.Vander Kooi, and Alan Daugherty. Structure and functions of angiotensinogen, jul 2016.

[171] Pamela Harding, David H. Sigmon, Marcos E. Alfie, Paul L. Huang, Mark C. Fishman, William H. Beierwaltes, and Oscar A. Carretero. Cyclooxygenase-2 mediates increased renal renin content induced by low- sodium diet. *Hypertension*, 29(1 II):297–302, 1997.

[172] Motoyuki Itoh, Cheol Hee Kim, Gregory Palardy, Takaya Oda, Yun Jin Jiang, Donovan Maust, Sang Yeob Yeo, Kevin Lorick, Gavin J. Wright, Linda Ariza-McNaughton, Allan M. Weismann, Julian Lewis, Settara C. Chandrasekharappa, and Ajay B. Chitnis. Mind bomb is a ubiquitin ligase that is essential for efficient activation of notch signaling by delta. *Developmental Cell*, 4(1):67–82, 2003.

[173] W. Saenger. Proteinase K. In *Handbook of Proteolytic Enzymes*, volume 3, pages 3240–3242. 2013.

[174] Masahiko Hirota, Masaki Ohmuraya, and Hideo Baba. The role of trypsin, trypsin inhibitor, and trypsin receptor in the onset and aggravation of pancreatitis. *Journal of Gastroenterology*, 41(9):832–836, 2006.

[175] Jesper V. Olsen, Shao En Ong, and Matthias Mann. Trypsin cleaves exclusively C-terminal to arginine and lysine residues. *Molecular and Cellular Proteomics*, 3(6):608–614, 2004.

[176] Michael Lämmerhofer. Chiral recognition by enantioselective liquid chromatography: Mechanisms and modern chiral stationary phases. *Journal of Chromatography A*, 1217(6):814–856, 2010.

[177] Kathleen M. Keating. Application of proteases to the identification of chiral modifications in synthetic peptides. *Journal of Biomolecular Techniques*, 10(2):72–75, 1999.

[178] Charles E Burnham, Charlyn L Hawelu-Johnson, Barry M Frank, and Kevin R Lynch. Molecular cloning of rat renin cDNA and its gene. *Biochemistry*, 84:5605–5609, 1987.

[179] Yahui Yan, Aiwu Zhou, Robin W. Carrell, and Randy J. Read. Structural basis for the specificity of renin-mediated angiotensinogen cleavage. *Journal of Biological Chemistry*, 294(7):2353–2364, 2019.

[180] Rosa M.A. Streatfeild-James, David Williamson, Robert N. Pike, Duane Tewksbury, Robin W. Carrell, and Paul B. Coughlin. Angiotensinogen cleavage by renin: Importance of a structurally constrained N-terminus. *FEBS Letters*, 436(2):267–270, oct 1998.

[181] L. T. SKEGGS, J. R. KAHN, and N. P. SHUMWAY. The preparation and function of the hypertensin-converting enzyme. *The Journal of experimental medicine*, 103(3):295–299, 1956.

[182] Mark C. Chappell, Martina N. Gomez, Nancy T. Pirro, and Carlos M. Ferrario. Release of angiotensin-(1-7) from the rat hindlimb: Influence of angiotensin-converting enzyme inhibition. In *Hypertension*, volume 35, pages 348–352, 2000.

[183] Manuel Luque, Piedad Martin, Nieves Martell, Carmen Fernandez, K. Bridget Brosnihan, and Carlos M. Ferrario. Effects of captopril related to increased levels of prostacyclin and angiotensin-(1-7) in essential hypertension. *Journal of Hypertension*, 14(6):799–805, 1996.

[184] Spyros Artavanis-Tsakonas, Matthew D. Rand, and Robert J. Lake. Notch signaling: Cell fate control and signal integration in development. *Science*, 284(5415):770–776, 1999.

[185] Eric W. Brunskill, Maria Luisa S. Sequeira-Lopez, Ellen S. Pentz, Eugene Lin, Jing Yu, Bruce J. Aronow, S. Steven Potter, and R. Ariel Gomez. Genes that confer the identity of the renin cell. *Journal of the American Society of Nephrology*, 22(12):2213–2225, 2011.

[186] R. A. Gomez, K. R. Lynch, R. L. Chevalier, A. D. Everett, D. W. Johns, N. Wilfong, M. J. Peach, and R. M. Carey. Renin and angiotensinogen gene expression and intrarenal renin distribution during ACE inhibition. Technical Report 6 (23/6), 1988.

[187] Fred A.M. Asselbergs, Joseph Rahuel, Frédéric Cumin, and Christian Leist. Scaled-up production of recombinant human renin in CHO cells for enzymatic and X-ray structure analysis. *Journal of Biotechnology*, 32(2):191–202, 1994.

[188] Zhongren Wu, Maria G. Cappiello, Boyd B. Scott, Yuri Bukhtiyarov, and Gerard M. McGeehan. Purification and characterization of recombinant human renin for X-ray crystallization studies. *BMC Biochemistry*, 9(1), 2008.

[189] Natalie Lassen, Tia Estey, Robert L. Tanguay, Aglaia Pappa, Mark J. Reimers, and Vasilis Vasiliou. Molecular cloning, baculovirus expression, and tissue distribution of the zebrafish aldehyde dehydrogenase 2. *Drug Metabolism and Disposition*, 33(5):649–656, 2005.

[190] Charles B. Kimmel, William W. Ballard, Seth R. Kimmel, Bonnie Ullmann, and Thomas F. Schilling. Stages of embryonic development of the zebrafish. *Developmental Dynamics*, 203(3):253–310, 1995.

[191] Le Qian, Feng Cui, Yang Yang, Yuan Liu, Suzhen Qi, and Chengju Wang. Mechanisms of developmental toxicity in zebrafish embryos (Danio rerio) induced by boscalid. *Science of the Total Environment*, 634:478–487, sep 2018.

[192] R.Ariel Gomez and Victoria F. Norwood. Developmental consequences of the renin-angiotensin system. *American Journal of Kidney Diseases*, 26(3):409–431, sep 1995.

[193] Magdalena Dabrowska, Wojciech Juzwa, Wlodzimierz J. Krzyzosiak, and Marta Olejniczak. Precise Excision of the CAG Tract from the Huntingtin Gene by Cas9 Nickases. *Frontiers in Neuroscience*, 12, 2018.

[194] Karin Pittman, Manuel Yúfera, Michail Pavlidis, Audrey J. Geffen, Willian Koven, Laura Ribeiro, José L. Zambonino-Infante, and Amos Tandler. Fantastically plastic: Fish larvae equipped for a new world. *Reviews in Aquaculture*, 5(SUPPL.1), may 2013.

[195] N F Smith, F B Eddyt, A D Struthers, and C Talbot. Renin, Atrial Natriuretic Peptide and Blood Plasma Ions in Parr and Smolts of Atlantic Salmon Salmo Salar L. and Rainbow Trout Oncorhynchus Mykiss (Walbaum) in Fresh Water and After Short-Term Exposure to Sea Water. *Journal of Experimental Biology*, 157(1):63–74, 1991.

[196] Johannes Stegbauer and Thomas M. Coffman. New insights into angiotensin receptor actions: From blood pressure to aging. *Current Opinion in Nephrology and Hypertension*, 20(1):84–88, 2011.

[197] W. Gary Anderson, Richard D. Pillans, Susumu Hyodo, Takehiro Tsukada, Jonathan P. Good, Yoshio Takei, Craig E. Franklin, and Neil Hazon. The effects of freshwater to seawater transfer on circulating levels of angiotensin II, C-type natriuretic peptide and arginine vasotocin in the euryhaline elasmobranch, Carcharhinus leucas. *General and Comparative Endocrinology*, 147(1):39–46, 2006.

[198] Alison Bendele, Jim Seely, Carl Richey, Gina Sennello, and George Shopp. Short communication: Renal tubular vacuolation in animals treated with polyethylene-glycol-conjugated proteins. *Toxicological Sciences*, 42(2):152–157, 1998.

[199] Anne M. Winkler. Albumin and Related Products. In *Transfusion Medicine and Hemostasis: Clinical and Laboratory Aspects: Second Edition*, pages 237–242. Elsevier Inc., jun 2013.

[200] Sonia Christou-Savina, Philip L. Beales, and Daniel P.S. Osborn. Evaluation of Zebrafish kidney function using a fluorescent clearance assay. *Journal of Visualized Experiments*, (96), 2015.

[201] Sebastien Andrew Rider, Finnius Austin Bruton, Richard George Collins, Bryan Ronald Conway, and John James Mullins. The efficacy of Puromycin and Adriamycin for induction of glomerular failure in larval zebrafish validated by an assay of glomerular permeability dynamics. *Zebrafish*, 15(3):234–242, jun 2018.

[202] A. Sauter, K. Machura, B. Neubauer, A. Kurtz, and C. Wagner. Development of renin expression in the mouse kidney. *Kidney International*, 73(1):43–51, 2008.

[203] R. Ariel Gomez, Brian Belyea, Silvia Medrano, Ellen S. Pentz, and Maria Luisa S. Sequeira-Lopez. Fate and plasticity of renin precursors in development and disease. In *Pediatric Nephrology*, volume 29, pages 721–726, 2014.

[204] Maria L.S. Sequeira Lopez and R. Ariel Gomez. The renin phenotype: Roles and regulation in the kidney. *Current Opinion in Nephrology and Hypertension*, 19(4):366–371, 2010.

[205] Maria Luisa S. Sequeira López, Ellen S. Pentz, Takayo Nomasa, Oliver Smithies, and R. Ariel Gomez. Renin cells are precursors for multiple cell types that switch to the renin phenotype when homeostasis is threatened. *Developmental Cell*, 6(5):719–728, 2004.

[206] Andrea Rossi, Zacharias Kontarakis, Claudia Gerri, Hendrik Nolte, Soraya Hölper, Marcus Krüger, and Didier Y.R. Stainier. Genetic compensation induced by deleterious mutations but not gene knockdowns. *Nature*, 524(7564):230–233, 2015.

[207] Mohamed A. El-Brolosy, Zacharias Kontarakis, Andrea Rossi, Carsten Kuenne, Stefan Günther, Nana Fukuda, Khrievono Kikhi, Giulia L.M. Boezio, Carter M. Takacs, Shih Lei Lai, Ryuichi Fukuda, Claudia Gerri, Antonio J. Giraldez, and Didier Y.R. Stainier. Genetic compensation triggered by mutant mRNA degradation. *Nature*, 568(7751):193–197, 2019.

[208] Maria Florencia Martinez, Silvia Medrano, Evan A. Brown, Turan Tufan, Stephen Shang, Nadia Bertoncello, Omar Guessoum, Mazhar Adli, Brian C. Belyea, Maria Luisa S. Sequeira-Lopez, and R. Ariel Gomez. Super-enhancers maintain renin-expressing cell identity and memory to preserve

multi-system homeostasis. *Journal of Clinical Investigation*, 128(11):4787–4803, oct 2018.

[209] Brigitte Angres, Heiko Steuer, Petra Weber, Michael Wagner, and Herbert Schneckenburger. A membrane-bound FRET-based caspase sensor for detection of apoptosis using fluorescence lifetime and total internal reflection microscopy. *Cytometry Part A*, 75(5):420–427, 2009.

[210] Valeriya M. Trusova, Galyna P. Gorbenko, Todor Deligeorgiev, and Nikolai Gadjev. Probing protein-lipid interactions by FRET between membrane fluorophores. *Methods and Applications in Fluorescence*, 4(3), 2016.

[211] Amanda Cobos-Correa, Johanna B. Trojanek, Stefanie Diemer, Marcus A. Mall, and Carsten Schultz. Membrane-bound FRET probe visualizes MMP12 activity in pulmonary inflammation. *Nature Chemical Biology*, 5(9):628–630, 2009.

Appendix A

Prorenin Coding Sequence

Size:1159bp
Restriction sites:EcoRI/Xhol (underlined)
Destination vector: pSECTAG2C
C-terminal TEV protease site (shaded)

gaattcttatggagggtaaaactgaagaaaatgccttccatacgagaaactctcaaggaaatgagcgtcacacca
gaattcttatggagggtaaaactgaagaaaatgccttccatacgagaaactctcaaggaaatgagcgtcacacca
gctcaagtgttatctgagattatgccaaaatatcaagaaccatcacccacaaacggcacagctccgacacctctg
atcaactacttagatactcaatattttggtgaaatcagcattggttcaccagctcagatgttcaacgttgtgttc
gacacgggttctgccaatctctgggttccctcacacagttgttctcctttatacacagcctgcttcacacacaac
agatatgatgcttccaaatccctcacacatattttcaacggcacaggattctccatccaatatgcttctggaaat
gtccggggctttctgagtgaggacgtggttgtggtgggcggtatcccagtggtgcaggtttttgcagaagccaca
gctcttcctgcaatccccttcatctttgccaaatttgatggagtgctaggaatgggctatccagatgtggccatt
gatggaattactcctgtgtttgatcggatcatgtctcagcatgttctgaaagagaatgttttctcggtgtactac
agcagggacccaacacatatccctggtggagagctggtgctgggggcacagatccgaattaccacactggacct
ttccattatataaacaccaaagagcaaggcaagtgggaggtcatcatgaaaggggtgtcggttggggcagatatc
ctgttttgcaaggatggctgtactgctgtgattgatacaggctcctcctacatcacaggccccgcttcctccatc
tcgattctgatgaaaacaattggagccgttgaactggcagaaggagggtatacagtgagctgtaatgtggtcagg
ttgttgcccactgttgcatttcatcttggtggtcaggaatattcactcacagatgaggactatattctctggcag
tcagagttcggggaggacatttgtactgtcacgttcaaagcattggatgtgccacccccctactggtcctgtctgg
atactgggggcaaacttcatagctcggtactacacagagtttgatcggggaaacaatcgcattggctttgcacga
gctgtcgaaaacctgtacttccaaggcactcgag

Protein Sequence
Size: 386 Amino Acids (42.2 kDa)
Restriction sites:EcoRI/Xhol (EF/TR)
Destination vector: pSECTAG2C
C-terminal TEV protease site (YFQG)

EFLWRVKLKK MPSIRETLKE MSVTPAQVLS EIMPKYQEPS PTNGTAPTPL INYLDTQYFG
EISIGSPAQM FNVVFDTGSA NLWVPSHSCS PLYTACFTHN RYDASKSLTH IFNGTGFSIQ
YASGNVRGFL SEDVVVVGGI PVVQVFAEAT ALPAIPFIFA KFDGVLGMGY PDVAIDGITP
VFDRIMSQHV LKENVFSVYY SRDPTHIPGG ELVLGGTDPN YHTGPFHYIN TKEQGKWEVI
MKGVSVGADI LFCKDGCTAV IDTGSSYITG PASSISILMK TIGAVELAEG GYTVSCNVVR
LLPTVAFHLG GQEYSLTDED YILWQSEFGE DICTVTFKAL DVPPPTGPVW ILGANFIARY
YTEFDRGNNR IGFARAVENL YFQGTR

Appendix B

Renin Coding Sequence

Size:1060bp
Restriction sites:EcoRI/Xhol (underlined)
Destination vector: pSECTAG2C
C-terminal TEV protease site (shaded)

gaattctatcaagaaccatcacccacaaacggcacagctccgacacctctgatcaactacttagatactcaatat
gaattctatcaagaaccatcacccacaaacggcacagctccgacacctctgatcaactacttagatactcaatat
tttggtgaaatcagcattggttcaccagctcagatgttcaacgttgtgttcgacacgggttctgccaatctctgg
gttccctcacacagttgttctcctttatacacagcctgcttcacacacaacagatatgatgcttccaaatccctc
acacatattttcaacggcacaggattctccatccaatatgcttctggaaatgtccggggctttctgagtgaggac
gtggttgtggtgggcggtatcccagtggtgcaggtttttgcagaagccacagctcttcctgcaatccccttcatc
tttgccaaatttgatggagtgctaggaatgggctatccagatgtggccattgatggaattactcctgtgtttgat
cggatcatgtctcagcatgttctgaaagagaatgttttctcggtgtactacagcagggacccaacacatatccct
ggtggagagctggtgctgggggcacagatccgaattaccacactggacctttccattatataaacaccaaagag
caaggcaagtgggaggtcatcatgaaaggggtgtcggttggggcagatatcctgttttgcaaggatggctgtact
gctgtgattgatacaggctcctcctacatcacaggccccgcttcctccatctcgattctgatgaaaacaattgga
gccgttgaactggcagaaggagggtatacagtgagctgtaatgtggtcaggttgttgcccactgttgcatttcat
cttggtggtcaggaatattcactcacagatgaggactatattctctggcagtcagagttcggggaggacatttgt
actgtcacgttcaaagcattggatgtgccacccccctactggtcctgtctggatactgggggcaaacttcatagct
cggtactacacagagtttgatcggggaaacaatcgcattggctttgcacgagctgtcgaaaacctgtacttccaa
ggcactcgag

Protein Sequence
Size: 353 Amino Acids (38.32 kDa)
Restriction sites:EcoRI/Xhol (EF/TR)
Destination vector: pSECTAG2C
C-terminal TEV protease site (YFQG)

EFYQEPSPTN GTAPTPLINY LDTQYFGEIS IGSPAQMFNV VFDTGSANLW VPSHSCSPLY
TACFTHNRYD ASKSLTHIFN GTGFSIQYAS GNVRGFLSED VVVVGGIPVV QVFAEATALP
AIPFIFAKFD GVLGMGYPDV AIDGITPVFD RIMSQHVLKE NVFSVYYSRD PTHIPGGELV
LGGTDPNYHT GPFHYINTKE QGKWEVIMKG VSVGADILFC KDGCTAVIDT GSSYITGPAS
SISILMKTIG AVELAEGGYT VSCNVVRLLP TVAFHLGGQE YSLTDEDYIL WQSEFGEDIC
TVTFKALDVP PPTGPVWILG ANFIARYYTE FDRGNNRIGF ARAVENLYFQ GTR